Role of cryptochromes in chromatin remodeling and DNA damage repair

A dissertation presented by

Yuzhao Hu

to the

School of Biological Sciences

in partial fulfillment of the requirements for the degree of

Doctor of Philosophy

in

Biological Sciences

at

Cold Spring Harbor Laboratory

August 2023

Abstract

Cryptochromes (CRYs) are UVA/blue light receptors found in both plants and animals. In animals, CRYs are involved in the entrainment of the circadian clock. In plants, CRYs play essential roles to regulate various aspects of plant growth and development. Originating from photolyases responsible for directly repairing UV-induced DNA damage, CRYs have undergone evolutionary changes and lost their enzymatic activity for DNA repair. Nevertheless, studies have shown that mammalian CRYs are involved in regulating the DNA damage response (DDR), but the detailed mechanism remains inadequately elucidated.

Thus, my research focused on investigating the involvement of plant CRYs in the DDR. My study demonstrates that CRY1 and CRY2 positively regulate plant resistance to UVC-induced DNA damage and enhance DNA damage repair. Surprisingly, examination of the CRY2 protein under UVC exposure reveals the induction of CRY2 nuclear speckles, indicating the activation of CRY2 photoreceptor by UVC. Furthermore, a time course transcriptomic experiment reveals that CRYs promote plant's transcriptional response to UVC. Notably, my study identified CAMTA transcription factors as potential downstream regulators of CRYs, mediating the DNA damage-induced transcriptional response. Together, these results characterize the positive roles of CRYs in regulating plant DDR and provide mechanistic insights into how CRYs mediate the DDR.

In a recent study conducted in the Pedmale laboratory, two deubiquitinases, UBP12 and UBP13, were identified as negative regulators of CRY2-mediated hypocotyl growth. Intriguingly, UBP12/13 have also been implicated in plant resistance to UVC, but their underlying mechanism remains unexplored. To address this gap in knowledge, my thesis research aimed to investigate whether UBP12/13 function within the same pathway as CRYs to regulate plant DDR. Through genetic experiments, I discovered that UBP12/13 act as negative regulators of DDR and operate in the same genetic pathway as CRYs to modulate plant resistance against DNA damage. Remarkably, UBP12/13 exhibit antagonistic effects on several aspects of CRYs' function in DDR. Specifically, UBP12/13

inhibits DNA damage repair and dampens the transcriptional response mediated by the CAMTA transcription factors under UVC exposure. Additionally, at the molecular level, UBP12/13 demonstrates a stronger interaction with the CRY2 protein upon UVC exposure, facilitating the destabilization of CRY2 and subsequent impairment of the role of CRYs in DDR. Collectively, these findings characterize UBP12/13 as crucial negative regulators in the CRY-mediated DDR pathway to alleviate the detrimental effects of DDR on normal cellular functions, such as cell cycle progression.

CRYs have been implicated in the regulation of large-scale chromatin condensation and decondensation. However, the precise mechanism by which CRYs govern these chromatin changes remains poorly understood. Notably, using affinity purification of CRY2 and mass spectrometry to identify interacting proteins, a novel group of CRY2 interactors was revealed: the ISWI chromatin remodeling complex, consisting of CHR11, CHR17, RLT1, RLT2, and ARID5. The homologs of ISWI chromatin remodelers in *Drosophila* and mammals have been known to actively participate in large-scale chromatin condensation and decondensation processes. Thus, the identification of the ISWI complex as CRY2 interactors positions them as promising candidates for mediating the large-scale chromatin changes associated with CRY function.

To validate the interaction between CRY2 and the ISWI complex, co-immunoprecipitation experiments were conducted, confirming the physical interaction between CRY2 and three different components of the ISWI complex: CHR11, RLT1, and ARID5. Intriguingly, the interaction between CRY2 and the ATPase subunit of the ISWI complex, CHR11, was found to be independent of light conditions. Moreover, my investigations revealed that the ISWI complex functions downstream of CRY2 in regulating blue light-mediated processes such as hypocotyl growth inhibition and floral transition. Notably, my findings demonstrate that the ISWI complex acts as a negative regulator of blue light-induced heterochromatin condensation during seedling development, opposing the role of CRY2 in this process. Collectively, these results identify the ISWI complex as novel downstream regulators within the CRY2-mediated blue light signaling pathway, presenting ISWI as promising candidates for mediating large-scale chromatin changes downstream of CRYs.

In summary, this thesis provides comprehensive insights into the pivotal roles of plant cryptochromes in DNA damage response and chromatin remodeling. The research establishes the critical involvement of CRYs and UBP12/13 deubiquitinases in plant DNA damage response, shedding light on their significant contributions to UVC-induced DNA damage repair and transcriptional regulation. Furthermore, the study identifies the ISWI chromatin remodeling complex as a novel interacting partner of CRY2, uncovering its participation in large-scale chromatin changes alongside CRYs. These findings greatly enhance our understanding of the molecular mechanisms underlying CRY-mediated chromatin regulation and hold implications for future investigations into DNA repair mechanisms and chromatin dynamics in plants.

Acknowledgements

I am deeply grateful to my Ph.D. advisor, Prof. Ullas Pedmale, for giving me the opportunity to work in his lab and for his invaluable mentorship throughout my Ph.D. journey. I am particularly grateful for his patience and guidance during the early years of my Ph.D. when I was learning essential scientific skills. I would also like to express my gratitude to all the members of the Pedmale lab, past and present, who have supported and encouraged me. I am especially grateful to Dr. Louise Lindbåck, who introduced me to many of the lab's practices and allowed me to work on one of her side projects, which turned into a large portion of the manuscript. Without Dr. Lindbåck's initial guidance and support, I would not have been able to accomplish this work. I am also thankful to Dr. Daniele Rosado, who worked closely with me on my RNA-seq analysis and helped me with writing the manuscript. Her efficiency and dedication have been a great influence on me. I would like to extend my sincere gratitude to Dr. Oliver Artz, a former postdoc in the Pedmale lab, for his support, kindness, and friendship. He has helped me navigate many challenges in the lab and in life, and I am deeply appreciative of his support.

I would also like to thank my thesis committee members, Prof. David Jackson, Prof. Christopher Vakoc, and Prof. Justin Kinney, for their invaluable guidance and feedback throughout my thesis research. My research collaborators, Prof. Yannick Jacob from Yale University, Prof. Fredy Barneche, and Prof. Clara Bourbousse from IBENS, France, also deserve my gratitude for their collaboration and support. I would like to acknowledge the staff at Uplands Farm, Mr. Timothy Mulligan, and Mr. Kyle Schlecht, for their contributions to my research by maintaining the plants I used. I would also like to thank the scientists working in the Delbruck-Page building on the CSHL campus for their generosity in lending reagents and providing scientific advice.

I owe an immeasurable debt of gratitude to my family, my mother, Ms. Qunxiong Tang, and my father, Mr. Xueman Hu, for their unwavering support and encouragement throughout my academic journey. They taught me the importance of kindness, honesty, and perseverance, and I am grateful for

their contributions to my personal and academic development. I would also like to thank my wife, Ms. Jialing Han, for her steadfast support and understanding during the challenging times of my Ph.D. program, especially during the COVID-19 pandemic when she was also pursuing her Bachelor's degree. Her sacrifices have allowed me to focus on my research, and I am deeply appreciative of her love and support. I am also grateful to my daughter, Miss Shihan Carolyn Hu, for being a cooperative and understanding presence in my life during my Ph.D. program. Her consideration and patience during the weekends when I work on my project have been a source of inspiration to me. I am confident that she will grow up to be an exceptional and passionate individual.

Finally, I would like to express my gratitude to the School of Biological Sciences (SBS) at CSHL for admitting me into their exceptional Ph.D. program and providing me with the necessary resources and support to pursue my research goals. I am grateful to the George A. and Marjorie H. Anderson Scholarship for funding my Ph.D. studies. I would like to thank Prof. Zach Lippman, Prof. Alexander Gann, Dr. Monn Monn Myat, Dr. Alyson Kass-Eisler, Ms. Kimberly Creteur, Ms. Kimberly Graham, and all the other staff and faculty members who have helped me in various ways during my time at SBS. I am also thankful for the camaraderie and support from my fellow classmates in the entering class of 2017, who have been a constant source of encouragement and inspiration.

Table of contents

List of Figures and Tables

List of Abbreviations

53BP1	P53 BINDING PROTEIN 1
6-4PP	6-4 pyrimidine pyrimidone photoproducts
ACF1	CHROMATIN ASSEMBLY FACTOR 1
ADP	Adenosine diphosphate
AHL22	AT-HOOK MOTIF NUCLEAR-LOCALIZED PROTEIN 22
AIPP3	ASI1-IMMUNOPRECIPITATED PROTEIN 3
AlkB	Alpha-ketoglutarate-dependent hydroxylase
ALKBH2	ALKB HOMOLOG 2, ALPHA-KETOGLUTARATE DEPENDENT DIOXYGENASE
ALKBH3	ALKB HOMOLOG 3, ALPHA-KETOGLUTARATE DEPENDENT DIOXYGENASE
alt-EJ	Alternative end-joining
ANOVA	Analysis of variance
AP	Apurinic/apyrimidinic
AP-MS	Affinity purification coupled with mass spectrometry
ARID5	AT-RICH INTERACTING DOMAIN 5
ARP6	ACTIN-RELATED PROTEIN 6
ATM	ATAXIA TELANGIECTASIA MUTATED
ATP	ADENOSINE TRIPHOSPHATE
ATPase	ADENOSINE TRIPHOSPHATASE
ATR	ATAXIA TELANGIECTASIA-MUTATED AND RAD3-RELATED
ATRIP	ATR INTERACTING PROTEIN
ATRX	ALPHA THALASSEMIA/MENTAL RETARDATION SYNDROME X-LINKED

ATX1	ARABIDOPSIS TRITHORAX 1
AutoN	N-TERMINAL AUTOINHIBITORY REGION
AUX/IAA	AUXIN/INDOLE-3-ACETIC ACID
BAH	BROMO-ADJACENT HOMOLOGY
BAHCC1	BAH DOMAIN AND COILED-COIL CONTAINING 1
BARD1	BRCA1 ASSOCIATED RING DOMAIN 1
BAS1	PHYB ACTIVATION TAGGED SUPPigvRESSOR 1
BAZ1A	BROMODOMAIN ADJACENT TO ZINC FINGER DOMAIN 1A
BER	Base excision repair
bHLH	Basic helix-loop-helix
BIC1	BLUE-LIGHT INHIBITOR OF CRYPTOCHROMES 1
BIC2	BLUE-LIGHT INHIBITOR OF CRYPTOCHROMES 2
BiFC	Bimolecular fluorescence complementation
BL	Blue light
BMAL1	BRAIN AND MUSCLE ARNT-LIKE 1
BPTF	BROMODOMAIN PHD FINGER TRANSCRIPTION FACTOR
BRCA1	BREAST CANCER GENE 1
BRCC36	BRCA1-BRCA2-CONTAINING COMPLEX 36
BRF	BAZ2B-CONTAINING REMODELING FACTOR
BRG1	BRAHMA-RELATED GENE-1
BUDR	BRCT DOMAIN UBIQUITIN-DEPENDENT RECRUITMENT MOTI
C	Cytosine
C4H	CINNAMATE-4-HYDROXYLASE
CAM7	CALMODULIN 7
CAMTA	CALMODULIN-BINDING TRANSCRIPTION ACTIVATOR
camta123	*camta1camta2camta3*

Cas9	CRISPR-ASSOCIATED PROTEIN 9
CCE	C-terminal CRY extension
CDC25A	CELL DIVISION CYCLE 25A
CDF2	CYCLING DOF FACTOR 2
CDK	CYCLIN-DEPENDENT KINASE
CECR2	CAT EYE SYNDROME CRITICAL REGION PROTEIN 2
CERF	CECR2-CONTAINING REMODELING FACTOR
CETN2	CENTRIN 2
CHD	CHROMODOMAIN-HELICASE-DNA BINDING
ChIP-seq	Chromatin immunoprecipitation sequencing
CHK2	CHECKPOINT KINASE 2
CHR11	CHROMATIN-REMODELING PROTEIN 11
CHR17	CHROMATIN-REMODELING PROTEIN 17
CIB1	CRYPTOCHROME-INTERACTING BASIC-HELIX-LOOP-HELIX 1
CLK	CLOCK
CLOCK	CIRCADIAN LOCOMOTER OUTPUT CYCLES KAPUT
CO	CONSTANS
COI1	CORONATINE INSENSITIVE 1
co-IP	Co-immunoprecipitation
COMPASS	COMPLEX PROTEINS ASSOCIATED WITH SET1
COP1	CONSTITUTIVE PHOTOMORPHOGENIC 1
CPD	Cyclobutane pyrimidine dimer
CPL2	BAH-PHD-CARBOXYL-TERMINAL DOMAIN PHOSPHATASE-LIKE 2
CRISPR	CLUSTERED REGULARLY INTERSPACED SHORT PALINDROMIC REPEATS

CRL4	CUL4-RING ubiquitin E3 ligase
CRY	Cryptochrome
CSA	COCKAYNE SYNDROME TYPE A
CSB	COCKAYNE SYNDROME TYPE B
CTAB	Cetyltrimethylammonium bromide
CtBP	C-TERMINAL BINDING PROTEIN
CTD	C-terminal domain
CtIP	C-TERMINAL BINDING PROTEIN
Cul	Cullin
CYC	CYCLE
DAPI	4’,6-diamidino-2-phenylindole
dCas9	catalytically dead Cas9
DDB1	DAMAGED DNA BINDING PROTEIN 1
DDP1	DDT-PHD PROTEIN 1
DDP2	DDT-PHD PROTEIN 2
DDP3	DDT-PHD PROTEIN 3
DDR	DNA damage response
DDR1	DDT-RELATED PROTEIN 1
DDR3	DDT-RELATED PROTEIN 3
DDR4	DDT-RELATED PROTEIN 4
DDR5	DDT-RELATED PROTEIN 5
DDRM1	DNA DAMAGE RESPONSE MUTANTS 1
DDW1	DDT-WAC PROTEIN 1
DEAD/H	Asp-Glu-Ala-Asp/His
DEG	Differentially expressed gene
DET1	DE-ETIOLATED 1

dISWI	DROSOPHILA ISWI
Dls1	DPB3-LIKE SUBUNIT
dMi-2	DROSOPHILA MI-2
DNA2	DNA REPLICATION HELICASE/NUCLEASE 2
DNA-PKcs	DNA-DEPENDENT PROTEIN KINASE CATALYTIC SUBUNIT
Dpb4	DNA POLYMERASE ε SUBUNIT 4
DREM	Dynamic regulatory events miner
DSB	Double-strand break
DTT	Dithiothreitol
DUB	Deubiquitinase
E.coli	*Escherichia coli*
EDTA	Ethylenediaminetetraacetic acid
EED	EMBRYONIC ECTODERM DEVELOPMENT
EMF1	EMBRYONIC FLOWER 1
ERCC1	EXCISION REPAIR CROSS COMPLEMENTATION GROUP 1
ETAA1	EWING'S TUMOR-ASSOCIATED ANTIGEN 1
EXO1	EXONUCLEASE 1
EZH2	ENHANCER OF ZESTE 2
FAAP24	FANCONI ANEMIA CORE COMPLEX ASSOCIATED PROTEIN 24
FAD	Flavin adenine dinucleotide
FANC	FANCONI ANEMIA COMPLEMENTATION GROUP
FBXL3	F-BOX AND LEUCINE RICH REPEAT PROTEIN 3
FDR	False discovery rate
FIP37	FKBP12 INTERACTING PROTEIN 37
FLC	FLOWERING LOCUS C
FPKM	Fragments per kilobase million

FT	FLOWERING LOCUS T
FUS	FUSCA
GFP	Green fluorescent protein
GG-NER	Global genome NER
GO	Gene ontology
H3K27me3	trimethylation of Histone H3 at lysine 27
H3K4me3	trimethylation of Histone H3 at lysine 4
HAUSP	HERPESVIRUS-ASSOCIATED UBIQUITIN-SPECIFIC PROTEASE
HDAC	HISTONE DEACETYLASE
HFR1	LONG HYPOCOTYL IN FAR-RED 1
HOX	HOMEOBOX
HP1β	HETEROCHROMATIN PROTEIN 1 BETA
HR	Homologous recombination
HRP	Horseradish peroxidase
HSA	HELICASE-SANT-ASSOCIATED
HY4	Elongated hypocotyl 4
HY5	Elongated hypocotyl 5
HYH	HY5-HOMOLOG
ID2	FANCI/FANCD2
IGV	Integrative Genomics Viewer
INO80	INOSITOL REQUIRING 80
INTS11	INTEGRATOR COMPLEX SUBUNIT 11
Ioc3	ISWI ONE COMPLEX PROTEIN 3
ISWI	IMITATION SWITCH
Itc1	IMITATION SWITCH TWO COMPLEX PROTEIN 1
JAMM	Jab1/Mov34/MPN+ proteases

JAZ	JASMONATE-ZIM-DOMAIN PROTEIN
JET	JETLAG
kDa	Kilodalton
LC-MS	Liquid-chromatography coupled to mass spectrometry
LD	Long day
LDS	Lithium dodecyl sulfate
LED	Light-emitting diode
LHP1	LIKE HETEROCHROMATIN PROTEIN 1
LIG4	DNA LIGASE 4
LRB	LIGHT-RESPONSE BROAD-COMPLEX, TRAMTRACK AND BRIC A BRACS
LS	Linsmaier and Skoog
LSD	Least significant difference
m^6A	N^6-methyladenosine
MAF4	MADS AFFECTING FLOWERING 4
MATH	Meprin and TRAF homology
MBD9	METHYL-CPG-BINDING DOMAIN 9
MDC1	MEDIATOR OF DNA DAMAGE CHECKPOINT 1
Mdm2	MURINE DOUBLE MINUTE 2
MERIT40	MEDIATOR OF RAP80 INTERACTIONS AND TARGETING 40 KDA
MHF1	MPH1-ASSOCIATED HISTONE-FOLD PROTEIN 1
MINDY	MOTIF INTERACTING WITH UBIQUITIN-CONTAINING NOVEL DUB FAMILY
MJD	MACHADO-JOSEPHIN DOMAIN PROTEASE
MMR	Mismatch repair

MOPS	3-(N-morpholino)propanesulfonic acid
MPK3	MAP KINASE 3
MPK3P	Phosphorylated MPK3
MPK6	MAP KINASE 6
MPK6P	Phosphorylated MPK6
MRE11	MEIOTIC RECOMBINATION 11
MRN	MRE11-RAD50-NBS1
MSI3	MULTICOPY SUPPRESSOR OF IRA1 3
MTA	MRNA ADENOSINE METHYLASE
MTB	METHYLTRANSFERASE B
MutH	MUTATOR H
MutL	MUTATOR L
MutS	MUTATOR S
NBS1	NIJMEGEN BREAKAGE SYNDROME 1
NER	Nucleotide excision repair
NHEJ	Non-homologous end-joining
NoRC	NUCLEOLAR REMODELING COMPLEX
NuRD	NUCLEOSOME REMODELING AND DEACETYLASE
NURF	NUCLEOSOME REMODELING FACTOR
OLIG2	OLIGODENDROCYTE TRANSCRIPTION FACTOR 2
OTU	OVARIAN TUMOR PROTEASE
OTUB2	OTU DEUBIQUITINASE, UBIQUITIN ALDEHYDE BINDING 2
OTUD4	OTU DEUBIQUITINASE 4
Paf1	Pol II-associated factor 1
PAIPP2	PARALOG OF AIPP2
PALB2	PARTNER AND LOCALIZER OF BRCA2

PARP1	POLY (ADP-RIBOSE) POLYMERASE 1
PBS	Phosphate-buffered saline
PCA	Principal component analysis
PCNA	PROLIFERATING CELL NUCLEAR ANTIGEN
PER	PERIOD
PER1	PERIOD 1
PER2	PERIOD2
PFA	Paraformaldehyde
PHD	PLANT HOMEODOMAIN
PHR	Photolyase homologous region
PHR1	PHOTOLYASE 1
PHY	PHYTOCHROME
PIF4	PHYTOCHROME INTERACTING FACTOR 4
PIF5	PHYTOCHROME INTERACTING FACTOR 5
PMSF	Phenylmethylsulfonyl fluoride
POLE3	DNA POLYMERASE EPSILON SUBUNIT 3
PPK	Photoregulatory protein kinases
PRC1	Polycomb repressive complex 1
PRC2	POLYCOMB REPRESSIVE COMPLEX 2
PRDM9	PR/SET DOMAIN CONTAINING PROTEIN 9
pRNA	Promoter RNA
PRR9	PSEUDO-RESPONSE REGULATOR 9
PTM	Post-translational modification
PWWP	Pro-Trp-Trp-Pro
RAD23B	RAD23 HOMOLOG B
RAP80	RECEPTOR-ASSOCIATED PROTEIN 80

RB	RETINOBLASTOMA PROTEIN
RBBP4	RB BINDING PROTEIN 4
rDNA	ribosomal RNA gene
RecA	RECOMBINASE A
RHF	Relative heterochromatin fraction
RLT1	RINGLET 1
RLT2	RINGLET 2
RNAi	RNA interference
RNA-seq	RNA-sequencing
RNF168	RING FINGER PROTEIN 168
RNF8	RING FINGER PROTEIN 8
RPA	REPLICATION PROTEIN A
RSF	REMODELING AND SPACING FACTOR
RT-qPCR	Reverse transcription-quantitative polymerase chain reaction
SANT	HAND-SWI3, ADA2, N-COR, AND TFIIB
SAV3	SHADE AVOIDANCE 3
SCF	SKP, CULLIN, F-BOX CONTAINING
SD	Standard deviation
SDG2	SET DOMAIN PROTEIN 2
SDS-PAGE	Sodium dodecyl-sulfate polyacrylamide gel electrophoresis
Ser1981	Serine at position 1981
Set1	SU(VAR)3-9, ENHANCER-OF-ZESTE AND TRITHORAX 1
SIRT6	SIRTUIN 6
SLIDE	SANT-LIKE ISWI DOMAIN

SMARCA5	SWI/SNF RELATED, MATRIX ASSOCIATED, ACTING DEPENDENT REGULATOR OF CHROMATIN, SUBFAMILY A, MEMBER 5
SOC1	SUPPRESSOR OF OVEREXPRESSION OF CO 1
SOG1	SUPPRESSOR OF GAMMA RADIATION 1
SPA	SUPPRESSOR OF PHYA-105
SSB	Single-strand break
ssDNA	Single-stranded DNA
STUBL4	SUMO-TARGETED UBIQUITIN E3 LIGASE 4
SWC6	SWR1 COMPLEX SUBUNIT 6
SWI/SNF	SWITCH/SUCROSE NON-FERMENTABLE
SWR1	SWI2/SNF2-RELATED 1
T	Thymine
TAF3	TATA-BOX BINDING PROTEIN ASSOCIATED FACTOR 3
TBS	Tris-buffered saline
TC-NER	Transcription-coupled NER
TCP17	TCP DOMAIN PROTEIN 17
TCP22	TCP DOMAIN PROTEIN 22
TF	Transcription factor
TFIIH	TRANSCRIPTION FACTOR II H
TIM	TIMELESS
TIP5	TTF-I INTERACTING PEPTIDE 5
TIR1	TRANSPORT INHIBITOR RESPONSE 1
TopBP1	DNA TOPOISOMERASE II BINDING PROTEIN 1
ToRC	TOUTATIS-CONTAINING CHROMATIN REMODELING COMPLEX

TSS	Transcription start site
TUBE	Tandem ubiquitin binding entities
UBP12	UBIQUITIN-SPECIFIC PROTEASE 12
UBP13	UBIQUITIN-SPECIFIC PROTEASE 13
UBP13oe	UBP13 overexpressing seedlings
UCH	UBIQUITIN C-TERMINAL HYDROLASE
Ume6p	UNSCHEDULED MEIOTIC GENE EXPRESSION 6 PROTEIN
USP	UBIQUITIN-SPECIFIC PROTEASE
USP34	UBIQUITIN SPECIFIC PROTEASE 34
USP7	UBIQUITIN SPECIFIC PROTEASE 7
USP9x	UBIQUITIN SPECIFIC PEPTIDASE 9 X-LINKED
UVR8	UV RESISTANCE LOCUS 8
VP	Valine-proline
WICH	WILLIAMS SYNDROME TRANSCRIPTION FACTOR-ISWI CHROMATIN REMODELING COMPLEX
WL	White light
WT	Wild type
XPC	XERODERMA PIGMENTOSUM COMPLEMENTATION GROUP C
XPF	XERODERMA PIGMENTOSUM COMPLEMENTATION GROUP F
XPG	XERODERMA PIGMENTOSUM COMPLEMENTATION GROUP G
XRCC1	X-RAY REPAIR CROSS COMPLEMENTING 1
XRCC4	X-RAY REPAIR CROSS COMPLEMENTING 4
yCHRAC	YEAST CHROMATIN ACCESSIBILITY COMPLEX
ZTL	ZEITLUPE
ZUP	ZINC-FINGER-CONTAINING UBIQUITIN PEPTIDASE

Chapter 1. Introduction

1.1 Cryptochromes in plants and animals

Cryptochromes (CRYs) are highly conserved proteins found in both animals and plants (Chaves et al. 2011), involved in various biological processes including light perception and circadian clock regulation. In plants, CRYs function as receptors for blue light, enabling plants to perceive and react to variations in light conditions (Wang and Lin 2020). For instance, plant CRYs are involved in the precise timing of vital processes like seed germination and flowering (Barrero et al. 2014; Guo et al. 1998). In *Drosophila*, CRYs contribute to the entrainment of the circadian clock (Chaves et al. 2011), which is crucial for maintaining daily rhythms. Mammalian CRYs have evolved to serve as specialized transcriptional repressors, playing a pivotal role in circadian rhythm regulation (Chaves et al. 2011). By selectively inhibiting gene activity during specific times of the day, mammalian CRYs help govern essential biological processes such as sleep and metabolism (Wisor et al. 2002; Lamia et al. 2011).

1.1.1 Photolyases and CRYs: diverse functions and evolutionary history

Photolyases are essential enzymes involved in the repair of DNA damage caused by UV radiation through a process known as photoreactivation (Sancar 2003). UV radiation induces two primary forms of DNA damage: cyclobutane pyrimidine dimers (CPDs) and 6-4 pyrimidine pyrimidone photoproducts (6-4PPs) (Sancar 2003). To address these DNA damages, two distinct classes of photolyases have been evolved: CPD photolyases that repair CPDs and 6-4 photolyases that repair 6-4PPs (Sancar 2003). Both types of photolyases contain the chromophore flavin adenine dinucleotide (FAD), enabling them to absorb energy from UVA/blue light and employ this energy to reverse UV-caused DNA damage (Carell et al. 2001). Photolyases exhibit remarkable fidelity in repairing UV-induced DNA damage, thereby preserving the integrity of the genetic material (Sancar 2003). Overall,

photolyases are captivating enzymes that have evolved to shield organisms from the detrimental effects of UV radiation (Weber 2005).

When the *CRY1* gene, known as *HY4*, was initially cloned and sequenced in *Arabidopsis*, it was revealed that CRY1 possesses a significant degree of sequence homology with photolyases (Ahmad and Cashmore 1993). Subsequent investigations led to the identification of CRYs in other algae and animal species as well (Mei and Dvornyk 2015). Notably, CRYs also bind the FAD chromophore (Lin et al. 1995). However, unlike photolyases, CRYs do not possess DNA repair enzymatic activity (Lin et al. 1995). Instead, they have acquired novel functions such as mediating light signaling pathways in plants and acting as transcriptional repressors for circadian rhythm in mammals (Chaves et al. 2011).

1.1.2 Function of CRYs in the model plant *Arabidopsis thaliana*

Arabidopsis possesses two CRY photoreceptors, namely CRY1 (Ahmad and Cashmore 1993) and CRY2 (Lin et al. 1998). Both CRY1 and CRY2 comprise of two protein domains: the N-terminal photolyase homologous region (PHR) and the C-terminal CRY extension (CCE) domain (Figure 1.1A) (Liu et al. 2016a). The PHR domain shares a high sequence homology with photolyases and has a FAD binding pocket, which enables CRYs to bind FAD and receive UVA/blue light (Figure 1.1A) (Liu et al. 2016a). On the other hand, the CCE domain is not homologous to photolyases (Figure 1.1A) but is believed to be responsible for carrying out the light signaling function of CRYs by interacting with downstream effectors of the signaling pathway (Liu et al. 2016a). While CRY2 is predominantly localized in the nucleus (Yu et al. 2007), CRY1 was found in both the nucleus and cytoplasm (Wu and Spalding 2007). Functionally, CRY1 responds to higher blue light intensities, whereas CRY2 is mainly functional in lower blue light intensities (less than 1 $\mu mol\ m^{-2}\ s^{-1}$) (Lin et al. 1998). When *cry1* and *cry2* mutants were grown under high blue light intensity, the *cry1* mutant exhibited a much taller hypocotyl phenotype compared to the wild type, while the *cry2* mutant was similar to the wild type (Lin et al. 1998). Conversely, under low intensities of blue light, the hypocotyl of *cry2* was longer than

the wild type, while *cry1* exhibited a shorter hypocotyl length compared to *cry2* (Lin et al. 1998). These findings suggest that CRY1 and CRY2 exhibit functional specialization in the regulation of hypocotyl growth under blue light (Lin et al. 1998).

Upon activation by blue light, CRYs undergo dimerization, tetramerization, and oligomerization (Figure 1.1B) (Liu et al. 2020; Sang et al. 2005; Palayam et al. 2021). Additionally, phosphorylation of CRY1 and CRY2 proteins occurs, with specific residues of CRY1 and CRY2 being identified as phosphorylation target sites following photoactivation (Gao et al. 2022; Liu et al. 2017). The photoregulatory protein kinases (PPKs) have been found to phosphorylate CRY1 and CRY2 proteins upon their activation by blue light, and these phosphorylation modifications are associated with the biological function of CRYs in regulating hypocotyl growth under blue light (Gao et al. 2022; Liu et al. 2017). Moreover, upon oligomerization, both CRY1 and CRY2 photoreceptors form nuclear speckles (Figure 1.1B) (Yu et al. 2009; Liu et al. 2022), but under different light intensities. Notably, CRY2 proteins undergo liquid-liquid phase separation (Wang et al. 2021) to form nuclear speckles in response to low to medium blue light intensities (7 μmol m^{-2} s^{-1}) (Zuo et al. 2012). Conversely, high blue light intensities (more than 100 μmol m^{-2} s^{-1}) are required for CRY1 to form nuclear speckles (Liu et al. 2022). Interestingly, although CRY1 is also localized in the cytoplasm, it exclusively forms speckles in the nucleus, suggesting the presence of either promoting factors in the nucleus or antagonizing factors in the cytoplasm for CRY1 speckle formation (Liu et al. 2022). The formation of CRY2 nuclear speckles has been linked to its role in regulating the circadian clock (Wang et al. 2021). When CRY2 is activated by blue light, its interacting partners, MRNA ADENOSINE METHYLASE (MTA), METHYLTRANSFERASE B (MTB), FKBP12 INTERACTING PROTEIN 37 (FIP37) (Wang et al. 2021), and TCP DOMAIN PROTEIN 22 (TCP22) proteins (Mo et al. 2022), co-localize with CRY2 in the nuclear speckles. Concentration of MTA, MTB, FIP37 and TCP22 within the CRY2 speckles facilitates the function of CRY2 in circadian clock control (Mo et al. 2022; Wang et al. 2021).

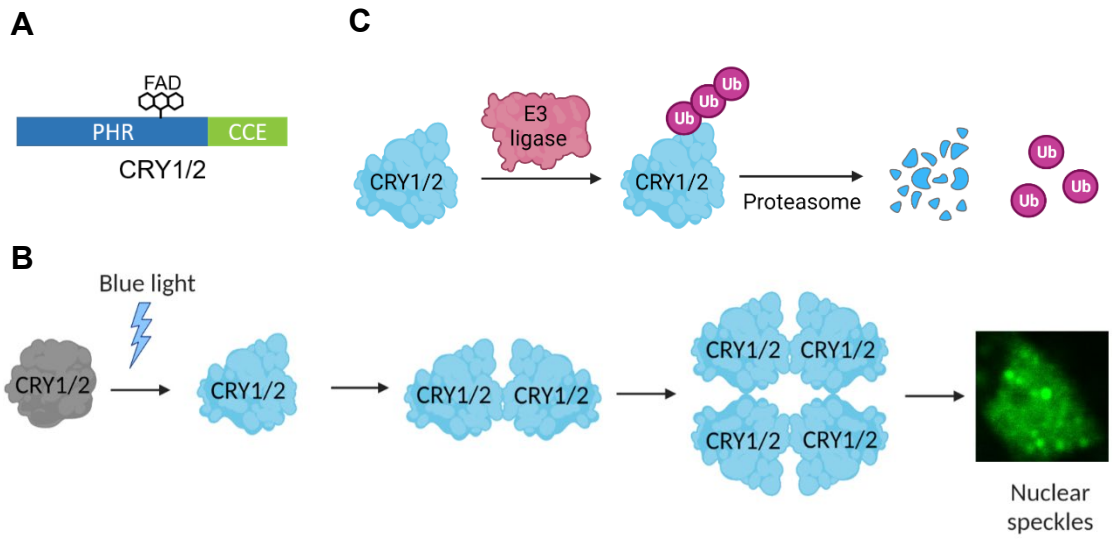

Figure 1.1 Domain structure and photoactivation of CRYs in *Arabidopsis*.
(A) CRY1 and CRY2 both contain the N-terminal PHR domain and the C-terminal CCE domain (Yu et al. 2010). CRYs are also non-covalently bound to the FAD chromophore, enabling them to sense blue/UVA light (Lin et al. 1995). (B) Upon activation by blue light, CRYs homodimerize and homotetramerize leading to nuclear speckles (Palayam et al. 2021). (C) Photoactivated CRYs are ubiquitinated by E3 ligases and further degraded by the proteasome (Chen et al. 2021; Yu et al. 2007).

Upon activation by blue light, the phosphorylated CRYs undergo ubiquitination (Figure 1.1C), serving as a desensitization mechanism for the CRY-mediated blue light signaling pathway (Chen et al. 2021). Initially, it was observed that CRY2 undergoes degradation under moderate blue light intensities (16 μmol m^{-2} s^{-1}), while CRY1 appears to be stable (Yu et al. 2007). However, recent findings have revealed that CRY1 also undergoes blue light-dependent ubiquitination and degradation, albeit at significantly higher blue light intensities (more than 100 μmol m^{-2} s^{-1}) compared to CRY2 (Miao et al. 2022). The ubiquitination of CRYs is mediated by two distinct types of E3 ligases: the Cullin 4-RING ubiquitin E3 ligase (CRL4)$^{\text{CONSTITUTIVE PHOTOMORPHOGENIC 1-SUPPRESSOR OF PHYA-105}}$ ($CRL4^{COP1\text{-}SPA}$) and the $CRL3^{\text{LIGHT-RESPONSE BROAD-COMPLEX, TRAMTRACK AND BRIC A BRACS}}$ ($CRL3^{LRBs}$) complexes (Miao et al. 2022; Chen et al. 2021). Mutation of COP1-SPA or LRBs leads to a substantial slowdown of CRY1 and CRY2 degradation (Chen et al. 2021; Miao et al. 2022). Ubiquitinated CRY1 and CRY2 are subsequently degraded by the 26S proteasome (Figure 1.1C) (Yu et al., 2007; Miao et al., 2022). It has been reported that the degradation of CRY1 and CRY2 may be associated with their nuclear speckle formation (Yu et al., 2009; Liu et al., 2022). This is supported by the observation that the CRY1 or CRY2-green fluorescent protein (GFP) fusion protein readily forms nuclear speckles in blue light, and its degradation is slower compared to the N-terminally tagged GFP-CRY1 or GFP-CRY2, which only forms nuclear speckles in blue light when pre-treated with the proteasome inhibitor MG132 to block CRY1 or CRY2 degradation (Yu et al., 2009; Liu et al., 2022).

Apart from regulating hypocotyl growth under blue light, CRYs are involved in another crucial developmental process in plants known as floral transition (Guo et al. 1998), which marks the transition from vegetative growth to reproductive growth (Battey and Tooke 2002). In *Arabidopsis*, CRY2 plays a critical role in the regulation of flowering time, as mutations in *CRY2* lead to a late flowering phenotype (Guo et al. 1998). However, the role of CRY1 in flowering time regulation remains controversial. A gain-of-function mutant of *CRY1* exhibited earlier flowering compared to the WT, suggesting a potential role of CRY1 in promoting floral transition (Exner et al. 2010). However, conflicting reports have emerged regarding the flowering time of the *cry1* mutant. While some studies

reported *cry1* mutant with a late flowering phentoype (Bagnall et al. 1996), others reported that *cry1* flowered around the same time as the WT (El-Din El-Assal et al. 2003). In summary, CRY2 is essential for plant floral transition, while the role of CRY1 in this process remains controversial.

The CRY-mediated light signaling pathway involves several molecular regulation modules (Ponnu and Hoecker 2022). Firstly, upon photoactivation, CRYs can inhibit the function of the $CRL4^{COP1\text{-}SPA}$ E3 ubiquitin ligase complex by at least two mechanisms (Ponnu et al. 2019). Light-activated CRY2 through its C-terminal valine-proline (VP) motif competes with the substrates of $CRL4^{COP1\text{-}SPA}$ for binding and subsequent ubiquitination and degradation (Ponnu et al. 2019), thus leading to the degradation of CRY2 and stabilization of other $CRL4^{COP1\text{-}SPA}$ substrates. Additionally, CRYs can inhibit the interaction between COP1 and SPA proteins thereby inhibiting the function of the $CRL4^{COP1\text{-}SPA}$ complex (Lian et al. 2011; Liu et al. 2011). As a result, substrates of the COP1-SPA E3 ligase, including transcription factors such as ELONGATED HYPOCOTYL 5 (HY5), HY5-HOMOLOG (HYH), CONSTANS (CO), and LONG HYPOCOTYL IN FAR-RED 1 (HFR1), are de-repressed upon blue light activation of CRYs (Ponnu and Hoecker 2022). The de-repression of HY5 leads to the activation of numerous light-responsive genes, ultimately inhibiting hypocotyl elongation in light (Wang and Lin 2020). De-repression of CO contributes to the activation of *FLOWERING LOCUS T* (*FT*) (Liu et al. 2008b), a key promoter of floral transition (PIN and NILSSON 2012). Another functional mechanism of CRY signaling involves the direct interaction between CRYs and basic helix–loop–helix (bHLH) transcription factors, including CRYPTOCHROME-INTERACTING BASIC-HELIX-LOOP-HELIX 1 (CIB1) (Figure 1.2A) (Liu et al. 2008a) and PHYTOCHROME INTERACTING FACTOR 4 and 5 (PIF4/5) (Figure 1.2B) (Pedmale et al. 2016). CRYs interact directly with CIB1 in a blue light-dependent manner (Figure 1.2A) (Liu et al. 2008a). CIB1, along with CO and CRY2, binds to the promoter of *FT* and promotes its transcription, thus promoting floral transition (Liu et al. 2018). CRY2 also directly interacts with PIF4/5 to repress their transcriptional activity under limiting blue light conditions (Figure 1.2B) (Pedmale et al. 2016). Moreover, CRY2 was found to bind to chromatin at overlapping sites with PIF4/5 transcription factors in low blue light shade conditions,

indicating that bHLH transcription factors can recruit CRY2 to specific target genes, regulating the expression of cell wall expansion genes and modulating hypocotyl growth (Pedmale et al. 2016).

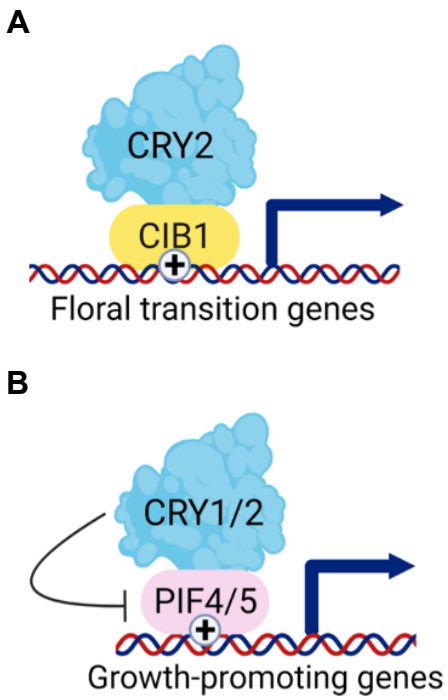

Figure 1.2 CRYs directly interact with transcription factors to regulate plant growth and development.
(A) CRY2 interacts directly with CIB1 transcription factor to promote the transcription of genes involved in floral transition (Liu et al. 2008a). (B) CRY1 and CRY2 interact directly with PIF4 and PIF5 transcription factors to inhibit their transcriptional activity, thereby inhibiting the transcription of growth-promoting genes (Pedmale et al. 2016; Ma et al. 2016).

In addition to ubiquitination and degradation (Chen et al. 2021), as well as spontaneous dark reversion (Bouly et al. 2007), there is another mechanism that downregulates CRY activity. CRY2 and BLUE-LIGHT INHIBITOR OF CRYPTOCHROMES 1 and 2 (BIC1/2) form a negative feedback loop that fine-tunes CRY2 photoactivation in plants (Wang et al. 2016). Upon blue light exposure, photoactivated CRY2 indirectly promotes the stabilization of HY5 protein (Wang et al. 2001). HY5 in turn binds to the promoter of *BIC1* and *BIC2* to induce their expression (Wang et al. 2016). BIC1 and BIC2 then bind to CRY2 in a blue light-dependent manner, inhibiting various aspects of CRY2 photo-response, such as CRY2 dimerization or oligomerization, photobody formation, phosphorylation, interaction with CIB1, and the physiological activity of CRY2 to inhibit hypocotyl growth and promote floral transition (Wang et al. 2016). Later structural studies reveal that BIC2 bind to CRY2 in a 1:1 ratio, with BIC2 acting as a "waist-belt" that wraps around the PHR domain of CRY2, inhibiting the photoreduction of FAD by light and occupying the CRY2 oligomeric interface to inhibit CRY2 oligomerization (Ma et al. 2020b). The binding affinity of BIC2 to CRY2 is also stronger than that between two CRY2 proteins (Ma et al. 2020b). Therefore, BIC2 binding inhibits the formation of CRY2 oligomers, rendering them inactive and unable to carry out normal physiological activities (Ma et al. 2020b).

In addition to regulating hypocotyl growth inhibition and flowering time (Wang et al. 2014), CRYs in *Arabidopsis* are involved in various other developmental processes (Wang et al. 2014). These developmental processes include the entrainment of the circadian clock (He et al. 2022), stomata development (Kang et al. 2009; Cao et al. 2021), stomata opening (Mao et al. 2005), as well as the suppression of leaf senescence (Kozuka et al. 2023), among others. Upon activation by blue light, CRYs undergo extensive conformational changes and exert their regulatory effects by directly and indirectly modulating transcription, playing crucial roles in various plant developmental processes (Lin and Todo 2005).

1.1.3 Role of CRYs in regulating the circadian clock in *Drosophila Melanogaster*

In fruit flies, there is a single copy of CRY known as DmCRY (Emery et al. 1998; Stanewsky et al. 1998), which functions as a photoreceptor primarily involved in entraining the circadian clock (Emery et al. 2000). The core molecular clock of fruit flies consists of two sets of proteins: the activating transcription factors CLOCK (CLK) and CYCLE (CYC), and the repressing transcription factors PERIOD (PER) and TIMELESS (TIM) (Nitabach and Taghert 2008). During the daytime, CLK and CYC activate the transcription of clock-related genes, including *PER* and *TIM* (Rosato et al. 2006). Consequently, throughout the day, PER and TIM gradually accumulate and peak around dusk (Nitabach and Taghert 2008). Subsequently, PER and TIM enter the nucleus, inhibit the activity of CLK and CYC, and suppress the expression of the clock-related genes including *PER* and *TIM* (Rosato et al. 2006). As PER and TIM mRNA and protein levels decline around dawn, CLK and CYC become reactivated, initiating a new daily cycle (Nitabach and Taghert 2008). DmCRY integrates the light information it receives to reset the molecular clock in the morning (Peschel et al. 2006; Koh et al. 2006). When DmCRY is activated by light in the morning, it interacts with TIM and the E3 ligase of TIM, namely JETLAG (JET) (Koh et al. 2006). Consequently, TIM undergoes ubiquitination by JET and subsequent degradation by the proteasome (Koh et al. 2006). Degradation of TIM renders PER unstable and induces PER degradation (Damulewicz and Mazzotta 2020). As a result of the destabilization of PER and TIM, CLK and CYC are relieved from inhibition and initiate a new daily cycle (Damulewicz and Mazzotta 2020). Importantly, following TIM degradation, DmCRY itself is also subject to degradation (Ozturk et al. 2013). The degradation of DmCRY subsequent to TIM degradation ensures that the circadian clock cannot be reset again immediately following an initial reset triggered by the photoactivation of DmCRY (Damulewicz and Mazzotta 2020).

1.1.4 Function of CRYs in mammals

In mammalian cells, CRYs play a crucial role as transcriptional repressors within the core molecular feedback circuit of the circadian clock (Takahashi 2017). The fundamental molecular clock

in mammalian cells consists of the activating transcription factors CIRCADIAN LOCOMOTER OUTPUT CYCLES KAPUT (CLOCK) and BRAIN AND MUSCLE ARNT-LIKE 1 (BMAL1), as well as the repressors CRY1, CRY2, PERIOD 1 (PER1), and PER2 (Takahashi 2017). CLOCK and BMAL1 initiate the transcription of numerous clock-related genes, including CRY1/2 and PER1/2 (Takahashi 2017). Subsequently, CRY1/2 and PER1/2 translocate back to the nucleus and inhibit the transcriptional activity of CLOCK and BMAL1, thereby suppressing the expression of clock-related genes including *CRY1/2* and *PER1/2* (Takahashi 2017). As the mRNA and protein levels of CRY1/2 and PER1/2 decrease, CLOCK and BMAL1 are de-repressed, initiating a new circadian cycle (Takahashi 2017). In contrast to *Drosophila* CRYs that serve as circadian photoreceptors, mammalian CRYs mainly function as core repressors within the negative feedback loop of circadian clock (Partch et al. 2014).

Apart from regulating the circadian clock, mammalian CRYs have also been implicated in the DNA damage response (DDR) (Kang and Leem 2014; Shafi et al. 2021; Papp et al. 2015). In mice, it has been observed that the ATAXIA TELANGIECTASIA-MUTATED AND RAD3-RELATED (ATR)-mediated DNA damage checkpoint response exhibits a circadian rhythm, and this time-of-day-dependent activity of ATR is compromised when cells lack CRY1 or both CRY1 and CRY2 (Kang and Leem 2014). This regulation of the rhythmic activity of ATR by CRYs is likely mediated by the rhythmic interaction between nuclear CRY1 and TIM (Kang and Leem 2014), since TIM is required for proper ATR activity (Kemp et al. 2010). Subsequently, another study suggested that DNA damage can differentially regulate the stability of mouse CRY1 and CRY2, and CRY1 and CRY2 regulate the transcriptional response to DNA damage (Papp et al. 2015). Upon genotoxic stress, CRY1 exhibits a stronger interaction with its deubiquitinase (DUB), HERPESVIRUS-ASSOCIATED UBIQUITIN-SPECIFIC PROTEASE (HAUSP), also called UBIQUITIN SPECIFIC PROTEASE 7 (USP7), leading to CRY1 stabilization (Papp et al. 2015). In contrast, during genotoxic stress, CRY2 shows a stronger interaction with its E3 ligase, F-BOX AND LEUCINE RICH REPEAT PROTEIN 3 (FBXL3), resulting in the destabilization of CRY2 protein (Papp et al. 2015). The destabilization of CRY2 upon

DNA damage transiently releases the transcriptional repression of DNA damage-responsive genes by CRY2. Later on, the transcription of DNA damage-responsive genes is repressed again by the increasing levels of CRY1 protein, causing a transient activation of DNA damage-responsive genes (Papp et al. 2015). Consequently, depletion of *CRY1* in cells leads to a stronger activation of DNA damage-responsive genes in response to DNA damage since CRY1 can no longer repress the transcription of these genes, while depletion of *CRY2* results in constitutive repression of DNA damage-responsive genes by CRY1, leading to the accumulation of DNA damage in cells (Papp et al. 2015). Furthermore, a separate study identified CRY1 as a tumor-specific regulator of DNA repair (Shafi et al. 2021). CRY1 amplification has been observed in prostate cancers, and overexpression of the CRY1 protein is associated with poor cancer outcomes (Shafi et al. 2021). Additional experiments have demonstrated that DNA damage stabilizes CRY1 protein in prostate cancer cells (Shafi et al. 2021). Cistrome and transcriptome analyses have revealed that CRY1 promotes the transcription of genes involved in homologous repair, thereby facilitating DNA damage repair in prostate cancer cells (Shafi et al. 2021). These findings underscore the significance of investigating the role of CRY1 in prostate cancer and suggest that targeting CRY1 may represent a potential therapeutic strategy for this disease (Shafi et al. 2021). In summary, CRYs in mammals not only function as core transcriptional suppressors in the molecular feedback loop of circadian clock, but also have important functions in DDR.

1.2 Relationship between CRYs and the chromatin

1.2.1 Role of CRYs in large-scale chromatin organization

Plant CRYs have been implicated in the regulation of higher order chromatin organization (Bourbousse et al. 2020). Within the *Arabidopsis* nucleus, condensed pericentromeric repeats and inactive ribosomal DNA form distinct structures known as chromocenters, which appear as densely staining nuclear bodies when visualized with DNA dyes like 4’,6-diamidino-2-phenylindole (DAPI) (van Zanten et al. 2011). Throughout plant development, the number of chromocenters in the nucleus

can dynamically change, reflecting the higher-order condensation or decondensation of the heterochromatin (van Zanten et al. 2012). Floral transition marks the switch from initial vegetative growth, which produces leaves, to later reproductive growth, generating floral organs for reproduction (Kinoshita and Richter 2020). During floral transition, the number of chromocenters in the nucleus temporarily decreases due to heterochromatin decondensation, followed by an increase in numbers of chromocenters once the plant enters the reproductive growth stage (Tessadori et al. 2007). This transient decondensation and re-condensation of heterochromatin during floral transition have been found to depend on the CRY2 photoreceptor (Tessadori et al. 2007). Interestingly, while CRY2 is known to regulate floral transition through CO and FT, the depletion of either *CO* or *FT* does not affect the transient decondensation of heterochromatin (Tessadori et al. 2007). This indicates that CRY2 regulates chromatin decondensation through a pathway independent of CO and FT (Tessadori et al. 2007). However, the specific mechanism by which CRY2 regulates large-scale chromatin decondensation remains unknown (Tessadori et al. 2007).

In addition to the floral transition, large-scale chromatin decondensation is also observed under decreasing environmental light intensity (van Zanten et al. 2010a). Transitioning plants from normal light intensity to low light intensity conditions, without altering the light quality, induces a gradual chromatin decondensation over a 96-hour period (van Zanten et al. 2010a). Remarkably, reverting the light intensity back to normal causes heterochromatin to recondense (van Zanten et al. 2010a). Interestingly, this decondensation of heterochromatin is not observed when plants are shifted from normal light conditions to complete darkness (van Zanten et al. 2010a). This suggests that the heterochromatin decondensation was not due to a general reduction of plant energy status but rather due to changes in light signaling (van Zanten et al. 2010a). Further investigations demonstrated that CRY2 is required for the reduction of chromatin compaction under low light intensity (van Zanten et al. 2010a). However, the mechanism through which CRY2 regulates large-scale chromatin decondensation under low light intensity remains unexplored (van Zanten et al. 2010a).

Another important developmental process involving large-scale chromatin changes is the light-regulated early development of *Arabidopsis* seedlings (Bourbousse et al. 2015). During the first three days of seedling development, cotyledon cells in both light-grown and dark-grown seedlings exhibit nuclear size expansion and formation of two to three chromocenters (Bourbousse et al. 2015). However, five days post seed imbibition, the nucleus from light-grown seedlings are much larger in size than the dark-grown ones (Bourbousse et al. 2015). Importantly, light-grown seedlings have a significantly greater number of chromocenters compared to dark-grown ones (Bourbousse et al. 2015). Further analysis revealed that blue light has the strongest impact on heterochromatin condensation during seedling development, while red and far-red light have minimal impact on chromatin condensation (Bourbousse et al. 2015). Importantly, the *cry1cry2* double mutant did not show blue light-induced heterochromatin condensation, suggesting that CRYs play a major role in light-induced heterochromatin condensation during early seedling development (Bourbousse et al. 2015).

These studies collectively emphasize the critical role of CRYs in the organization of higher-order chromatin structure. However, the underlying mechanism of how CRYs regulate this type of large-scale chromatin condensation and decondensation remain poorly understood (Bourbousse et al. 2015). Therefore, further investigations are imperative to elucidate the mechanism by which CRYs regulate higher-order chromatin structure.

1.2.2 Associating plant CRYs with the chromatin

Early in 2000, it was discovered that the GFP-CRY2 fusion protein in *Arabidopsis* accumulates on anaphase chromosomes in dividing root cells (Cutler et al. 2000), suggesting an association of CRY2 proteins with chromatin. Moreover, it is known that plant CRYs can interact with bHLH transcription factors to associate with the chromatin (Ponnu and Hoecker 2022). Notably, the first identified blue light-dependent interactor of CRY2 is a bHLH transcription factor (TF) named CIB1 (CRY-interacting basic-helix-loop-helix) (Liu et al. 2008a). In addition to CIB1, CRYs are known to physically interact with another group of bHLH TFs, namely PIF4 and PIF5, to regulate plant growth under limiting blue

light conditions and under high temperature (Pedmale et al. 2016; Ma et al. 2016). Therefore, plant CRYs are associated with the chromatin through the interaction with transcription factors to finely modulate plant growth and development.

CRYs have also been found to interact with chromatin remodeling proteins, including the SWI2/SNF2-RELATED 1 (SWR1) complex, to associate with chromatin and modulate gene expression through histone H2A.Z deposition (Mao et al. 2021). A yeast-two-hybrid screen using CRY1 as bait identified SWR1 COMPLEX SUBUNIT 6 (SWC6), a subunit of the SWR1 complex (Mao et al. 2021). Further biochemical assays demonstrated that CRY2 also interacts with SWC6, and both CRY1 and CRY2 interact with another subunit of the SWR1 complex, ACTIN-RELATED PROTEIN 6 (ARP6) (Mao et al. 2021). Notably, the interaction between CRYs and the SWR1 complex appears to enhance the interaction between SWC6 and ARP6, thereby promoting the function of the SWR1 complex (Mao et al. 2021). The SWR1 complex also interacts with HY5 and is recruited to HY5 target genes (Mao et al. 2021). Moreover, CRYs indirectly promote the recruitment of the SWR1 complex to genomic loci through the stabilization of HY5 proteins (Mao et al. 2021). This study underscores the association of CRYs with chromatin through their interaction with the SWR1 chromatin remodeling complex, elucidating the role of CRYs in regulating histone H2A.Z deposition and gene expression (Mao et al. 2021).

1.3 DNA damage response in plants and animals

DNA serves as the genetic material in most cellular organisms. The integrity of DNA is crucial for accurate transmission of genetic information from one generation to the next (Chatterjee and Walker 2017). However, DNA is constantly exposed to both internal and external mutagenic factors which cause DNA damage (Chatterjee and Walker 2017). Endogenously, DNA damage can arise from spontaneous chemical reactions occurring on DNA bases, such as hydrolysis, oxidation, and alkylation, leading to DNA mismatches and subsequent point mutations during DNA replication (Huang and Zhou

2021). Externally, various environmental factors can induce damages in DNA and cause single-strand breaks (SSBs) and double-strand breaks (DSBs) (Huang and Zhou 2021). High-energy radiation can directly damage chromatin and result in DNA DSBs (Mavragani et al. 2019). UV radiation induces CPDs and 6-4PPs, which distort the DNA double helix, impairing transcription and DNA replication processes (Rastogi et al. 2010). Consequently, these diverse forms of DNA damage necessitate efficient repair through distinct DNA damage repair mechanisms to preserve the integrity of the genetic material (Chatterjee and Walker 2017).

1.3.1 DNA damage response in animals and plants

Organisms have also developed a comprehensive signaling and response pathway known as the DDR to mitigate the negative effects of DNA damage (Jackson and Bartek 2009). The DDR plays a vital role in regulating the transcription of thousands of genes upon genotoxic stress (Workman et al. 2006). Moreover, DDR induces cellular responses such as cell cycle arrest or checkpoint activation, which provide cells with sufficient time to efficiently repair the DNA damage before progressing to the next stage of the cell cycle (Zhou and Elledge 2000). Additionally, the DDR triggers programmed cell death or apoptosis to eliminate cells with irreparable DNA damage (Wang 2001). This integrated DDR ensures the preservation of genomic integrity and promotes the survival of healthy cells (Jackson and Bartek 2009).

The DDR in animal cells is orchestrated by key regulators, namely the checkpoint kinases ATAXIA TELANGIECTASIA MUTATED (ATM) and ATR, along with their respective substrates CHECKPOINT KINASE 2 (CHK2) and CHK1 (Figure 1.3A) (Blackford and Jackson 2017). ATM is mainly activated in response to DNA DSBs, while ATR is activated by ssDNA (Marechal and Zou 2013). Upon activation, ATM and ATR kinases phosphorylate and activate CHK2 and CHK1 kinases, respectively (Figure 1.3A) (Smith et al., 2010). Subsequently, CHK1 and CHK2 phosphorylate downstream factors, initiating a signaling cascade that ultimately leads to the transcriptional activation

of DNA repair genes, cell cycle checkpoints, and apoptosis or senescence (Figure 1.3A) (Smith et al., 2010).

The ATM kinase, a large protein of 370 kilodalton (kDa), is recruited to DNA DSBs by the MEIOTIC RECOMBINATION 11 (MRE11)-RAD50-NIJMEGEN BREAKAGE SYNDROME 1 (NBS1) complex (MRN complex) (Uziel 2003). Initially, ATM exists in an inactive homodimer state upon recruitment to the DSB sites (Lee and Paull 2005). The MRN complex stimulates ATM activity by facilitating ATM autophosphorylation at serine at position 1981 (Ser1981), leading to the conversion of ATM into active monomers (Lee and Paull 2005). Once activated, ATM proteins remain bound to the DNA damage sites for several hours and phosphorylate numerous substrates, establishing a signaling hub on the chromatin at the damage site (Blackford and Jackson 2017). Proteomic studies have identified hundreds of ATM substrates, many of which are kinases, indicating the existence of a multi-layered phosphorylation cascade of ATM-mediated responses in the cell (Mu et al. 2007).

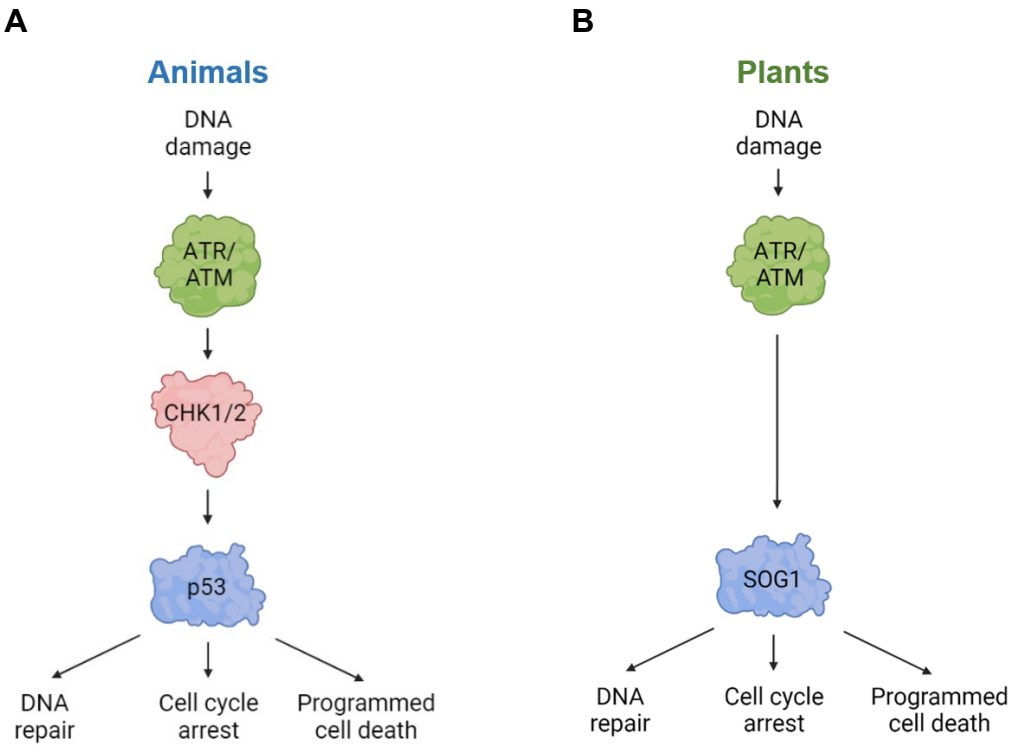

Figure 1.3 DNA damage response is partially conserved in animals and plants.
(A) DNA damage response pathway in animals. DNA damage is sensed by ATR or ATM kinases (Blackford and Jackson 2017), which activate CHK1 or CHK2 kinases (Smith et al., 2010). CHK1/2 kinases activate p53 transcription factor (Lavin and Gueven 2006), which in turn activate a transcriptional program including genes involved in DNA repair, cell cycle arrest and programmed cell death (Lane 1992). (B) DNA damage response pathway in plants. DNA damage is sensed by ATR or ATM kinases (Nisa et al. 2019), while activate SOG1 transcription factor (Yoshiyama 2015). SOG1 in turn activates a transcriptional program including genes involved in DNA repair, cell cycle arrest and programmed cell death (Bourbousse et al. 2018).

One of the ATM-mediated signaling pathway is the ATM-CHK2-p53 cascade (Figure 1.3A) (Lavin and Gueven 2006). Both ATM and CHK2 kinases have the capability to phosphorylate the tumor suppressor protein p53, leading to p53 stabilization and translocation to the nucleus (Lavin and Gueven 2006). The p53 transcription factor plays a crucial role in regulating the transcription of thousands of genes during DDR (Figure 1.3A) (Kenzelmann Broz et al. 2013). Mutations in p53 are frequently observed in various types of human cancers, earning p53 the name "Guardian of the Genome" (Lane 1992). The genes induced by p53 are involved in multiple pathways including DNA damage repair, cell cycle arrest, apoptosis and senescence (Lane 1992). One of the genes induced by p53 is p21 (Lavin and Gueven 2006). p21 serves as a CYCLIN-DEPENDENT KINASE (CDK) inhibitor, preventing the phosphorylation of RETINOBLASTOMA PROTEIN (RB) by CDK (Engeland 2022). The resulted hypophosphorylated form of RB in turn inhibits the cell cycle-promoting E2F transcription factors, resulting in the inhibition of several cell cycle genes and preventing the G1/S transition (Engeland 2022). Consequently, both p53 and p21 act as tumor suppressors to inhibit cell cycle progression (Engeland 2022).

Another significant function of ATM in DNA damage response is phosphorylating histone H2AX (Burma et al. 2001). ATM phosphorylates H2AX at serine 139, leading to the formation of γH2AX (Burma et al. 2001) . γH2AX recruits the MEDIATOR OF DNA DAMAGE CHECKPOINT 1 (MDC1) protein to DNA damage sites (Stucki et al. 2005). γH2AX and MDC1 form a complex and establish a DNA damage signaling pathway near the DNA damage sites that involves a series of phosphorylation and ubiquitination (Lou et al. 2006) events to recruit other DNA repair proteins (Mattiroli and Penengo 2021).

Unlike ATM, which cells can survive without, the loss of ATR is detrimental to proliferating cells and leads to embryonic lethality (Brown and Baltimore 2000). Consequently, the function of ATR is typically studied by downregulating *ATR* gene expression rather than knocking out this gene (Saldivar et al. 2017). As previously mentioned, ATR is primarily recruited to ssDNA, and this recruitment is dependent on the partner protein of ATR, namely ATR INTERACTING PROTEIN

(ATRIP) (Ball et al. 2005). However, binding to ATRIP and ssDNA is insufficient for complete activation of ATR (Haahr et al. 2016; Mordes et al. 2008). Instead, ATR requires activating proteins such as DNA TOPOISOMERASE II BINDING PROTEIN 1 (TopBP1) and EWING'S TUMOR-ASSOCIATED ANTIGEN 1 (ETAA1) to stimulate its kinase activity (Haahr et al. 2016; Mordes et al. 2008). Once activated, ATR phosphorylates a wide range of substrates, some of which overlap with ATM, including H2AX and p53 (Saldivar et al. 2017). One crucial substrate of ATR is CHK1 (Zhang and Hunter 2014). Activated CHK1 phosphorylates CELL DIVISION CYCLE 25A (CDC25A), which leads to the degradation of CDC25A (Zhao et al. 2002). CDC25A is a phosphatase responsible for removing inhibitory phosphorylation marks from CDKs (Shen and Huang 2012). Therefore, inactivation of CDC25A by the ATR-CHK1 pathway inhibits CDKs and slows down cell cycle progression, allowing cells more time to repair DNA damage (Zhao et al. 2002).

DDR in plants are similar to animals, which encompasses DNA damage repair, cell cycle arrest, and programmed cell death pathways (Nisa et al. 2019). Like animals, plants also have the conserved ATM and ATR kinases (Figure 1.3B), which are mainly activated by DSBs and ssDNA, respectively (Nisa et al. 2019). However, there are some important differences between plant and animal DDR. Unlike animals, plant cells lack homologs of CHK1, CHK2, and p53 (Manova and Gruszka 2015). Instead, plants have a functionally equivalent substitute for p53, the SUPPRESSOR OF GAMMA RADIATION 1 (SOG1) transcription factor, which is essential for the DDR-induced checkpoint response (Figure 1.3B) (Yoshiyama 2015). Plant ATM and ATR kinases directly phosphorylate SOG1, leading to the activation of SOG1 (Figure 1.3B) (Yoshiyama 2015). SOG1 in turn regulates the transcriptional response to genotoxic stress, as revealed by transcriptomic studies of the *sog1* mutant, which lost the majority of gene induction upon genotoxic stress (Bourbousse et al. 2018). Loss of function in the plant *SOG1* gene results in increased resistance to DSB-inducing chemicals because of the inability to induce cell cycle arrest upon DNA damage (Yoshiyama et al. 2009). At the same time, unrestricted cell cycle progression in the *sog1* mutant leads to a higher rate of spontaneous mutation in

leaf cells (Yoshiyama et al. 2009), suggesting the pivotal role for SOG1 in plant DDR to protect genome integrity.

1.3.2 Types of DNA repair mechanisms

Several DNA repair mechanisms have been evolved to safeguard the integrity of DNA (Chatterjee and Walker 2017). These mechanisms include direct reversal repair, base excision repair (BER), nucleotide excision repair (NER), mismatch repair (MMR), the Fanconi anemia pathway, homologous recombination (HR) repair and non-homologous end joining (NHEJ) repair of DNA damage (Jeggo et al. 2016).

Direct reversal repair primarily targets base damages in DNA (Yi and He 2013). Specific types of DNA damage can be directly reversed without involving DNA excision or synthesis (Yi and He 2013). Examples of direct reversal include the repair of pyrimidine dimers by photolyases (Weber 2005), repair of O-alkylated DNA bases by alkyltransferases and dioxygenases (Soll et al. 2017), and repair of N-alkylated DNA bases by alpha-ketoglutarate-dependent hydroxylase (AlkB) family dioxygenases (Fedeles et al. 2015).

BER is responsible for correcting various forms of DNA base damages, including oxidation, alkylation, and deamination (Krokan and Bjoras 2013). Damaged DNA bases typically do not cause significant distortion to the DNA double helix and are primarily repaired during the G1 phase of the cell cycle through BER (Krokan and Bjoras 2013). In BER, DNA glycosylases recognize and remove the damaged bases, followed by the removal of 1 to 10 bases by apurinic/apyrimidinic (AP) endonuclease (Wallace 2014). Subsequently, DNA polymerases and ligases replace the excised bases with correct DNA sequences (Krokan and Bjoras 2013).

In contrast to BER, NER is primarily involved in repairing bulky DNA base lesions that cause distortion of the DNA double helix, such as pyrimidine dimers formed between two adjacent pyrimidines on the same DNA strand (Marteijn et al. 2014). NER encompasses two major sub-pathways: global genome NER (GG-NER) and transcription-coupled NER (TC-NER), which differ in how DNA

damage was recognized (Scharer 2013). GG-NER involves sensor proteins that scan the entire genome to identify DNA damage, while TC-NER recognizes DNA damage indirectly through the DNA damage-caused stalling of RNA polymerase II during transcription (Spivak 2015). Despite different recognition mechanisms, GG-NER and TC-NER converge on the same factors to excise the damaged DNA and synthesize a new DNA strand to restore the intact DNA double strand (Marteijn et al. 2014). For recognition of DNA damage, GG-NER relies on the XERODERMA PIGMENTOSUM COMPLEMENTATION GROUP C (XPC)/ RAD23 HOMOLOG B (RAD23B)/ CENTRIN 2 (CETN2) protein complex, with assistance from the UV-DDB complex, which is specialized in identifying UV-induced pyrimidine dimers (Petruseva et al. 2014). In TC-NER, the COCKAYNE SYNDROME TYPE A (CSA)-COCKAYNE SYNDROME TYPE B (CSB) complex recognizes the stalled RNA polymerase II (van der Weegen et al. 2020). Once DNA damage is recognized, both GG-NER and TC-NER recruit the TRANSCRIPTION FACTOR II H (TFIIH) complex (Kokic et al. 2019). The helicase activity of TFIIH helps expose the DNA damage sites to proteins involved in precise excision at the 5' and 3' ends of the damage site, including endonucleases XERODERMA PIGMENTOSUM COMPLEMENTATION GROUP F (XPF), EXCISION REPAIR CROSS COMPLEMENTATION GROUP 1 (ERCC1) and XERODERMA PIGMENTOSUM COMPLEMENTATION GROUP G (XPG) (Graf et al. 2011). After the damaged DNA is excised, DNA polymerases and ligases synthesize and ligate new DNA strands to complete NER (Chatterjee and Walker 2017; Huang and Zhou 2021).

MMR primarily occurs when there are mismatches in base pairs or small deletions/insertions in the double-stranded DNA (Jiricny 2006). Base pair mismatches often arise from errors made by DNA polymerase during DNA replication (Li 2008). Therefore, the primary function of MMR is to ensure the accuracy of DNA replication and correct errors made by DNA polymerases (Iyer et al. 2006). MMR has been reported to enhance DNA replication fidelity by 100-fold (Lujan et al. 2014). When mismatch repair is disrupted, it can lead to genome-wide instability due to an increased rate of errors during DNA replication (Iyer et al. 2006). The proteins involved in MMR are highly conserved between *Escherichia coli* (*E. coli*) and humans (Hofstatter and Lahr 2021). In *E. coli* cells, the initial recognition

and incision of DNA mismatches are carried out by the MUTATOR S (MutS), MUTATOR L (MutL), and MUTATOR H (MutH) proteins (Modrich 2016). MutS recognizes the base pair mismatch (Grilley et al. 1989), MutL interacts with MutS (Grilley et al. 1989), and recruits and stimulates MutH to make an incision on the unmethylated newly synthesized strand near the site of the mismatch (Ban 1998). Subsequently, exonucleases remove the newly synthesized mismatched strand, and DNA polymerases and DNA ligases complete the MMR process (Li 2008).

The repair of interstrand crosslinks is carried out by the Fanconi anemia pathway, which is associated with Fanconi anemia disease (Walden and Deans 2014). Defects in any of the 16 FANCONI ANEMIA COMPLEMENTATION GROUP (FANC) genes (FANCA-FANCQ) in the Fanconi anemia pathway can cause the Fanconi anemia disease (Bogliolo and Surrallés 2015). In patients with Fanconi anemia disease, endogenous aldehydes in cells crosslink DNA bases on complementary DNA strands, obstructing transcription and DNA replication (Garaycoechea et al. 2012). In these patients, hematopoietic stem cells are particularly vulnerable to interstrand crosslinks, resulting in replication stress, bone marrow failure, and increased susceptibility to leukemia (Garaycoechea et al. 2012). The repair process for interstrand crosslinks through the Fanconi anemia pathway involves several protein complexes (Walden and Deans 2014). First, the anchor complex, consisting of FANCM, FANCONI ANEMIA CORE COMPLEX ASSOCIATED PROTEIN 24 (FAAP24), MPH1-ASSOCIATED HISTONE-FOLD PROTEIN 1 and 2 (MHF1 and 2), recognizes the interstrand crosslinks (Niedernhofer 2007). Subsequently, the anchor complex recruits the core complex, which includes FANCA, FANCB, FANCC, FANCE, FANCF, FANCG, FANCL, FAAP20, and FAAP100 (Huang et al. 2014). The core complex in turn monoubiquitinates the FANCI/FANCD2 (ID2) heterodimer (Boisvert and Howlett 2014). Monoubiquitinated ID2 heterodimer then recruits downstream factors, such as nucleases and repair factors, to complete the DNA repair process (Boisvert and Howlett 2014).

All of the aforementioned repair pathways primarily address damage to DNA bases or nucleotides within intact DNA strands. However, DNA damage can also occur in the form of DNA strand breaks, including SSBs and the more severe DSBs (Chapman et al. 2012; Abbotts and Wilson

2017). SSBs are typically repaired by common factors involved in BER, NER, or MMR (Abbotts and Wilson 2017). On the other hand, DSBs are repaired by three specialized pathways: HR, NHEJ, and alternative end-joining (alt-EJ) pathways (Scully et al. 2019). HR utilizes homology from a sister chromatid to accurately repair the DSB, resulting in error-free repair, but this pathway is restricted to the S and G2 phases of the cell cycle when sister chromatids are present (Wright et al. 2018). In contrast, NHEJ repairs DSBs throughout the cell cycle, without extensive sequence homology, and is error-prone, often leading to mutations, deletions, and insertions (Chang et al. 2017). Although NHEJ is prone to errors, it is crucial for mitigating large-scale chromatin translocations (Chang et al. 2017). The CLUSTERED REGULARLY INTERSPACED SHORT PALINDROMIC REPEATS (CRISPR)-CRISPR-ASSOCIATED PROTEIN 9 (Cas9) system utilizes the NHEJ pathway to introduce mutations, deletions, or insertions at DSB sites created by the Cas9 enzyme (Cong et al. 2013). The alt-EJ pathway is distinct from classical NHEJ but also repairs DSBs without extensive sequence homology and is error-prone (Sallmyr and Tomkinson 2018).

The NHEJ pathway initiates with the formation of a ring-like structure by the Ku70/Ku80 heterodimer, which rapidly binds to the two ends of the DNA DSBs in the time scale of a few seconds (Zahid et al. 2021). The Ku70/80 dimer then recruits other factors, including the DNA-DEPENDENT PROTEIN KINASE CATALYTIC SUBUNIT (DNA-PKcs) (Yue et al. 2020), the MRN complex (Quennet et al. 2011), the Artemis DNA processing protein (Chang and Lieber 2016), and the X-RAY REPAIR CROSS COMPLEMENTING 4 (XRCC4)-DNA LIGASE 4 (LIG4) DNA ligation complex to repair DNA (Grawunder et al. 1997). Together, the DNA-PKcs and the MRN complex work in conjunction with the Ku70/80 dimers to bridge the two broken DNA ends (Zhao et al. 2020). Subsequently, Artemis exhibits nuclease activity to process the DNA ends (Chang and Lieber 2016), and XRCC4 stabilizes LIG4 for efficient ligation of the broken DNA ends (Grawunder et al. 1997). Since the entire NHEJ process does not rely on extensive sequence homology, it can introduce mutations during the DNA end processing steps (Zhao et al. 2020).

The alt-EJ pathway is an end-joining repair mechanism that operates independently of classical NHEJ factors, such as Ku70/80 (Mansour et al. 2010). The alt-EJ pathway initiates with DNA end resection carried out by the MRN complex (Taylor et al. 2010). POLY (ADP-RIBOSE) POLYMERASE 1 (PARP1) may also play a role in alt-EJ repair by facilitating the recruitment of the MRN complex and bridging the two DNA ends (Wang et al. 2006). DNA polymerase theta has been shown to be important for filling DNA gaps during alt-EJ repair (Chan et al. 2010). Finally, DNA ligase III, in complex with X-RAY REPAIR CROSS COMPLEMENTING 1 (XRCC1), is crucial for ligating the two DNA ends and completing the DNA DSB repair process during alt-EJ (Sallmyr and Tomkinson 2018).

HR is a complex repair pathway that involves multiple steps (Wright et al. 2018). It begins with DNA end processing, resulting in the formation of long 3' DNA overhangs (Wright et al. 2018). Subsequently, a nucleoprotein filament containing 3' single-stranded DNA (ssDNA) and the recombinase RAD51 forms, facilitating the annealing of the 3' overhangs to the homologous DNA on the sister chromatid (Wright et al. 2018). Complementary DNA synthesis then occurs, utilizing the homologous DNA as a template to complete the HR repair process (Wright et al. 2018).

HR involves two stages of DNA end resection (Liu and Kong 2021). The initial short-range resection is carried out by the MRN complex's 3'-5' exonuclease activity, which is stimulated by C-TERMINAL BINDING PROTEIN (CtIP) (Sartori et al. 2007). This is followed by long-range end resection, performed by EXONUCLEASE 1 (EXO1) and DNA REPLICATION HELICASE/NUCLEASE 2 (DNA2) (Karanja et al. 2012). The resulting long 3' ssDNA tail is immediately bound by the abundant REPLICATION PROTEIN A (RPA) complex, consisting of RPA1, RPA2, and RPA3 (Li and Heyer 2008). Subsequently, RAD51 displaces the RPA complex to form an ssDNA-RAD51 nucleoprotein filament, which plays a crucial role in HR by facilitating homology search and invasion of complementary DNA (Sung and Robberson 1995). Following the homology search, in cases where both ends of the DNA DSB invade the same DNA duplex, a double holiday junction is formed, aiding the repair process (Li and Heyer 2008). However, if only one DNA end

invades, DNA synthesis occurs solely on the invaded end. Finally, DNA polymerase delta, along with other DNA polymerases, synthesizes the nascent DNA to complete the repair of the DNA DSB (Li and Heyer 2008).

Components of various BRCA1 complexes in animals	
BRCA1-C	BRCA1, BARD1, MRE11, RAD50, NBS1 and CtIP
BRCA1-P	BRCA1, BARD1, BRCA2, PALB2 and RAD51
BRCA1-A	BRCA1, BARD1, Abraxas, RAP80, BRCC36, BRCC45, and MERIT40

Table 1.1 List of proteins constituting the three different BRCA1 complexes in animals.

BREAST CANCER GENE 1 (BRCA1) is a protein associated with breast cancer that plays a crucial role in multiple steps of HR by forming distinct BRCA1 complexes (Chen et al. 2018). One of the BRCA1 complexes, BRCA1-C, which consists BRCA1, BRCA1 ASSOCIATED RING DOMAIN 1 (BARD1), MRN complex and CtIP, participates in DNA end resection (Table 1.1) (Greenberg et al. 2006). Another BRCA1 complex, BRCA1-P, includes BRCA1, BARD1, BRCA2, PARTNER AND LOCALIZER OF BRCA2 (PALB2), and RAD51 (Table 1.1) (Savage and Harkin 2015). The BRCA1-P complex assists in the replacement of the RPA complex by RAD51 and facilitates the homology search step performed by the RAD51 protein (Savage and Harkin 2015).

In conclusion, the complex interplay between various DNA repair mechanisms serves to protect the integrity of genetic material from both endogenous and exogenous genotoxic agents, ensuring the accurate inheritance of genetic information (Gartner and Engebrecht 2022). Collectively, these repair mechanisms play a critical role in maintaining genome stability and preserving the continuity of life (Gartner and Engebrecht 2022).

1.4 Ubiquitination and DUBs in plant and animal DDR

1.4.1 Ubiquitin, E3 ligase and DUBs

Ubiquitin is a small protein consisting of 76 amino acids with a molecular weight of 8.6 kDa (Swatek and Komander 2016). The process of adding ubiquitin to a protein is known as ubiquitination, which can involve the addition of a single ubiquitin molecule (mono-ubiquitination) or the formation of a chain of multiple ubiquitin molecules (Akutsu et al. 2016). The most studied function of ubiquitination is to tag substrate proteins for degradation by proteasomes (Wilkinson 2000). However, ubiquitination can also impact the cellular localization or activity of the substrate protein (Xu and Jaffrey 2011). Ubiquitination typically involves a series of reactions catalyzed by E1, E2, and E3 enzymes (Scheffner et al. 1995). The E1 enzyme activates a ubiquitin molecule, which is then

conjugated to the E2 enzyme. Finally, the E3 ligase transfers the activated ubiquitin molecule from the E2 enzyme to the substrate protein (Scheffner et al. 1995).

In the human genome, there are two E1 enzymes, approximately 50 E2 enzymes, and over 1000 E3 enzymes (Zhao et al. 2012). In *Arabidopsis thaliana*, there are two E1 enzymes, 37 E2 enzymes, and more than 1300 E3 enzymes (Ramadan et al. 2015). The abundance of E3 enzymes suggests that they play a crucial role in determining the substrate specificity for ubiquitination (Cowan and Ciulli 2022). Consequently, many E3 ligases are regulated by external and internal signals to modulate their substrate proteins and finely tune biological processes (Yang et al. 2021). For example, *Arabidopsis* TRANSPORT INHIBITOR RESPONSE 1 (TIR1), an F-box protein that is part of the SKP, CULLIN, F-BOX CONTAINING $(SCF)^{TIR1}$ E3 ligase complex, acts as the receptor for the plant hormone auxin (Dharmasiri et al. 2005). When auxin binds to TIR1, it strengthens the interaction between TIR1 and its substrates, the AUXIN/INDOLE-3-ACETIC ACID (AUX/IAA) proteins, leading to ubiquitination and subsequent degradation of the AUX/IAAs by the proteasome, leading to the activation of the auxin signaling pathway (Dharmasiri et al. 2005). Similarly, *Arabidopsis* CORONATINE INSENSITIVE 1 (COI1), the receptor for another plant hormone called jasmonic acid, is also an F-box protein that is part of the SCF^{COI1} E3 ligase complex (Yan et al. 2009). Binding of jasmonic acid to COI1 enables COI1 to ubiquitinate the JASMONATE-ZIM-DOMAIN PROTEIN (JAZ) proteins, resulting in their degradation, thereby relieving the transcriptional repression of downstream genes by JAZ proteins and activating the jasmonic acid signaling pathway (Yan et al. 2009).

Mono-ubiquitination occurs when a single ubiquitin molecule attaches its C-terminal tail to a lysine residue on the substrate protein (Hicke 2001). In contrast, polyubiquitination involves the attachment of multiple ubiquitin proteins to form a ubiquitin chain on the substrate's lysine residue (Li and Ye 2008). Ubiquitin chains can be linked through different amino acid residues (Akutsu et al. 2016). There are seven lysine residues (K6, 11, 27, 29, 33, 48, and 63) and an N-terminal methionine residue (M1) on ubiquitin proteins that can be linked to the C-terminal amino acid of another ubiquitin molecule (Rittinger and Ikeda 2017), resulting in K6, K11, K27, K29, K33, K48, K63 and M1-linked ubiquitin

chains. The positions at which ubiquitins are attached within the chain can be the same or different, resulting in homogeneous or heterogeneous ubiquitin chains, respectively (Ohtake and Tsuchiya 2016). The attachment of a single ubiquitin or multiple ubiquitins to another ubiquitin within the chain leads to unbranched or branched ubiquitin chains, respectively (French et al. 2021).

The K48-linked ubiquitin chain is the most extensively characterized type of ubiquitin chains (Mallette and Richard 2012). Proteins tagged with a K48 polyubiquitin chain are primarily targeted for degradation by the proteasome (Mallette and Richard 2012). Another ubiquitin chain that has been extensively studied is the K63-linked chain, which mainly regulate the substrate proteins in non-proteolytic manners (Erpapazoglou et al. 2014). However, it has been reported that K48 ubiquitin chains can also serve as non-proteolytic signals (Flick et al. 2004), while K63-linked chains can also mark a protein substrate for degradation (Ohtake et al. 2018). These K48 and K63-linked chains are considered canonical ubiquitin chains, in contrast to the non-canonical chains linked through M1, K6, K11, K27, K29, and K33 (Tracz and Bialek 2021). Recent studies have started to elucidate the functions of non-canonical ubiquitin chains in processes such as DDR and immunity (Tracz and Bialek 2021).

The ubiquitination of substrate proteins is reversible (Komander et al. 2009). E3 ligases catalyze the addition of ubiquitin to substrate proteins, while DUBs remove ubiquitins from substrate proteins, often leading to substrate stabilization (Lange et al. 2022). Some DUBs are associated with the proteasome and remove ubiquitin chains to recycle ubiquitin molecules (Shin et al. 2020). However, most DUBs act independently of the proteasome and catalyze the removal of ubiquitin from specific substrate proteins (Mofers et al. 2017). In the *Arabidopsis* genome, there are approximately 64 DUBs (Yan et al. 2000), which is much less than the over 1300 E3 ligases (Ramadan et al. 2015). This indicates that DUBs are less substrate-specific than E3 ligases, with each DUB often acting on multiple substrates (Mevissen and Komander 2017). For instance, the plant UBP12 and UBP13 DUBs have many substrates, including proteins involved in plant immunity, leaf senescence, cell size, root meristem maintenance, and JA signaling pathway (Zhou et al. 2021). Thus, studying both E3 ligases

and DUBs and their substrate specificity provides a more comprehensive understanding of the post-translational regulation of gene expression (Shi and Grossman 2010).

DUBs are categorized into two main groups, (Estavoyer et al. 2022), cysteine-dependent proteases, with a catalytic triad consisting of cysteine and histidine residues (Estavoyer et al. 2022) and Jab1/Mov34/MPN+ proteases (JAMM) DUBs, which uses a zinc atom coordinated by surrounding amino acids as the catalytic center (Shrestha et al. 2014). Furthermore, based on the protein domain difference, cysteine-dependent proteases DUBs can be categorized into six groups, including UBIQUITIN-SPECIFIC PROTEASEs (USPs), UBIQUITIN C-TERMINAL HYDROLASEs (UCHs), OVARIAN TUMOR PROTEASEs (OTUs), MACHADO-JOSEPHIN DOMAIN PROTEASEs (MJDs), ZINC-FINGER-CONTAINING UBIQUITIN PEPTIDASE (ZUP), and MOTIF INTERACTING WITH UBIQUITIN-CONTAINING NOVEL DUB FAMILY (MINDY) (Estavoyer et al. 2022). These different DUBs participate in various cellular processes, ensuring precise regulation of biological networks at the post-translational level (Estavoyer et al. 2022).

1.4.2 Role of ubiquitination in the DNA damage response

Ubiquitination plays a crucial role in regulating various cellular processes, particularly in DNA damage repair pathways and the DDR (Ghosh and Saha 2012). Ubiquitination serves as a mechanism for the regulation of proteins involved in DDR and DNA repair through ubiquitination-induced degradation (Brinkmann et al. 2015). Additionally, ubiquitination of histone tails serves as a significant signal near DNA damage sites to recruit DNA repair proteins (Uckelmann and Sixma 2017).

The ubiquitination signaling near double-strand DNA breaks is initiated by γH2AX(Huen et al. 2007). γH2AX recruits the MDC1 protein to the DNA damage sites (Stucki et al. 2005; Kolas et al. 2007). MDC1 then facilitates the recruitment of the E3 ligase RING FINGER PROTEIN 8 (RNF8) (Kolas et al. 2007). RNF8, in turn, catalyzes the ubiquitination of histone H1 (Mailand et al. 2007; Kolas et al. 2007; Huen et al. 2007; Thorslund et al. 2015). Ubiquitinated H1 acts as a platform for the recruitment of another E3 ligase, RING FINGER PROTEIN 168 (RNF168), through the ubiquitin

binding motif of RNF168 (Thorslund et al. 2015). RNF168 subsequently ubiquitinates histone H2A and H2AX at positions K13 or K15 (Mattiroli et al. 2012).

Histone ubiquitination, catalyzed by RNF8 and RNF168, is a critical signal that facilitates the recruitment of essential DNA repair proteins to the site of DNA damage (Sekiguchi and Matsushita 2022). Among these DNA repair proteins, P53 BINDING PROTEIN 1 (53BP1), the BRCA1-A complex (consisting BRCA1, BARD1, Abraxas, RECEPTOR-ASSOCIATED PROTEIN 80 (RAP80), BRCA1-BRCA2-CONTAINING COMPLEX 36 (BRCC36), BRCC45, and MEDIATOR OF RAP80 INTERACTIONS AND TARGETING 40 KDA (MERIT40)) (Table 1.1) and BRCA1-P complexes are of particular significance (Savage and Harkin 2015; Fradet-Turcotte et al. 2013). 53BP1 functions as a key regulator in the repair of DSBs, influencing the choice between NHEJ and HR pathways (Daley and Sung 2014). Specifically, during the G1 phase of the cell cycle, 53BP1 acts as a barrier, inhibiting DNA end resection and promoting the NHEJ pathway (Gupta et al. 2014). However, in the S or G2 phase, BRCA1 and CtIP counteract the inhibitory role of 53BP1 by promoting DNA resection, thereby facilitating the HR pathway as the preferred method for DSB repair (Escribano-Díaz et al. 2013). The ubiquitination of histones induced by RNF8 and RNF168 also recruits the BRCA1-A complex (Uckelmann and Sixma 2017). The RAP80 protein in the BRCA1-A complex possesses a tandem ubiquitin-interacting motif domain that binds to ubiquitin chains, thereby facilitating the recruitment of the BRCA1-A complex (Kim et al. 2007). The BRCA1-A complex in turn inhibits DNA end resection at DSB sites, promoting NHEJ, and inhibiting HR (Coleman and Greenberg 2011). Additionally, recent research has shown that RNF168-mediated H2A ubiquitination recruits the BRCA1-P complex (Krais et al. 2021). The BARD1 protein in the BRCA1-P complex contains a BRCT DOMAIN UBIQUITIN-DEPENDENT RECRUITMENT MOTIF (BUDR) domain that specifically recognizes H2A ubiquitination (Becker et al., 2021). As discussed earlier, the BRCA1-P complex is crucial for HR repair (Krais et al. 2021). Therefore, the ubiquitination of histones by RNF8 and RNF168 plays a vital role in recruiting a diverse range of DNA damage repair proteins, enabling an effective cellular response to DNA damage (Uckelmann and Sixma 2017).

1.4.3 Role of DUBs in DDR and DNA repair pathways

DUBs play a crucial role in regulating the histone ubiquitination signaling pathway triggered by DNA DSBs (Cao and Yan 2012). Several DUBs have been identified that counteract the E3 ligase activity of RNF8 or RNF168 on histone, thereby exerting important functions in DDR and repair (Le et al. 2019). For instance, BRCC36 and OTU DEUBIQUITINASE, UBIQUITIN ALDEHYDE BINDING 2 (OTUB2) function as antagonists of histone ubiquitination near DNA damage sites (Kato et al. 2014; Shao et al. 2009). BRCC36, a JAMM DUB, is recruited to DNA damage sites through RAP80, which binds to ubiquitinated histones, as both BRCC36 and RAP80 are part of the BRCA1-A complex (Shao et al. 2009). Depletion of BRCC36 restores ubiquitin foci near DNA damage sites in RNF8-depleted cells, suggesting that BRCC36 and RNF8 have opposing roles in ubiquitination-mediated DDR (Shao et al. 2009). Moreover, as a component of the BRCA1-A complex, BRCC36 collaborates with RAP80 to restrain DNA end resection and promote NHEJ rather than HR repair of DSBs (Harris and Khanna 2011). On the other hand, OTUB2 is known to antagonize the ubiquitination of histones by RNF8, resulting in decreased recruitment of RNF168 to DNA damage sites (Kato et al. 2014). Consistently, depletion of OTUB2 accelerates the recruitment of RNF168, RAP80, and 53BP1 to DNA damage loci during the early phase of DDR (Kato et al. 2014). Consequently, the increased recruitment of RAP80 and 53BP1 restricts DNA end resection, favoring NHEJ over HR repair of DSBs (Kato et al. 2014).

Apart from regulating histone ubiquitination, DUBs also directly deubiquitinate critical DNA repair proteins (Le et al. 2019). Following DNA damage, RNF168 undergoes ubiquitination and becomes targeted for protein degradation (Sy et al. 2013). However, the DUB UBIQUITIN SPECIFIC PROTEASE 34 (USP34) deubiquitinates and stabilizes RNF168 (Sy et al. 2013). Depletion of USP34 leads to the rapid degradation of RNF168 and diminished histone ubiquitination near the DSB site (Sy et al. 2013). Similarly, USP7 promotes DNA damage repair by deubiquitinating and stabilizing RNF168 (Zhu et al. 2015). Disrupting USP7 function results in reduced histone H2A ubiquitination and impaired localization of BRCA1 at the DSB site, which can be rescued by introducing RNF168

through ectopic expression (Zhu et al. 2015). While it remains unclear whether the roles of USP7 and USP34 in stabilizing RNF168 are redundant or regulated by distinct signals to fine-tune DNA damage repair, the post-translational regulation of RNF168 by DUBs serves as a compelling example of how DUBs exert control over critical factors in DNA damage repair (Le et al. 2019).

In addition to their involvement in DSB repair, DUBs also play a role in other DNA repair pathways, such as NER and direct DNA alkylation reversal (Le et al. 2019). USP7 is a multifunctional DUB that regulates various processes, including different DNA damage repair pathways (Valles et al. 2020). Besides its role in DSB repair, USP7 also governs both GG-NER and TC-NER pathways (He et al. 2014; Zhu et al. 2020). In GG-NER, XPC is crucial for recognizing bulky DNA lesions (Scharer 2013). USP7 has been identified as a DUB that stabilizes XPC, promoting efficient NER (He et al. 2014). Disruption of USP7 can lead to increased XPC ubiquitination and reduced DNA damage repair efficiency (He et al. 2014). In TC-NER, CSB is responsible for recognizing stalled RNA pol II at DNA damage sites and recruiting DNA repair proteins (Fousteri and Mullenders 2008). The protein stability of CSB is also regulated by USP7 (Zhu et al. 2020). Disruption of USP7 results in CSB destabilization and TC-NER deficiency (Zhu et al. 2020). Apart from regulating the NER, DUBs also modulate direct reversal of DNA alkylation, which is primarily mediated by ALKB HOMOLOG 2, ALPHA-KETOGLUTARATE DEPENDENT DIOXYGENASE (ALKBH2) and ALKBH3 (Duncan et al. 2002). A protein complex formed by three DUBs, OTU DEUBIQUITINASE 4 (OTUD4), USP7, and UBIQUITIN SPECIFIC PEPTIDASE 9 X-LINKED (USP9x), is known to stabilize ALKBH2 and ALKBH3 (Zhao et al. 2015). Interestingly, the deubiquitination of ALKBH2/3 only requires the catalytic activity of USP7 and USP9x, while OTUD4 primarily serves as a scaffolding protein within the OTUD4-USP7-USP9x complex (Zhao et al. 2015). Disruption of this OTUD4-USP7-USP9x complex leads to the destabilization of ALKBH2/3 and increased cellular sensitivity to DNA alkylating agents (Zhao et al. 2015). In summary, DUBs play crucial roles in various aspects of DDR and DNA repair, through modulating histone ubiquitination and the ubiquitination of DNA repair proteins (Kee and Huang 2016).

1.5 Chromatin remodeling

1.5.1 Types of chromatin remodelers and their main functions

Within each human cell, there are DNA strands that extend over 2 meters in length, yet these DNA strands are highly compacted within the nucleus, which has a diameter of less than 10 micrometers (Piovesan et al. 2019). This remarkable compaction of DNA is achieved through the utilization of chromatin's basic units known as nucleosomes, and the subsequent layering of nucleosomes to form a condensed chromatin fiber (Ozer et al. 2015). Nucleosomes consist of approximately 146 base pairs of DNA wrapped around a histone octamer, which comprises two copies each of histones H3, H4, H2A, and H2B (Cutter and Hayes 2015). Additionally, monomeric histone H1 molecules bind to the linker DNA between each nucleosome (Hergeth and Schneider 2015). In cellular contexts, nucleosomes act as a formidable barrier for most DNA-related processes, including DNA replication, DNA-dependent RNA transcription, and DNA damage repair (Millán-Zambrano et al. 2022). To grant access to the machinery responsible for these DNA-dependent processes, the presence of chromatin remodelers is crucial (Clapier et al. 2017). Chromatin remodelers are specialized enzymes that can relocate nucleosomes along the DNA, generating a locally accessible chromatin environment conducive to DNA-related processes (Reyes et al. 2021).

Chromatin remodelers are divided into four major subfamilies depending on their domain structures: IMITATION SWITCH (ISWI), CHROMODOMAIN-HELICASE-DNA BINDING (CHD), SWITCH/SUCROSE NON-FERMENTABLE (SWI/SNF), and INOSITOL REQUIRING 80 (INO80) (Tyagi et al. 2016). In addition to these four families of chromatin remodelers, there are also orphaned ADENOSINE TRIPHOSPHATASE (ATPase)-dependent chromatin remodelers that do not belong to any of the four major families (Wang et al. 2019). One example of orphaned chromatin remodeler is ALPHA THALASSEMIA/MENTAL RETARDATION SYNDROME X-LINKED (ATRX), which is involved in histone H3.3 deposition (De La Fuente et al. 2011). Chromatin remodelers possess DNA translocase activity and are homologous to the ADENOSINE TRIPHOSPHATE (ATP)-binding

helicases of the Asp-Glu-Ala-Asp/His (DEAD/H) family (Laurent et al. 1992). However, there is a distinction between chromatin remodelers and DNA helicases. DNA helicases can insert one of their protein domains between the DNA double strands to facilitate DNA replication by separating the strands (Abdelhaleem 2009). In contrast, chromatin remodelers translocate along the DNA without inserting their protein domains between the complementary DNA strands (Hargreaves and Crabtree 2011). All four families of chromatin remodelers contain an ATPase domain composed of two RECOMBINASE A (RecA)-like lobes separated by an insertion domain (Yan and Chen 2020). This ATPase domain of chromatin remodelers is responsible for ATP hydrolysis and drives the movement of remodelers along the DNA (Yan and Chen 2020).

The different subfamilies of chromatin remodelers are distinguished by their specific protein domains, their interaction partners, and their unique functions on the chromatin (Sahu et al. 2020). The SWI/SNF subfamily exhibits an N-terminal HELICASE-SANT-ASSOCIATED (HSA) domain that can bind to actin or actin-related proteins (Figure 1.4) (Euskirchen et al. 2012). At the C-terminal end, SWI/SNF proteins possess a bromodomain responsible for recognizing acetylated lysine residues on histone tails (Figure 1.4) (Tang et al. 2010). The ISWI chromatin remodelers possesses N-TERMINAL AUTOINHIBITORY REGION (AutoN) and NegC domains that play a crucial role in regulating the enzymatic activity of the remodeler by modulating the two RecA-like lobes (Figure 1.4) (Bartholomew 2014). Additionally, ISWI proteins feature C-terminal HAND, SWI3, ADA2, N-COR, AND TFIIB (SANT) and SANT-LIKE ISWI DOMAIN (SLIDE) domains (Figure 1.4), known to bind extranucleosomal DNA (Dang and Bartholomew 2007). The CHD family is distinguished by the presence of two tandem chromodomains capable of recognizing methylated lysine residues on histone tails (Figure 1.4) (Marfella and Imbalzano 2007). The C-terminal region of CHD contains a NegC domain (Figure 1.4), similar to the NegC domain of the ISWI subfamily, followed by a DNA-binding domain encompassing SANT and SLIDE domains (Figure 1.4) (Clapier and Cairns 2009). The INO80 subfamily distinguishes itself by having a longer insertion domain between the two RecA-like lobes compared to the other subfamilies (Figure 1.4) (Bao and Shen 2007). Additionally, the N-terminal

region of the INO80 subfamily contains HSA domain (Figure 1.4), similar to the SWI/SNF subfamily (Eustermann et al. 2018).

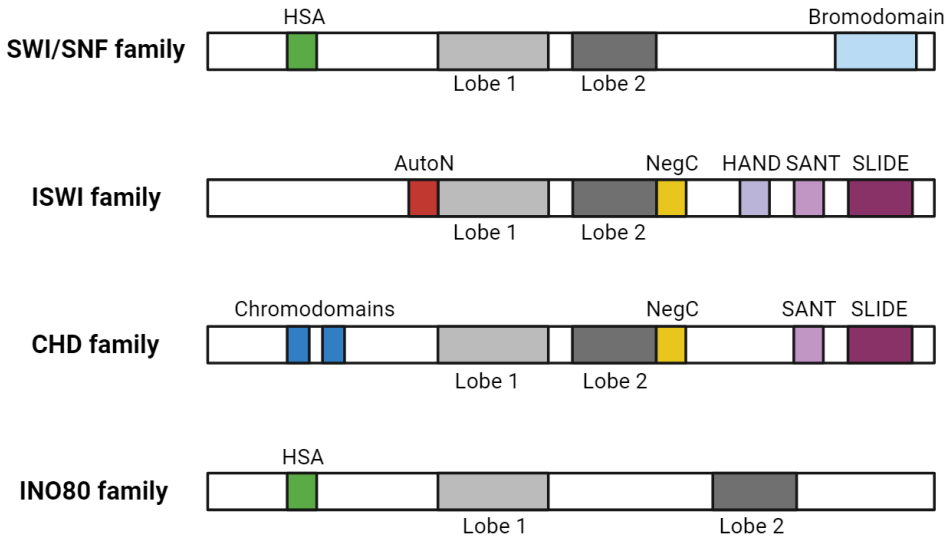

Figure 1.4 Protein domains of various chromatin remodeler families.
SWI/SNF family remodelers have an N-terminal HSA domain, two RecA-like lobes and a C-terminal bromodomain. ISWI family remodelers have an N-terminal AutoN domain, two RecA-like lobes, C-terminal NegC, HAND, SANT and SLIDE domains. CHD family remodelers have two tandem N-terminal chromodomains, two RecA-like lobes, C-terminal NegC, SANT and SLIDE domains. INO80 family remodelers have an N-terminal HSA domain and two RecA-like lobes sepepated by a long insertion.

Chromatin remodelers perform three main functions on chromatin: chromatin assembly and organization, chromatin access, and nucleosome editing (Clapier et al. 2017). The ISWI and CHD proteins primarily participate in chromatin assembly and organization (Clapier et al. 2017). ISWI and CHD play a role in assembling the pre-nucleosome complex, which involves incorporating newly synthesized DNA and the corresponding histones into nucleosomes (Clapier et al. 2017). Additionally, ISWI and CHD contribute to fine-tuning the spacing between nucleosomes, thereby contributing to the establishment of an evenly spaced nucleosome pattern in newly synthesized chromatin (Clapier et al. 2017). On the other hand, the SWI/SNF subfamily primarily functions in chromatin access by moving nucleosomes along DNA or displacing histone dimers or entire nucleosomes (Yudkovsky et al. 1999). SWI/SNF chromatin remodelers enable access to the DNA by chromatin-related proteins and are often associated with the creation of nucleosome-free regions and the activation of gene transcription (Centore et al. 2020). The INO80 subfamily, which includes the SWR1 complexes and the INO80 complexes, is mainly involved in nucleosome editing (Gerhold and Gasser 2014). INO80 complexes are responsible for substituting histone H2A.Z with H2A (Papamichos-Chronakis et al. 2011), while SWR1 complexes perform the reverse, replacing H2A with H2A.Z (Kobor et al. 2004). However, it is worth noting that there can be cross-over functions between the different subfamilies of chromatin remodelers. For example, INO80 subfamily may also participate in nucleosome spacing and chromatin access functions (Udugama et al. 2011).

Although the various subfamilies of chromatin remodelers differ in their domains and functions, they often share a common mechanism for driving DNA translocation (Yan and Chen 2020). Recent structural and biophysical evidence supports a "DNA wave" model to explain how chromatin remodelers move along DNA, particularly for the ISWI, CHD, and SWI/SNF subfamilies (Yan and Chen 2020). When the chromatin remodeler is bound to the nucleosome but not actively hydrolyzing ATP, it is in a “closed” state that creates a +1 bp DNA bulge at the remodeler's binding site (Yan and Chen 2020). Upon ATP binding and hydrolysis, this +1 bp DNA bulge is translocated along the DNA strand, creating a wave that propagates through the DNA (Yan and Chen 2020). This movement results

in the +1 bp movement of the remodeler and the nucleosome relative to the DNA at the end of the remodeling cycle (Yan and Chen 2020). Therefore, for each ATP hydrolysis event, the nucleosome moves along the DNA by approximately 1 bp (Yan and Chen 2020).

In summary, chromatin remodelers play a vital role in modulating the structure and accessibility of chromatin, allowing for the regulation of DNA-related processes (Clapier et al. 2017). The different subfamilies of chromatin remodelers, including ISWI, CHD, SWI/SNF, and INO80, possess unique protein domains and functions that contribute to chromatin assembly and organization, chromatin access, and nucleosome editing (Clapier et al. 2017). Furthermore, these chromatin remodelers share a common mechanism of DNA translocation, involving a "DNA wave" model driven by ATP hydrolysis (Yan and Chen 2020). Understanding the diverse functions and mechanisms of chromatin remodelers is essential for unraveling the complexities of chromatin dynamics and its impact on gene expression and genome maintenance (Tyagi et al. 2016).

1.5.2 Regulation of chromatin remodelers by their intrinsic domains

Chromatin remodeling activities are intricately regulated to finely tune various chromatin-related processes (Clapier et al. 2017). The functionality of chromatin remodelers is primarily regulated at three levels (Clapier et al. 2017). Firstly, the accessibility of the substrate nucleosome to the RecA-like lobes of the remodeler can be tightly regulated (Clapier et al. 2017). Secondly, the rate of ATP turnover determines the efficiency of the chromatin remodelers (Clapier et al. 2017). Finally, the probability of ATP hydrolysis being coupled to DNA translocation influences the overall remodeling process (Clapier et al. 2017). These regulatory mechanisms ensure precise control and coordination of chromatin remodeling to meet specific cellular requirements (Clapier et al. 2017).

The functionality of chromatin remodelers can be regulated by intrinsic domains through auto-inhibition (Reyes et al. 2021). In the case of ISWI chromatin remodelers, intrinsic protein domains play a crucial role in regulating their ATPase activity and DNA translocation (Clapier and Cairns 2012). For instance, both the AutoN and NegC domains of ISWI act as inhibitors of its function (Clapier and

Cairns 2012). The AutoN domain binds to the two RecA-like lobes, inactivating the ATP hydrolysis process by keeping the lobes in an inactive conformation (Clapier and Cairns 2012). Similarly, the NegC domain inhibits the coupling of ATP hydrolysis and DNA translocation by disrupting the interaction between the two RecA-like lobes of ISWI (Clapier and Cairns 2012). Interestingly, the AutoN domain structurally resembles a basic patch (R17–19) of histone H4 (Clapier and Cairns 2012). When ISWI binds to the basic patch of histone H4, the basic patch competes with the AutoN domain for binding to the ATPase domain, effectively removing the auto-inhibition (Clapier and Cairns 2012). Furthermore, the presence of linker DNA can prevent the NegC domain from binding to the RecA-like lobes, releasing the inhibition and enabling the coupling of ATP hydrolysis to DNA translocation (Clapier and Cairns 2012). These intrinsic domains of ISWI create an "inhibition of inhibition" module within the enzyme, ensuring activation of the remodeling activity only in the appropriate chromatin environment with the presence of the basic patch of histone H4 and the linker DNA (Barisic et al. 2019).

Another example of chromatin remodeling activity regulated by intrinsic domains is found in the CHD chromatin remodelers (Hauk et al. 2010). Structural analysis reveals that the N-terminal chromodomain of CHD is strategically positioned in the DNA-binding cleft of CHD, thus inhibiting the CHD remodeler from binding to DNA (Hauk et al. 2010). Consistent with this observation, depletion of the chromodomain leads to increased DNA affinity and enhanced DNA-stimulated ATP hydrolysis by the CHD remodeler (Hauk et al. 2010).

In summary, chromatin remodelers are subject to regulation by intrinsic protein domains that modulate their ATPase activity and DNA translocation (Narlikar et al. 2013). The ISWI remodelers utilize the AutoN and NegC domains to exert auto-inhibition, which can be relieved by binding to histone H4 and the linker DNA (Clapier and Cairns 2012). Similarly, the chromodomain of CHD remodelers plays a role in inhibiting DNA binding (Hauk et al. 2010). Understanding the regulatory mechanisms involving intrinsic domains is crucial for comprehending the precise control of chromatin remodeling activity and its impact on chromatin structure and function (Narlikar et al. 2013).

1.5.3 Targeting of chromatin remodelers to genomic loci

Chromatin remodelers play a critical role in global nucleosome regulation (Ocampo et al. 2016). Notably, ISWI complexes are involved in establishing an evenly spaced pattern of nucleosomes in the majority of protein coding genes (Li et al. 2014). However, chromatin remodeling complexes also exhibit locus-specific control over chromatin-based processes, including the transcriptional regulation of a select group of genes (Bowman and McKnight 2017). The targeting of chromatin remodelers to specific genomic loci primarily occurs through two mechanisms. Firstly, certain domains within the ATPases or accessory subunits of chromatin remodeling complexes can recognize specific histone modifications (Petty and Pillus 2013). Secondly, transcription factors or non-coding RNAs can recruit chromatin remodeling complexes to specific genomic loci, thereby modulating gene expression (Erdel et al. 2011). Understanding these mechanisms is pivotal in unraveling the intricate regulation of chromatin remodeling activity and its impact on chromatin structure and gene function (Erdel et al. 2011).

The ATPases and accessory subunits of chromatin remodeling complexes possess various domains that exhibit binding affinity towards modified histones, contributing to target specificity of chromatin remodelers (Clapier et al. 2017). For instance, the CHD family remodelers are characterized by a conserved chromodomain that can bind to methylated lysine residues on histones (Flanagan et al. 2005), while the SWI/SNF family chromatin remodelers possess a bromodomain located near their C-terminal region, facilitating recognition of acetylated lysine residues on histone tails (Sanchez and Zhou 2009). Additionally, many accessory subunits of chromatin remodeling complexes contain PLANT HOMEODOMAIN (PHD) or Pro-Trp-Trp-Pro (PWWP) domains that specifically recognize methylated histones (Sanchez and Zhou 2011; Rona et al. 2016). Through their interactions with modified histones, these protein domains enable chromatin remodeling complexes to attain a certain level of target specificity, ultimately contributing to the precise modulation of chromatin structure and function (Erdel et al. 2011).

Targeting chromatin remodeling complexes to specific loci also involves their interaction with transcription factors that recognize specific cis-DNA elements (Erdel et al. 2011). For example, the NUCLEOSOME REMODELING AND DEACETYLASE (NuRD) complex, which possesses both CHD chromatin remodeling activity and histone deacetylation activity, is known to be recruited to specific target genes through interactions with transcription factors (Basta and Rauchman 2015). In *Drosophila*, the NuRD complex ATPase subunit, DROSOPHILA MI-2 (dMi-2), interacts with the hunchback transcription factor to bind to and repress the transcription of HOMEOBOX (HOX) genes (Kehle 1998). The SWI/SNF chromatin remodeling complex is well-known for its interaction with numerous transcription factors to bind to specific target genes (Centore et al. 2020). For instance, the BRAHMA-RELATED GENE-1 (BRG1) ATPase subunit of the SWI/SNF complex is recruited to oligodendrocyte-specific enhancers by OLIGODENDROCYTE TRANSCRIPTION FACTOR 2 (OLIG2), contributing to the establishment of oligodendrocyte identity (Yu et al. 2013). Furthermore, the *Arabidopsis* SWR1 chromatin remodeling complex, which belongs to the INO80 subfamily, is recruited by the HY5 transcription factor to facilitate the exchange of histone H2A by histone H2A.Z, thereby inhibiting the transcription of HY5 target genes (Mao et al. 2021).

In summary, chromatin remodelers play crucial roles in modulating nucleosome dynamics on chromatin, thereby contributing to the regulation of various chromatin-related processes such as chromatin assembly, DNA replication, DNA repair, and transcription (Clapier and Cairns 2009). The activity of chromatin remodelers can be regulated by intra-molecular inhibitory domains or through interactions with other proteins (Clapier et al. 2017). In addition to their involvement in global chromatin remodeling, chromatin remodeling complexes are directed to specific genomic loci by interacting with specific histone modifications or transcription factors (Erdel et al. 2011). This targeted localization enables chromatin remodelers to regulate the spatial and temporal transcription of specific genes (Erdel et al. 2011).

1.6 Function of the ISWI chromatin remodelers in eukaryotic organisms

1.6.1 Components of ISWI complexes

The ISWI complexes are highly conserved among eukaryotes, including yeast, plant, fruit fly, and human (Bartholomew 2014). The ISWI complexes typically consist of an ATPase catalytic core subunit along with a few accessory proteins (Li et al. 2021). In the yeast species *Saccharomyces cerevisiae*, two ISWI ATPase homologs, Isw1 and Isw2, give rise to four distinct ISWI complexes: Isw1a (Isw1 and ISWI ONE COMPLEX PROTEIN 3 (Ioc3)), Isw1b (Isw1, Ioc2, and Ioc4), Isw2 (Isw2 and IMITATION SWITCH TWO COMPLEX PROTEIN 1 (Itc1)), and YEAST CHROMATIN ACCESSIBILITY COMPLEX (yCHRAC) (Isw2, Itc1, DNA POLYMERASE ε SUBUNIT 4 (Dpb4), and DPB3-LIKE SUBUNIT (Dls1)) (Table 1.2) (Toto et al. 2014). *Arabidopsis*, on the other hand, possesses two ISWI ATPase homologs, CHROMATIN-REMODELING PROTEIN 11 (CHR11) and CHR17, which form three different complexes: CRA (CHR11/17, RINGLET 1 and 2 (RLT1/2), and AT-RICH INTERACTING DOMAIN 5 (ARID5)), CDM (CHR11/17, DDT-PHD PROTEIN 1/2/3 (DDP1/2/3), and MULTICOPY SUPPRESSOR OF IRA1 3 (MSI3)), and CDD (CHR11/17, DDT-WAC PROTEIN 1 (DDW1), and DDT-RELATED PROTEIN 1/3/4/5 (DDR1/3/4/5)) (Table 1.2) (Tan et al. 2020). In *Drosophila*, there is a single ISWI ATPase homolog, DROSOPHILA ISWI (dISWI), which forms six distinct ISWI complexes: CHRAC (dISWI, CHROMATIN ASSEMBLY FACTOR 1 (ACF1), CHRAC14, and CHRAC16), ACF (dISWI and ACF1), NUCLEOSOME REMODELING FACTOR (NURF) (dISWI, NURF301, NURF38, and NURF55), REMODELING AND SPACING FACTOR (RSF) (dISWI and RSF1), TOUTATIS-CONTAINING CHROMATIN REMODELING COMPLEX (ToRC) (dISWI, TTF-I INTERACTING PEPTIDE 5 (TIP5), and C-TERMINAL BINDING PROTEIN (CtBP)), and NUCLEOLAR REMODELING COMPLEX (NoRC) (dISWI and TIP5) (Table 1.2) (Toto et al. 2014). In human cells, two ISWI ATPase homologs, SWI/SNF RELATED, MATRIX ASSOCIATED, ACTING DEPENDENT REGULATOR OF CHROMATIN, SUBFAMILY A, MEMBER 5 (SMARCA5) and SMARCA1, form at least 16 distinct ISWI complexes,

including ACF-1 (SMARCA1 and BROMODOMAIN ADJACENT TO ZINC FINGER DOMAIN 1A (BAZ1A)), ACF-5 (SMARCA5 and BAZ1A), CHRAC-1 (SMARCA1, BAZ1A, CHRAC1, and DNA POLYMERASE EPSILON SUBUNIT 3 (POLE3)), CHRAC-5 (SMARCA5, BAZ1A, CHRAC1, and POLE3), WILLIAMS SYNDROME TRANSCRIPTION FACTOR-ISWI CHROMATIN REMODELING COMPLEX (WICH)-1 (SMARCA1 and BAZ1B), WICH-5 (SMARCA5 and BAZ1B), NORC-1 (SMARCA1 and BAZ2A), NORC-5 (SMARCA5 and BAZ2A), RSF-1 (SMARCA1 and RSF1), RSF-5 (SMARCA5 and RSF1), BAZ2B-CONTAINING REMODELING FACTOR (BRF)-1 (SMARCA1 and BAZ2B), BRF-5 (SMARCA5 and BAZ2B), NURF-1 (SMARCA1, BROMODOMAIN PHD FINGER TRANSCRIPTION FACTOR (BPTF), RB BINDING PROTEIN 4 (RBBP4), and RBBP7), NURF-5 (SMARCA5 and BPTF), CECR2-CONTAINING REMODELING FACTOR (CERF)-1 (SMARCA1 and CAT EYE SYNDROME CRITICAL REGION PROTEIN 2 (CECR2)), and CERF-5 (SMARCA5 and CECR2) (Table 1.2) (Toto et al. 2014; Oppikofer et al. 2017). These different ISWI complexes often possess distinct functions due to the different accessory subunits that associate with the core ATPase (Li et al. 2021).

1.6.2 Role of ISWI in regulation of gene expression

The ISWI complex exhibits dual regulatory functions in transcription, either positively or negatively, depending on the target genes (Corona and Tamkun 2004). ISWI complexes are frequently recruited to specific genes through interactions with transcription factors or non-coding RNAs, thereby modulating gene expression (Corona and Tamkun 2004). Upon recruitment near the promoter regions of specific genes, the ISWI complex can reposition nucleosomes in different directions, influencing the accessibility of the RNA polymerase transcriptional machinery to the promoters, thereby regulating transcription (Levendosky and Bowman 2019).

Components of ISWI complexes in different organisms		
Organism	**Complex**	**Component**
Yeast	Isw1a	Isw1 and Ioc3
	Isw1b	Isw1, Ioc2, and Ioc4
	Isw2	Isw2 and Itc1
	yCHRAC	Isw2, Itc1, Dpb4, and Dls1
Arabidopsis	CRA	CHR11, CHR17, RLT1, RLT2 and ARID5
	CDM	CHR11, CHR17, DDP1, DDP2, DDP3 and MSI3
	CDD	CHR11, CHR17, DDW1, DDR1, DDR3, DDR4 and DDR5
Drosophila	CHRAC	dISWI, ACF1, CHRAC14, and CHRAC16
	ACF	dISWI and ACF1
	NURF	dISWI, NURF301, NURF38, and NURF55
	RSF	dISWI and RSF1
	ToRC	dISWI, TIP5 and CtBP
	NoRC	dISWI and TIP5
Human	ACF-1	SMARCA1 and BAZ1A
	ACF-5	SMARCA5 and BAZ1A
	CHRAC-1	SMARCA1, BAZ1A, CHRAC1, and POLE3
	CHRAC-5	SMARCA5, BAZ1A, CHRAC1, and POLE3
	WICH-1	SMARCA1 and BAZ1B
	WICH-5	SMARCA5 and BAZ1B
	NORC-1	SMARCA1 and BAZ2A
	NORC-5	SMARCA5 and BAZ2A
	RSF-1	SMARCA1 and RSF1
	RSF-5	SMARCA5 and RSF1
	BRF-1	SMARCA1 and BAZ2B
	BRF-5	SMARCA5 and BAZ2B
	NURF-1	SMARCA1, BPTF, RBBP4 and RBBP7
	NURF-5	SMARCA5 and BPTF
	CERF-1	SMARCA1 and CECR2
	CERF-5	SMARCA5 and CECR2

Table 1.2 Protein components of ISWI complexes in yeast, *Arabidopsis*, *Drosophila* and human.

The ISWI complex could be recruited to specific genomic target genes to repress their transcription. In yeast, the Isw2 complex is recruited to target genes by the UNSCHEDULED MEIOTIC GENE EXPRESSION 6 PROTEIN (Ume6p) transcription factor (Goldmark et al. 2000). The Isw2 complex then establishes a nuclease-inaccessible chromatin state near the Ume6p binding sites, leading to gene repression *in vivo* (Goldmark et al. 2000). Another chromatin remodeling complex, the NoRC complex, is recruited by the non-coding RNA "promoter RNA" (pRNA) to the ribosomal RNA gene (rDNA) promoter (Mayer et al. 2008). Subsequently, the NoRC complex recruits DNA methyltransferases and histone deacetylases to silence rDNA transcription (Santoro et al. 2002). Conversely, the ISWI complex has also been shown to positively regulate gene transcription. In *Drosophila*, the NURF complex is recruited by Armadillo transcription factor to target genes to promote transcription (Song et al. 2009). In the absence of the NURF complex, the expression of Armadillo target genes is diminished (Song et al. 2009). Additionally, the GAGA pioneer transcription factor in *Drosophila* can recruit the NURF complex to target genes (Judd et al. 2021). This recruitment of the NURF complex facilitates the release of RNA polymerase pausing and enhances RNA polymerase elongation at these specific genes by precisely positioning the +1 nucleosomes (Judd et al. 2021).

In summary, the ISWI complex dynamically modulates transcription *in vivo* through nucleosome sliding near promoters and the recruitment of other epigenetic regulators (Erdel and Rippe 2011). The ISWI complexes are often recruited to specific genes through interactions with transcription factors or non-coding RNAs (Erdel and Rippe 2011).

1.6.3 Role of ISWI in DDR

The ISWI complexes play a pivotal role in regulating various DNA damage repair pathways, such as NER and DSB repair (Aydin et al. 2014b). In human cells, NER is the primary mechanism employed to rectify UV-induced DNA damage (Sinha and Häder 2002). Remarkably, SMARCA5 is indispensable for NER-mediated repair of UV-induced DNA damage, as demonstrated by heightened

sensitivity to UV radiation in cells with *SMARCA5* knockdown (Aydin et al. 2014a). Subsequent investigations have revealed the recruitment of SMARCA5 to sites of UV-induced DNA damage, facilitating the recruitment of CSB to stalled RNA polymerases, thereby governing transcription-coupled NER (Aydin et al. 2014a). Furthermore, the UV-induced DNA damage sites recruit ACF1 and WSTF, which are accessory subunits of the ACF and WICH ISWI complexes, respectively (Aydin et al. 2014a). Notably, the depletion of either ACF1 or WSTF results in reduced CSB recruitment, indicating the involvement of both the ACF and WICH complexes in regulating transcription-coupled NER (Aydin et al. 2014a). These findings collectively suggest that the ISWI complex is a crucial factor in the NER repair pathway (Aydin et al. 2014a).

The ISWI complex also plays a crucial role in regulating the DSB repair pathway (Karl et al. 2022). In a RNAi screen conducted in *Caenorhabditis elegans*, it was discovered that the ISWI chromatin remodeler was required for resistance against ionizing radiation-induced DNA damage. (van Haaften et al. 2006). Similarly, SMARCA5, the ISWI homolog in human cells, was found to be required for both NHEJ and HR-mediated repair of DNA DSBs (Smeenk et al. 2012). SMARCA5 is rapidly recruited to sites of DNA damage caused by laser-microirradiation (Smeenk et al. 2012). Recruitment of SMARCA5 to DNA damage sites is functionally required for DNA damage repair. Several proteins have been shown to mediate the recruitment of SMARCA5 to DNA damage sites, including RNF168 and SIRTUIN 6 (SIRT6) (Smeenk et al. 2012; Toiber et al. 2013). Notably, RNF168 undergoes poly(ADP-ribosyl)ation upon DNA damage, and the poly(ADP-ribosyl)ated form of RNF168 interacts with SMARCA5 (Smeenk et al. 2012). Importantly, SMARCA5 and RNF168 exhibit mutual dependence in their accumulation at DNA damage sites, highlighting the requirement of SMARCA5 for the recruitment of RNF168 and the downstream histone ubiquitination signaling (Smeenk et al. 2012). Consistently, depletion of SMARCA5 renders human cells hypersensitive to ionizing radiation (Smeenk et al. 2012). SIRT6, a histone deacetylase known for its role in maintaining genome stability, has been identified as an interactor of SMARCA5 through mass spectrometry experiments (Toiber et al. 2013). Notably, the interaction between SIRT6 and SMARCA5 is enhanced in response to ionizing

radiation-induced DNA damage (Toiber et al. 2013). Subsequent experiments demonstrated that SIRT6 can recruit SMARCA5 to DNA damage sites (Toiber et al. 2013). Silencing either SIRT6 or SMARCA5 renders cells hypersensitive to ionizing radiation, underscoring their importance in DNA damage repair (Toiber et al. 2013). Furthermore, depletion of both SIRT6 and SMARCA5 yields a similar phenotype as depletion of either protein alone, indicating that SIRT6 and SMARCA5 function in the same genetic pathway to regulate DNA damage repair (Toiber et al. 2013).

1.6.4 Role of ISWI in higher order chromatin changes

The ISWI complex is involved in higher-order chromatin changes (Corona et al. 2007). Expression of a dominant negative mutant of *Drosophila* ISWI leads to decompaction of polytene and diploid chromosomes during metaphase (Corona et al. 2007). Notably, expression of the dominant negative mutant of *Drosophila* ISWI also results in a significant reduction in histone H1 incorporation into metaphase chromosomes, which is strongly associated with the large-scale chromosome decompaction (Corona et al. 2007). Additional evidence from a subsequent study demonstrates that knockdown of the *H1* gene in *Drosophila* yields a similar chromosome decompaction phenotype (Siriaco et al. 2009). These findings highlight the importance of the ISWI complex in large-scale chromosome compaction in *Drosophila* cells (Corona et al. 2007). Another association between the ISWI complex and higher-order chromatin changes is observed in the involvement of the WICH complex in DNA replication (Poot et al. 2004). Depletion of WSTF, a subunit of the WICH complex, leads to a more condensed state of newly synthesized chromatin (Poot et al. 2004). Remarkably, the function of the ISWI complex in higher order chromatin changes differs in fruit fly and human cells, as ISWI positively regulates chromatin condensation in *Drosophila* cells during mitosis and negatively regulates chromatin condensation in newly synthesized chromatin in human cells (Poot et al. 2004; Corona et al. 2007). These observations suggest that the ISWI complex may modulate large-scale chromatin condensation in both negative and positive manners, depending on the specific context.

1.7 The effects of histone modifications on transcription

1.7.1 General description of histone modifications

The nucleosome consists of two copies each of four different core histones: histone H2A, H2B, H3, and H4 (Cutter and Hayes 2015). Histones undergo various post-translational modifications that contribute to their functional diversity (Millán-Zambrano et al. 2022). The first functional link between histone modification and gene transcription was demonstrated in a study published in 1996 (Brownell et al. 1996). In this study, histone acetylation was shown to activate gene expression in *Tetrahymena thermophila* (Brownell et al. 1996). Since then, numerous studies have characterized the function of various histone modifications, contributing to our understanding of epigenetics (Millán-Zambrano et al. 2022).

Histone modifications can be targeted to specific amino acids (Peterson and Laniel 2004). For instance, histone acetylation can target lysine, serine, and threonine residues, while histone ubiquitination specifically targets lysine residues (Millán-Zambrano et al. 2022). Histone methylation can occur on lysine and arginine residues, while adenosine diphosphate (ADP) ribosylation targets lysine and glutamic acid residues on histones. Phosphorylation can affect serine, threonine, tyrosine, and histidine residues of histones (Millán-Zambrano et al. 2022). The extensive research on the function of histone modifications has led to the proposal of an "epigenetic" code, analogous to the genetic code encoded by DNA sequences (Turner 2007). This "epigenetic" code theory suggests that specific histone modifications or combinations thereof direct the readout of transcription and other chromatin-related processes, such as DNA replication and DNA repair (Turner 2007). Consequently, the terms "writer," "reader," and "eraser" have been used to describe specialized proteins involved in depositing, recognizing, and removing histone modifications, respectively (Biswas and Rao 2018). However, the relationship between histone modifications and chromatin-related processes is complex and context-dependent (Peterson and Laniel 2004). Establishing a causal relationship between histone modifications and chromatin-related processes had been challenging due to the lack of targeted approaches to modify

histone modifications at specific genomic loci (Yu et al. 2008). Nonetheless, recent advancements, such as catalytically dead Cas9 (dCas9) protein fused with histone writers and erasers, have provided insights into the instructive roles of histone modifications in chromatin-related processes at specific genomic loci (Brocken et al. 2018).

1.7.2 Regulation of transcription by histone modifications

Transcriptional regulation plays a crucial role in cellular and organismal adaptation to both external and internal stimuli (Burdge et al. 2007). Cell signaling pathways, originating from external or internal signals, involve various components that ultimately modulate changes in gene transcription and regulation of diverse biological processes (Weidemüller et al. 2021). Given the pivotal role of transcription, the investigation of histone modifications in regulating gene transcription has been extensively pursued, resulting in a wealth of knowledge in the field (Morgan and Shilatifard 2020).

Histone modifications can influence transcription through primarily two mechanisms (Millán-Zambrano et al. 2022). Firstly, histone modifications can alter the intrinsic properties of nucleosomes, resulting in less compacted chromatin and improved DNA accessibility for transcription machinery (Grunstein 1997). Secondly, histone modifications can recruit transcription regulators, thereby indirectly regulating transcription (Millán-Zambrano et al. 2022). Histone acetylation is known to alter the intrinsic properties of nucleosomes to facilitate transcription activation (Grunstein 1997). Acetylation of lysine residues on histones neutralizes the positive charges of histones and weakens the interaction between histones and DNA, leading to chromatin decompaction and facilitating active transcription (Grunstein 1997). In addition to modulating the intrinsic properties of nucleosomes, histone modifications such as trimethylation of Histone H3 at lysine 4 (H3K4me3) and trimethylation of Histone H3 at lysine 27 (H3K27me3) can impact transcription by recruiting transcription regulators that modulate the transcription machinery (Millán-Zambrano et al. 2022). H3K4me3 is associated with active transcription, while H3K27me3 is associated with transcriptional repression (Millán-Zambrano et al. 2022).

One of the pioneering studies investigating the relationship between H3K4me3 and active transcription was conducted in yeast (Santos-Rosa et al. 2002). The researchers identified that the yeast SU(VAR)3-9, ENHANCER-OF-ZESTE AND TRITHORAX 1 (Set1) protein is responsible for depositing H3K4me2 and H3K4me3 marks at genes, with only H3K4me3 being exclusively associated with active gene transcription (Santos-Rosa et al. 2002). Crucially, when the methyltransferase domain of Set1 was deleted, a reduction in gene expression was observed, indicating that the deposition of H3K4me3 potentially plays a role in regulating the transcriptional activity of specific genes (Santos-Rosa et al. 2002).

H3K4me3 exhibits a peak around the transcription start site (TSS) of protein coding genes across various organisms (Barski et al. 2007; Millán-Zambrano et al. 2022). Moreover, genes that display higher expression levels tend to have increased levels of H3K4me3 deposition near the TSS (Millán-Zambrano et al. 2022). Notably, the breadth of the H3K4me3 peak has also been found to positively correlate with gene expression, particularly in the case of tumor suppressor genes in humans (Chen et al. 2015). In normal cells, tumor suppressor genes such as p53 are characterized by broad H3K4me3 peaks, spanning more than 4 kilo base pairs (Chen et al. 2015). However, in tumor cells, the tumor suppressor genes exhibit considerably thinner H3K4me3 peaks, which correspond to the lower expression levels of tumor suppressor genes in tumor cells (Chen et al. 2015). Another study observed a connection between the breadth of H3K4me3 peaks and transcriptional consistency: genes with broader H3K4me3 peaks tend to have reduced transcriptional noise (Benayoun et al. 2015).

Although the positive correlation between H3K4me3 deposition and gene transcription is well established, there is still debate about whether H3K4me3 is instructive for transcription or simply a record of active transcription, with evidence supporting both possibilities (Howe et al. 2017). Some evidence suggests that H3K4me3 is a record of active transcription (Howe et al. 2017). For example, it has been demonstrated in different organisms that the transcription machinery is responsible for the recruitment of H3K4 methyltransferases (Ding et al. 2011; Lee and Skalnik 2008; Milne et al. 2005; Krogan et al. 2003). Moreover, loss of H3K4me3 does not result in a global decrease in nascent

transcription, suggesting that expression of the majority of protein coding genes may not depend on H3K4me3 deposition (Clouaire et al. 2012).

Evidence also exists that supports an instructive role for H3K4me3 in transcription (Wang et al. 2023). For example, H3K4me3 has been shown to be recognized by the PHD domain of TATA-BOX BINDING PROTEIN ASSOCIATED FACTOR 3 (TAF3), a subunit of the basal transcription factor complex TFIID, which is a component of the transcription machinery (Lauberth et al. 2013). This interaction between H3K4me3 and TFIID enhances the recruitment of the transcription machinery to specific genes, thereby promoting transcription (Lauberth et al. 2013). Furthermore, recent studies have demonstrated that loss of H3K4me3 disrupts the release of paused RNA polymerase (Wang et al. 2023). Depletion of the shared subunits of the COMPLEX PROTEINS ASSOCIATED WITH SET1 (COMPASS) complexes, which is responsible for H3K4 methylation, resulted in the fast loss of H3K4me3 marks (Wang et al. 2023). This acute loss of H3K4me3 did not impact transcription initiation but led to prolonged pausing of RNA polymerase II and reduced transcriptional elongation (Wang et al. 2023). Additional experiments identified INTEGRATOR COMPLEX SUBUNIT 11 (INTS11) protein as responsible for the regulation of pause-release of RNA pol II by H3K4me3, thereby modulating transcriptional output (Wang et al. 2023).

Establishing a causal role of H3K4me3 in the control of transcription at specific genomic loci has historically been challenging (Brocken et al. 2018). However, recent developments in the CRISPR/Cas9 system have allowed for editing histone modification at targeted genomic loci by fusing dCas9 with histone modification-modulating enzymes, providing insight into the causal roles of histone modifications on the transcription of specific genes (Brocken et al. 2018). For instance, when the Set domain of human H3K4 methyltransferase PR/SET DOMAIN CONTAINING PROTEIN 9 (PRDM9) was fused to dCas9 and targeted to specific genes, H3K4me3 levels and transcription levels of the targeted genes were upregulated, establishing a causal role of H3K4me3 in gene transcription activation (Cano-Rodriguez et al. 2016). It should be noted that the epigenetic editing of H3K4me3 reactivated gene expression in a context-dependent manner (Cano-Rodriguez et al. 2016). Specifically, stable

reactivation of gene transcription was observed when the binding regions of the dCas9 fusion protein did not have methylated DNA (Cano-Rodriguez et al. 2016). This context-dependent H3K4me3 modification nonetheless demonstrates the instructive role of H3K4me3 in gene transcription activation (Cano-Rodriguez et al. 2016).

H3K27me3 is another well-established histone modification associated with gene repression (Wiles and Selker 2017). H3K27me3 deposition is mediated by the POLYCOMB REPRESSIVE COMPLEX 2 (PRC2) complex, which includes the methyltransferase catalytic subunit ENHANCER OF ZESTE 2 (EZH2) (Duan et al. 2020). H3K27me3 functions instructively in gene repression by virtue of its recognition by BROMO-ADJACENT HOMOLOGY (BAH) domain-containing proteins that are conserved across different species (Wiles et al. 2020). In humans, the BAH DOMAIN AND COILED-COIL CONTAINING 1 (BAHCC1) protein possesses a BAH domain that specifically binds to the H3K27me3 histone modification (Fan et al. 2020). BAHCC1 interacts with HISTONE DEACETYLASE (HDAC), thereby facilitating histone deacetylation and establishing a connection between the recognition of H3K27me3 and gene repression (Fan et al. 2020). In *Arabidopsis*, a recently discovered BAH-PHD-CARBOXYL-TERMINAL DOMAIN PHOSPHATASE-LIKE 2 (CPL2) complex acts as a reader of H3K27me3 and is involved in mediating transcriptional repression (Zhang et al. 2020). The BAH-PHD-CPL2 complex consists of the BAH domain-containing protein ASI1-IMMUNOPRECIPITATED PROTEIN 3 (AIPP3), which recognizes H3K27me3, along with the PHD domain-containing proteins AIPP2 and PARALOG OF AIPP2 (PAIPP2), and the CPL2 protein (Zhang et al. 2020). Notably, the CPL2 subunit of this complex functions as a phosphatase for the RNA pol II C-terminal domain (CTD). This dephosphorylation of the RNA pol II CTD leads to the inhibition of RNA pol II release, ultimately resulting in transcriptional silencing (Zhang et al. 2020).

Similar to H3K4me3, the functional role of H3K27me3 at specific genomic loci has also been investigated using dCas9-mediated epigenetic editing (Fukushima et al. 2019). In two separate studies, fusion of the dCas9 protein with the EZH2 H3K27 methyltransferase successfully induced the deposition of H3K27me3 and led to the repression of targeted genes (Chen et al. 2019; O'Geen et al.

2017). Conversely, when dCas9 was fused with a computationally designed PRC2 inhibitor protein called EMBRYONIC ECTODERM DEVELOPMENT (EED) binder, it effectively reduced H3K27me3 deposition at target genes and resulted in gene activation (Levy et al. 2022). These dCas9-mediated epigenetic editing experiments provided compelling evidence for the instructive role of H3K27me3 in the regulation of gene repression.

In summary, histone modifications play a crucial role in various chromatin-related processes, particularly in the regulation of gene transcription, which is vital for fine-tuning developmental processes in diverse organisms (Millán-Zambrano et al. 2022). While the epigenetic code hypothesis is not yet as well-characterized as genetic codes, the recent emergence of the CRISPR/Cas9 biotechnology tool has provided a means to investigate the causal role of histone modifications in gene transcription with greater precision and targeting capabilities (Brocken et al. 2018).

Chapter 2. Cryptochromes and UBP12/13 deubiquitinases antagonistically regulate the DNA damage response in plants.

This chapter is available on the bioRxiv preprint server (2023) under the title "Cryptochromes and UBP12/13 deubiquitinases antagonistically regulate DNA damage response in Arabidopsis" by Yuzhao Hu, Daniele Rosado, Louise N. Lindbäck, Julie Micko, and Ullas V. Pedmale (Hu et al. 2023; doi: https://doi.org/10.1101/2023.01.15.524001). *I thank Louise N. Lindbäck for phenotypic studies and performing RT-qPCR analysis and Daniele Rosado for her help with the RNA-seq analysis.*

2.1 Summary

Cryptochromes (CRYs) are evolutionarily conserved blue-light receptors that evolved from bacterial photolyases that repair damaged DNA. Today, CRYs have lost their ability to repair damaged DNA; however, prior reports suggest that human CRYs can respond to DNA damage. Currently, the role of CRYs in the DNA damage response (DDR) is lacking, especially in plants. Therefore, we evaluated the role of plant CRYs in DDR along with UBP12/13 deubiquitinases, which interact with and regulate the CRY2 protein. We found that *cry1cry2* was hypersensitive, while *ubp12ubp13* was hyposensitive to UVC-induced DNA damage. Elevated UV-induced cyclobutane pyrimidine dimers (CPDs) and the lack of DNA repair protein RAD51 accumulation in *cry1cry2* plants indicate that CRYs are required for DNA repair. On the contrary, CPD levels diminished and RAD51 protein levels elevated in plants lacking UBP12 and UBP13, indicating their role in DDR repression. Temporal transcriptomic analysis revealed that DDR-induced transcriptional responses were subdued in *cry1cry2,* but elevated in *ubp12ubp13* compared to WT. Through transcriptional modeling of the time-course transcriptome, we found that genes quickly induced by UVC (15 min) are targets of CAMTA 1-3 transcription factors, which we found are required for DDR. This transcriptional regulation seems, however, diminished in the *cry1cry2* mutant, suggesting that CAMTAs are required for CRY2-

mediated DDR. Furthermore, we observed enhanced CRY2-UBP13 interaction and formation of CRY2 nuclear speckles under UVC, suggesting that UVC activates CRY2 similarly to blue light. Together, our data reveal the temporal dynamics of the transcriptional events underlying UVC-induced genotoxicity and expand our knowledge of the role of CRY and UBP12/13 in DDR.

2.2 Introduction

Genome integrity is essential for all living organisms, but it is especially important for plants because they are stationary and primarily grow post-embryonically. DNA damage can lead to the loss or alteration of essential genes, which can affect plant growth, development, and overall health (Manova and Gruszka 2015). Additionally, DNA damage can also lead to the production of abnormal proteins that can disrupt normal cellular processes or cause other negative effects (Alhmoud et al. 2020). Since plants rely on light as an energy source, they are inevitably exposed to DNA damage caused by both UV radiation in sunlight and the production of reactive oxygen species in chloroplasts due to excess light (Roldán-Arjona and Ariza 2009; Gill et al. 2015). UV radiation is particularly damaging because it leads to the formation of cyclobutane pyrimidine dimer (CPD) in DNA, which inhibits DNA replication and RNA transcription (Pfeifer et al. 2005). Therefore, it is important for organisms to have effective DNA repair mechanisms to prevent and mitigate the negative consequences of DNA damage. Once such mechanism conserved in the eukaryotes is the DNA damage response (DDR), which generally encompasses three important aspects: 1) induction of DNA repair, 2) checkpoint response that halts the cell cycle, and 3) programmed cell death to eliminate cells with irreparable DNA damage (Groelly et al. 2022).

In plants and animals, similar DDR mechanisms exist, where the DNA repair and cell-cycle arrest are initiated by two kinases, ATAXIA TELANGIECTASIA-MUTATED AND RAD3-RELATED (ATR) and ATAXIA-TELANGIECTASIA MUTATED (ATM), which are activated by ssDNA or DNA double-strand breaks (DSBs), respectively (Savitsky et al. 1995; Weinert et al. 1994). Upon activation,

ATR and ATM target different downstream factors in animals and plants. In animals, ATR and ATM phosphorylate Checkpoint kinase 1 and 2 (Chk1 and Chk2), respectively (Smith et al., 2010). ATR, ATM, Chk1, and Chk2 then phosphorylate and activate a master regulator of DDR, p53 transcription factor (TF), which induces the transcription of thousands of genes to orchestrate DDR (Linzer and Levine 1979). In contrast, plant genomes lack orthologs of Chk1, Chk2 and p53 (Manova and Gruszka 2015) instead, ATR and ATM activate a different TF, SUPPRESSOR OF GAMMA RADIATION 1 (SOG1), which is largely required for the induction of the transcriptional network of DDR (Bourbousse et al. 2018).

UV-induced CPD can be detected and repaired by the nucleotide excision repair (NER) pathway (Marteijn et al. 2014). There are two NER pathways, the global genome NER (GG-NER), which scans the whole genome to detect CPD, and the transcription-coupled NER (TC-NER), which senses the CPD-induced stalling of RNA polymerase II during transcription (Marteijn et al. 2014). Interestingly, both GG-NER and TC-NER require Cullin 4 (CUL4)-RING ubiquitin E3 ligase (CRL4): the former relies on $CRL4^{\text{DNA DAMAGE BINDING 2 (DDB2)}}$ to recognize CPD, while the latter require $CRL4^{\text{COCKAYNE SYNDROME A(CSA)}}$ to assemble the DNA repair machinery (Lee and Zhou 2007). In plants, apart from NER, photolyases can harness energy from blue/UVA light to repair CPD without DNA excision (Sancar 1994). Evolutionarily, photolyases are homologous to plant and animal cryptochromes (CRY) (Chaves et al. 2011). Plant CRYs perceive blue light to fine-tune growth and development (Cashmore et al. 1999). Blue-light-activated CRYs dimerize and tetramerize to interact with downstream signaling partners (Palayam et al. 2021). Upon exposure to blue light, CRYs also form nuclear speckles (Yu et al. 2009; Liu et al. 2022), where CRY2 carries out its function (Wang et al. 2021). The photoactive CRYs are then ubiquitinated by two E3 ligase complexes, CONSTITUTIVE PHOTOMORPHOGENIC 1 (COP1) and SUPPRESSOR OF PHYA-105 (SPA) in complex with CRL4 ($CRL4^{\text{COP1-SPA}}$), and LIGHT RESPONSE BROAD-COMPLEX, TRAMTRACK AND BRIC A BRACS (LRB) in complex with CRL3 ($CRL3^{\text{LRBs}}$) (Chen et al. 2021; Liu et al. 2016b), and further degraded by 26S proteasomes (Yu et al. 2007; Liu et al. 2022), desensitizing the CRY-mediated blue

light signaling pathway (Miao et al. 2022; Chen et al. 2021). Recently, we found that two deubiquitinases (DUBs), UBIQUITIN-SPECIFIC PROTEASE 12 (UBP12) and UBP13 (UBP12/13), interact with CRY2 in a blue light-dependent manner and stabilize COP1 (Lindback et al. 2022), which contributes to the blue light-specific degradation of CRY2 mediated by COP1 (Lindback et al. 2022).

Ubiquitination marks are important for both plant and animal DDR. For example, SOG1 in plants is stabilized through ubiquitination by DNA DAMAGE RESPONSE MUTANTS 1 (DDRM1), contributing to the homologous recombination (HR) repair upon DNA damage (Wang et al. 2022). Moreover, animal p53 is ubiquitinated by the E3 ligase MURINE DOUBLE MINUTE 2 (Mdm2), leading to the degradation of p53 and the depletion of p53 from the nucleus (Brooks and Gu 2011). Therefore, DUBs that removes the ubiquitination marks have been identified as important regulators of DDR, especially in animals. For example, the UBP12/13 homolog in animals, ubiquitin-specific protease 7 (USP7), deubiquitinates p53 and Chk1 to stabilize them (Valles et al. 2020). In addition, USP3 deubiquitinates histone H2A and H2AX, negatively regulating the recruitment of DNA damage repair proteins (Sharma et al. 2014). However, despite the role of ubiquitination in the DDR being largely conserved in plants, how plant DUBs are regulating the DDR remains largely unexplored.

Present-day CRYs have lost their enzymatic activity to repair pyrimidine dimers directly (Hsu et al. 1996), but continue to bind preferentially to CPD-containing DNA and regulate DDR in mammals (Özgür and Sancar 2003; Papp et al. 2015). Evidence in *Arabidopsis* suggests that CRYs affect the activity of the UVB receptor UV RESISTANCE LOCUS 8 (UVR8) in a blue-light dependent manner and, therefore, are involved in UVB tolerance under natural light conditions (Tissot and Ulm 2020; Rai et al. 2020, 2019). However, the role of plant CRYs in the DDR is not well understood. In this study, we demonstrate that CRYs act as positive regulators of DDR in plants when exposed to UVC, promoting the repair of UV-induced CPDs and the expression of DDR-related genes. Additionally, we show two known CRY2 regulators, UBP12 and UBP13 DUBs, counteract the activity of CRYs, thus revealing the important role of deubiquitinases in DDR in plants. Through transcriptomic analysis of CRY and UBP12/13 mutants during DDR, we identify CALMODULIN-BINDING

TRANSCRIPTION ACTIVATORs (CAMTAs) as novel regulators of DDR that potentially act downstream of the CRY-UBP12/13 module. Furthermore, we also find that UVC enhances CRY2-UBP13 interaction, resulting in the degradation of CRY2. Furthermore, we observed the formation of punctate nuclear bodies (photobodies) of CRY2 upon UVC exposure. In summary, we reveal that the CRYs-UBP12/13 module is harnessed by plants to not only optimize growth in accord with visible light signals, but also establish resistance against UV-caused DNA damage.

2.3 Results

2.3.1 CRY1/2 promote, whereas UBP12/13 inhibit resistance against DNA damage

To elucidate the role of CRY1 and CRY2 (CRY1/2) and UBP12/13 in the DDR, we examined the phenotype of *Arabidopsis* single and double CRY1 and CRY2 mutants along with UBP13 overexpressing seedlings (*UBP13oe*) and the double mutant *ubp12ubp13*, as UBP12 and UBP13 are genetically redundant (Cui et al. 2013; Lindback et al. 2022). To induce DDR, we employed UVC, which is a known genotoxin (Molinier et al. 2005). We treated 4-day-old light-grown seedlings with 0, 5500, 8000 J/m^2 UVC, then grew them back under light for 6 days before inspecting their phenotype (Figure 2.2A). At 5500 and 8000 J/m^2 UVC, *cry1*, *cry2*, *cry1cry2* and *UBP13oe* showed pale cotyledons, while *ubp12ubp13* and wild-type (WT) did not (Figures 2.1A and 2.2B). To assess plant growth and survival after DNA damage, we measured seedling weight after UVC treatment. The *cry1*, *cry2*, *cry1cry2* mutants and *UBP13oe* line had lower weights (Figures 2.1B and 2.2C), while *ubp12ubp13* had a ~1.5 times higher weight than the WT after UVC (Figures 2.1B). These results suggest that CRY1/2 positively regulate while UBP12/13 negatively regulate DDR. UBP13 interacts with CRY2 and regulates its blue light signaling pathway (Lindback et al. 2022). Therefore, we examined whether UBP12/13 also act in the same genetic pathway as CRY1/2 during DDR. We examined *cry1cry2;UBP13oe* seedlings upon DNA damage and found that *cry1cry2;UBP13oe* exhibited pale cotyledons and had a lower fresh weight than WT (Figures 2.1A and 2.1B), phenocopying *cry1cry2*

mutants (Figures 2.1A and 2.1B), indicating that UBP13 functions in the same genetic pathway as CRY1/2 to regulate DDR.

Next, to explore whether CRYs are involved in resistance against other genotoxins, we used zeocin, which induces DSBs (Takahashi et al. 2021). *KU70* is required for DSB repair (Tamura et al. 2002), therefore, we used the *ku70* mutant as a positive control. We treated 4-day-old WT, *ku70*, *cry1cry2* seedlings with 0, 4, and 8 μM zeocin for 8 days. As expected, *ku70* was hypersensitive to zeocin as it had a lower fresh weight than WT (Figure 2.2D). However, the fresh weight of *cry1cry2* and WT was similar after zeocin treatment (Figure 2.2D), indicating that CRYs are not required to resist DSB. Therefore, we focused on the UVC-induced DDR for the scope of our study. Our combined results suggest that CRY1 and CRY2 both play a positive role in DDR. Furthermore, UBP12 and UBP13 function in the same genetic pathway as CRY1/2 to negatively regulate DDR.

2.3.2 Loss of CRY1 and CRY2 leads to higher CPD accumulation and lower DNA repair

Absorption of UV results predominately in CPD-type DNA damage, where cytosine (C) to thymine (T) or CC to TT mutations occur (Pfeifer et al. 2005) (Figure 2.1C). Changes in CPD levels can be used to track the progress of DNA damage repair after UVC exposure (Castells et al. 2010). Therefore, to examine whether DNA damage repair is misregulated in *cry1cry2* and *ubp12ubp13*, we measured CPD levels in these mutants by dot-blot analysis after UVC exposure. 5-day-old light-grown plants were treated with UVC (6000 J/m^2) and recovered in light for 1 min and 180 min. Genomic DNA was then extracted and dot-blotted at different serial dilutions to increase the dynamic range of detection. Using an anti-CPD antibody, we detected CPD in WT, *cry1cry2*, and *ubp12ubp13* 1 min after UVC exposure (Figures 2.1D and 2.2E), indicating accumulation of DNA damage in all three genotypes. In WT, the accumulated CPD decreased at 180 min suggesting CPD repair, as expected, while *ubp12ubp13* exhibited even lower CPD levels at 180 min (Figures 2.1D, 2.1E and 2.2E), suggesting enhanced CPD repair. Importantly, CPD levels in *cry1cry2* remained mostly unchanged 180 min after UVC exposure (Figures 2.1D, 2.1E and 2.2E), indicating impaired CPD repair in this mutant.

UVC and UVB stresses induce the phosphorylation and consequent activation of MAP KINASE 3 (MPK3) and 6 (MPK6) (Ulm et al. 2001; Besteiro et al. 2011), which are gradually dephosphorylated as plants recover from the stress (Besteiro et al. 2011). Also, in this context, deficiencies in CPD repair are related to the hyper-phosphorylation of the two kinases[43]. Similarly, mutants with sustained levels of phosphorylated MPK3 ($MPK3^P$) and $MPK6^P$ following UVB radiation are hypersensitive to this genotoxic treatment (Besteiro et al. 2011). Since we observed differences in sensitivity to UVC-induced DNA damage and CPD repair rates, we wondered if MPK3 and MPK6 were differentially phosphorylated in *cry1cry2* and *ubp12ubp13* mutants relative to WT. For this, we extracted proteins from 5-day-old seedlings that were either untreated (0 min) or treated by UVC and collected after 10 min or 20 min of recovery. We detected the phosphorylated forms of the two kinases in an immunoblot using an anti- $MPK3^P$ and -$MPK6^P$ antibody (Besteiro et al. 2011). In all three genotypes, $MPK3^P$ and -$MPK6^P$ were only detected after UVC treatment and decreased after 20 min of recovery (Figure 2.1F). We then quantified the levels of $MPK6^P$, which is the most abundant of the two detected MPKs (Figure 2.1F). Compared to WT, levels of $MPK6^P$ were increased in the hypersensitive *cry1cry2* and decreased in the resistant *ubp12ubp13* after UVC (Figures 2.1F and 2.2F). Therefore, $MPK6^P$ dephosphorylation during recovery was delayed in *cry1cry2* mutant and accelerated in *ubp12ubp13*, correlating with CPD levels in these genotypes (Figures 2.1D, 2.1E and 2.2E), which might explain their different sensitivities to UVC treatment (Figures 2.1A and 2.1B).

Apart from CPDs, UV also induces DSBs, the repair of which requires BREAST CANCER GENE 1 (BRCA1) and RAD51 (Culligan et al. 2006). Moreover, DNA damage induces the expression of *BRCA1* and *RAD51* (Ogita et al. 2018). Therefore, to check for the DNA repair activity in WT, *cry1cry2* and *ubp12ubp13*, we measured the expression of *BRCA1* and *RAD51* in these three genotypes 1.5 h after UVC by reverse transcription-quantitative polymerase chain reaction (RT-qPCR). In WT, *BRCA1* and *RAD51* were induced by UVC compared to untreated samples (Figure 2.2G), suggesting normal DNA repair activity. In contrast, *BRCA1* and *RAD51* were not induced in *cry1cry2* upon UVC (Figure 2.2G), suggesting impaired DNA repair activity. Moreover, *BRCA1* and *RAD51* gene

expression in *ubp12ubp13* was already higher than WT in untreated samples, then diminished after UVC treatment (Figure 2.2G), suggesting that *ubp12ubp13* had increased DNA repair activity. Because RAD51 protein is directly involved in DNA damage repair and DNA damage induces the accumulation of RAD51 protein (Li et al. 2004b; Ulm et al. 2004; Rodriguez et al. 2018), we next measured the accumulation of RAD51 protein after UVC to corroborate the qPCR assays. We treated 5-day-old seedlings with UVC (6000 J/m^2) and allowed them to recover for either 1 or 2 h before total proteins were extracted for immunoblot analysis using an anti-RAD51 antibody. In WT, RAD51 levels increased at 1 h after UVC exposure when compared with the untreated samples (0 h) and then recovered to basal levels at 2 h indicating normal DNA repair activity (Figures 2.1G and 2.2H). In contrast, induction of RAD51 was not observed in *cry1cry2* at either 1 h or 2 h after UVC exposure indicating the absence of DNA repair activity (Figures 2.1G and 2.2H). Interestingly, RAD51 levels were already higher in *ubp12ubp13* untreated seedlings when compared to WT and *cry1cry2*, but its levels diminished at 1 h and 2 h after UVC (Figures 2.1G and 2.2H), suggesting enhanced DNA repair activity. Altogether, these results indicate that *cry1cry2* has impaired while *ubp12ubp13* has enhanced DNA repair activity under UVC. Collectively, these findings reinforce that CRYs positively mediate DDR, while UBP12/13 negatively regulate DDR.

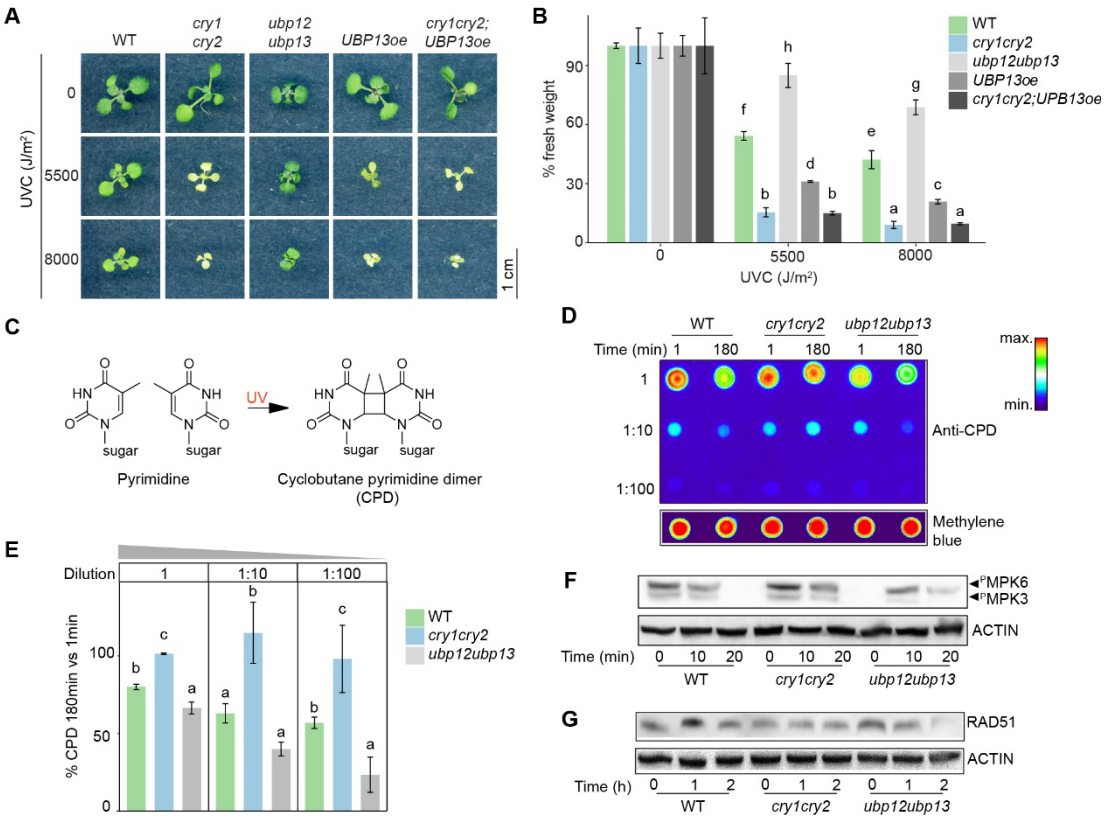

Figure 2.1: *Arabidopsis* plants deficient in CRY1 and CRY2 are susceptible to UVC-induced DNA damage, while mutants of UBP12 and UBP13 are not.

(A) Phenotype of representative 10-day-old seedlings of the indicated genotypes treated with indicated intensities of UVC. 4-day-old light-grown seedlings were treated with UVC and then returned to white light for 6 days before examination of the phenotype. (B) Fresh weight of 10-day-old seedlings of the indicated genotypes treated with indicated UVC doses as described in (A). Fresh weight was normalized to the untreated (0 J/m^2) samples of the same genotype. (C) Schematic diagram illustrating the UV-induced formation of a CPD from two adjacent pyrimidines (two thymine bases shown as an example). (D) Representative dot blot showing CPD levels on the genomic DNA from the indicated genotypes. After treating 5-day-old seedlings with 6000 J/m2 UVC, genomic DNA was extracted after 1 or 180 minutes and serially diluted and CPD was detected using an anti-CPD antibody by immunoblotting. Serial dilutions of the genomic DNA were blotted: 1, 1:10, and 1:100. The immunoblot has been pseudo-colored to reflect the difference in intensities of CPD levels. Methylene blue staining shows equal loading of genomic DNA. (E) Quantification of CPD levels using replicates of the dot blot shown in (D). The percentage of CPD was derived by normalizing the CPD level at 180 min to 1 min of the same genotype. One-way analysis of variance (ANOVA) analysis was separately performed for each serial dilution. (F, G) Immunoblot analysis of phosphorylated MPK6 and MPK3 (F) and RAD51 (G) in indicated genotypes at indicated time points after UVC exposure. 5-day-old seedlings were untreated (0 min) or treated with 6000 J/m2 UVC and collected after 10 or 20 min in (F) and 1 or 2 h in (G). ACTIN was used to normalize the amount of total protein. For (B) and (E), different letters indicate $p<0.05$ for one-way ANOVA analysis followed by Fisher's least significant difference (LSD) posthoc test. Data show means ± standard deviation (SD), n = 3 independent replicates.

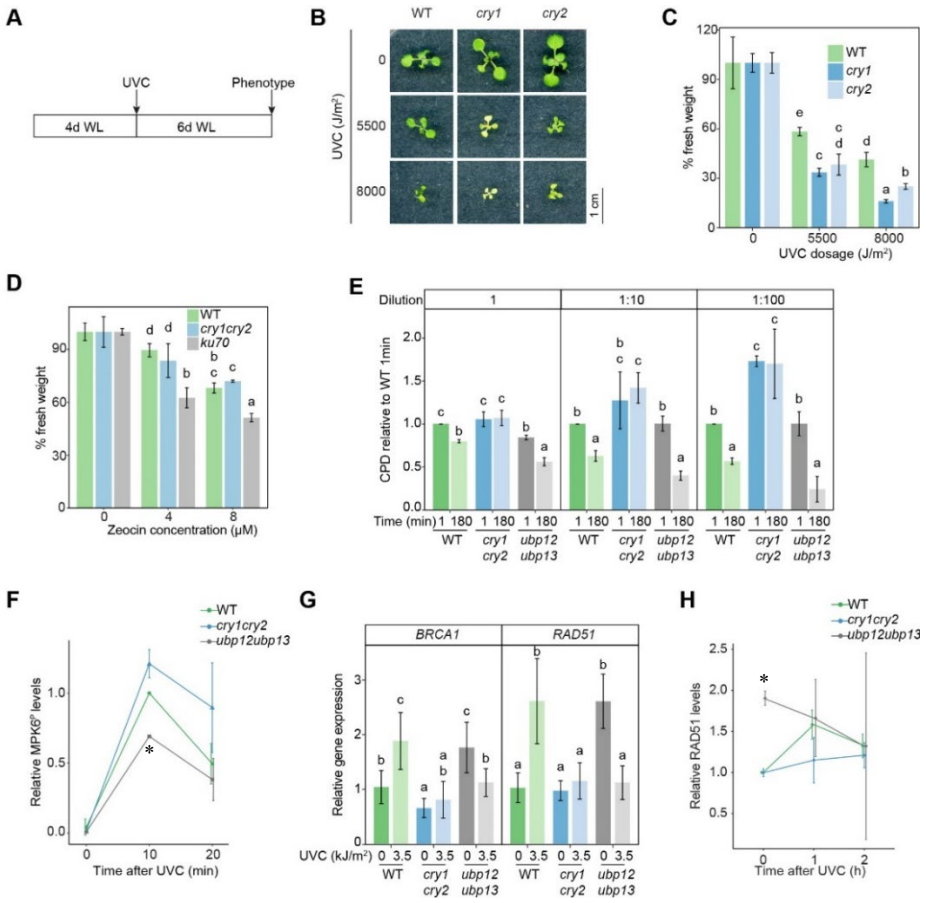

Figure 2.2: *cry1cry2* mutants were hypersensitive to UVC while *ubp12ubp13* mutants were hyposensitive to UVC.

(A) Schematic diagram illustrating the UVC treatment and phenotyping. 4-day-old seedlings grown in continuous white light (WL) were treated with UVC and grown in continuous WL for another 6 d before examination of phenotype. (B) Phenotype of representative 10-day-old seedlings of the indicated genotypes treated with indicated UVC doses as described in (A). (C) Fresh weight of 10-day-old seedlings of the indicated genotypes treated with indicated UVC doses as described in (A). Fresh weight was normalized to the untreated (0 J/m^2) samples of the same genotype, n = 3. (D) Fresh weight of 12-day-old seedlings of the indicated genotypes treated with indicated concentrations of zeocin. 4-day-old seedlings grown in light and regular growth medium were transferred to a growth medium containing zeocin and grown for another 8 d before examination of phenotype. Fresh weight was normalized to the untreated (0 μM) samples of the same genotype. n = 3. (E) Quantification of relative CPD levels using replicates of the dot blot shown in Figure 1D. The CPD levels were normalized to the average levels in WT at 1 min after UVC exposure for each dilution. One-way ANOVA analysis was separately performed for each dilution. n = 3. (F) Quantification of phosphorylated MPK6 (MPK6^P) levels from replicates of Figure S1I. MPK6^P levels were normalized to WT at 10 min for each blot. n = 2. (G) Relative expression of *BRCA1* and *RAD51* genes derived from RT-qPCR analysis. 3-day-old etiolated seedlings were untreated (0 kJ/m^2) or treated with 3.5 kJ/m^2 of UVC and incubated in white light for 1.5 h before tissue collection. n = 3. (H) Quantification of RAD51 protein levels using replicates of Figure S1G. RAD51 levels were normalized to WT at 0 h for each blot. n = 2. For (C), (D), (E) and (G), different letters mean $p<0.05$ for one-way ANOVA analysis followed by Fisher's LSD posthoc test. For (C-H), data show means ± standard deviation (SD) of independent replicates. For (F) and (H), asterisks indicate $p<0.05$ for Student's t test compared to WT at the same time point.

2.3.3 CRYs promote while UBP12/13 inhibit the transcriptional response to UVC

To obtain further insights into how genetic losses of CRYs and UBP12/13 affect the transcriptional response to DNA damage, we analyzed a time-course transcriptome by RNA-sequencing (RNA-seq) in WT, *cry1cry2,* and *ubp12ubp13* after UVC. First, to select optimal sampling time points for the RNA-seq, we did an exploratory RT-qPCR assay in WT at 0, 15, 30, 60, 120 and 180 min after UVC. We then analyzed four known UV-responsive genes, *BRCA1*, *RAD51*, *PHOTOLYASE 1* (*PHR1*) and *CINNAMATE-4-HYDROXYLASE* (*C4H*) (Molinier et al. 2005; Jin 2000; Kliebenstein et al. 2002) (Figure 2.4A). We found that *BRCA1* was strongly induced early in our time course, 15 min after the UVC treatment (Figure 2.4A). *PHR1* expression peaked at 60 min (Figure 2.4A), while *BRCA1*, *RAD51* and *C4H* peaked at 180 min after UVC (Figure 2.4A). Since these three time points (15, 60 and 180 min) seemed to cover early as well as peak induction of our selected marker genes (Figure 2.4A), they were chosen for the RNA-seq experiment.

5-day-old seedlings of WT, *cry1cry2* and *ubp12ubp13* were harvested before (0 min) and 15, 60 and 180 min after UVC treatment (Figure 2.3A). Biological replicates in the RNA-seq are highly similar as evidenced by the high Pearson's correlation coefficient (0.92 to 1) (Figure 2.4B) and the close proximity of replicates in the principal component analysis (PCA) plot (Figure 2.4C). To explore the pathways by which CRYs and UBP12/13 regulate the transcriptional response to DNA damage, we obtained differentially expressed genes (DEGs) from the RNA-seq. We identified DEGs (defined as false discovery rate-adjusted p value (q value) < 0.05) for each genotype by comparing the gene expression at 15 min, 60 min and 180 min to 0 min, respectively. DEGs in *cry1cry2* and *ubp12ubp13* relative to WT were obtained by comparing the gene expression in the corresponding mutant to WT at all four time points.

We then used these DEG lists to perform gene ontology (GO) enrichment analysis (Table S1). The top 10 GO terms enriched in the upregulated genes in WT at 15, 60 and 180 min included many stress-related GO terms (Figure 2.4D, Table S1), consistent with known studies reporting that UVC can induce stress responses (Tsurumoto et al. 2022). Importantly, in *cry1cry2* and *ubp12ubp13* these stress-

related GO terms were enriched in the downregulated and upregulated genes relative to WT, respectively (Figure 2.4D), suggesting that the transcriptomic response to UVC-induced DNA damage is less prominent in *cry1cry2* and enhanced in *ubp12ubp13*. Next, we found that the GO term "response to UV" was significantly enriched in the genes upregulated in WT (Figure 2.3B, Table S1), as expected. Importantly, this GO term was enriched in genes downregulated in *cry1cry2* and upregulated in *ubp12ubp13* relative to the WT (Figure 2.3B, Table S1). The expression of genes in the GO term "response to UV" was not significantly changed in *cry1cry2* or *ubp12ubp13* relative to WT at 0 min, but was lower in *cry1cry2* and higher in *ubp12ubp13* compared to WT at 60 min (Figure 2.3C, Table S2), suggesting that, after UVC treatment, genes in the known UV-responsive pathways are less induced in *cry1cry2* and more induced in *ubp12ubp13* compared to WT. Upon UV-induced DNA damage, DDR can trigger programmed cell death to protect genome integrity (Danon et al. 2004). Accordingly, the GO term "programmed cell death" is highly enriched in the upregulated genes in WT (Figure 2.3B). Moreover, this GO term is enriched in the downregulated genes in *cry1cry2* and upregulated genes in *ubp12ubp13* relative to WT (Figure 2.3B). The expression of genes involved in the GO term "programmed cell death" also showed less induction in *cry1cry2* at 60 min compared to WT (Figure 2.3D, Table S2), suggesting that the UVC-induced programmed cell death may be diminished in *cry1cry2*, possibly contributing to the hypersensitive phenotype of *cry1cry2* (Figures 2.1A and 2.1B). Altogether, these results suggest that DNA damage-induced transcriptional responses are weaker in *cry1cry2* and stronger in *ubp12ubp13* compared to WT.

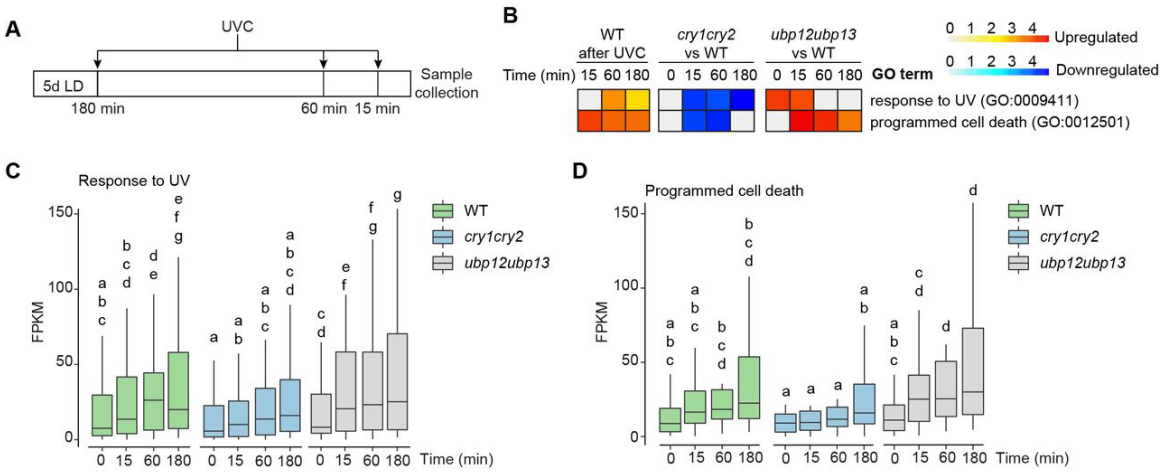

Figure 2.3: CRYs promote while UBP12 and UBP13 inhibit DNA damage-induced stress response. (A) Schematic diagram illustrating the UVC treatment for the RNA-seq samples. 5-day-old light-grown seedlings were treated with 6000 J/m^2 of UVC and collected after 0, 15, 60, and 180 min of recovery time in white light. (B) Heatmap of the GO terms "response to UV" and "programmed cell death" in the upregulated genes in WT, downregulated genes in *cry1cry2* relative to WT and upregulated genes in *ubp12ubp13* relative to WT at indicated time points after UVC. The fold enrichment of non-statistically significant GO terms (false discovery rate ≥0.05) was manually set to 0. (C, D) Boxplot showing the expression levels (fragments per kilobase million, FPKM) of genes in the GO term "response to UV" (C) and "programmed cell death" (D) in WT, *cry1cry2* and *ubp12ubp13*. Only genes downregulated in *cry1cry2* relative to WT are shown. Different letters indicate $p<0.05$ for two-way ANOVA analysis followed by Fisher's LSD posthoc test.

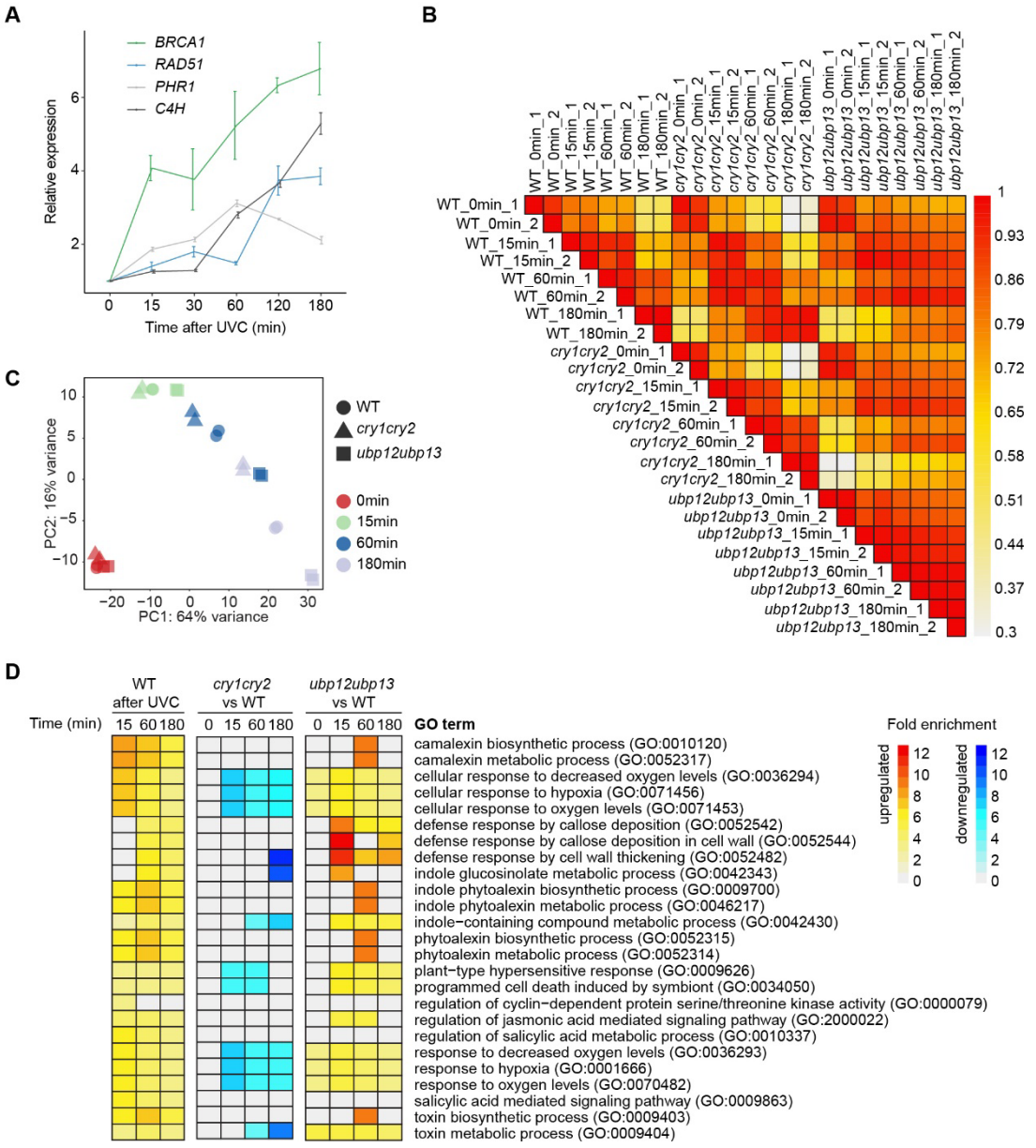

Figure 2.4: Transcriptional response to UVC is diminished in *cry1cry2* and enhanced in *ubp12ubp13*.

(A) Relative expression of UV-responsive genes at indicated time points after UVC treatment derived from qRT-PCR analysis. 5-day-old light-grown WT seedlings were treated with 6000 J/m^2 of UVC and collected after 0, 15, 30, 60, 120, and 180 min. Data show means ± SD. n = 3. (B) Pearson's correlation coefficient between all 24 RNA-seq samples. Coefficient was calculated based on the FPKM values of all genes in the transcriptome. (C) Principal component analysis of all RNA-seq samples using normalized read counts. (D) Heatmap of the top 10 GO terms enriched in the upregulated genes of WT at 15, 60 and 180 min.

2.3.4 CAMTAs mediate DDR

To gain insights into how the DEGs in WT are coordinately regulated during the UVC-induced DDR, we performed a Dynamic Regulatory Events Miner (DREM) analysis to generate a model of the underlying gene regulatory network (Ernst et al. 2007; Schulz et al. 2012). DREM analysis takes time-course gene expression data as input, assigns genes into different groups based on similar expression patterns and predicts which transcription factors might be responsible for modulating the expression of each group of genes (Ernst et al. 2007; Schulz et al. 2012). We first analyzed the expression of the DEGs in the WT along the time course after UVC and uncovered seven groups of co-expressed genes (W1-7) in the DREM model (Figure 2.5A). In the WT DREM model, SOG1, WRKYs and CAMTAs were predicted to regulate the induction of gene expression upon UVC treatment (Figure 2.5A). Since CAMTAs were predicted to regulate the most upregulated branch (consisting of paths W1, 2 and 7) for the early gene expression change at 15 min (Figure 2.5A), we next focused on studying the role of CAMTAs in the UVC-induced DDR. First, to corroborate the DREM prediction, we performed a *de novo* motif search in the promoters of the genes within the W1, 2 and 7 paths (Figure 2.5A, Table S2) (Heinz et al. 2010), and found a highly enriched "CGCGTT" motif (Figure 2.5B), which is a known CAMTA-binding DNA element, the rapid stress response element (Benn et al. 2014), suggesting the CAMTAs can bind to the promoters of genes in the W1, 2, and 7 paths. Furthermore, when all DEGs were considered, *de novo* motif search identified CAMTA-binding motifs enriched in the promoters of only the upregulated but not downregulated genes in WT after UVC treatment (Figures 2.6A and 2.6B). These results suggest that CAMTAs might be required for the induction of DEGs in WT during DDR. CAMTA 1, 2 and 3 are involved in various abiotic and biotic stress responses (Iqbal et al. 2020), but their possible role in DDR remains unexplored. To address this, we treated *camta1camta2camta3* (hereafter *camta123*) triple mutant with UVC. Similar to *cry1cry2*, the *camta123* mutant had pale cotyledons and a lower fresh weight than WT after UVC treatment (Figures 2.5C and 2.5D), suggesting that CAMTAs are indeed required for DDR.

We next asked whether CRYs and UBP12/13 would regulate the DDR through CAMTAs as well. To test this hypothesis, we generated DREM models using expression of the DEGs derived from *cry1cry2* and *ubp12ubp13* (Figures 2.6C and 2.6D) along the time course. In both the *cry1cry2* and *ubp12ubp13* models, SOG1 and WRKYs were predicted to regulate gene expression after UVC (Figures 2.6C and 2.6D). However, CAMTAs were only predicted in the *ubp12ubp13* but not in the *cry1cry2* DREM model (Figures 2.6C and 2.6D). This suggests that CAMTAs may be dysregulated in the *cry1cry2* mutant. To explore this possibility, we compared the expression of CAMTA3 target genes in *cry1cry2* and *ubp12ubp13* to WT, respectively. We obtained UVC-inducible CAMTA3 target genes by overlapping the upregulated genes in WT after UVC in our RNA-seq data with targets of CAMTA3 previously identified by chromatin immunoprecipitation sequencing (ChIP-seq) (Table S2) (Matsumura et al. 2022). Compared to WT, these CAMTA3 target genes were less induced in *cry1cry2* and more induced in *ubp12ubp13* at 15 min and 60 min after UVC (Figure 2.5E, Table S2). Interestingly, the UVC-inducible CAMTA3 target genes are enriched in GO terms related to stress responses (Figure 2.5F, Table S3), which is similar to the upregulated GO terms in WT after UVC (Figure 2.4D), suggesting that CRYs and UBP12/13 may antagonistically regulate the DNA damage-induced transcriptional changes partially through the CAMTAs.

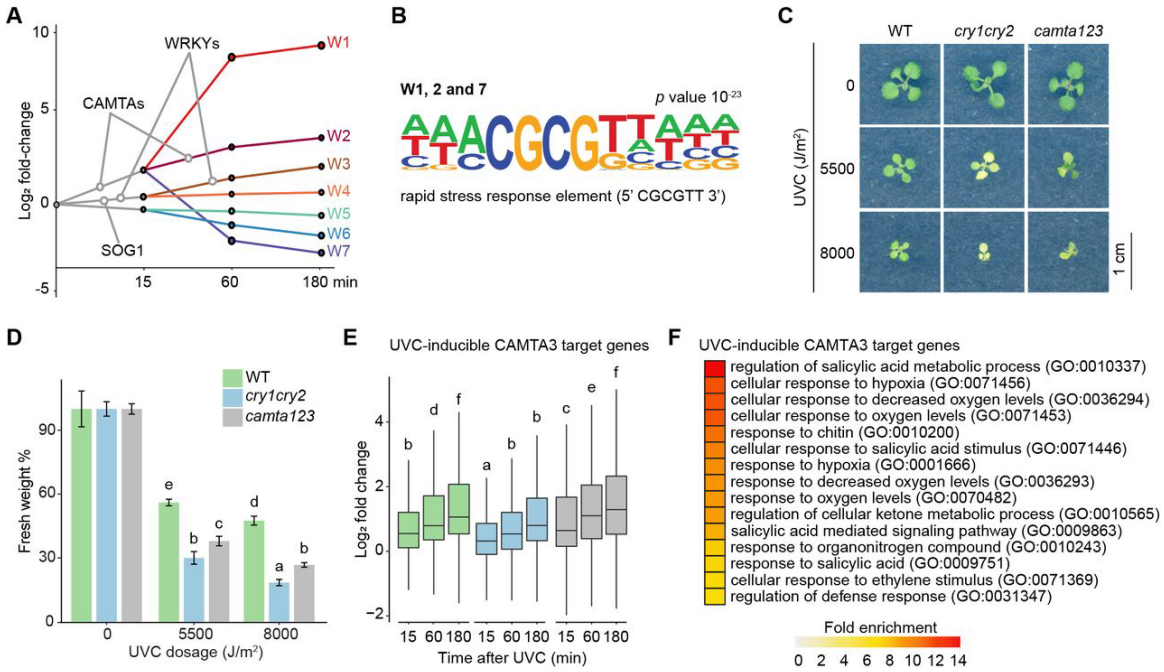

Figure 2.5: CAMTAs are required for DDR.

(A) Groups of co-expressed DEGs in WT after UVC. 7 co-expressed groups of genes (W1-7) were identified. CAMTAs, SOG1 and WRKYs TFs were predicted to regulate the indicated groups. (B) Consensus sequence of the top cis-regulatory motif found in the promoters of W1, 2 and 7 genes shown in (A). (C) Phenotype of representative 10-day-old seedlings of the indicated genotypes treated with indicated UVC doses. 4-day-old light-grown seedlings were treated with UVC and then returned to white light for 6 days before examination of the phenotype. (D) Fresh weight of 10-day-old seedlings of the indicated genotypes treated with indicated UVC doses as in (C). Fresh weight was normalized to the untreated (0 J/m^2) samples of the same genotype. n = 3 independent replicates. (E) Log_2 fold change of gene expression of UVC-inducible CAMTA3 target genes in indicated genotypes at indicated time points. (F) Heatmap showing the fold enrichment of the top 15 GO terms enriched in UVC-inducible CAMTA3 target genes. For (D) and (E), data show means ± SD. Different letters mean $p<0.05$ for ANOVA analysis followed by Fisher's LSD posthoc test.

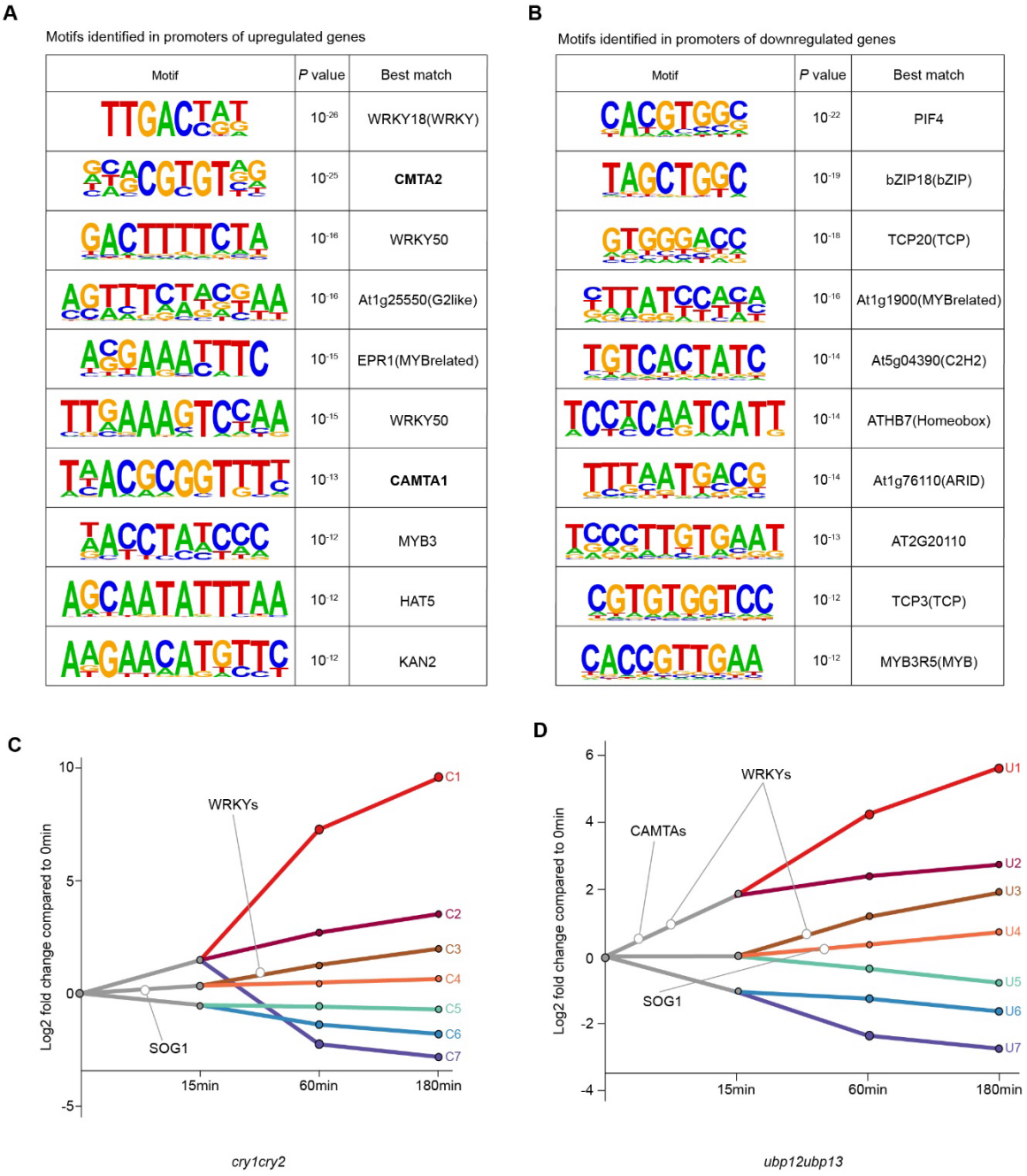

Figure 2.6: CAMTAs regulate transcriptional responses to UVC.
(A, B) Top 10 significant *cis*-regulatory motifs identified in the promoters of all upregulated (A) and downregulated (B) genes in WT after UVC. (C, D) DREM model showing co-expressed gene groups and predicted transcription factors of all DEGs in *cry1cry2* (C) and *ubp12ubp13* (D) after UVC.

2.3.5 UVC induces the UBP12/13-dependent CRY2 degradation

We found that UBP12/13 and CRYs had opposite functions in the response to UVC (Figures 2.1B, 2.1E and 2.3C), which is reminiscent of the opposite roles of UBP13 and CRY2 in blue light signaling pathway (Lindback et al. 2022), where UBP13 interacts with CRY2 in a blue light-dependent manner (Lindback et al. 2022). Therefore, we asked whether UVC could also enhance the interaction between CRY2 and UBP13, similar to blue light. To address this, we treated 5-day-old seedlings expressing both FLAG-CRY2 and UBP13-HA with or without UVC and performed co-immunoprecipitation (co-IP) analysis using a FLAG antibody. The UVC light was obtained through a light-emitting diode (LED) lamp, which did not contain UVA or blue light (Figure 2.8A). This UVC LED lamp also induced the hypersensitive phenotype of the *cry1cry2* mutant (Figure 2.8B). We found that compared to untreated samples, UVC-treated seedlings exhibited enhanced interaction between CRY2 and UBP13 (Figure 2.7A). This result suggests that UVC can strengthen the interaction between CRY2 and UBP13.

Blue light-enhanced interaction between UBP13 and CRY2 promotes COP1-mediated CRY2 degradation (Lindback et al. 2022), therefore, we next asked whether UVC also induces CRY2 degradation. To test this hypothesis, we treated 5-day-old *cry2* mutant seedlings expressing FLAG-CRY2 with UVC and analyzed FLAG-CRY2 protein levels after 0, 1, and 3 h. We found that FLAG-CRY2 protein levels diminished 1 h after UVC and partially recovered 3 h after UVC (Figures 2.7B and 2.8C), suggesting that UVC can induce CRY2 degradation. Next, we asked whether UVC-induced CRY2 degradation was dependent on UBP12/13. We treated *ubp12ubp13* seedlings expressing FLAG-CRY2 with UVC, and found that FLAG-CRY2 was more stable in the *ubp12ub13* mutant background than in the *cry2* mutant background in UVC (Figures 2.7B and 2.8C). This result suggests that UVC-induced CRY2 degradation is partially dependent on UBP12/13. In blue light, UBP12/13 regulates CRY2 degradation through COP1 (Lindback et al. 2022). Therefore, we next examined whether COP1 plays a role in UVC response. To address this hypothesis, we treated *cop1-4* and *COP1oe* seedlings with UVC and found that *cop1-4* is hyposensitive while *COP1oe* is hypersensitive to DNA damage

(Figures 2.8D and 2.8E), suggesting that COP1, similar to UBP12/13, promotes plant resistance against UVC-induced DNA damage. Together, these results indicate that UBP12/13 may regulate DDR by interacting with CRY2 and modulating CRY2 degradation.

2.3.6 UVC induces the formation of CRY2 nuclear speckles

Upon exposure to blue light, CRY1 and CRY2 form punctate nuclear speckles, also known as photobodies (Liu et al. 2022; Yu et al. 2009). Since we found that UVC could enhance the CRY2-UBP13 interaction and induce UBP12/13-dependent CRY2 degradation, similar to blue light, we next examined if UVC could also induce CRY2 speckles. We treated 4-day-old dark-grown *cry2;CRY2-mCitrine* and *cry2;mCitrine-CRY2* seedlings with blue light, UVC light from the LED lamp or continued darkness to observe speckle formation of CRY2. To excite mCitrine in confocal microscopy, a blue light source is often used (Thompson and Wolniak 2008). Therefore, to prevent microscopy-induced CRY2 speckles, we used a mild fixative to crosslink proteins in seedlings before confocal imaging (Yu et al. 2009). C-terminally tagged CRY2, such as CRY2-GFP, is known to readily form speckles in blue light while N-terminally tagged CRY2, like GFP-CRY2, requires blocking of proteasome-mediated protein degradation to form speckles in blue light (Yu et al. 2009). Therefore, we first examined the formation of speckles of CRY2-mCitrine in *Arabidopsis* seedlings. As expected, in darkness we did not observe CRY2-mCitrine speckles (Figures 2.7C and 2.8F), while in blue light (40 μmol m^{-2} s^{-1}) and UVC (approximately 1800 J/m^2) speckles formed after 2 min (Figures 2.7C and 2.8F). Next, we examined whether mCitrine-CRY2 could also form speckles under UVC. mCitrine-CRY2 did not form speckles in the dark (Figure 2.8G), in contrast, it formed nuclear speckles after 30 min of blue light (40 μmol m^{-2} s^{-1}) and under UVC (30 min; approximately 100 J/m^2) (Figure 2.8G). Together, these results suggest that UVC can induce the formation of CRY2 nuclear speckles.

The ability of CRY2 to absorb blue light to form speckles is dependent on its covalently bound chromophore, flavin adenine dinucleotide (FAD) (Banerjee et al. 2007; Che et al. 2015). To test if CRY2 requires its light-sensing property to form speckles under UVC, we generated $CRY2^{D387A}$ where

aspartic acid 387 was substituted with alanine within the FAD-binding pocket, rendering it light-insensitive (Liu et al. 2008a). mCitrine-CRY2^{D387A} did not form speckles in dark, blue light, or UVC (Figure 2.8H), suggesting that CRY2 requires its light-sensing ability to form nuclear speckles under UVC. To check whether CRY2 forms nuclear speckles in UVC when expressed in a heterologous system, we transiently expressed CRY2-mCitrine as well as CRY2^{D387A}-mCitrine in *Nicotiana benthamiana*. We found that CRY2-mCitrine formed nuclear speckles under blue light and UVC (Figure 2.7D), while CRY2^{D387A}-mCitrine remained uniformly distributed in the nucleus in dark, blue light and UVC (Figure 2.7E). This result strengthens the conclusion that *Arabidopsis* CRY2 requires its light-sensing activity to form nuclear speckles under UVC. Taken together, our data suggested that UVC induces similar changes in CRY2 as blue light, including enhancing the interaction between CRY2 and UBP13, inducing CRY2 degradation and triggering CRY2 nuclear speckle formation.

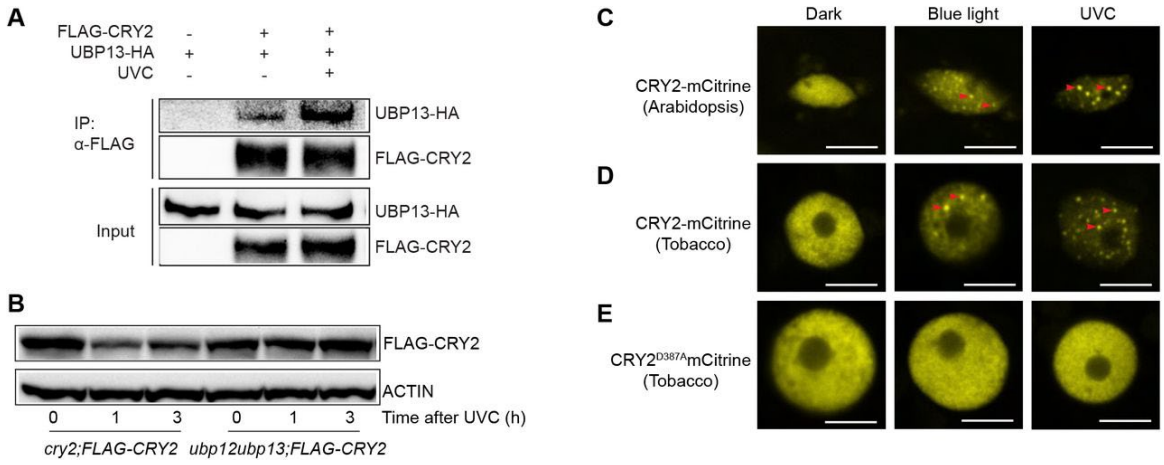

Figure 2.7: CRY2 interaction with UBP13 and nuclear speckle formation is induced by UVC.
(A) Co-IP immunoblot showing enhanced pulldown of UBP13-HA by FLAG-CRY2 after UVC treatment. 4-day-old light-grown seedlings expressing FLAG-CRY2 and UBP13-HA were dark adapted for 24 h, then treated or untreated with approximately 1800 J/m^2 of UVC from the LED source and collected after 10 min incubation in the dark. Seedlings expressing only UBP13-HA without UVC treatment were used as a negative control for the co-IP. (B) Immunoblot analysis of FLAG-CRY2 levels after UVC treatment in the *cry2* and *ubp12ubp13* mutant backgrounds. 5-day-old light-grown seedlings were treated with 6000 J/m^2 of UVC and collected after 0, 1, and 3 h. (C-E) Representative confocal microscopy images of nuclei in plants expressing CRY2-mCitrine (C, D) or CRY2^{D387A}-mCitrine (E) fusions in the dark and after blue light or UVC in transgenic *Arabidopsis* seedlings (C) and infiltrated *Nicotiana benthamiana* leaves (D, E). Samples were fixed before imaging. The scale bar is 5 μm. For (C-D), red arrowheads indicate representative nuclear speckles.

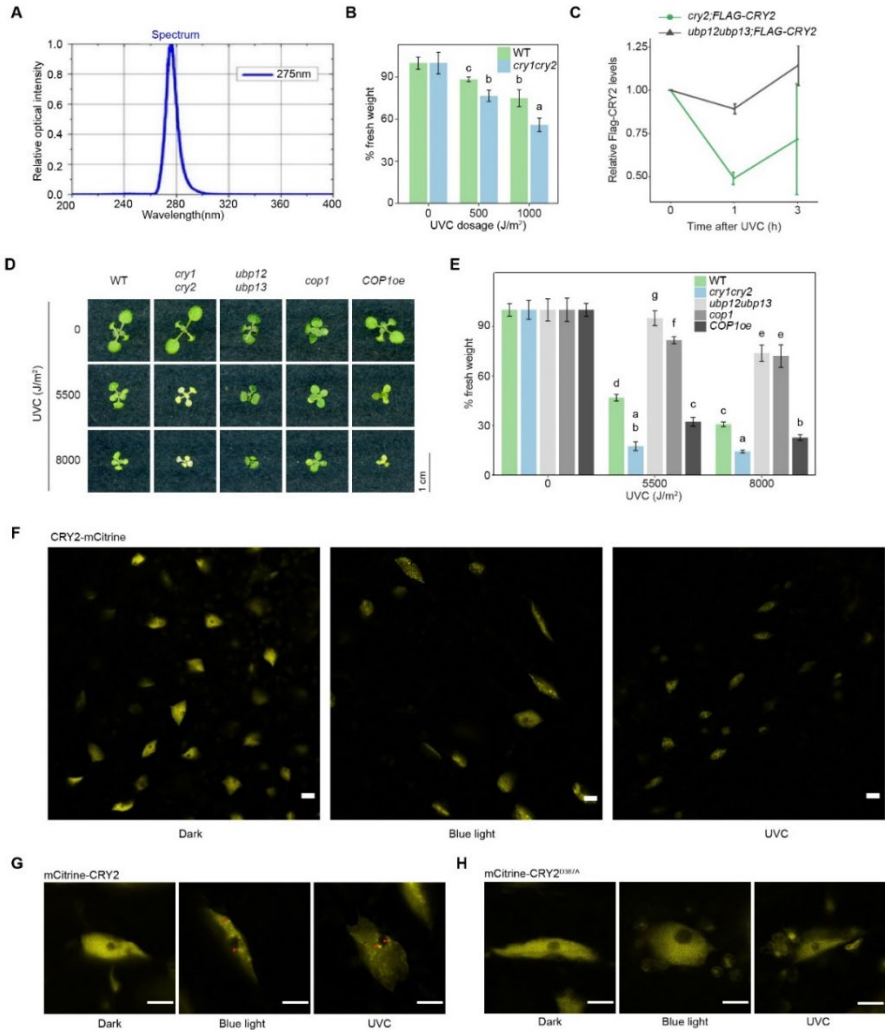

Figure 2.8: UVC induces CRY2 speckle formation.
(A) Spectrum of the light emitted by the UVC LED source adapted from the data sheet provided by the manufacturer (International Light Technologies 2022). (B) Fresh weight of 10-day-old seedlings with indicated genotypes treated with indicated UVC doses by the UVC LED source. 5-day-old light-grown seedlings were treated with UVC and incubated in light for another 5 days before examination of phenotype. Fresh weight was normalized to the untreated (0 J/m^2) samples of the same genotype. n = 3. (C) Quantification of FLAG-CRY2 levels using replicates of Figure 4B. FLAG-CRY2 levels were normalized to the 0 h sample of the same genetic background. Data show means ± SD, n = 2. (D) Phenotype of representative 10-day-old seedlings of the indicated genotypes treated with indicated UVC doses. 4-day-old light-grown seedlings were treated with UVC and then returned to white light for 6 days before examination of the phenotype. (E) Fresh weight of 10-day-old seedlings of the indicated genotypes treated as in (D). The fresh weight percentage was calculated as described in (C). n = 3. (F- H) Representative confocal microscopy images of transgenic *Arabidopsis* seedlings expressing CRY2 and mCitrine fusions. Seedlings were dark grown and either kept in dark or treated with blue light or UVC and fixed before imaging. C-terminal CRY2-mCitrine fusion in (F), and N-terminal mCitrine-CRY2 and mCitrine-CRY2^{D387A} in (G) and (H), respectively. For (B) and (E), different letters mean $p<0.05$ for one-way ANOVA analysis followed by Fisher's LSD posthoc test. Data show means ± SD. For (F-H), the scale bar is 5 μm.

2.4 Discussion

In this study, we demonstrate that DDR is favorably regulated by CRYs in *Arabidopsis*. We also show that UBP12 and UBP13 negatively regulate many aspects of CRY-mediated DDR, including CPD repair and induction of DNA repair genes (Figures 2.1 and 2.2). Through transcriptomic analysis, we found that CRYs and UBP12/13 antagonistically regulate the transcriptional response to DNA damage (Figures 2.3 and 2.4) and identified CAMTA transcription factors as novel regulators of DDR (Figures 2.5 and 2.6). Upon further investigation, we unexpectedly discovered that CRY2 responds to UVC in a manner similar to blue light, such as interacting stronger with UBP13, undergoing UBP12/13-dependent degradation, and forming nuclear speckles (Figures 2.7 and 2.8). Together, our results reveal key roles for CRYs and UBP12/13 in the DDR and suggest a mechanism where UBP12/13 destabilizes CRY2 during the DDR.

Evolved from photolyases, present-day CRYs have lost their enzymatic activity to repair pyrimidine dimers (Hsu et al. 1996), however, they still bind to damaged DNA (Özgür and Sancar 2003), indicating that although CRYs cannot directly repair UV-damaged DNA, they might have a residual function in sensing or responding to DNA damage (Papp et al. 2015). There is evidence in mammals in favor of this hypothesis, as DNA damage affects CRY protein stability: CRY1 is stabilized, while CRY2 is destabilized (Shafi et al. 2021; Papp et al. 2015). The roles of CRYs in DDR can also differ between paralogs (*i.e.* CRY1 and CRY2) and homologs (*e.g.*, human and mouse) (Papp et al. 2015; Shafi et al. 2021). For instance, in human cell lines, stabilized CRY1 promotes DNA repair by regulating genes involved in HR repair of DSBs (Shafi et al. 2021), while mouse CRY1 can function as a transcriptional repressor (Papp et al. 2015). Mouse CRY2 inhibits the transcription of DNA damage responsive genes, therefore, destabilization of CRY2 upon DNA damage releases gene expression and induces DNA damage response (Papp et al. 2015). Here we show that upon UVC-induced DNA damage, plant CRY2 proteins are destabilized, as in mice (Shafi et al. 2021), and that that CRY1 and CRY2 together promote DNA repair by regulating the transcription of genes involved in HR, as well as

RAD51 protein (Figures 2.1G, 2.2G and 2.2H), which is similar to the role of human CRY1 (Shafi et al. 2021). Therefore, our study suggests that not only animal CRYs, but also plant CRYs play a residual role in DDR. Further investigations would be required to address the effects of UVC on CRY1 stabilization in plants and the its functional consequences to DDR.

In mammalian cells, CPDs are mainly repaired by the NER pathway, which removes one strand of DNA containing the damaged site and replaces it with newly synthesized DNA (Marteijn et al. 2014). Unlike mammals, plants have the PHR1 photolyase, which uses energy from light to efficiently repair CPD without DNA excision (Jiang et al. 1997). For this reason, it was thought that photolyase-dependent repair in plants was the major repair pathway of CPDs in light conditions and the NER repair was only relevant in the dark (Molinier et al. 2008). However, a recent study suggests that both photolyases and the NER pathway are important for repairing UV-induced DNA damage in light, as there is a synergistic genetic interaction between *PHR1* and the NER-related *CUL4*, *DDB1A* and *DDB2* (Molinier et al. 2008). Our study finds that CRYs promote the repair of CPDs under light (Figures 2.1C-E, 2.2E). In this context, CRYs may regulate the repair of CPDs either by PHR1 photolyase-mediated repair or by NER. On one hand, CRYs may regulate the expression of *PHR1* through the light signaling pathway. For instance, the TF ELONGATED HYPOCOTYL 5 (HY5) induces the expression of *PHR1* in light (Lee et al. 2007; Castells et al. 2010), but is in turn repressed by another light signaling component, DE-ETIOLATED 1 (DET1) (Castells et al. 2010). Thus, since CRYs are known to positively regulate HY5 protein stability (Ponnu et al. 2019), it is plausible that CRYs indirectly induce *PHR1* via HY5 under UVC, which is consistent with our observation that CRYs promote CPD repair, opposite to DET1 (Castells et al. 2010). On the other hand, it is also plausible that CRYs regulate NER through the $CRL4^{COP1/SPA}$ complex. First, CRYs can repress the activity of COP1 (Ponnu et al. 2019; Lau et al. 2019), which we found is a negative regulator of the DDR (Figures 2.8D and 2.8E). Second, similar to COP1, DET1 forms a complex with CUL4 and DDB1 to regulate NER in collaboration with DDB2 (Castells et al. 2011). Therefore, the $CRL4^{COP1/SPA}$ complex may serve as a mediator between CRY-mediated light signaling and the NER-mediated repair of CPDs. In addition, the finding that

CRYs are not required for DSB repair (Figure 2.2D) further suggests that photolyase-mediated repair and the NER are the two most plausible DNA repair pathways that could be regulated by CRYs.

DDR, however, isn't regulated just at the transcriptional level. Proteins involved in DDR are regulated by post-translational modifications (PTMs) (Oberle and Blattner 2010). After phosphorylation, ubiquitination is the second most prevalent PTM (Gross et al. 2015), which alters protein stability and protein-protein interactions. For example, p53 is destabilized by ubiquitination (Hafner et al. 2019). Moreover, ubiquitination of histone H2AX promotes the recruitment of DNA repair proteins to DNA damage sites (Doil et al. 2009). DUBs, proteases that remove ubiquitination from target proteins, play an important role in animal DDR, for instance, USP7, the ortholog of UBP12/13 in animals, stabilizes p53 (Li et al. 2002) and the Chk1 kinase (Alonso-de Vega et al. 2014), which is essential for the initiation of the DDR (Sanchez et al. 1997). However, there are only a few papers exploring the role of DUBs in plant DDR. Recently, Al Khateeb et al. suggest that UBP12, a plant DUB, acts as a positive regulator of UVC tolerance in the dark (Al Khateeb et al. 2019). In contrast to their study, our study finds that UBP12/13 act as negative regulators of DDR in light conditions (Figures 2.1, 2.2, 2.3 and 2.4). This variation in results may arise from the difference in experimental procedures, suggesting that the function of UBP12/13 is distinct in the light versus dark. Although our study suggests that UBP12/13 likely regulate the DDR through CRYs (Figures 2.7A and 2.7B), we cannot rule out the possibility that UBP12/13 could target other DDR-related proteins. For instance, UBP12/13 can deubiquitinate histone H2A (Derkacheva et al. 2016). Because histone ubiquitination marks are important signals in DDR for the recruitment of DNA damage repair proteins (Mattiroli and Penengo 2021), it is plausible that the negative role of UBP12/13 in plant DDR could also result from removing of histone ubiquitination marks.

DDR promotes DNA damage repair, inhibits the cell cycle to allow sufficient time for DNA repair, and induces apoptosis in cells that have irreparable DNA damage (Jackson and Bartek 2009). Constitutive activation of the latter two aspects of DDR in the absence of DNA damage could lead to undesired cell cycle arrest and cell death (Hafner et al. 2019). Therefore, organisms evolved

mechanisms to desensitize the DDR. For example, p53 can induce the expression of its E3 ligase, Mdm2, which in turn leads to p53 degradation, serving as a negative feedback loop to halt the p53 signaling pathway when DNA damage is repaired (Hafner et al. 2019). This inhibition of p53 by Mdm2 is also important for normal cell survival as Mdm2-deficient mice are embryonically lethal due to the cytotoxicity caused by ectopic activation of p53 (Jones et al. 1995). Similarly, we show that UBP12/13 serve as a brake for CRY-mediated DDR in plants (Figures 2.1, 2.2, 2.3, 2.4, 2.7A and 2.7B). This inhibition of CRY function by UBP12/13 is also crucial for normal plant growth since the loss of UBP12 and UBP13 leads to over-accumulation of CRY2 and subsequently constitutive activation of stress responses resulting in stunted growth phenotypes (Lindback et al. 2022).

CAMTA transcription factors are conserved across many animal and plant species (Bouché et al. 2002). In animals, CAMTAs regulate nervous system-related processes and cardiac growth (Song et al. 2006; Long et al. 2014; Bas-Orth et al. 2016; Schraivogel et al. 2011), while in plants, they are mainly implicated in abiotic stress and immune responses (Iqbal et al. 2020). In both groups, the role of CAMTAs in DDR remains unexplored. Our study shows that CAMTA TFs play a novel role in UVC-induced DDR (Figures 2.5 and 2.6). Many TFs are important for DDR, especially SOG1, as gamma irradiation-induced gene expression is largely diminished in the *sog1* loss of function mutant (Bourbousse et al. 2018; Yoshiyama et al. 2009). However, using public databases (Winter et al. 2007), we found that induction of the *CAMTA3* gene 20 min after gamma irradiation is largely unaffected by the genetic loss of *SOG1* (Bourbousse et al. 2018), suggesting that CAMTAs might play a SOG1-independent role in the DDR, similar to E2Fa, a known SOG1-independent TF (Horvath et al. 2017). To test whether CAMTAs function in the DDR independent of SOG1, the *camta123* triple mutant could be crossed to the *sog1* mutant to generate the *camta123sog1* quadruple mutant. If CAMTAs function in the DDR independent of SOG1, the *camta123sog1* quadruple mutant should have a more severe UVC hypersensitive phenotype than both the *camta123* and the *sog1* mutant. CAMTAs can bind to calmodulin proteins that are important for the calcium signaling pathway (Iqbal et al. 2020). In animals, the calcium signaling pathway is required for the DDR. Intracellular calcium level is increased upon

DNA replication stress, which in turn activates the calcium signaling pathway and inhibits Exonuclease 1 (Exo1) from making aberrant nicks in replication forks, thus maintaining genome stability (Li et al. 2019). Therefore, further investigations would provide insights into whether calcium signaling play a role in plant DDR and if this role is dependent on the CAMTAs and CRYs.

CRYs are well-characterized blue/UVA light receptors (Guo et al. 1998; Lin et al. 1998), and evidence suggests that human CRY1 and the chromophore common to all CRYs, FAD, can absorb light in the UVB/UVC spectrum (YAGI et al. 1959; Zeng et al. 2018). However, whether UVC light is functionally relevant for CRYs has never been explored. Blue light triggers the formation of CRY2 nuclear speckles (Yu et al. 2009), where photoactivated CRY2 carries out its function (Wang et al. 2021). Our unexpected finding that CRY2 requires its light-sensing property to form nuclear speckles in UVC (Figures 2.7 and 2.8) suggests that this light stimulus could trigger the photoactivation of CRY2. This discovery not only provides the first evidence that the UVC light spectrum is functionally relevant for CRYs, but also justifies future research to explore if CRY2 could act as a bona fide UVC light receptor, with experiments to be performed such as the spectroscopic examination of CRY2 upon UVC exposure.

Recent studies have shown that CRYs and the UVB receptor, UVR8, functionally interact (Tissot and Ulm 2020; Rai et al. 2019, 2020). Even though *cry1*, *cry1cry2* and *uvr8* mutants survive under natural and simulated sunlight (*i.e.*, supplemented with UVB), *cry1uvr8* double and *cry1cry2uvr8* triple mutants do not, suggesting that CRYs and UVR8 redundantly contribute to plant survival in sunlight (Tissot and Ulm 2020; Rai et al. 2019, 2020). Paradoxically, CRY proteins induce the dimerization and, therefore, inactivation of UVR8 in a blue-light-dependent manner (Tissot and Ulm 2020; Rai et al. 2019, 2020). Moreover, CRYs likely oppose UVR8-induced gene expression under UVB, suggesting that CRYs would function as a brake to UVR8 hyper-activation (Tissot and Ulm 2020; Rai et al. 2019, 2020). In this context, the mechanism of how CRYs positively contribute to plant survival under UVB remains largely unknown. In our study, we further extended the function of CRYs into the UVC spectrum and showed that CRYs play a role in UVC-induced DDR, and presented

evidence that CRYs could regulate DNA repair after UVC exposure to contribute to plant growth and survival. Therefore, beyond revealing a novel role for CRYs, UBP12/13 and CAMTAs in UVC, our findings might point to how CRYs help plants to survive under other types of genotoxic stresses, such as UVB.

2.5 MATERIALS AND METHODS

2.5.1 Plant genotypes and growth conditions used

Arabidopsis thaliana Columbia (*Col-0*) ecotype was used as background for mutants and transgenic lines. *cry1-304* (Mockler et al., 1999), *cry2-1* (Lin et al. 1998), *cry1-304 cry2-1* (Mockler et al., 1999), *ubp12-2w ubp13-3* (Cui et al. 2013), *ku70* (Kannan et al. 2008), *cop1-4* (Deng et al. 1992) and *camta123* (Kim et al. 2020) mutants have been previously described. *Col-0;UBQ10$_{pro}$:UBP13-6xHA* (*UBP13oe*) (Lindback et al. 2022), *cry2-1;UBQ10$_{pro}$:UBP13-6xHA;CRY2$_{pro}$:2xStrep-6xHis-3xFLAG-CRY2* (Lindback et al. 2022), *ubp12-2w ubp13-3;UBQ10$_{pro}$: 2xStrep-6xHis-3xFLAG-CRY2* (*ubp12ubp13;CRY2oe*) (Lindback et al. 2022), *Col-0;UBQ10$_{pro}$:COP1-6xHis-3xFLAG* (*COP1oe*) (Lindback et al. 2022), and *cry2-1;UBQ10$_{pro}$:2xStrep-6xHis-3xFLAG-CRY2* (*cry2;CRY2oe*) (Pedmale et al. 2016) lines have been described previously. After surface sterilization, seeds were plated on 0.5× Linsmaier and Skoog (LS) medium (HiMedia Laboratories) containing 0.8% agar, stratified for 2 days in darkness at 4°C and then grown at 22°C under 100 μmol m^{-2} s^{-1} white light from a LED source in a growth chamber (Percival Scientific) unless otherwise specified.

2.5.2 Molecular cloning and transformation of *Arabidopsis* and *Nicotiana benthamiana.*

Promoters and coding sequences were amplified from genomic or cDNA pool of Col-0 (WT) plants or subcloned from plasmids by PCR and cloned into Gateway donor plasmids including pDONR221, pDONRP4-P1R and pDONRP2R-P3 (Thermo Fisher Scientific) using BP Clonase II (Thermo Fisher Scientific). CRY2^{D387A} was generated by replacing the aspartate 387 with an alanine

through site-directed mutagenesis (Oligos listed in Table S4). Three-fragment Gateway cloning technology was used to combine the Gateway donor constructs with pB7m34GW or pK7m34GW destination plasmids (Karimi et al. 2007) using LR Clonase II (Thermo Fisher Scientific). Binary destination plasmids were transformed into *Agrobacterium tumefaciens* (GV3101) and then transformed into *Arabidopsis* plants using the floral dip method (Clough and Bent 1998). *cry1-304 cry2-1;UBQ10pro:UBP13-6xHA* (*cry1cry2;UBP13oe*) line was generated by transforming *cry1cry2* with *pB7m34GW-UBQ10$_{pro}$:UBP13-6xHA* plasmid. *cry2* plants were transformed either with *pK7m34GW-UBQ10$_{pro}$:CRY2-mCitrine*, *pB7m34GW-CRY2$_{pro}$:mCitrine-CRY2* or *pB7m34GW-CRY2$_{pro}$:mCitrine-CRY2^{D387A}* plasmids to generate *cry2;CRY2-mCitrine*, *cry2;mCitrine-CRY2* or *cry2;mCitrine-CRY2^{D387A}*, respectively. *pK7m34GW-UBQ10$_{pro}$:CRY2-mCitrine* and *pB7m34GW-UBQ10$_{pro}$:CRY2^{D387A}-mCitrine* were transformed into *Agrobacterium* and used to infiltrate *Nicotiana benthamiana* plants as described before (Lindback et al. 2022).

2.5.3 UVC sensitivity assay

UVC treatment was performed using a UV Crosslinker 1800 (Stratagene) or with a UVC-emitting LED lamp (peak wavelength 270-280 nm), (Cat# E275-80-Module; International Light Technologies). Plants were grown in continuous white light for 4 days at 22°C, then treated with 5500 or 8000 J/m^2, and returned to continuous white light for another 5-6 days before phenotyping and measurement of fresh weight. Three biological replicates of fresh weight measurement were performed. For each biological replicate, the total fresh weight of 10-24 seedlings was measured and the fresh weight per seedling was calculated. Fresh weight percentages were calculated by normalizing the fresh weight measurement at the indicated UVC dose to the 0 J/m^2 treatment group of the same genotype.

2.5.4 Zeocin sensitivity assay

Plants were grown under long days (LD) for 4 days, then transferred to plates containing 0, 4 or 8 μM of zeocin (Thermo Fisher Scientific) and grown for further 8 days in LD before fresh weight

measurement. Three biological replicates of fresh weight measurements were performed. Fresh weight and fresh weight percentage relative to 0 μM were calculated as described above.

2.5.5 CPD dot blot assay

5-day-old seedlings grown in LD were treated with 6000 J/m^2 UVC using the UV crosslinker and then transferred to 100 μmol m^{-2} s^{-1} white light for 1 min or 180 min before flash freezing in liquid nitrogen. Genomic DNA was extracted with the cetyltrimethylammonium bromide (CTAB) method (Porebski et al. 1997) , denatured by incubating at 100°C for 10 min and placed on ice immediately for 15 min, and quantified using a Qubit fluorometer (Thermo Fisher Scientific) and a Qubit ssDNA assay kit (Thermo Fisher Scientific). Serial dilutions (1, 1:10, 1:100) of the genomic DNA were blotted onto a Whatman Nytran SuPerCharge nylon blotting membrane (MilliporeSigma) and baked at 80°C for 2 h, then soaked in tris-buffered saline (TBS) with Tween-20 (TBST) (20 mM Tris-HCl, 150 mM NaCl, 0.05% Tween-20, pH 7.6) for 20 min before blocking with 5% fat-free milk in TBST for 30 min. After blocking, the membrane was incubated with an anti-CPD antibody (Cosmo Bio USA) at 1:1000 dilution prepared in 1% fat-free milk made in TBST overnight at 4°C before washing with TBST three times, 5 min each. Following the wash, the membrane was incubated with 1:10,000 dilution of anti-mouse-horseradish peroxidase (anti-mouse-HRP) antibody (Bio-Rad) at room temperature for 1 h and washed again three times in TBST, 5 min each wash. Imaging was performed in a Chemidoc imaging system (Bio-Rad) following the addition of SuperSignal West Dura Extended Duration Substrate (Thermo Fisher Scientific) to the membrane. Methylene blue staining was performed by incubating the blotted and baked nylon membrane with staining buffer (0.04% methylene blue, 0.5 M sodium acetate, pH 5.2) for 10 min, then de-stained with distilled water for 5 min before imaging. The CPD dot blots were quantified with ImageJ (Schneider et al. 2012).

2.5.6 Protein extraction and Immunoblotting

Total protein was extracted by grinding frozen *Arabidopsis* tissue in lithium dodecyl sulfate (LDS) buffer (106 mM Tris-HCl, 141 mM Tris, 2% LDS, 10% glycerol, 0.51 mM EDTA, 0.22 mM

Coomassie Brilliant Blue G 250 (SERVA Electrophoresis GmbH), 0.175 mM phenol red, 10% tris(2-carboxyethyl)phosphine). After centrifugation at 13000 rpm for 5 min, proteins were separated by sodium dodecyl-sulfate polyacrylamide gel electrophoresis (SDS-PAGE) in either homemade 7% or 4-12% gradient Bis-Tris polyacrylamide gel (Thermo Fisher Scientific) using 3-(N-morpholino)propanesulfonic acid (MOPS) running buffer (40 mM MOPS, 10 mM sodium acetate, 1 mM EDTA, pH 7) and transferred to nitrocellulose membrane (MilliporeSigma). After transfer, the nitrocellulose membrane was incubated in 5% fat-free milk made in TBST for 30 min, followed by incubation with primary antibodies in 1% fat-free milk made in TBST for 1 h. Then the membrane was washed three times with TBST and incubated with the secondary antibodies in 1% fat-free milk made in TBST for 1 h. The blots were washed three times with TBST and detection was performed as described above. The following antibodies were used: anti-RAD51 (Cat# AB63799, Abcam), anti-phospho-p44/42 MAPK (Erk1/2) (Thr202/Tyr204) (Cell Signaling Technology), anti-actin (MP Biomedicals) as primary antibodies. Goat-anti-mouse-HRP (Bio-Rad) and goat-anti-rabbit-HRP (Bio-Rad) were used as secondary antibodies. Conjugated anti-HA-HRP (Cat#12013819001, MilliporeSigma) and anti-FLAG-HRP (Thermal Fisher Scientific) antibodies were used to detect HA- and FLAG-tagged proteins, respectively. All immunoblot experiments were repeated at least twice. Quantification of the immunoblot was performed in ImageJ software (Schneider et al. 2012) by measuring the mean gray value of bands subtracted by the mean gray value of the background.

2.5.7 *In vivo* co-immunoprecipitation

4-day-old *cry2-1;UBQ10*$_{pro}$*:UBP13-6xHA;CRY2*$_{pro}$*: 2xStrep-6xHis-3xFLAG*-CRY2 seedlings grown under continuous white light were dark adapted for 24 h, then treated with continued darkness or UVC LED source (approximately 1800 J/m^2). Tissue was collected after 10 min, immediately frozen and later ground in liquid nitrogen. Each 1 g of tissue was dissolved in 2 ml of SII buffer (100 mM sodium phosphate [pH 8], 150 mM NaCl, 5 mM EDTA, 5 mM EGTA, 0.1% Triton X-100, 1× protease inhibitors (Sigma), 50 μM MG132) and sonicated (Branson Ultrasonics) on the ice at 40% power, with

0.5 s on/off cycles for a total of 10 s. The protein extracts were then clarified by two rounds of centrifugation at 13000 rpm for 10 min at 4°C. Protein concentration was inferred by spectroscopy using Bradford reagent (Bio-Rad), and normalized for inputs and co-IPs. For co-IPs, proteins were then mixed with anti-FLAG antibody (Thermal Fisher Scientific) for 1 h at 4 °C and incubated with protein-G magnetic beads (Bio-rad) for 0.5 h at 4 °C. Beads were washed 3× with 0.75 ml of SII buffer and proteins were eluted with 20 µl of 2× LDS buffer and boiled at 95°C for 5 min before immunoblot analysis, as described above.

2.5.8 Laser scanning confocal microscopy

For CRY2-mCitrine, 4-day-old dark-grown *Arabidopsis cry2;UBQ10pro::CRY2-mCitrine* seedlings were incubated in MG132 buffer (0.5× LS medium, 50 µM MG132) for 5-8 h in the dark at room temperature. Samples were then treated with 40 µmol m^{-2} s^{-1} of blue light or UVC LED (approximately 1800 J/m^2 in total) for 2 min or kept in continued darkness. Seedlings were immediately fixed in 4% PFA with a vacuum for 20 min, then washed for 5 min twice in phosphate-buffered saline (PBS) before cotyledon cells were imaged. For mCitrine-CRY2 and mCitrine-CRY2^{D387A}, 4-day-old dark-grown *cry2;CRY2pro::mCitrine-CRY2* or *cry2;CRY2pro::mCitrine-CRY2^{D387A}* seedlings were incubated in MG132 buffer (0.5× LS medium, 50 µM MG132) for 0.5 h in the dark at room temperature. Then treated for 30 min with 40 µmol m^{-2} s^{-1} of blue light or UVC LED (approximately 100 J/m^2 in total) or continued darkness. Seedlings were fixed in 1% PFA for 10 min and washed twice in PBS for 5 min. Hypocotyl cells were imaged in this case.

UBQ10pro::CRY2-mCitrine or *UBQ10pro::CRY2^{D387A}-mCitrine* were transiently expressed in *N. benthamiana* following agroinfiltration of leaves. For this, plants were grown for approximately four weeks in the greenhouse environment. Three leaves were infiltrated per condition, and then plants were kept in white light for 1 day and dark incubated for 2 days to allow for CRY2 accumulation. After this time, leaves were infiltrated with 50 µM MG132 for 0.5 h, prior to treatment with blue light (40 µmol m^{-2} s^{-1}) or UVC LED (approximately 4500 J/m^2 in total) for 5 min or continued darkness. Leaves were

fixed in 4% PFA for 20 min with a vacuum, then kept in 1× PBS and imaged under the confocal microscope. All confocal microscopy was performed using the LSM900 confocal microscope (Zeiss) using a 488 nm laser and images were captured at the emission range of 410 to 545 nm**.**

2.5.9 mRNA sequencing and analysis

Five-day-old seedlings grown under LD conditions were untreated (0 min) or treated with 6000 J/m^2 UVC and collected after 15, 60 and 180 min. Two biological replicates were harvested for each sample and frozen in liquid nitrogen. RNA was extracted using a Direct-zol RNA miniprep kit (Zymo Research) and quantified using a Qubit fluorometer (Thermo Fisher Scientific). 500 ng of total RNA was used for mRNA isolation using NEBNext poly(A) mRNA Magnetic Isolation Module (New England Biolabs) and the purified mRNA was used to construct libraries using the NEBNext Ultra II Directional RNA Library Prep Kit for Illumina (New England Biolabs) following manufacturer instructions. Single-end sequencing of 76 bp was performed on NextSeq500 (Illumina) to a total of 40 million reads per sample on average. The sequencing reads were mapped to the *Arabidopsis thaliana* Col-0 genome (TAIR10) using STAR version 2.7.5c (Dobin et al. 2013). Differential gene expression analysis was performed using Cufflinks version 2.2.1 (Trapnell et al. 2012). R environment version 4.1.0 (R Foundation) and its packages (ggplot2, RColorBrewer, corrplot, DESeq2 (Love et al. 2014)) were used for statistical analysis and to visualize the results. Principal component analysis was performed using DESeq2 (Love et al. 2014). GO term analysis was performed using PANTHER (Mi and Thomas 2009).

2.5.10 RT-qPCR analysis

Total RNA was extracted from frozen *Arabidopsis* seedlings using the Direct-zol RNA miniprep kit (Zymo Research). cDNA from RNA was synthesized using the iScript cDNA Synthesis Kit (Bio-Rad) and qPCR was performed using the indicated oligos (Table S4) (QuantStudio 6 Pro PCR system; Thermo Fisher Scientific) using Power SYBR Green Master Mix (Thermo Fisher Scientific).

Expression values were normalized to the *UBC28* reference gene and calculated using the $2^{-\Delta\Delta Ct}$ method (Livak and Schmittgen 2001).

2.5.11 DREM analysis

DREM analysis was performed as previously described (Bourbousse et al. 2018). For each genotype (WT, *cry1cry2* and *ubp12ubp13*), the $\log_2$ fold change of the expression of all the DEGs along the time course in the corresponding genotype was used as inputs for DREM models (Schulz et al. 2012). The TF-gene interaction file derived from Bourbousse et al (Bourbousse et al. 2018) was used as input for the DREM analysis.

2.5.12 Discovery of *de novo* motifs

The *de novo* motif search by HOMER (Heinz et al. 2010) was performed using lists of target genes (genes within the W2 group from the DREM model, all upregulated genes in WT after UVC, and all downregulated genes in WT after UVC) as input. The following code was used in a Linux environment: "findMotifs.pl /file/path/to/gene/names arabidopsis /file/path/to/output -noconvert -start -500 -end 50 -nogo".

Chapter 3. UBP12 and UBP13 deubiquitinases destabilize the CRY2 blue light receptor to regulate *Arabidopsis* growth

This chapter is previously published in Current Biology (2022), Volume 32, Issue 15, Pages 3221-3231, under the title "UBP12 and UBP13 deubiquitinases destabilize the CRY2 blue light receptor to regulate Arabidopsis growth" by Louise N. Lindbäck, Yuzhao Hu, Amanda Ackermann, Oliver Artz, and Ullas V. Pedmale* (Lindback et al. 2022). *Author contributions: conceptualization by U.V.P. and L.N.L.; methodology by U.V.P. and L.N.L.; L.N.L. performed most of the experiments with the following exceptions: U.V.P. performed RNA-seq analysis, O.A. performed the CRY1 immunoblot, Y.H. and U.V.P. performed the in vitro coIP and COP1 immunoblots, A.A. performed phenotypic analysis, L.N.L. and U.V.P. wrote the manuscript, and all authors reviewed and commented on the manuscript. In this published work, I mainly performed the in vitro coIP experiments and the immunoblots to evaluate COP1 protein, together with Prof. Ullas V. Pedmale. I will denote my contributions in the legends of each figure of Chapter 3.*

3.1 Summary

Light is a crucial exogenous signal sensed by cryptochrome (CRY) blue light receptors to modulate growth and the circadian clock in plants and animals. However, how CRYs interpret light quantity to regulate growth in plants remains poorly understood. Furthermore, CRY2 protein levels and activity are tightly regulated in light to fine-tune hypocotyl growth; however, details of the mechanisms that explain precise control of CRY2 levels are not fully understood. We show that in *Arabidopsis*, UBP12 and UBP13 deubiquitinases physically interact with CRY2 in light. UBP12/13 negatively regulates CRY2 by promoting its ubiquitination and turnover to modulate hypocotyl growth. Growth and development were explicitly affected in blue light when UBP12/13 were disrupted or

overexpressed, indicating their role alongside CRY2. UBP12/13 also interacted with and stabilized COP1, which is partially required for CRY2 turnover. Our combined genetic and molecular data support a mechanistic model in which UBP12/13 interact with CRY2 and COP1, leading to the stabilization of COP1. Stabilized COP1 then promotes the ubiquitination and degradation of CRY2 under blue light. Despite decades of studies on deubiquitinases, the knowledge of how their activity is regulated is limited. Our study provides insight into how exogenous signals and ligands, along with their receptors, regulate deubiquitinase activity by protein-protein interaction. Collectively, our results provide a framework of cryptochromes and deubiquitinases to detect and interpret light signals to control plant growth at the most appropriate time.

3.2 Introduction

Multicellular organisms undergo growth and development during their lifetime within the scope of their genetic and developmental constraints. Unchecked growth often leads to neoplasia in animals and loss of fitness in plants. Furthermore, growth is either restricted or promoted at the most appropriate time based on many endogenous and exogenous signals. Light is one of those exogenous signals utilized by organisms to regulate their growth and physiology. In animals, light affects mood, behavior, metabolism, growth, and entrainment of the circadian clock (Fernandez et al. 2018; Bedrosian and Nelson 2017). In plants, light is not only a source of energy but also provides information about their geographical location, allowing them to change their body plan to better adapt to their environment and entrain their biological clocks (Chory 2010).

Specialized photoreceptors in plants perceive UV-B, blue, red, and far-red light to monitor their quality and quantity to survey their environment. Blue light (BL)-absorbing cryptochromes (CRYs) are one of those evolutionarily conserved photoreceptors found in broad lineages, including yeast, flies, plants, and animals (Pedmale et al. 2016; Sancar 2003). CRYs evolved from DNA photolyases that utilize UV-A/BL as an energy source to repair damaged DNA. Present-day CRYs have retained the

light absorption properties of photolyases but cannot bind DNA directly (Sancar 2003). CRYs are known to entrain the circadian clock, regulate metabolism, and control other crucial processes. The loss of animal CRYs is also associated with tumorigenesis, diabetes, and neuronal disorders (Hirota et al. 2012; Lamia et al. 2011). The main functions of plant CRYs are their regulation of light-dependent development termed photomorphogenesis, control of stem/hypocotyl growth, and photoperiodic flowering (Lin et al. 1998). CRYs can modulate these wide range of processes by governing gene expression through their interaction with signaling partners, often with bHLH transcription factors such as BMAL1 and CLOCK in animals, with PIFs and CIBs in plants (Pedmale et al. 2016; Ma et al. 2016; Koike et al. 2012; Liu et al. 2008a). Central to CRY-mediated signaling in diverse species is its targeted ubiquitination and proteasomal degradation. The degradation of CRYs is hypothesized to be necessary for their desensitization and the reset of downstream signaling (Godinho et al. 2007; Liu et al. 2016b).

In *Arabidopsis*, CRY1 is a nucleocytoplasmic protein, whereas CRY2 is nuclear and readily forms nuclear speckles in BL (Yu et al. 2007). Photoactivated CRYs undergo phosphorylation and oligomerize as tetramers, which have been described as their physiologically active form (Ma et al. 2020a; Palayam et al. 2021). One of the functions of photoactive CRYs is to dampen the activity of the COP1-SPA (constitutive photomorphogenic 1-suppressor of PhyA-105), which serves as a substrate-specific adaptor of the Cullin 4-RING ubiquitin E3 ligase (CRL4). Inactivation of $CRL4^{COP1\text{-}SPA}$ by CRYs leads to accumulation of transcription factors essential for plant development and growth (Jang et al. 2005; Seo et al. 2003). CRY2 abundance is regulated by light, accumulating in darkness or vegetational shade, and rapidly turning over under prolonged and high intensities of BL (Pedmale et al. 2016; Yu et al. 2007). Therefore, the levels and activity of CRY2 protein are tightly regulated to fine-tune hypocotyl growth and photomorphogenesis. In mammals, SCF^{FBXL3} and SCF^{FBXL21} function as E3 ubiquitin ligases to facilitate the ubiquitination of CRYs (Godinho et al. 2007; Siepka et al. 2007; Busino et al. 2007; Yoo et al. 2013). Recently, $CRL4^{COP1\text{-}SPA}$ and $CRL3^{LRBs}$ have been shown to be necessary for CRY2 degradation in *Arabidopsis* (Liu et al. 2016b; Weidler et al. 2012; Lau et al. 2019; Ponnu et al. 2019; Chen et al. 2021). However, the mechanism of action on how *Arabidopsis* CRY2 is

ubiquitinated by the $CRL4^{COP1\text{-}SPA}$ complex in light remains poorly understood (Chen et al. 2021; Wang et al. 2001; Holtkotte et al. 2017).

Protein ubiquitination is a key reversible post-translational modification. Protein polyubiquitination serves mainly as a signal for proteasomal degradation, whereas monoubiquitination is often associated with non-degradation-independent functions (Mevissen and Komander 2017). The E3 ubiquitin ligases ubiquitinate their target proteins with high specificity to cause their degradation. Ubiquitination can be reversed by deubiquitinating enzymes (DUBs) to prevent the target protein from degradation (Mevissen and Komander 2017). DUBs are evolutionarily conserved proteases that generally trim ubiquitin chains and/or remove ubiquitin covalently bound to proteins (Komander et al. 2009). In plants and animals, DUBs comprise five major gene families: ubiquitin-specific proteases (UBP/USP), ubiquitin-carboxyl terminal hydrolases (UCHs), ovarian tumor proteases (OUTs), Machado-Joseph disease protein domain proteases (MJDs), and Jab1/MPN+/MOV34 proteases (Komander et al. 2009; March and Farrona 2018; Lai et al. 2020). However, unlike E3 ligases, the role of DUBs in mediating key cellular processes is slowly emerging, especially in plants. Furthermore, the molecular functions and substrates of the large number (~64) of DUBs in plants remain largely unidentified.

CRY2 levels and activity are critical for plant growth in light, especially during photomorphogenesis, a process in which newly germinated seedlings establish themselves to become photoautotrophic and ensure success as an organism. Details of the mechanisms that account for precise control of CRY2 levels by ubiquitination are not fully understood. In this study, we identify UBP12- and UBP13 DUB-mediated regulation of CRY2 degradation as a mechanism to regulate hypocotyl growth in light. However, it was unexpected that the critical function of UBP12/13 in this process did not depend on its deubiquitination activity to stabilize and prevent the CRY2 degradation. Instead, UBP12 and UBP13 used their influence to mediate CRY2 degradation indirectly by stabilizing COP1. Hypocotyl growth was disrupted in seedlings lacking UBP12 and UBP13 or when they were overexpressed, specifically in BL. Our combined genetic and molecular data support a mechanistic

model in which UBP12/13 physically interact with CRY2 and COP1, leading to stabilization of COP1 and modulation of its activity in BL. Stabilized COP1 then promotes ubiquitination and degradation of CRY2 in BL. This mechanism of attenuation of CRY2 is unusual among the reported mechanisms but probably typifies the mitigation of the receptor in an ever-changing light environment of the plant. This regulation by the CRY2-UBP12/13-COP1 axis is particularly essential to optimize plant growth and development.

3.3 Results

3.3.1 UBP13 through its MATH domain interacts with CRY2

To identify novel regulators of CRY2 abundance in *Arabidopsis*, we examined the protein complex associated with CRY2 by affinity purification followed by mass spectrometry analysis. We used a previously described transgenic line expressing Flash-CRY2 (also called *CRY2oe*) under a constitutive *UBQ10* promoter that complements *cry2* mutant (Pedmale et al. 2016) grown under a subdued BL to affinity purify the CRY2-protein complex. Analysis of the proteins co-purified with CRY2 identified its previously known interacting partners that include COP1, SPAs, CRY1, and BIC1 (Figure 3.2A) (Weidler et al. 2012; Wang et al. 2001, 2016). Among these proteins there were UBP12 and UBP13 (Figures 3.1A and 3.1B). *Arabidopsis* UBP12 and UBP13 share a 91% amino acid sequence identity, suggesting that their biological function is likely redundant (Figure 3.2B) (Cui et al. 2013). Orthologs of the UBP12/13 proteins can be found in other plant species, invertebrates, and vertebrates (Figure 3.2C), suggesting evolutionary conservation. Previously, UBP12/13 have been shown to have functions in immunity, flowering, jasmonate signaling, and leaf development (Vanhaeren et al. 2020; Jeong et al. 2017; Lee et al. 2019; Cui et al. 2013).

In an *in vitro* pull-down assay, we co-immunoprecipitated FLAG-UBP13 along with Myc-CRY2, validating their ability to physically interact (Figure 3.2D). UBP12/13 are nucleocytoplasmically localized (Cui et al. 2013; Derkacheva et al. 2016), whereas CRY2 is a nuclear protein (Yu et al. 2007).

Therefore, to visualize their subcellular site of interaction, we used bimolecular fluorescence complementation (BiFC) in *Nicotiana benthamiana*, which revealed that CRY2 interacted with UBP13 in the nucleus of epidermal cells (Figure 3.1C). *Arabidopsis* encodes approximately 64 DUBs, which comprise 27 members of the UBP subfamily (Liu et al. 2008c). Among them, only UBP12 and UBP13 contain the meprin and TRAF homology (MATH) domain, which aid in protein-protein interactions, especially with various receptors (Figures 3.2B and 3.3A) (Liu et al. 2008c; Ye et al. 1999). To test whether the MATH domain mediates CRY2-UBP13 interactions, we immunoprecipitated Flash-CRY2 co-expressed with either UBP13-6xHA or UBP13 without its MATH domain (UBP13ΔMATH-6xHA) from *N. benthamiana* protein extracts. Immunoblotting for HA revealed that CRY2 did not co-immunoprecipitate with UBP13ΔMATH (Figure 3.1D), and we validated that this was not due to inadvertent changes in subcellular localization and thus loss of its interaction with CRY2 (Figure 3.3B). In contrast, the MATH domain of UBP13 (FLAG-MATH^{UBP13}) alone was sufficient to interact with Myc-CRY2 in an *in vitro* pull-down assay (Figure 3.2E), indicating that the MATH domain of UBP13 mediates the interaction with CRY2.

To address whether light influenced the interaction between CRY2 and UBP13, we performed co-immunoprecipitation using transgenic *Arabidopsis* seedlings co-expressing Flash-CRY2 and UBP13-6xHA. In addition, 4-day-old seedlings were dark adapted for 24 h and then exposed to BL for 10 min (30 μmol m^{-2} s^{-1}) or mock treated (dark). The protein extracts were immunoprecipitated with anti-FLAG antibody and immunoblotting with anti-HA antibody revealed that the interaction of CRY2 with UBP13 was greatly enhanced in BL (Figure 3.1E). Together, these findings suggest that UBP12/13 are new components in the CRY signaling pathway, that UBP13 interacts with CRY2 in the nucleus through its MATH domain, and that BL enhances their interaction.

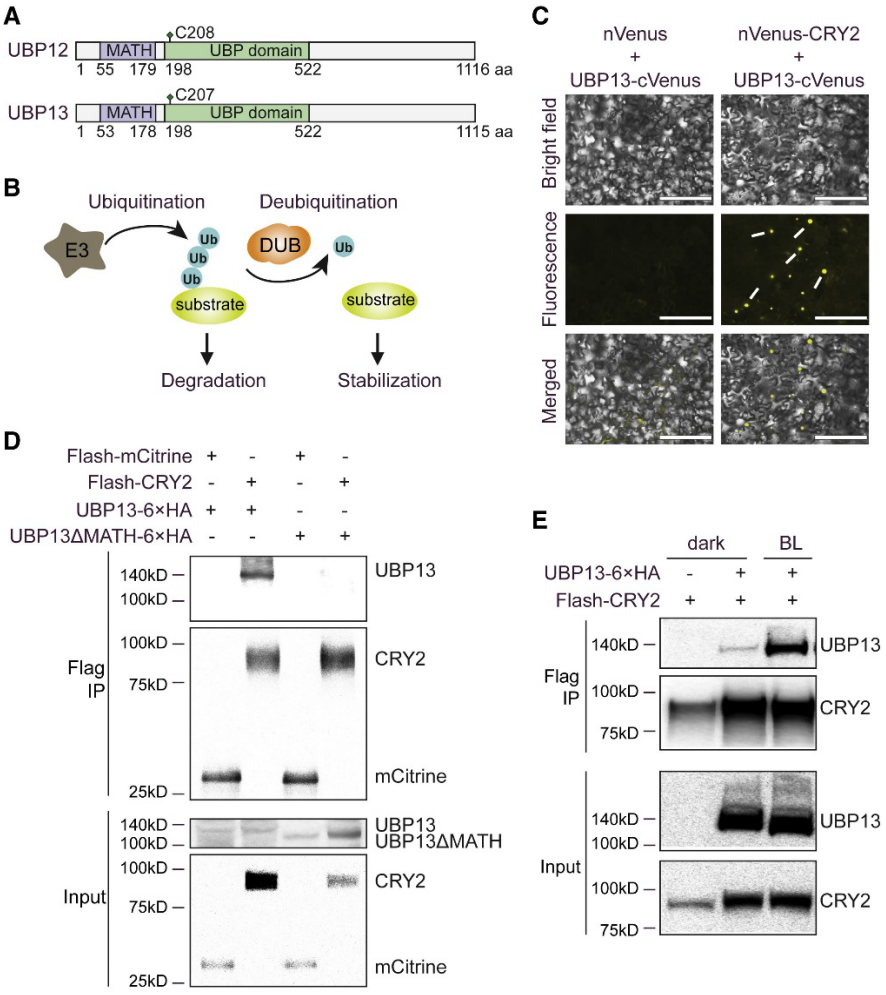

Figure 3.1: UBP13 physically interacts with CRY2 and their contact is enhanced in light.
Schematic representation of *Arabidopsis* UBP12 and UBP13 proteins indicating the position of MATH and UBP domains and cysteine catalytic residue (C208 or C207). aa, amino acids. (B) Role of E3 ubiquitin ligases (E3) and deubiquitinases (DUB) in controlling the fate of their target proteins by catalyzing their ubiquitination or deubiquitination. Ub, ubiquitin. (C) BiFC analysis of nVenus-CRY2 and UBP13-cVenus in *N. benthamiana* leaf epidermal cells. nVenus indicates the amino terminus of the Venus protein alone. The nucleus of the cells is indicated by white bars. Scale bar, 200 μm. (D) Co-immunoprecipitation of the indicated proteins expressed in *N. benthamiana* using an anti-FLAG antibody. Flash-mCitrine serves as a negative control. (E) Co-immunoprecipitation of the indicated proteins from *Arabidopsis* transgenic seedlings using an anti-FLAG antibody. Four-day-old seedlings were dark adapted for 24 h and then either exposed to BL (30 μmol m^{-2} s^{-1}) for 10 min or mock treated in the dark before protein extraction. **Contribution**: I did not contribute data to this figure.

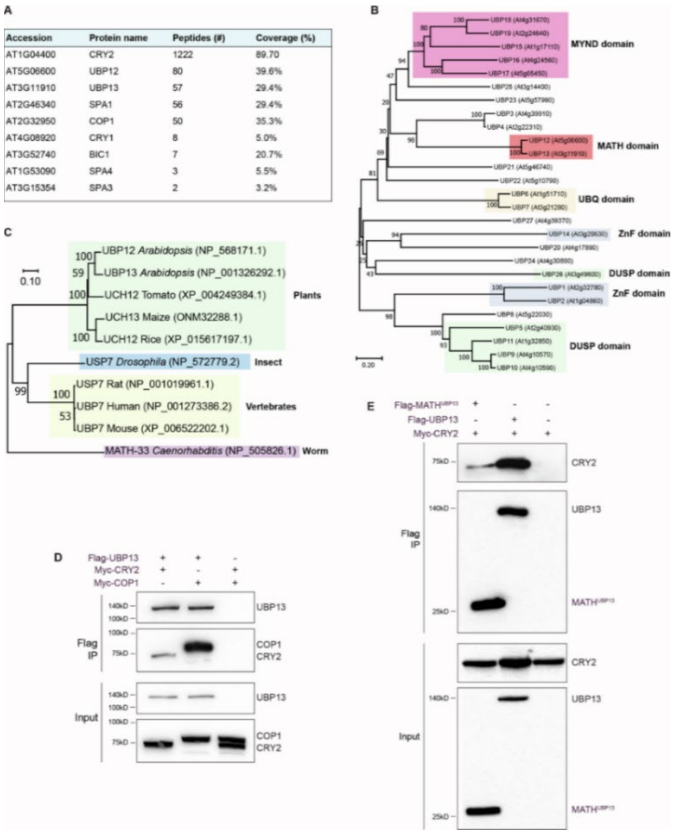

Figure 3.2: MATH-domain containing UBP12 and UBP13 deubiquitinases interact with CRY2 and COP1.

(A) Summary of *Arabidopsis* proteins that include the count of peptides and sequence coverage that form a protein complex with Flash-CRY2 (*CRY2oe*) as determined by affinity purification- mass spectrometry analysis. (B) Phylogenetic analysis of 27 members of the UBP subfamily in Arabidopsis. The evolutionary history was inferred using the neighbor-joining method. The optimal tree with the sum of branch length = 18.12934367 is shown. The percentage of replicate trees in which the associated taxa clustered together in the bootstrap test (1001 replicates) are shown next to the branches. The tree is drawn to scale, with branch lengths in the same units as those of the evolutionary distances used to infer the phylogenetic tree. The evolutionary distances were computed using the Poisson correction method and are expressed in units of the number of amino acid substitutions per site. Abbreviations: UBP, ubiquitin specific protease; MYND, myeloid; MATH, meprin and TRAF homology; UBQ, ubiquitin homologues; ZnF, zinc finger; DUSP, domain in ubiquitin-specific proteases. (C) Phylogenetic analysis of *Arabidopsis* UBP12 and UBP13 proteins along with their orthologs in major plant and animal species. The evolutionary history was inferred using the Neighbor-Joining method. The optimal tree with the sum of branch length = 2.40603150 is shown. The percentage of replicate trees in which the associated taxa clustered together in the bootstrap test (1001 replicates) are shown next to the branches. (D) *In vitro* co-immunoprecipitation of Flag-UBP13 with Myc-COP1 or Myc-CRY2. Flag-UBP13 was immunoprecipitated using an anti-Flag antibody and the indicated proteins were detected using anti-Myc and anti-Flag antibodies. The experiment was performed at least twice. (E) *In vitro* co-immunoprecipitation of Flag-UBP13 or Flag- $MATH^{UBP13}$ with Myc-CRY2. FlagUBP13 and Flag-$MATH^{UBP13}$ were immunoprecipitated using an anti-Flag antibody and the indicated proteins were detected using an anti-Myc and anti-Flag antibodies. **Contribution**: Myself and Prof. Ullas V. Pedmale together performed the experiments that resulted in the data shown in Figure 3.2D and Figure 3.2E.

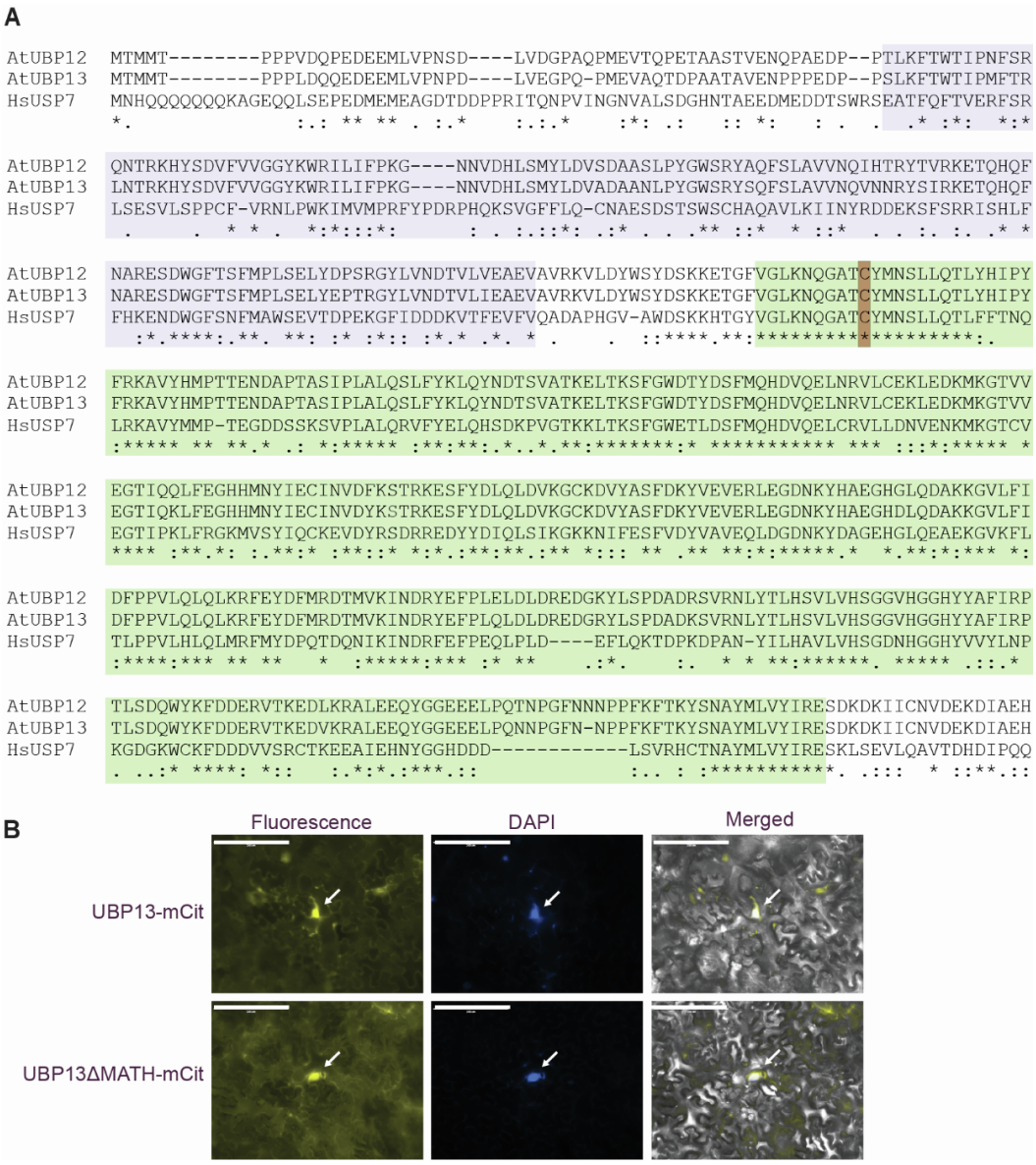

Figure 3.3: *Arabidopsis* UBP12 and UBP13 is closely related to the mammalian USP7, related to Figure 3.1.

(A) Partial amino acid sequence alignment of amino acid sequence for the *Arabidopsis* UBP12, UBP13, and human USP7 deubiquitinases indicating the conserved domains and catalytic residues between them. Asterisks (*) indicate conserved amino acid residues, colons (:) indicate conservation between amino acid groups of similar properties, periods (.) indicate conservation between amino acid groups of weakly similar properties, and dashes (-) indicate gaps introduced to maximize alignment. The active cysteine residue is indicated by an orange box, the purple shaded region indicates the location of *Arabidopsis* UBP13's MATH domain (aa 53-178), and the green shaded area indicates the location of *Arabidopsis* UBP13's UBP domain (aa 198-522). (B) Microscopic analysis of the abaxial epidermal cells of *N. benthamiana* leaves expressing UBP13-mCitrine (mCit) or without its MATH domain. DAPI (blue fluorescence) was used as a stain the nucleus. Arrows indicate fluorescence signal and DAPI stain in the nucleus. Scale bar = 200 µm. The experiment was repeated at least 3 times with identical results. **Contribution**: I did not contribute data to this figure.

3.3.2 UBP12 and UBP13 control hypocotyl growth and CRY2 levels in BL

CRY2 mediates inhibition of hypocotyl growth under low fluence of BL (<1 μmol m^{-2} s^{-1}) (Lin et al. 1998). CRY2 protein levels regulate hypocotyl growth in BL, as its reduced levels result in a long hypocotyl phenotype, and higher levels lead to shorter hypocotyl (Figures 3.4C and 3.4D) (Lin et al. 1998; Pedmale et al. 2016). Therefore, we investigated the role of UBP12/13 in the regulation of CRY2 and hypocotyl growth. We measured hypocotyl length of the single mutant alleles of *UBP12* (*12-1* and *12-2w*) and *UBP13* (*13-1* and *13-3*), together with their double mutant *ubp12-2w ubp13-3* (*ubp12ubp13*), *cry2*, and wild type (WT) after growth in BL (1 μmol m^{-2} s^{-1}) for 4 days. Loss of either *UBP12* or *UBP13* did not affect hypocotyl length (Figures 3.4A and 3.4B), indicating biological redundancy (Figure 3.2B) as previously reported (Cui et al. 2013). *ubp12ubp13* developed a hypersensitive short hypocotyl phenotype, whereas *cry2* mutant had an expected long hypocotyl phenotype insensitive to BL (Figures 3.4A and 3.4B). Next, we measured the hypocotyl length of *ubp12ubp13* and *cry2*, along with CRY2 (*CRY2oe/Flash-CRY2*) and UBP13 (*UBP13oe/UBP13-6xHA*) overexpressing seedlings grown for 4 days in BL (1 μmol m^{-2} s^{-1}). The short hypocotyls of *ubp12ubp13* mimicked that of *CRY2oe* (Figures 3.4C and 3.4D), whereas *UBP13oe* had a long hypocotyl, comparable with *cry2* (Figures 3.4C, 3.4D, and 3.5A–3.5C). The BL-specific phenotype of *UBP13oe* and *ubp12ubp13* was not observed in red or white light (Figures 3.5D and 3.5E). Significant hypocotyl growth and open cotyledon defects were not observed in dark-grown *ubp12ubp13* and *UBP13oe* seedlings (Figures 3.5F and 3.5G).

To assess whether UBP12/13 regulate CRY2, we performed an immunoblot analysis using an anti-CRY2 antibody on protein extracts obtained from the above genotypes grown in BL at 1 μmol m^{-2} s^{-1}. CRY2 levels were much higher in *ubp12ubp13* than in WT and *CRY2oe*, whereas *UBP13oe* had a reduced amount of CRY2 (Figures 3.4E and 3.11A) in BL, although we did not observe the same in white light or in darkness (Figures 3.5H, 3.5I, 3.11D, and 3.11E). Although we did not detect a prominent decrease in CRY2 in *UBP13oe* compared with *ubp12ubp13*, the lack of inhibition of hypocotyl growth was evident in multiple independent transgenic lines of *UBP13oe* (Figures 3.5A and

3.5B). The effect of UBP12/13 was specific to CRY2, as we did not observe changes in CRY1 levels determined by immunoblotting using an anti-CRY1 antibody, in seedlings grown under BL at 1 μmol m^{-2} s^{-1} (Figures 3.4F and 3.11B). The unexpected result that UBP12/13 negatively regulate CRY2 protein levels is the opposite of the expectation of a DUB. Since DUBs are generally known to prevent the degradation of their target proteins (Komander et al. 2009; March and Farrona 2018), one would hypothesize that loss of UBP12 and UBP13 will lead to lower CRY2 levels and a longer hypocotyl. Likewise, it can be postulated that overexpression of UBP12/13 results in increased stabilization of CRY2, resulting in a shorter hypocotyl. However, our results suggest that UBP12 and UBP13 have the opposite effect, destabilizing CRY2 to regulate its protein levels and CRY2-dependent hypocotyl inhibition under BL. Furthermore, our results indicate that UBP12/13 modulate hypocotyl growth under BL.

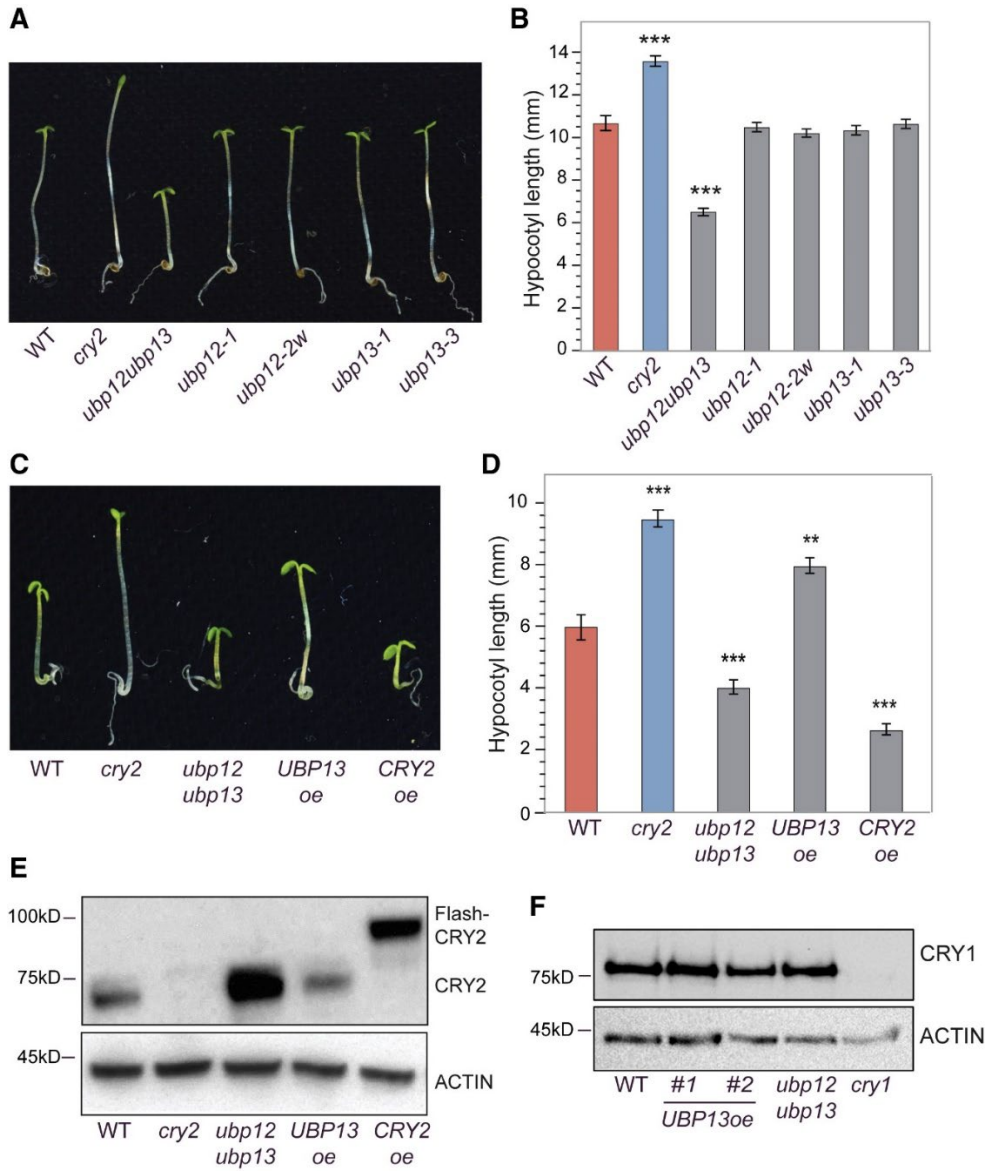

Figure 3.4: UBP12 and UBP13 negatively regulate the CRY2 protein and modulate hypocotyl growth in BL.

(A–D) Phenotype and hypocotyl length of 4-day-old seedlings of the indicated genotypes grown under BL (1 μmol m^{-2} s^{-1}). (E) Immunoblot analysis of CRY2 in 4-day-old seedlings grown in BL (1 μmol m^{-2} s^{-1}). CRY2 was detected using an anti-CRY2 antibody. ACTIN serves as a loading control. (F) Immunoblot analysis of CRY1 in 4-day-old seedlings grown under BL (1 μmol m^{-2} s^{-1}). CRY1 was detected using an anti-CRY1 antibody. ACTIN serves as a loading control. For (B) and (D), data are shown as mean ± SE, n = 16, and repeated at least three times (Student's t test: $^{***}p < 0.001$; $^{**}p < 0.01$).

Contribution: I did not contribute data to this figure.

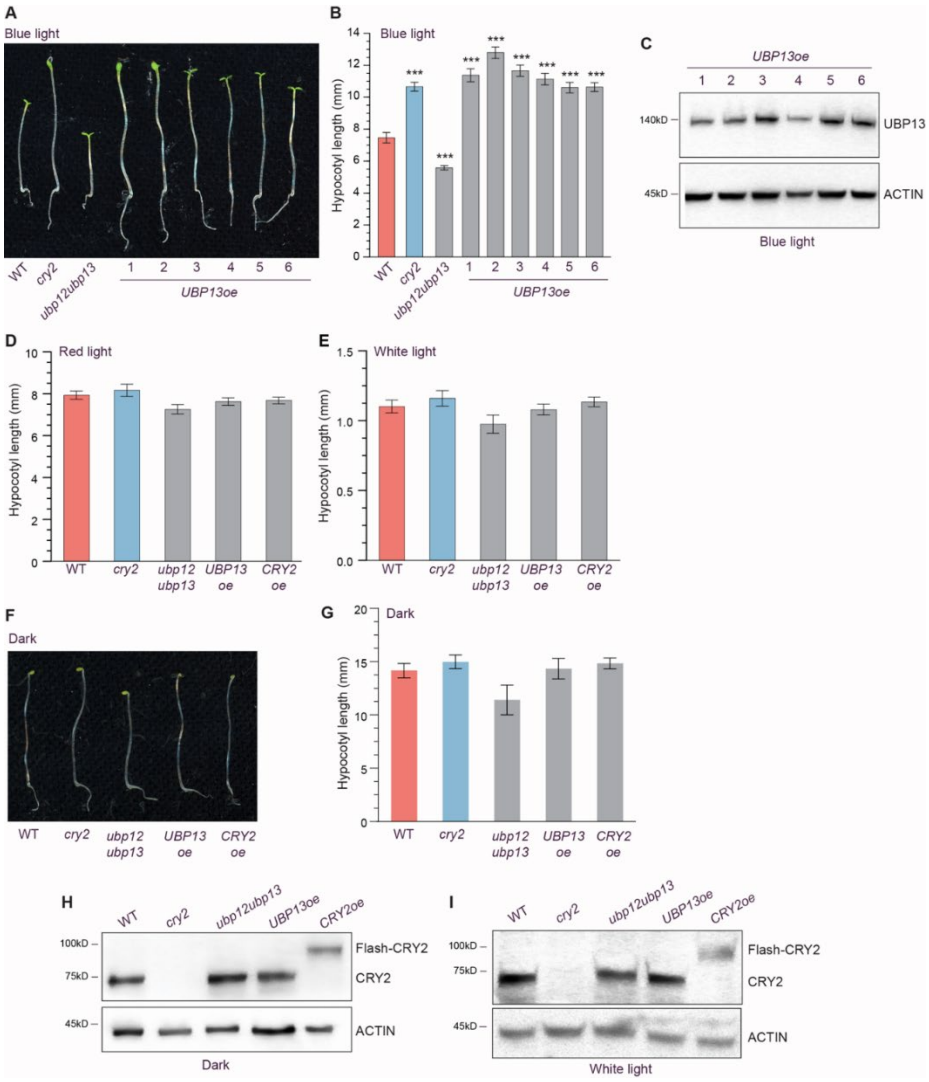

Figure 3.5: UBP12 and UBP13 regulate hypocotyl growth under blue light, related to Figure 3.4. (A) and (B) Hypocotyl length analysis of the indicated genotypes. Seedlings were grown for 4 days in 1 µmol m^{-2} s^{-1} BL before measuring their hypocotyl length. At least 15 seedlings per genotype were used for the measurements. Data are shown as means ± SE. Student's t-test: ***p < 0.001. (C) Immunoblot analysis of UBP13-6×HA (*UBP13oe*) in independent transgenic lines after 4 days of growth in constant BL (1 µmol m^{-2} s^{-1}). The UBP13-6×HA protein from the total protein lysate was detected using an anti-HA antibody. ACTIN detected using an anti-ACTIN antibody serves as a loading control. (D) Hypocotyl length analysis of the indicated genotypes under constant red light for 4 days (20 µmol m^{-2} s^{-1}). Data are shown as means ± SE. At least 15 seedlings were measured for each genotype. (E) Hypocotyl length analysis of the indicated genotypes under constant white light for 4 days (100 µmol m^{-2} s^{-1}). Data are shown as means ± SE. At least 15 seedlings were measured for each genotype. (F) and (G) Phenotype and hypocotyl length analysis of the indicated genotypes in 4-day-old dark grown seedlings. Data are shown as means ± SE. At least 15 seedlings were measured for each genotype. (H) and (I) Immunoblot analysis of CRY2 using an anti-CRY2 antibody from the total protein extracts in the indicated genotypes. Seedlings of the indicated genotypes were grown for 4 days in dark (F) or 100 µmol m^{-2} s^{-1} white light (G) before protein extraction. ACTIN detected with anti-ACTIN antibody is shown as a loading control. All immunoblots were repeated at a minimum of 2-3 times and a representative blot is shown. **Contribution**: I did not contribute data to this figure.

3.3.3 Genotypes with similar hypocotyl phenotypes have similar gene expression patterns

To corroborate whether genotypes that exhibit similar long hypocotyls (*UBP13oe* and *cry2*) and short hypocotyls (*ubp12ubp13* and *CRY2oe*) had similar underlying gene expression profiles, we analyzed their transcriptomes. We performed an RNA-sequence analysis on WT, *cry2*, *ubp12ubp13*, *CRY2oe*, and *UBP13oe* seedlings grown under BL (1 μmol m^{-2} s^{-1}) for 4 days using two biological replicates that correlated well with each other (Pearson's *R* between 0.98 and 0.99) (Figure 3.7A). We identified significant differentially expressed genes (DEGs; false discovery rate, FDR < 0.05) in these mutants and transgenics compared with WT (Table S1). The unbiased hierarchical clustering of DEGs identified two nodes: one for *ubp12ubp13* and *CRY2oe*, and the other for *cry2* and *UBP13oe* (Figure 3.6A). A gene ontology (GO) analysis further supported that *cry2* and *UBP13oe* have comparable gene expression changes and also between *ubp12ubp13* and *CRY2oe* (Figure 3.7B). We found that genes comprising of "light stimulus" and "light intensity" GO terms were overrepresented in *CRY2oe* and *ubp12ubp13* (Figure 3.6B; Data S1), indicating active light-dependent signaling and gene expression changes leading to hypocotyl growth inhibition (Pedmale et al. 2016; Huang et al. 2019). In contrast, genes belonging to "cell wall organization" or "microtubule assembly" GO terms, characteristic of a growing or uninhibited hypocotyl (Pedmale et al. 2016; Sasidharan and Pierik 2010), were upregulated in *cry2* and *UBP13oe* (Figure 3.6B; Data S1). CRYs in animals and plants mostly modulate gene expression through their interaction with the bHLH family of transcription factors, like PIFs, that bind to the E/G-box promoter elements of the genes (Pedmale et al. 2016; Koike et al. 2012). Therefore, we reasoned that increased CRY2 activity will result in the expression of genes with an overrepresentation of E/G-box cis-elements in their promoters. Indeed, among the promoter sequences of genes commonly upregulated in *CRY2oe* and *ubp12ubp13*, we identified the G-box [CACGTG] cis-motif, but not in those of *cry2* and *UBP13oe* (Figure 3.7C). These observations indicate that phenotypic changes due to changes in gene expression are sensitive to the levels of CRY2 and further reinforce that UBP12/13 are involved in regulating CRY2 and hypocotyl growth in BL.

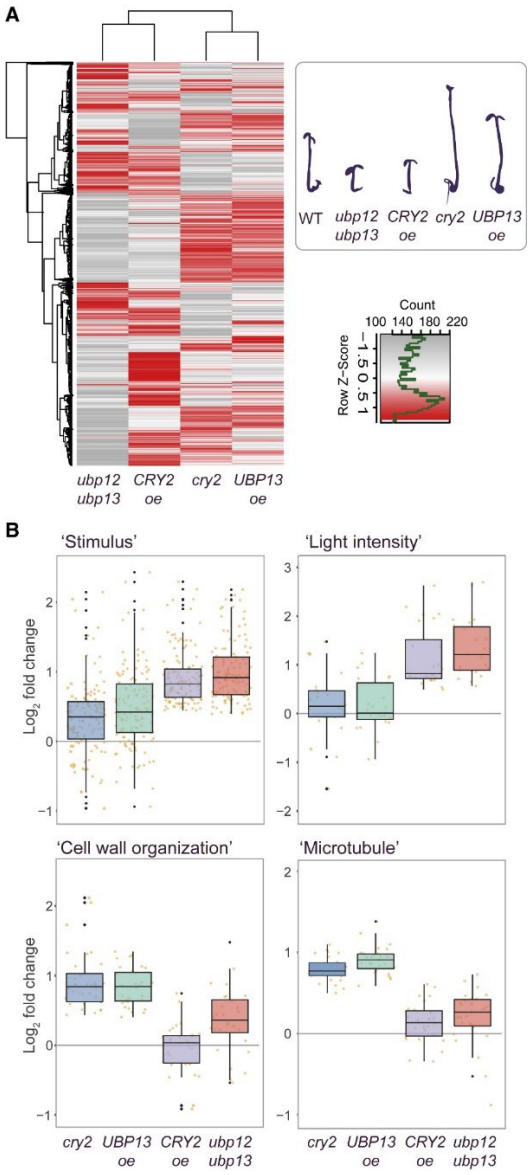

Figure 3.6: Genotypes with similar hypocotyl phenotypes have similar gene expression patterns. (A) Unbiased hierarchical clustering of differentially expressed genes from the RNA sequencing analysis performed on the indicated genotypes compared with the WT. RNA sequencing was performed on mRNA isolated from 4-day-old seedlings grown under 1 μmol m^{-2} s^{-1} BL. (B) Boxplot of representative expression pattern of the genes constituting the indicated GO (gene ontology) terms in the specified genotypes. Center lines are the medians; box limits indicate the 25th and 75th percentiles; whiskers extend 1.5 times the interquartile range from the 25th and 75th percentiles; outliers are represented by black dots. Orange jitter indicates individual data points. **Contribution**: I did not contribute data to this figure.

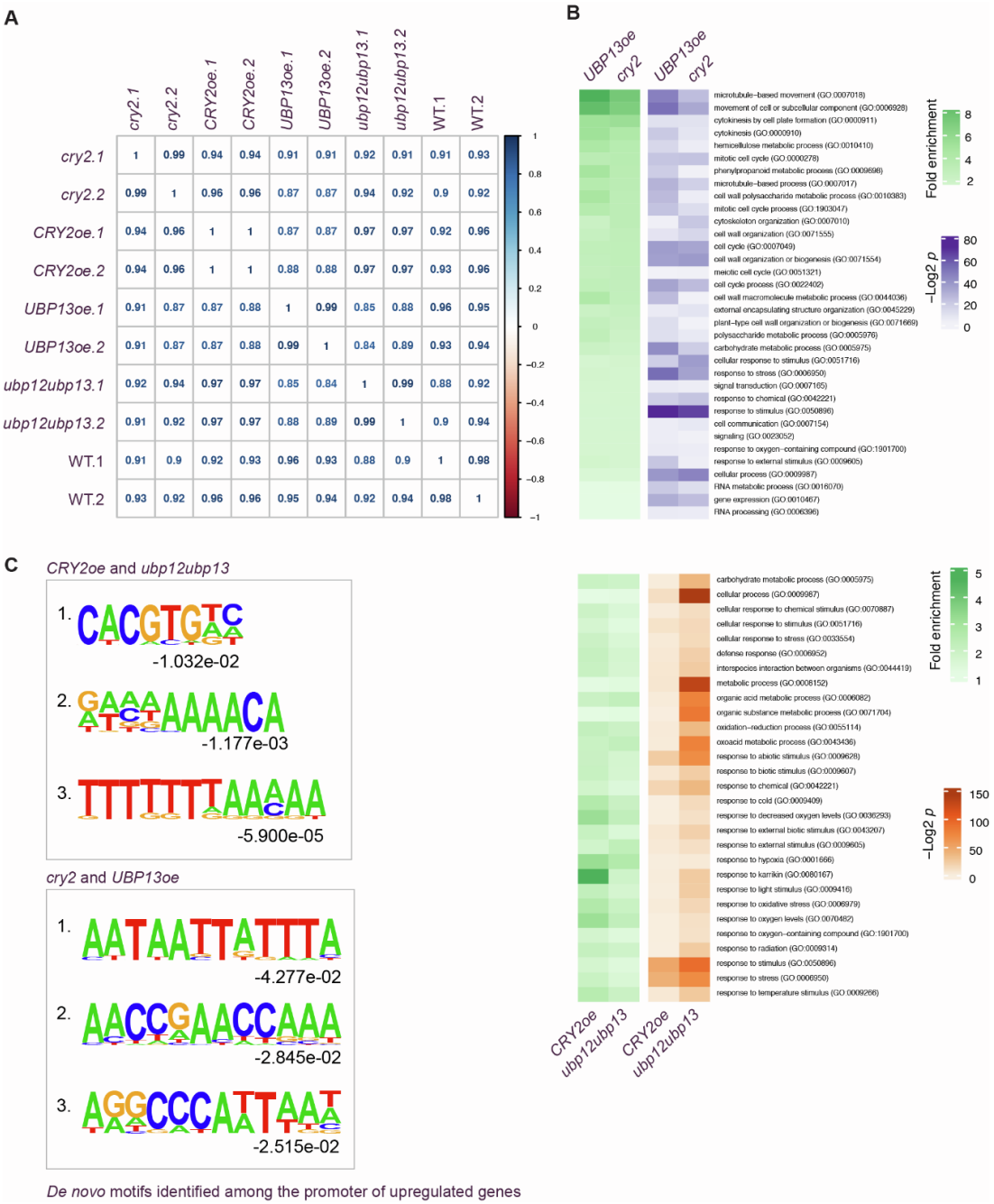

Figure 3.7: Qualitative analysis of RNA-seq data and the discovery of cis-elements, and Gene Ontology (GO) enrichment in the differentially expressed genes, related to Figure 3.6.
(A) Pearson's correlation between the biological replicates among the indicated genotypes used in the RNA-sequencing analysis. Numerals '1' and '2' in the genotype names indicate independent biological replicates. (B) Top and common (ranked by fold enrichment) of significantly enriched GO (gene ontology) terms derived from genes that are upregulated in *ubp12ubp13* and *CRY2oe*, which has a short hypocotyl under blue light; and between *cry2* and *UBP13ox*, which has a long hypocotyl phenotype. (C) Top three *de novo* promoter cis-elements identified in the promoters of genes that are upregulated in the indicated genotypes and comparison. 500 bp upstream from the start codon of the gene was used as a promoter sequence to identify cis-elements. **Contribution**: I did not contribute data to this figure.

3.3.4 The MATH domain and catalytic activity of UBP13 are required to regulate hypocotyl growth

To gain insight into the role of UBP12/13 in the regulation of the CRY2 protein, we generated the *cry2ubp12ubp13* triple mutant. The hypocotyl length of *cry2ubp12ubp13* in BL was similar to that of *cry2* (Figure 3.8A), indicating that *CRY2* is epistatic to *UBP12* and *UBP13* and that CRY2 and UBP12/13 function together to regulate hypocotyl growth. As the loss of UBP12 and UBP13 (in *ubp12ubp13*) increases CRY2 levels (Figure 3.4E) and leads to hypersensitive hypocotyl in BL (Figures 3.4C and 3.4D), we examined whether overexpression of CRY2 in *ubp12ubp13* (*ubp12ubp13;CRY2oe*) can further reduce the hypocotyl length of *ubp12ubp13*. *ubp12ubp13;CRY2oe* exhibited enhanced hypocotyl inhibition compared with *CRY2oe* and *ubp12ubp13* alone (Figure 3.8A), which is indicative of increased abundance and stabilization of CRY2.

When we overexpressed UBP13ΔMATH (*UBP13ΔMATHoe*), we did not observe any defects in hypocotyl growth under BL, which reinforces that the MATH domain that mediates the contact of UBP13 with CRY2 is required for the hyposensitive phenotype seen in *UBP13oe* (Figures 3.8B and 3.10A). We also tested whether the enzymatic activity of UBP13, which catalyzes the hydrolysis of the bonds between ubiquitin and its substrate, affects the hypocotyl growth. We overexpressed catalytically inactive UBP13 (*UBP13^{CD}oe*), carrying Cys207Ser substitution in its catalytic box (Cui et al. 2013) (Figures 3.3A and 3.10A). Hypocotyl growth in independent *UBP13^{CD}oe* seedlings was identical to that of WT, indicating that UBP13 enzymatic activity is required to mediate hypocotyl growth (Figure 3.8B). Collectively, these results indicate that the physical interaction of UBP13 with CRY2 and the enzymatic activity of UBP13 are required to regulate the abundance of CRY2 and hypocotyl growth in BL.

3.3.5 The loss of UBP12 and UBP13 leads to impaired ubiquitination of CRY2 in BL

Since our results indicate that UBP12/13 and CRY2 function together and that UBP12/13 negatively regulate CRY2, we tested whether UBP12/13 control the ubiquitination of CRY2. Dark-

grown seedlings expressing Flash-CRY2 (*cry2;Flash-CRY2*), or in *ubp12ubp13* mutant (*ubp12ubp13;Flash-CRY2*), were exposed to BL (30 μmol m^{-2} s^{-1}) for 30 min or kept in the dark before total proteins were extracted. We then captured total ubiquitinated proteins from these protein extracts using the tandem ubiquitin binding entities (TUBEs) method (Figure 3.8C) (Hjerpe et al. 2009). Immunoblotting with anti-ubiquitin antibody confirmed that ubiquitinated proteins were captured from both dark- and BL-treated seedlings (Figure 3.8D). Immunoblotting with anti-FLAG antibody to detect Flash-CRY2, we observed the enrichment of ubiquitinated Flash-CRY2 (Figure 3.8D, lanes 1–3) in *cry2;Flash-CRY2* after exposure to BL, which was consistent with the previous reports that BL stimulates CRY2 ubiquitination (Liu et al. 2016b). However, we observed little ubiquitination of Flash-CRY2 in *ubp12ubp13* seedlings (Figure 3.8D, lanes 4–6). Our findings suggest that UBP12/13 control the ubiquitination of CRY2 in BL.

3.3.6 UBP13 interacts with COP1 and increases its stability to mediate CRY2 degradation in BL

Our data so far indicate that the UBP12/13-CRY2 complex likely regulates the activity of another protein, which, in turn, likely destabilizes CRY2. We reasoned that one such candidate is COP1, since it is partially required for the turnover of CRY2 (Figures 3.10B and 3.11F). COP1 and SPAs interact with CRY2 (Weidler et al. 2012; Lau et al. 2019; Ponnu et al. 2019; Chen et al. 2021; Wang et al. 2001, 2015), and we also identified them in the same protein complex containing CRY2 and UBP12/UBP13 (Figure 3.2A). Therefore, we proceeded to test whether UBP12/13 influences COP1. First, we found that FLAG-UBP13 immunoprecipitated Myc-COP1 in an *in vitro* pull-down experiment, indicating their direct contact (Figure 3.2D). Additionally, we found that FLAG-UBP13 immunoprecipitated Myc-COP1 and Myc-CRY2 simultaneously *in vitro*, indicating their ability to form a ternary complex consisting of CRY2, UBP13, and COP1 (Figure 3.9A). We determined that the UBP13-COP1 interaction occurs preferentially in the nucleus, as determined by BiFC in *N. benthamiana* (Figure 3.10C). Co-immunoprecipitation using plant extracts demonstrated that both

UBP13-6xHA and UBP13ΔMATH-6xHA interacted with COP1-6xHis-3xFLAG (Figure 3.9B), suggesting that the MATH domain, which mediates the UBP13-CRY2 interaction, is not required for the contact between UBP13 and COP1. We observed an increase in Myc-COP1 pull-down under light compared with dark when FLAG-UBP13 was immunoprecipitated in the presence of Myc-CRY2 *in vitro* (Figure 3.10D), which is in agreement with a previous report that light enhanced COP1-CRY2 interaction (Holtkotte et al. 2017).

Next, we determined COP1 levels in *ubp12ubp13*, *UBP13oe*, and COP1 tagged with 6xHis-3xFLAG overexpressing (*COP1oe*) seedlings grown in BL and in the dark. Immunoblotting with an anti-COP1 antibody revealed that COP1 was present in a much higher abundance in *UBP13oe* and undetectable in *ubp12ubp13* in BL (Figures 3.9C and 3.11C), but not in the dark (Figures 3.10E and 3.11G), indicating that UBP12/13 stabilize COP1 in BL. We found that *COP1oe* exhibited a long hypocotyl phenotype insensitive to BL similar to *cry2* and *UBP13oe* seedlings, whereas *cop1* had a shorter hypocotyl (Figures 3.9D and 3.9E). When we overexpressed COP1 in *ubp12ubp13* (*ubp12ubp13;COP1oe*), its hypocotyl growth was not affected in the dark but was significantly reduced in BL, comparable with *ubp12ubp13* (Figures 3.9F and 3.10F), supporting the idea that UBP12/13 are required for COP1's activity. Together, our combined molecular and genetic data suggest that UBP13 physically interacts with COP1 along with CRY2. Furthermore, UBP12/13 are necessary for the stability and activity of COP1 in BL. Stabilized COP1 then promotes ubiquitination and turnover of photoactive-CRY2 under BL to modulate hypocotyl growth (Figure 3.12).

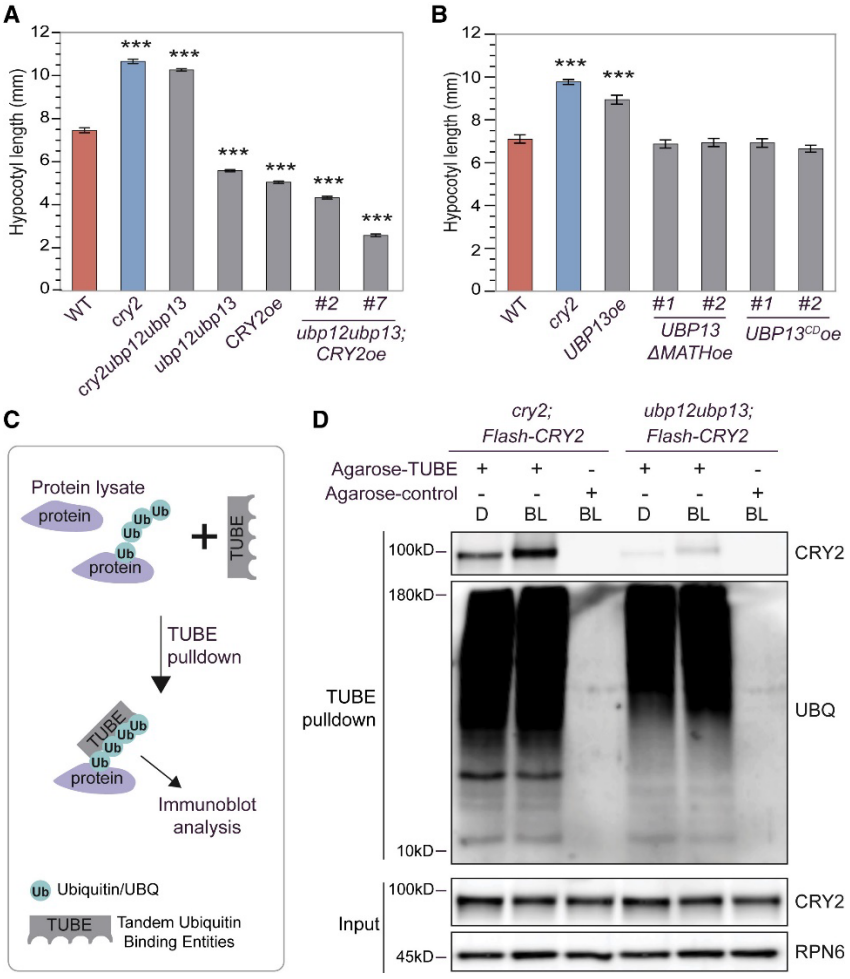

Figure 3.8: UBP12 and UBP13 are required for the ubiquitination and degradation of CRY2 in BL.

(A and B) Hypocotyl length of 4-day-old seedlings of the indicated genotypes grown in BL (1 μmol m^{-2} s^{-1}). (C) Illustration of a tandem ubiquitin binding entities (TUBE) pull-down method to enrich ubiquitinated proteins from total protein extracts. (D) TUBE pull-down of protein extracts from 4-day-old indicated transgenic seedlings either treated with 30 μmol m^{-2} s^{-1} BL for 30 min or mock treated in the dark. Agarose-control beads without TUBE served as negative control. Immunoblotting with an anti-FLAG antibody detected Flash-CRY2; anti-ubiquitin (P4D1) antibody detected total ubiquitinated (UBQ) proteins. RPN6 was used as a loading control. The experiment was repeated at least 3 times with similar results. D, dark; BL, blue light. For (A) and (B), data are shown as mean ± SE, n = 15, and repeated at least three times (Student's t test: ***$p < 0.001$). Numerals following the pound indicates independent transgenic lines. **Contribution**: I did not contribute data to this figure.

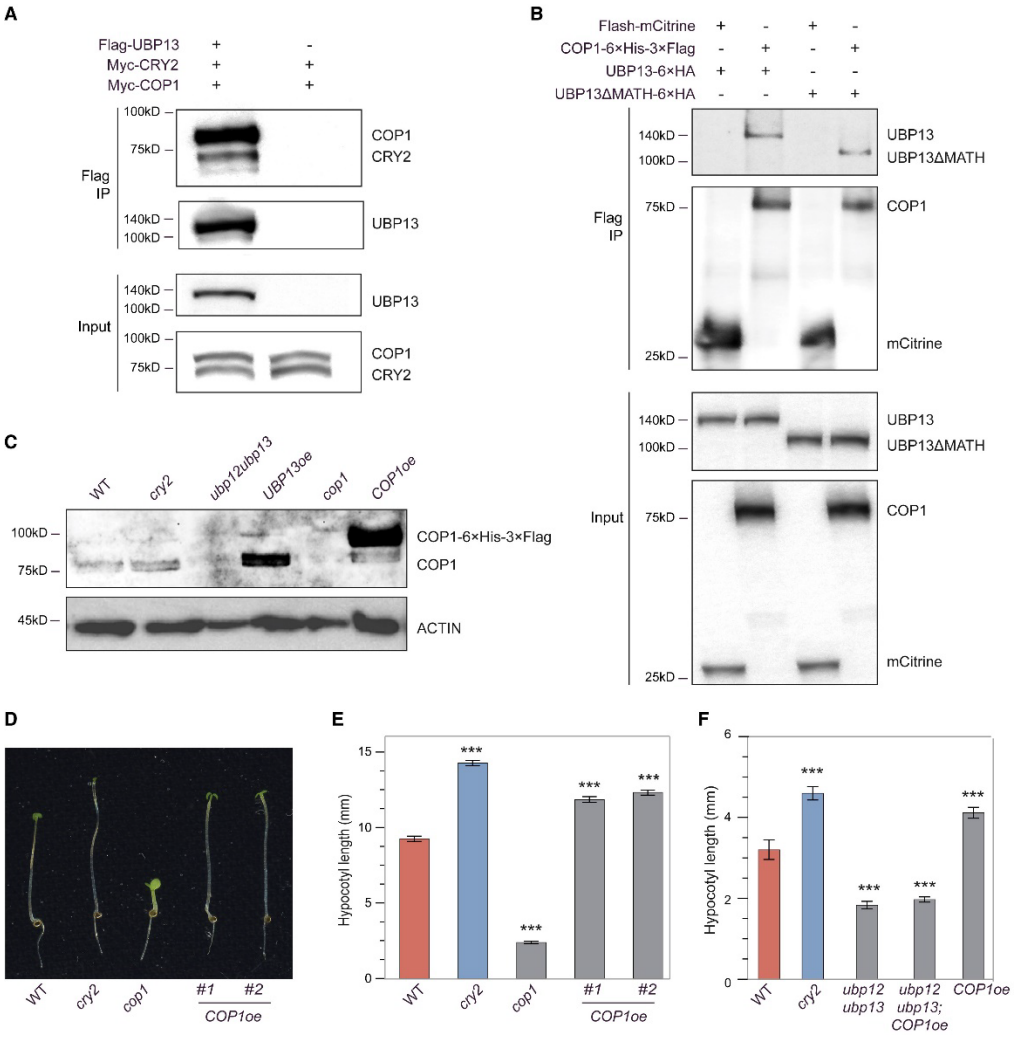

Figure 3.9: UBP13 interacts with COP1 and is required for its stability and activity in BL.
(A) *In vitro* co-immunoprecipitation of the indicated proteins using an anti-FLAG antibody. (B) Co-immunoprecipitation of the indicated proteins expressed in *N. benthamiana* using an anti-FLAG antibody. Flash-mCitrine serves as a negative control. (C) Immunoblot analysis of COP1 (detected by an anti-COP1 antibody) in 4-day-old seedlings of the indicated genotypes grown under BL (1 µmol m^{-2} s^{-1}). ACTIN serves as a loading control. (D and E) Phenotype and hypocotyl length of the indicated 4-day-old genotypes grown under 1 µmol m^{-2} s^{-1} BL. (F) Hypocotyl length of the indicated genotypes grown for 3 days in 1 µmol m^{-2} s^{-1} BL. For (E) and (F), data are shown as mean ± SE, n = 15, and repeated at least two-three times (Student's t test: ***$p < 0.001$). Numerals following the pound indicates independent transgenic lines. **Contribution**: Myself and Prof. Ullas V. Pedmale together performed the experiments that resulted in the data shown in Figure 3.9A and Figure 3.9C.

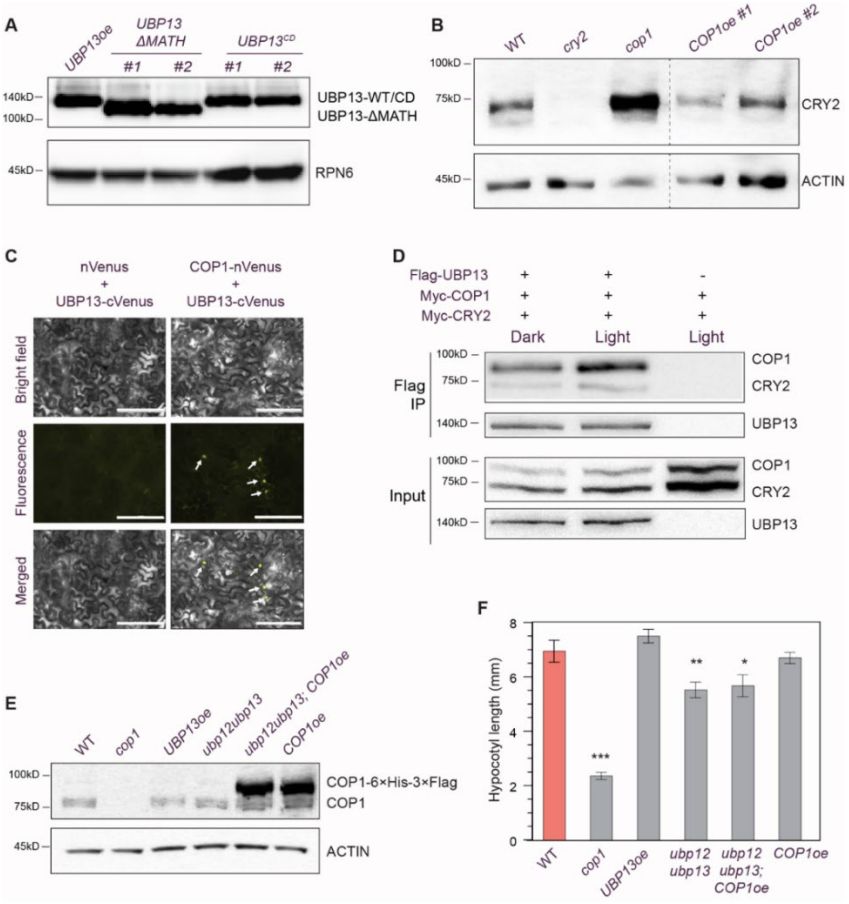

Figure 3.10: COP1 interacts with UBP13 and CRY2, related to Figures 3.8 and 3.9.
(A) Immunoblot analysis of UBP13-6×HA (*UBP13oe*), UBP13^{CD}-×HA, UBP13ΔMATH-6×HA in 4day-old *Arabidopsis* transgenic seedlings grown under blue light (1 µmol m^{-2} s^{-1}) and the specific proteins were detected using an anti-HA antibody. RPN6 detected using an anti-RPN6 antibody is shown as a loading control. (B) Immunoblot analysis of the CRY2 protein from the total protein isolated from the indicated genotypes using an anti-CRY2 antibody. Seedlings were grown for 4 days in 1 µmol m^{-2} s^{-1} blue light before protein extraction. ACTIN detected using an anti-ACTIN antibody is shown as a loading control. The dashed vertical line indicates that the blot has been cut and compared on the same blot. At least three immunoblots were performed and a representative blot is shown. (C) Microscopic images of the BiFC of the indicated proteins in the abaxial epidermal cells of *N. benthamiana* leaves. nVenus indicates the amino-terminal half of the venus fluorescent protein. cVenus indicates the carboxyl-terminal half of the venus protein. Arrows indicate fluorescence signal in the nucleus. Scale bar = 200 µm. The experiment was repeated at least 3 times with identical results. (D) *In vitro* co-immunoprecipitation of Flag-UBP13 with Myc-COP1 and Myc-CRY2 in the dark and light. Flag-UBP13 was immunoprecipitated using an anti-Flag antibody and the indicated proteins were detected using anti-Myc and anti-Flag antibodies. The experiment was performed at least twice. (E) Immunoblot analysis of COP1 protein in the total protein extracts from the indicated genotypes grown in the dark for 4 days. COP1 protein was detected using an anti-COP1 antibody. ACTIN detected using anti-ACTIN antibody serves as a loading control. A representative blot from at least two individual experiments is shown. (F) Hypocotyl length of seedlings of the indicated genotypes grown in the dark for 3 days. 11-13 seedlings were measured and the data are shown as means ± SE. Student's t-test: ***$p < 0.001$; **$p<0.01$; *$p<0.05$. **Contribution**: Myself and Prof. Ullas V. Pedmale together performed the experiments that resulted in the data shown in Figure 3.10D and Figure 3.10E.

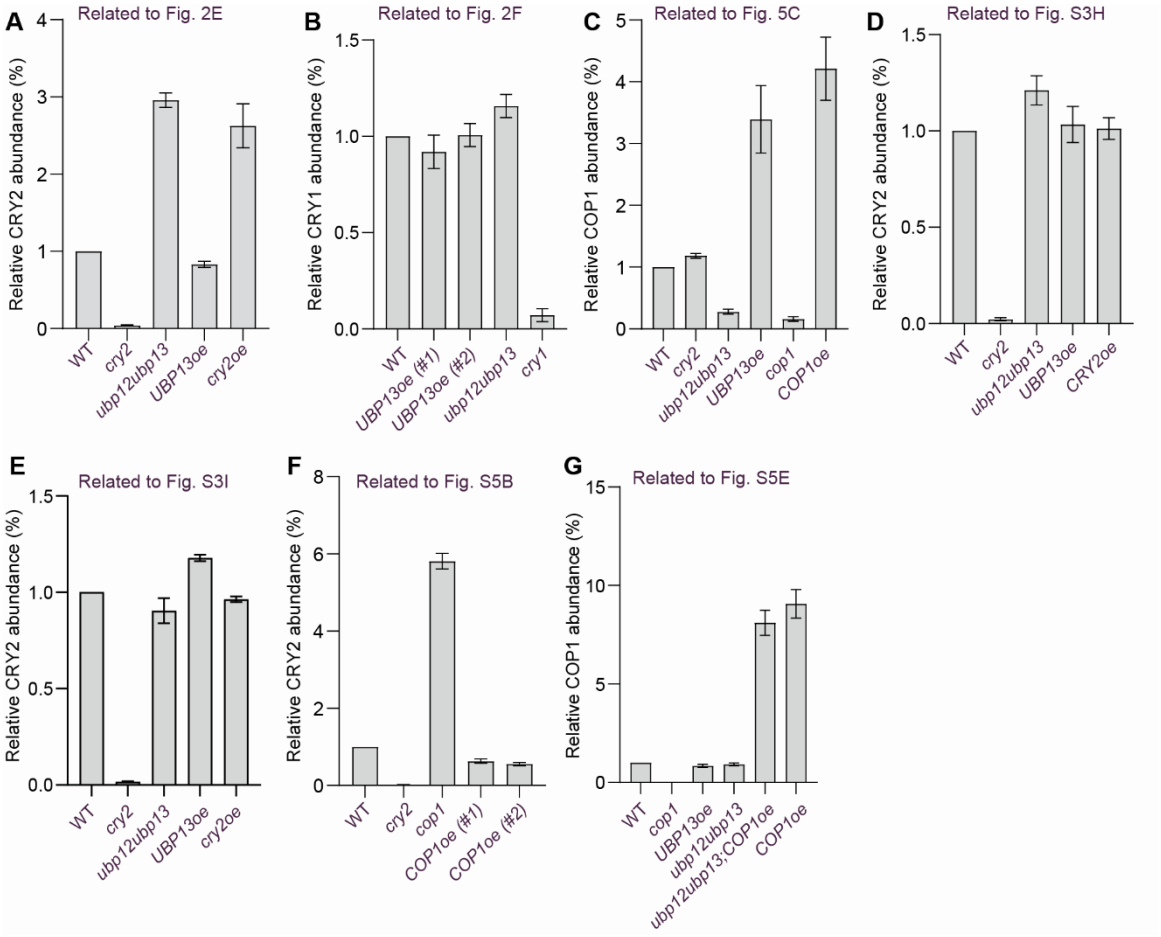

Figure 3.11: Quantification of protein levels in the immunoblots, related to Figures 3.4, 3.9, 3.5, and 3.10.

(A) to (F) Quantification of the indicated protein levels in the immunoblots (using replicates) shown in the indicated figures. The protein level for each genotype is compared to the WT and adjusted to the ACTIN loading control using ImageJ software (https://imagej.nih.gov). **Contribution**: Myself and Prof. Ullas V. Pedmale together performed the experiments that resulted in the data shown in Figure 3.11C and Figure 3.11G.

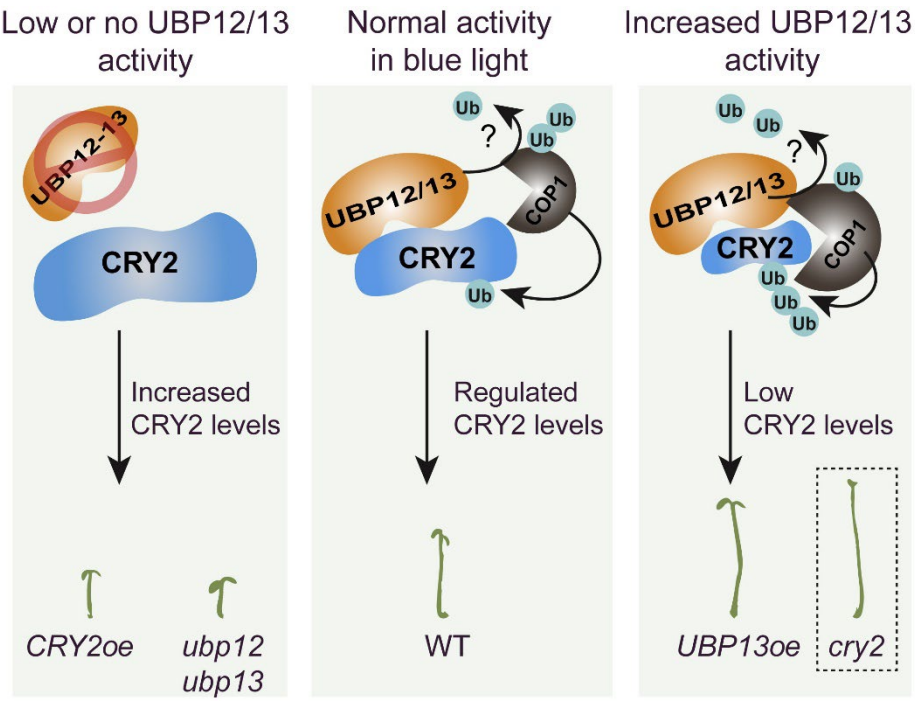

Figure 3.12: Model illustrating the role of UBP12/13 in the regulation of CRY2 and COP1 to modulate hypocotyl growth in BL.
During optimal photomorphogenesis (middle), CRY2-UBP12/13 complex recruits the COP1 E3 ubiquitin ligase and UBP12/13 stabilizes COP1 under BL. This stabilized COP1 (as part of $CRL4^{COP1-SPA}$) then targets CRY2 for degradation, leading to optimal hypocotyl growth. Loss of UBP12/13 (as in *ubp12ubp13*) leads to an increase in CRY2 levels due to the lack of stabilization of COP1. Therefore, the hypocotyl phenotype of *ubp12ubp13* resembles *CRY2oe* (right). Consequently, increased UBP12/13 activity results in enhanced stabilization of COP1, leading to ubiquitination and degradation of CRY2, as *UBP13oe* seedlings have a BL insensitive phenotype similar to the *cry2* mutant (left). **Contribution**: I did not contribute data to this figure.

3.4 Discussion

Our study established a critical role for UBP12 and UBP13 in the CRY-mediated signaling pathway to regulate hypocotyl growth. UBP12/13 physically interacted with CRY2 and promotes its ubiquitination and turnover indirectly under BL. UBP12/13 also interacted directly with COP1 to stabilize and modulate its activity to cause CRY2 turnover. Consistent with this model, specifically in BL, we show that the *ubp12ubp13* and *cop1* displayed a short hypocotyl phenotype, similar to *CRY2oe*, indicating that they contain increased levels of CRY2. Plants overexpressing UBP13 and COP1 exhibited long hypocotyls, phenocopying *cry2* indicating lower levels or loss of CRY2. CRY2 turnover was accelerated in *UBP13oe* but was substantially stabilized and accumulated in *ubp12ubp13*. Additionally, COP1 was unstable and barely detectable in *ubp12ubp13*, whereas it stabilized when UBP13 was overexpressed in BL and not in the dark. Together, our results reveal a key role for UBP12/13 in the regulation of hypocotyl growth and demonstrate a mechanism by which UBP12/13 regulates CRY2 abundance by stabilizing COP1 in BL. This abundance of CRY2 affects the sensitivity of hypocotyl to light.

UBP12/13 belong to an ancient lineage that consists of USP7 (ubiquitin-specific protease 7) and other related DUBs in metazoans and *Drosophila* (Figure 3.3A) (Cui et al. 2013; Heimbucher and Hunter 2015; Tian et al. 2012). The *Arabidopsis* and human genomes code for 64 and 90 DUBs, in contrast, they have a large number of E3 ubiquitin ligases, 1,400 in *Arabidopsis* and 700 in humans (March and Farrona 2018; Lai et al. 2020; Vierstra 2009; George et al. 2018). The smaller number of DUBs suggests that each DUB can multitask and have a variety of substrates. This is indeed reflected in other studies, where UBP12/13 and USP7 regulate and are associated with multiple protein substrates that function in many diverse signaling pathways. In plants, UBP12/13 constitute the polycomb repressive complex 1 (PRC1) to regulate gene expression (Derkacheva et al. 2016; Lecona et al. 2015). UBP12/13 modulate the jasmonate hormone pathway by binding to the MYC2 transcription factor (Park et al. 2019) and associates with the RGRF1/2 receptors during root development (An et al. 2018).

The DA1, DAR1, and DAR2 peptidases are deubiquitinated by UBP12/13 to modulate plant development (Vanhaeren et al. 2020). UBP12/13 interact with the ZEITLUPE (ZTL) photoreceptor with ubiquitin ligase activity, which is essential for the circadian clock (Lee et al. 2019). USP7 interacts with the EBNA1 from Epstein-Barr virus, tumor suppressor p53, and its ubiquitin ligase, MDM2 (Saridakis et al. 2005; Li et al. 2004a). USP7 also interacts with mammalian CRYs, but it deubiquitinated them, in contrast to our study (Papp et al. 2015; Hirano et al. 2016).

UBP12/13 negatively regulated CRY2 by facilitating its ubiquitination and degradation through COP1. In this regard, UBP12/13 mirrored the function of an E3 ubiquitin ligase, underscoring a previously undocumented role for these DUBs. This is in stark contrast to all studies conducted to date on UBP12/13 and USP7. In previous studies and consistent with its function as a deubiquitinating protein, ectopic overexpression of USP7 and UBP12/13 stabilized their interacting partners. In contrast, their loss of function led to the destabilization of their target proteins. For example, in mammals, p53, CRY1/2, and MDM2 were stabilized when USP7 was overexpressed and were destabilized and degraded when USP7 was absent (Li et al. 2004a; Papp et al. 2015; Li et al. 2002). Similarly, UBP12/13 positively controlled the stability of MYC2, ZTL, RGRF1/2, DA1, DAR1, and DAR2 in *Arabidopsis* (Vanhaeren et al. 2020; Jeong et al. 2017; Lee et al. 2019; An et al. 2018).

We found that light enhanced the CRY2-UBP13 interaction, and the MATH domain of UBP13 provided substrate specificity. Furthermore, UBP13 interacted with COP1 in a region distinct from its MATH domain. DUBs are known to bind to ubiquitin ligases; for example, USP7 binds to MDM2 and RNF2/RING2, whereas UBP12/13 has been shown to interact with ZTL (Li et al. 2002; Maertens et al. 2010; Cummins et al. 2004). Interestingly, USP7 deubiquitinated MDM2 and its target p53, likewise, our data indicated that UBP12/13 interact with CRY2 and COP1 simultaneously. Like many other E3 ligases, COP1 undergoes autoubiquitylation as a self-regulation mechanism (Seo et al. 2003; de Bie and Ciechanover 2011). Here, UBP12/13 stabilized COP1 and positively promoted its activity in BL. Our data support a mechanistic model in which photoactivated CRY2 interacts with UBP12/13, and this complex likely recruits COP1. We hypothesize that UBP12/13 likely deubiquitinates COP1,

leading to its stabilization. Stabilized COP1 as part of the $CRL4^{COP1\text{-}SPA}$ ubiquitin ligase then ubiquitinates CRY2 (Figure 3.12). This dual mechanism of attenuation of CRY2 and stabilization of COP1 is unusual among the reported mechanisms but likely typifies the desensitization of the receptor in an ever-changing light environment of the plant. This regulation by the CRY2-UBP12/13-COP1 axis is particularly essential to maintain a correct balance between the active and inactive CRY2 protein pool to optimize hypocotyl growth during photomorphogenesis.

Despite decades of research on DUBs, how their catalytic activity and protein-substrate specificity are regulated is not well known. Few examples are available on the role of phosphorylation and ubiquitination in the regulation of catalytic activity and localization of DUBs. For example, phosphorylation of mammalian OTUB1, USP10, and ATXN3 results in their nuclear localization (Herhaus et al. 2015; Mueller et al. 2009; Yuan et al. 2010). However, how DUB activity is enhanced or inhibited by protein-protein interactions is poorly understood, especially in plants. Our results suggest that the interaction of UBP12/13 with photoactive CRY2 probably regulates its activity and subsequent activation of COP1. COP1 overexpression in *ubp12ubp13* seedlings did not lead to hypocotyl elongation compared with *COP1oe* alone in BL (Figure 3.9F). Similarly, in the absence of UBP12/13, the ubiquitination of CRY2 was reduced (Figure 3.8D). This suggests that UBP12/13 are required for the normal function of COP1, and UBP12/13 are themselves possibly regulated by photoactivated CRY2. Therefore, our findings provide insight and a framework for testing how ligands and their receptors regulate DUB activity through protein-protein interactions.

CRL4 E3 ubiquitin ligases can initiate different types of proteolytic as well as non-proteolytic ubiquitination, including polyubiquitination and monoubiquitination (Dumbliauskas et al. 2011; Choi et al. 2020). Likewise, extensive studies on USP7 have revealed that it can deubiquitinate mono- and poly-ubiquitinated substrates. USP7 cleaves K6-, K11-, K33-, K48-, and K63-linked ubiquitin chains and less efficiently, K27 and K29 chains (Pozhidaeva and Bezsonova 2019). Future studies are required on the nature of the ubiquitin chains cleaved by UBP12/13 and their role in stabilizing COP1, if by deubiquitination, and the detailed account by which UBP12/13, CRY2, and COP1 form a multiprotein

complex. Interestingly, we observed enrichment of G-boxes, commonly bound by PIFs, in the promoters of genes upregulated in *ubp12ubp13* and *CRY2oe*. Many of these upregulated genes are also directly regulated by PIF3, PIF4, and PIF5 (Pedmale et al. 2016; Zhang et al. 2013), and it is plausible that UBP12/13 could directly or indirectly modulate their activities.

CRYs, UBP/USP deubiquitinases, and COP1 are present in all major evolutionary lineages, pointing to a recent common ancestor in which these proteins originated before plants and animals diverged (Komander et al. 2009; Cui et al. 2013; Liu et al. 2008c; Han et al. 2020). Importantly, light-dependent degradation of CRYs is preserved in flies, mammals, and plants to regulate their activity (Godinho et al. 2007; Siepka et al. 2007; Busino et al. 2007; Peschel et al. 2009). However, the CRY-COP1 interaction observed in plants is not conserved in mammals (Rizzini et al. 2019). USP7 interacts with CRYs; however, contrary to our findings in plants, USP7 stabilized mammalian CRY1/CRY2 by deubiquitination (Papp et al. 2015; Hirano et al. 2016). Thus, the interaction between CRYs and DUBs is mirrored in mammals and plants, but their roles and regulatory logic are reversed. Furthermore, contrary to the current assumption that DUBs generally stabilize proteins, our findings accentuate their importance in facilitating protein turnover. My study opens the door to future investigations on the deubiquitinase-dependent stabilization of proteins and their roles in a multitude of development and growth programs.

3.5 Experimental model and subject details

Plants of *Arabidopsis thaliana* ecotype Columbia (Col-0) was used as a wild type (WT) and mutants and transgenics in this ecotype were generated and analyzed. *Arabidopsis* mutants used in this study have been previously described: *cry1-304* (Mockler et al., 1999), *cry2-1* (Lin et al. 1998), *ubp12-1* (GABI_244E11), *ubp12-2w* (GABI_742C10), *ubp13-1* (SALK_128312), *ubp13-3* (SALK_130784), *ubp12-2w ubp13-3* (Cui et al. 2013), and *cop1-4* (McNellis et al. 1994). Transgenic line *cry2-1;UBQ10$_{pro}$:9xMyc-6xHis-3xFlag-CRY2* (*Flash-CRY2/CRY2oe*) has been reported previously

(Pedmale et al. 2016). For all experiments, seeds were plated on 0.5× Linsmaier and Skoog (LS) medium (HiMedia Laboratories) with 0.8% agar, stratified for 2 days at 4°C in darkness and grown under the indicated light conditions in a LED growth chamber (Percival Scientific). *Nicotiana benthamiana* (tobacco) was grown under long days (16/8h day/night cycle) in the greenhouse or in a growth incubator at 22°C. Leaves of 3-4-week-old *N. benthamiana* were used for infiltration to transiently express proteins.

3.6 Method details

3.6.1 Cloning and generation of *Arabidopsis* transgenic lines

All coding and promoter sequences were amplified from a cDNA pool from WT plants or a known plasmid containing the coding sequence using standard PCR techniques and cloned in one of the Gateway donor vectors (pDONR-221, pDONR-P4P1R, or pDONR-P2RP3; Thermo Fisher) using BP Clonase II (Thermo Fisher). We used multisite Gateway cloning technique to combine the donor constructs with either pB7m34GW or pK7m34GW binary destination vectors (Karimi et al. 2007) using LR Clonase II (Thermo Fisher) to generate the final expression constructs. Agrobacterium tumefaciens (GV3101) containing the expression constructs were used to transform *Arabidopsis* by the floral dip method (Clough and Bent 1998) to generate the transgenic lines. *Arabidopsis UBIQUITIN 10* (*UBQ10*) constitutive promoter was used to drive the expression of UBP13, UBP13^{CD}, and UBP13ΔMATH tagged with 6xHA epitope tag. UBP13^{CD} was generated by replacing Cys207 with a Ser residue in the UBP13 coding sequence by site-directed mutagenesis and UBP13ΔMATH line was generated by deleting the MATH domain residues 1-178 a.a. by PCR. CRY2 overexpressing lines in *ubp12ubp13* was generated by transforming with a *UBQ10$_{pro}$:Flash-CRY2* construct. COP1 overexpressing lines in WT was generated by transforming with a *UBQ10$_{pro}$:COP1-6xHis-3xFlag* construct using the Gateway technique. All the transgenic lines were selected on growth media supplemented with appropriate antibiotics. Transgenic plants containing a single insertion of the transgene was selected on the basis of

its segregation (~3:1 resistant: sensitive) on selective media in the T2 generation. Plants containing a single transgene were characterized for functionality based on its ability to complement its mutant or by monitoring transgene expression by immunoblotting. T3 or later generation of transgenic lines were used for the experiments. A list of primers used for cloning and genotyping is provided in Table S2.

3.6.2 Hypocotyl length measurements

As indicated, genotypes were grown in 1 μmol m^{-2} s^{-1} constant blue light (BL), 20 μmol m^{-2} s^{-1} constant red light or 100 μmol m^{-2} s^{-1} constant white light in a LED chamber at 22°C (Percival Scientific). Following the growth period, seedlings were placed horizontally on agar LS media and imaged using a flatbed scanner (Epson). Hypocotyl length was then measured using ImageJ software. For all measurements, at least 15 seedlings were measured and the experiment was repeated at least 3 times.

3.6.3 Co-immunoprecipitation of proteins in *N. benthamiana* and *Arabidopsis*

For co-immunoprecipitation (co-IP) assays in *N. benthamiana*, *Agrobacterium tumefaciens* containing the indicated constructs along with p19 (Lombardi et al. 2009) were infiltrated into the leaves and after 3 days the leaves were flash-frozen using liquid nitrogen. The constructs used were *$UBQ10_{pro}$:Flash-CRY2*, *$UBQ10_{pro}$:Flash-mCitrine*, *$UBQ10_{pro}$:UBP13-6xHA*, *$UBQ10_{pro}$:UBP13ΔMATH-6xHA*, and *$UBQ10_{pro}$:COP1-6xHis-3xFlag*. For co-IP assays in *Arabidopsis*, stable transgenic lines expressing *$CRY2_{pro}$:Flash-CRY2* and *$UBQ10_{pro}$:UBP13-6xHA* was used which was made by transforming *$UBQ10_{pro}$:UBP13-6xHA* into *cry2;$CRY2_{pro}$:Flash-CRY2* expressing line. 4-day old *Arabidopsis* etiolated seedlings were collected in the dark or exposed to 30 μmol m^{-2} s^{-1} BL for 10 min before sample collection and flash freezing in liquid nitrogen. Frozen plant tissue from *Arabidopsis* or *N. benthamiana* was finely ground by mortar and pestle using liquid nitrogen and then resuspended in SII buffer (100 mM sodium phosphate pH 8.0, 150 mM NaCl, 5 mM EDTA, 5 mM EGTA, 0.1% Triton X-100, 10 mM NaF, 1.5× protease inhibitor cocktail (VWR), 20 μM bortezomib (MedChemExpress) and 20 mM N-ethylmaleimide). The extracts were sonicated using a sonicator

(Branson) at 30% amplitude, 0.5 S on/off for a total of 10 S and clarified by 2× high speed centrifugation for 10 min at 4°C. Proteins were then quantified by Bradford assay. 2 mg of total protein was then incubated with anti-Flag antibody (M2 clone, MilliporeSigma) for 1 h with gentle rotation at 4°C and then protein-G coated magnetic beads (Thermo Fisher) were added and incubated for an additional 30 min. The beads were then washed 3× with 0.8 mL of SII buffer and the proteins were eluted from it using 2× Laemmli sample buffer by heating at 90°C for 5 minutes.

3.6.4 *in vitro* co-immunoprecipitation

The coding sequence of CRY2, COP1, UBP13, and Flag-MATH^{UBP13} were cloned in a modified pTnT vector (Promega) containing Gateway recombination sequence (Thermo Fisher) (Pedmale et al. 2016; Nito et al. 2013) to express them in an *in vitro* translation system. 1 to 1.5 µg of plasmid DNA for each construct (Myc-COP1, Myc-CRY2, Flag-UBP13, Flag-MATH^{UBP13}, or empty vector) were used to synthesize proteins using a transcription / transcription coupled system using the TNT SP6 Wheat Germ system (Promega) in the presence of 20 µm of FAD (MilliporeSigma) at 25°C for 2.5 hours. Equal quantities of *in vitro* synthesized proteins in the indicated combinations were mixed with 140 µl of IVIP buffer (140 mM NaCl, 2.7 mM KCl, 1 mM Na2HPO4, 1.8 mM KH2PO4, pH 7.3, 0.1% Igepal CA-630 (MilliporeSigma), 0.1% BSA, 1× plant protease inhibitor cocktail (MilliporeSigma), and 50 µM MG132 (VWR)) with gentle rotation at room temperature for 10 min. 2 µg of anti-Flag antibody (M2 clone, MilliporeSigma) was added to the mix and then incubated for 1 hour at 4°C with gentle rotation. This was followed by an incubation with protein-G magnetic beads (Bio-Rad) (prewashed with IVIP buffer) for 30 min with gentle rotation to collect the immunoprecipitates. The beads were then pelleted using a magnet and washed 3× with 0.7 mL of IVIP buffer (without the protease inhibitor cocktail and MG132) with gentle rotation. Proteins from the beads were then eluted with 2× SDS-PAGE sample buffer and subjected to the immunoblot assay. To assay for interaction in the dark, all the steps were done under dim red light.

3.6.5 Tandem Ubiquitin Binding Entities (TUBE) pulldown

Immunoprecipitation of ubiquitinated proteins from *cry2;UBQ10$_{pro}$:Flash-CRY2* and *ubp12ubp13;UBQ10$_{pro}$:Flash-CRY2* seedlings was performed as previously described (Zhang et al. 2017) with some minor modifications. 4-day old etiolated seedlings were first pre-treated by transferring them to liquid 0.5× MS medium containing 0.01% Silwet L-77 and 20 μM MG132, then vacuum infiltrated for 10 min and kept in dark for 2 hours. Thereafter, the seedlings were either kept in dark or transferred to 30 μmol m^{-2} s^{-1} BL for 30 min before being collected. Total proteins were using a buffer containing 100 mM MOPS, pH 7.6, 150 mM NaCl, 0.1% NP40, 1% Triton X-100, 0.1% SDS, 20 mM Iodoacetamide, 1 mM PMSF, 2 μg/mL aprotinin, 40 μM MG132, 5 μM PR-619, 1 mM 1,10-Phenanthroline and 2× Complete protease inhibitor cocktail and PhosStop cocktail (MilliporeSigma). 2 mg total protein was incubated with 30 μl agarose-TUBE2 or agarose-control beads (tebu-bio, Le Perray-en-Yvelines, France) for 5 hours at 4°C with gentle rotation. The agarose beads were washed three times with the extraction buffer and eluted with 2× Laemmli sample buffer at 90°C. The eluate was used for immunoblot analysis using anti-Flag-HRP (M2 clone, MilliporeSigma) for detection of Flash-CRY2, and anti-ubiquitin (P4D1)-HRP (Santa Cruz Biotechnology) antibody was used to detect ubiquitin and ubiquitinated proteins. Anti-RPN6 antibody was used to monitor uniform loading.

3.6.6 Immunoblot analysis

Immunoblot analysis was performed as described previously (Pedmale and Liscum 2007). Proteins were separated in 10% or 4-12% gradient Bis-Tris polyacrylamide gel (Thermo Fisher) using SDS-MOPS running buffer and transferred to reinforced nitrocellulose membrane (MilliporeSigma) electrophoretically. After transfer, the nitrocellulose membrane was incubated in 5% fat-free milk prepared in TBST (20 mM Tris-HCl pH 7.6, 150 mM NaCl, 0.05% Tween-20) for 30 min, followed by incubation with respective primary and secondary antibodies in 1% fat-free milk in TBST for 1-2 hrs with gentle shaking. The blots were washed 3× with TBST followed by chemiluminescent detection of protein using homemade substrate or commercially available (Dura substrate; Thermo Fisher). The

blots were imaged using a CCD camera (Canon) or on a radiographic film. Antibodies used for immunoblots are as follows: a polyclonal antibody against the C-terminal of CRY2 (SEGKNLEGIQDSSDQ) was produced in rabbit (Antibody Research Corporation, St. Louis) and used to detect CRY2. The anti-CRY1 antibody has been described (Liu et al. 2016b). Anti-COP1 antibody to detect COP1 is described previously (Maier et al. 2013). Anti-Flag-HRP (M2 clone, MilliporeSigma), anti-Myc-HRP (9E10 clone, Santa Cruz Biotechnology), anti-HA-HRP (3F10 clone, MilliporeSigma), anti-HA (HA-7 clone, MilliporeSigma) were used to detect the respective epitope-tagged proteins. Appropriate goat-anti-mouse-HRP and goat-anti-rabbit-HRP (Bio-Rad) was used as a secondary antibody. An anti-ACTIN antibody (MP Biomedicals) was used as a loading control. All immunoblot experiments were repeated at least 2-3 times with similar results.

3.6.7 Transient expression in *N. benthamiana* leaves

5 mL overnight cultures of *Agrobacterium tumefaciens* (GV3101) containing the expression constructs were centrifuged at 4000 g at room temperature for 15 min. The bacterial pellet was then resuspended in infiltration buffer (10 mM MgCl2, 10 mM MES pH 5.6, and 200 µM acetosyringone) and incubated at room temperature for at least 2 h. Each *Agrobacterium* suspension containing the desired construct was then mixed in an equal ratio along with RNA silencing suppressor p19 (Lombardi et al. 2009) to a final OD600 nm = 1.0 before infiltrating the abaxial side of *N. benthamiana* leaves using a needleless 1 mL syringe. 2-3 days post infiltration, the leaves were used for the appropriate experiments.

3.6.8 Cloning and localization of UBP13-mCitrine and UBP13ΔMATH-mCitrine

The UBP13-WT and UBP13ΔMATH were cloned into pDONR-221 vector. The UBP13 promoter sequence used was the 2043 bp upstream of the start codon of UBP13 ORF (Cui et al. 2013) and was cloned into the pDONR-P4P1R vector. These entry clones were then recombined with mCitrine (in pDONR-P2RP3) along with the pB7m34GW destination vector. The *$UBP13_{pro}$:UBP13-mCitrine* and *$UBP13_{pro}$:UBP13ΔMATH-mCitrine* constructs were then transformed into *A. tumefaciens*,

and then infiltrated into *N. benthamiana* leaves. The plants were kept for 1-day in light and then 1-day in dark, and subsequently leaf discs were taken. The leaf discs were then counterstained by immersing them in 0.02 µg/mL DAPI in water for 3 min and rinsed 2× in water before imaging the abaxial side using an inverted fluorescence microscope (Evos, Thermo Fisher) or a confocal laser scanning microscope (LSM 900; Zeiss). A list of primers used for cloning is provided in Table S2.

3.6.9 Bimolecular fluorescence complementation (BiFC)

CRY2, UBP13, and COP1 coding regions were cloned into pDONR-P2RP3 or pDONR-221 vectors to obtain the Gateway entry clones. These entry clones were then recombined together with either *UBQ10* or *CaMV 35S* promoter (in pDONR-P4P1R vector) and cVenus/nVenus (in pDONR-P2RP3 or pDONR-221) entry constructs along with pB7m34GW or pK7m34GW destination vectors using LR II clonase (Thermo Fisher). The final expression constructs $35S_{pro}$*:nVenus-CRY2*, $UBQ10_{pro}$*:UBP13-cVenus*, $UBQ10_{pro}$*:COP1-nVenus* and $UBQ10_{pro}$*:nVenus* were transformed into *A. tumefaciens*, mixed equally in the desired combinations and infiltrated into abaxial side of *N. benthamiana* leaves as described earlier. Fluorescence signal was analyzed 2-days post infiltration (1-day light/1-day dark) on the abaxial side of leaf discs using a fluorescence microscope.

3.6.10 RNA-sequencing and analysis

Seedlings in biological replicates were grown for 4 days in 1 µmol m^{-2} s^{-1} constant blue light and frozen in liquid nitrogen prior to RNA extraction. Total RNA was extracted using the RNeasy Plant Mini kit (Qiagen) and quantified using a Flurometer (Qubit 2.0, Thermo Fisher). 500 ng of total RNA was used to isolate poly(A)-mRNA using the NEBNext poly(A) mRNA Isolation Module (NEB) and the purified mRNA was used to construct sequencing libraries using the Ultra II Directional RNA library Prep Kit for Illumina (NEB). Single end short read sequencing of 76 bp were performed on NextSeq instrument (Illumina). Two biological replicates were sequenced. The sequencing reads were mapped to the *Arabidopsis thaliana* Col-0 reference genome (TAIR10) using the STAR aligner (Dobin et al. 2013). Since the Pearson's correlation *R* between the independent biological replicates were

between 0.98 – 0.99, the subsequent analysis was performed on two biological replicates for each genotype. Differential gene expression analysis was performed using Cuffdiff for Linux operating system (Trapnell et al. 2012). The list of DEGs is provided in Table S1. R environment (R Foundation) and its packages (ggplot2, ComplexHeatMap, RColorBrewer, gPlots, corrplot) was used for statistical analysis and to visualize the results. *De novo* cis-motifs in the promoters were identified using HOMER (Heinz et al. 2010).

3.6.11 Gene Ontology analysis

GO term enrichment was performed on Panther Classification System (Mi et al. 2021). The up-regulated and the statistically significant (FDR <0.05) upregulated genes were used to identify the enriched GO terms after Fisher's Exact test and Bonferroni correction. List of GO terms and associated genes described in this study are provided in Data S1.

3.6.12 Phylogenetic analysis

For phylogenetic analysis of the 27 UBP proteins in *Arabidopsis*, the full-length amino acid sequences based on TAIR10 genome were used. For phylogenetic analysis of UBP12/13 orthologs in other plant species, insect, vertebrate and worms, the amino acid sequence was obtained from NCBI. The alignment of the protein sequences was performed using ClustalW (MEGA-X Software). The phylogenetic tree was constructed using MEGA-X by identifying conserved positions of the alignment using the Neighbor-Joining method with bootstrap test set to 1001 replicates.

3.6.13 Affinity purification

5-day-old *cry2-1;UBQ10$_{pro}$:9xMyc-6xHis-3xFlag-CRY2* (*Flash-CRY2/CRY2oe*) and WT control seedlings grown in white light were exposed to attenuated blue light conditions for ~16 h as previously described (Pedmale et al. 2016). Total protein was extracted as previously described using SII buffer (Pedmale et al. 2016). Roughly 28 mg of total protein was incubated with 150 µl of protein-G-Dynabeads (Thermo Fisher) coupled to Flag antibody (M2 clone, MilliporeSigma). Protein complex

was eluted with 3×-Flag peptide (MilliporeSigma) and precipitated with TCA. Liquid-chromatography coupled to mass spectrometry (LC-MS) was performed using standard techniques.

3.6.14 Quantification and statistical analysis

We used R and Microsoft Excel to perform statistical analysis. For RNA-seq analysis, we used Cuffdiff. Enriched GO terms were determined using Fisher's Exact test with Bonferroni correction on the Panther platform. All numbers of plants used for the experiments and the statistical method employed can be found in the corresponding figure legends.

Chapter 4. Cryptochrome 2 interacts with the ISWI complex to regulate hypocotyl elongation and flowering time

4.1 Introduction

Cryptochromes modulate gene expression to control developmental processes, such as hypocotyl elongation and floral transition, by interacting with various transcription factors (TFs). For example, CRY2 interacts with PHYTOCHROME INTERACTING FACTOR 4 and 5 (PIF4/5) TFs to modulate plant response to low blue light shade (Pedmale et al. 2016) and interacts with CRYPTOCHROME-INTERACTING BASIC-HELIX-LOOP-HELIX 1 (CIB1) TF to bind to the *FLOWERING LOCUS T* (*FT*) gene and regulate flowering time (Liu et al. 2008a). Cryptochromes are known to be associated with chromatin and early studies have demonstrated that a GFP::CRY2 fusion protein accumulates on anaphase chromosomes in plant cells (Cutler et al. 2000). Furthermore, presence of CRYs is required for higher-order chromatin organization, namely the decondensation of heterochromatin during shifts in light intensity and floral transition (Tessadori et al. 2007; van Zanten et al. 2010b). Recent studies have shown that CRYs physically interact with the SWI2/SNF2-RELATED 1 (SWR1) chromatin-remodeling complex to modulate the deposition of the histone variant H2A.Z on chromatin (Mao et al. 2021), but there is no clear connection between the SWR1 complex and in higher-order chromatin organization. Therefore, the molecular mechanism by which CRYs facilitate higher-order chromatin decondensation remains largely unknown.

Previously, my laboratory conducted an affinity purification coupled with mass spectrometry (AP-MS) experiment to identify novel interactors of CRY2. Interestingly, among the proteins identified were CHROMATIN-REMODELING PROTEIN 11 (CHR11), CHR17, RINGLET 1 (RLT1), RLT2 and AT-RICH INTERACTING DOMAIN 5 (ARID5). These proteins collectively form the CHR11/17-RLT1/2-ARID5 (CRA) IMITATION SWITCH (ISWI) chromatin remodeling complex in *Arabidopsis*

(Tan et al. 2020). In plants, there exist multiple ISWI chromatin remodeling complexes, each consisting of ATPase subunits CHR11 and CHR17, along with different accessory subunits, thereby forming distinct complexes (Tan et al. 2020). The ISWI complex is essential for nucleosome sliding, leading to the establishment of an evenly-spaced nucleosome pattern within gene bodies (Li et al. 2014). Moreover, the ISWI proteins modulate expression of genes involved in floral transition to regulate flowering time (Li et al. 2012). Within the CRA ISWI complex, RLT1/2 act as mediators for the interaction between CHR11/17 and ARID5, while ARID5 is known to bind to AT-rich DNA sequences and histone H3K4me3 modifications (Tan et al. 2020). In this study, I confirmed the interaction between CRY2 and three ISWI proteins, namely CHR11, RLT1, and ARID5. Notably, I observed that mutations in *rlt1rlt2* and *arid5* were epistatic to the *cry2* mutation, exerting regulatory control over CRY2-dependent processes, including hypocotyl growth under blue light and floral transition. Additionally, my investigation revealed that *rlt1rlt2* and *arid5* mutations resulted in increased heterochromatin condensation during seedling development under blue light, in contrast to decreased heterochromatin condensation observed in the *cry2* mutant. These findings strongly suggest a critical role for the ISWI complex in the regulation of CRY-dependent processes.

4.2 Results

4.2.1 CRY2 physically interacts with the ISWI chromatin remodeling complex in a light-independent manner

Using AP-MS, we identified five novel CRY2 interactors which belong to the ISWI chromatin remodeling complex including CHR11, CHR17, RLT1, RLT2 and ARID5. To confirm these interactions, I conducted co-immunoprecipitation (co-IP) assays in *Nicotiana Benthamiana*, where I co-expressed CRY2 with either CHR11, RLT1, or ARID5, as well as with the positive control UBP13 (Figures 4.1A-C), a known CRY2-interacting partner (Lindback et al. 2022). Consistently, I found that UBP13 protein co-immunoprecipitated with the CRY2 protein. More importantly, I observed that

CRY2 co-immunoprecipitated with CHR11, RLT1, and ARID5 (Figures 4.1A-C), respectively, indicating a physical interaction between CRY2 and the ISWI complex.

CRY2 has two modes of interaction with its partners, light-dependent and independent. CIB1 (Liu et al. 2008a) and PIF4/5 (Pedmale et al. 2016) are known to interact with CRY2 in a light-dependent manner. In contrast, CRY2 interacts with TCP DOMAIN PROTEIN 22 (TCP22) (Mo et al. 2022) and the N^6-methyladenosine (m^6A) writer complex comprising MESSENGER RNA ADENOSINE METHYLASE (MTA), METHYLTRANSFERASE B (MTB) and FKBP12 INTERACTING PROTEIN 37 (FIP37) (Wang et al. 2021) in both light and dark conditions. To determine whether the interaction between CRY2 and the ISWI complex is light-dependent, I performed an *in vitro* co-IP assay using CIB1 as a positive control for light-dependent interaction with CRY2 (Liu et al. 2008a). Consistently, CRY2 co-immunoprecipitated more CIB1 proteins in the light than in the dark *in vitro* (Figure 4.1D). However, the amount of CRY2 protein co-immunoprecipitated with CHR11 *in vitro*, the catalytic subunit of the ISWI complex (Tan et al. 2020), was similar between light and dark conditions (Figure 4.1D), suggesting a light-independent interaction. Therefore, my data suggest that CRY2 physically interacts with subunits of the ISWI complex in plants in a light-independent manner.

4.2.2 *rlt1rlt2* and *arid5* mutations are epistatic to *cry2* mutation in regulating flowering time

CRY2 has been previously identified to promote floral transition (Mockler et al., 1999), while the ISWI complex has been shown to inhibit flowering (Tan et al. 2020). Since I discovered that ISWI proteins interact with CRY2, I aimed to investigate whether ISWI and CRY2 function within the same genetic pathway to regulate flowering time. To achieve this, I generated *cry2rlt1rlt2* triple mutant and *cry2arid5* double mutant through crosses involving the *cry2* loss-of-function mutant and *rlt1rlt2* and *arid5* mutants, respectively. I examined the flowering time of WT, *cry2*, *rlt1rlt2*, *arid5*, *cry2rlt1rlt2* and *cry2arid5* under long-day conditions. The *rlt1rlt2* and *arid5* mutants exhibited earlier flowering,

with average times of 23.5 and 23.8 days, respectively, compared to the WT, which flowered at an average of 27.9 days (Figure 4.2A), consistent with the previously reported early flowering phenotype of the *rlt1rlt2* and *arid5* mutants (Tan et al. 2020). In contrast, *cry2* displayed a delayed flowering time, with an average of 37.3 days (Figure 4.2A), as expected (Mockler et al., 1999). Notably, *cry2rlt1rlt2* and *cry2arid5* exhibited average flowering times of 26.5 and 28.2 days, respectively (Figure 4.2A), which were similar to the WT. Importantly, the flowering times of *cry2rlt1rlt2* (26.5 days) and *cry2arid5* (28.2 days) are more comparable to *rlt1rlt2* (23.5 days) and *arid5* (23.8 days) than to *cry2* (37.3 days) (Figure 4.2A), suggesting that *RLT1/2* and *ARID5* are partially epistatic to *CRY2* in the regulation of flowering time.

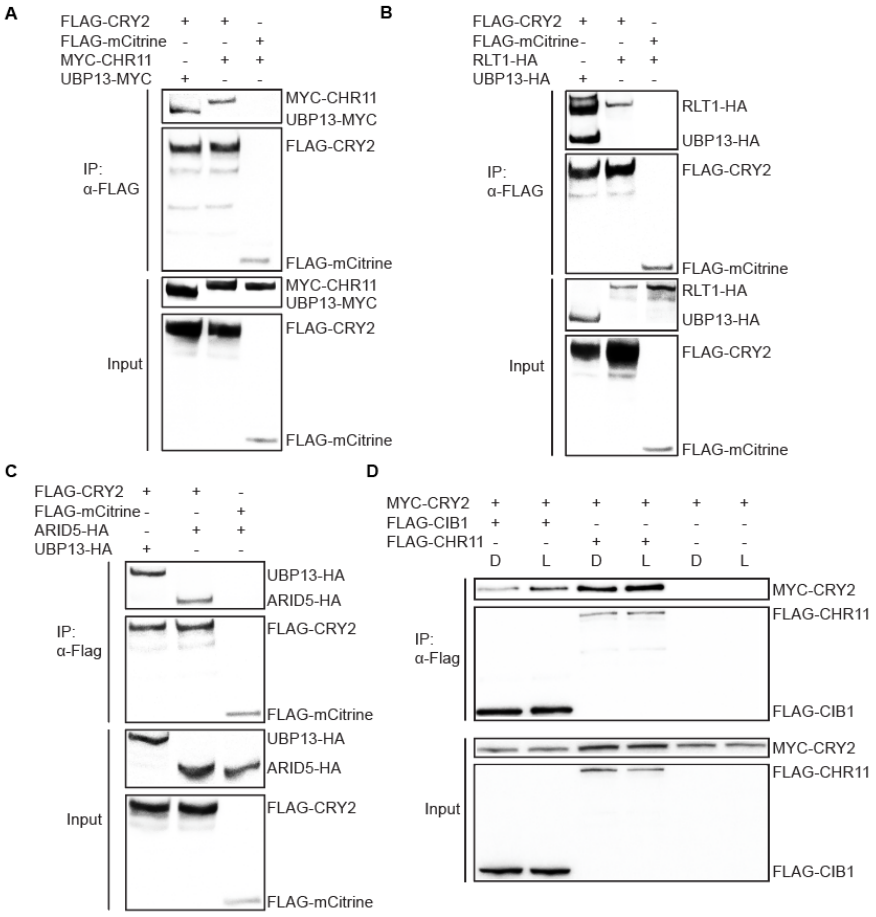

Figure 4.1 Light-independent interaction between CRY2 and the ISWI complex.
(A) Co-IP assay of the indicated recombinant proteins expressed in *N. benthamiana* to test the interaction between CRY2 and CHR11. UBP13-MYC was used as a positive control, and FLAG-mCitrine was used as a negative control. (B) Co-IP assay of the indicated recombinant proteins expressed in *N. benthamiana* to test the interaction between CRY2 and RLT1. UBP13-HA was used as a positive control, and FLAG-mCitrine was used as a negative control. (C) Co-IP assay of the indicated recombinant proteins expressed in *N. benthamiana* to test the interaction between CRY2 and ARID5. UBP13-HA was used as a positive control, and FLAG-mCitrine was used as a negative control. (D) *In vitro* co-IP assay of the indicated recombinant protein performed in both dark and light conditions. Immunoprecipitation was performed using an anti-FLAG antibody, and FLAG-CIB1 was used as a positive control.

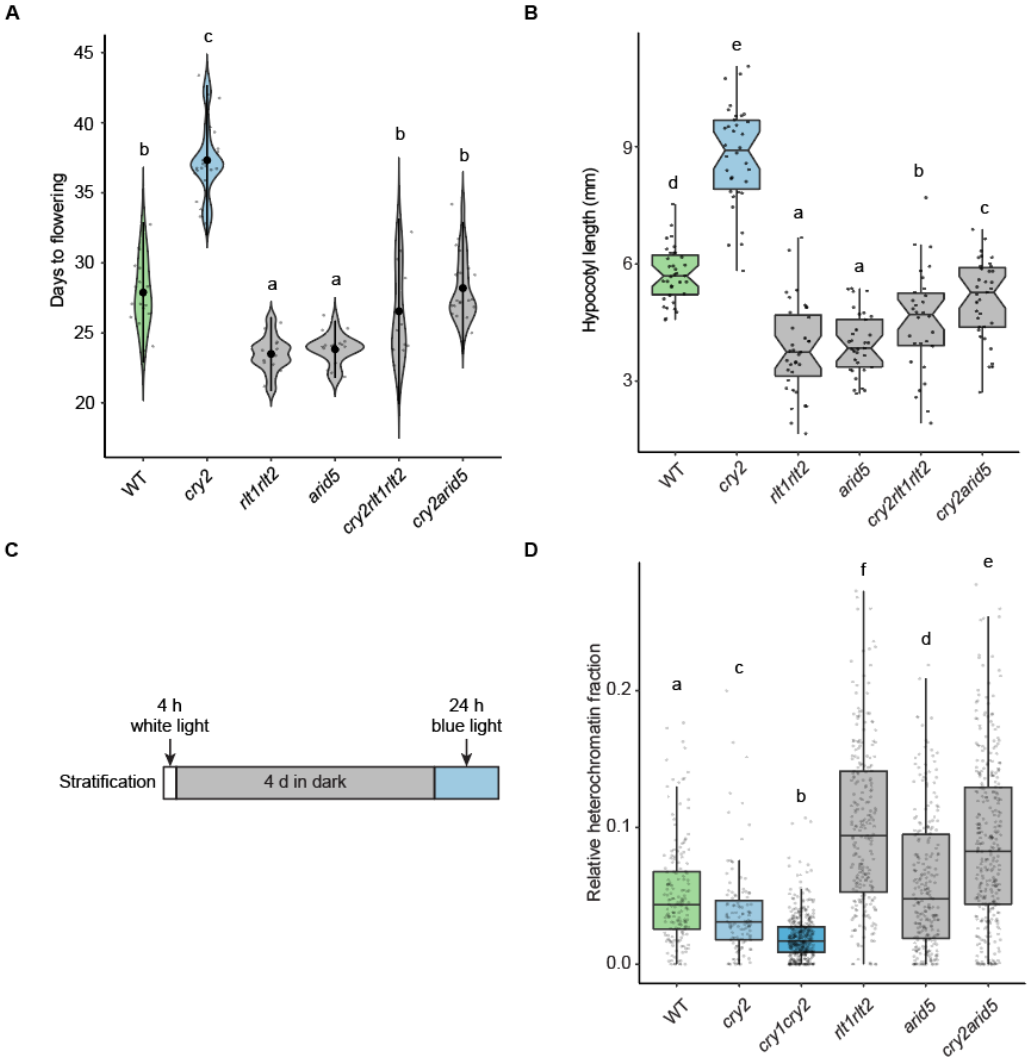

Figure 4.2 CRY2 and ISWI complex antagonistically regulate various processes during *Arabidopsis* development.

(A) Diagram depicting the days to flowering of the indicated genotypes. (B) Diagram showing the hypocotyl length of 4-day-old seedlings of the indicated genotypes grown under 0.8 μmol m^{-2} s^{-1} blue light. (C) Schematic diagram illustrating the growth conditions for the seedlings used for examining the chromatin compaction phenotypes. (D) Diagram showing the relative heterochromatin fraction (RHF) of the indicated genotypes. (A-B) Different letters indicate $p < 0.05$ for one-way ANOVA analysis followed by Fisher's least significant difference (LSD) posthoc test. Data show means ± standard deviation (SD).

4.2.3 *rlt1rlt2* and *arid5* mutations are epistatic to *cry2* mutation in regulating hypocotyl growth in blue light

In addition to regulating flowering time, CRY2 has been shown to inhibit hypocotyl growth under low intensities of blue light (less than 1 μmol m^{-2} s^{-1}) (Lin et al. 1998). Given the interaction between CRY2 and the ISWI complex, I hypothesized that ISWI might also play a role in the regulation of hypocotyl growth under blue light. To investigate this hypothesis, I measured the hypocotyl length of WT, *cry2*, *rlt1rlt2*, *arid5*, *cry2rlt1rlt2*, and *cry2arid5* seedlings grown under 0.8 μmol m^{-2} s^{-1} of blue light for four days. The *cry2* mutant displayed an average hypocotyl length of 8.78 mm, which was longer than that of the WT seedlings (5.73 mm) (Figure 4.2B). These results are consistent with the reported role of CRY2 in inhibiting hypocotyl growth under blue light. Interestingly, *rlt1rlt2* and *arid5* exhibited average hypocotyl lengths of 3.83 mm and 3.96 mm, respectively, which were shorter than the WT (5.73 mm) (Figure 4.2B). This suggests an antagonistic regulation of hypocotyl elongation in response to blue light by the ISWI complex and CRY2. Furthermore, the hypocotyls of *cry2rlt1rlt2* (average hypocotyl length of 4.53 mm) and *cry2arid5* mutants (average hypocotyl length of 5.09 mm) were shorter than the WT, similar to the *rlt1rlt2* and *arid5* mutants (Figure 4.2B). These findings indicate that the *RLT1/2* and *ARID5* genes are epistatic to the *CRY2* gene in the regulation of hypocotyl growth. In conclusion, my findings suggest that the ISWI complex and CRY2 exhibit an antagonistic relationship in the regulation of hypocotyl growth in response to blue light, with the genes encoding ISWI proteins being epistatic to *CRY2* in this process.

4.2.4 CRY2 and the ISWI complex antagonistically regulate blue light-mediated chromatin condensation during seedling development

Although cryptochromes are known to be required for heterochromatin during early seedling development under blue light (Bourbousse et al. 2015), the underlying mechanism remains poorly understood. Given the role of ISWI proteins in regulating chromatin condensation in fruit flies (Corona et al. 2007), I investigated whether ISWI proteins might play a similar role in CRY-mediated

heterochromatin condensation in *Arabidopsis*. To test this hypothesis, I grew WT and *cry2*, *arid5*, *rlt1rlt2*, and *cry2arid5* for three days in darkness followed by one day in blue light (Figure 4.2C). I then assessed heterochromatin condensation in the cotyledon cell nucleus by quantifying the relative heterochromatin fraction (RHF), defined as the sum of DNA fluorescence intensity of chromocenters relative to the entire nucleus (Soppe et al. 2002). RHF serves as a quantitative indicator of the extent of heterochromatin condensation (Soppe et al. 2002). The *cry2* mutants exhibited reduced RHF compared to WT under blue light (Figure 4.2D), indicating that heterochromatin was less condensed in this mutant, consistent with the positive role of CRYs in heterochromatin condensation (Bourbousse et al. 2015). Conversely, the *rlt1rlt2* and *arid5* mutants displayed an opposite phenotype, with increased RHF relative to WT (Figure 4.2D), suggesting that RLT1/2 and ARID5 negatively regulate heterochromatin condensation. Notably, the *cry2arid5* mutants exhibited significantly higher RHF than WT (Figure 4.2D), similar to the *arid5* mutant, indicating that CRY2 and ARID5 regulate heterochromatin compaction under blue light through the same genetic pathway but in opposite directions

4.3 Discussion

My study has uncovered a novel interactor of the plant blue light receptor CRY2, namely the ISWI complex comprising of CHR11, CHR17, RLT1, RLT2, and ARID5. I demonstrated that the physical interaction between CRY2 and the CHR11 subunit of the ISWI complex is light-independent. I also identified a genetic interaction between *CRY2* and the ISWI genes in regulating floral transition, blue light-induced hypocotyl growth inhibition and heterochromatin condensation during seedling development. These findings provide novel insights into the molecular mechanisms underlying CRY2-mediated plant responses to blue light (Lindback et al. 2022), and open up new avenues for further investigations into the role of the ISWI complex in chromatin remodeling in response to light.

4.3.1 Role of the ISWI complex in higher-order chromatin structure organization

The modulation of large-scale chromatin organization by CRYs has been long recognized, with roles of CRYs in both chromatin decondensation and condensation during different developmental processes (Bourbousse et al. 2020). Specifically, during floral transition, both heterochromatin and euchromatin undergoes transient decondensation before flowering and recondensation after flowering (Tessadori et al. 2007), which relates to the shift from vegetative growth to reproductive growth. This decondensation and recondensation of chromatin during floral transition is absent in the *cry2* mutant and is independent of the flowering time (Tessadori et al. 2007). Additionally, a decrease in light intensity can cause heterochromatin decondensation that can be reversed by re-elevating environmental light intensity, a process also dependent on CRY2 (van Zanten et al. 2010b). More recently, it has been observed that during seedling development heterochromatin in the nucleus of cotyledon cells undergoes condensation, and this process is regulated by blue light and cryptochromes (Bourbousse et al. 2015). However, how cryptochromes regulate large-scale chromatin condensation and decondensation remains poorly understood.

My study demonstrates that CRY2 and the ISWI complex interact and regulate chromatin condensation during seedling development in an antagonistic manner. Previous studies suggest that the ISWI complex is involved in higher-order chromatin changes (Siriaco et al. 2009; Deuring et al. 2000; Corona et al. 2007). For instance, in *Drosophila*, loss of ISWI homolog function leads to decondensation of both mitotic and polytene chromosomes (Corona et al. 2007), which may be linked to the regulation of the linker histone H1 by the ISWI complex (Siriaco et al. 2009). My findings reveal that the *rlt1rlt2* mutant shows enhanced heterochromatin condensation in blue light during seedling development, indicating a conserved role of the ISWI complex in regulating chromatin condensation in both *Drosophila* and *Arabidopsis*. Interestingly, the *iswi* mutation in *Drosophila* leads to decondensed chromatin (Corona et al. 2007), while the mutation in ISWI genes in *Arabidopsis* results in more condensed heterochromatin. This discrepancy may be due to the different accessory subunits

of the ISWI complex in these two organisms that regulate the context-dependent function of the ISWI complexes.

Over two decades ago, it was observed that the GFP::CRY2 fusion protein accumulates on chromosomes during anaphase of cell division (Cutler et al. 2000), but the function of CRY2 on chromosomes remained unexplored. Since the ISWI complex is part of the major chromosomal components and localizes to chromosomes during anaphase in *Xenopus* cells (Yokoyama et al. 2009), it is possible that ISWI is involved in the accumulation of CRY2 on anaphase chromosomes. Further investigations could shed light on whether the ISWI complex is required for the accumulation of CRY2 on chromosomes and the underlying mechanism.

4.3.2 Light-independent interaction between CRY2 and the ISWI complex

Several CRY2 interactors have shown a stronger affinity for CRY2 under blue light conditions compared to darkness (Ponnu and Hoecker 2022), including transcription factors CIB1 (Liu et al., 2008a) and PIF4/5 (Pedmale et al. 2016), E3 ligase COP1 (Holtkotte et al. 2017), and deubiquitinase UBP12/13 (Lindback et al. 2022). Upon activation by blue light, CRY2 engages with these light-dependent interactors to transmit blue light signaling and regulate downstream processes (Ponnu and Hoecker 2022). Furthermore, recent studies have identified and characterized light-independent interactors of CRY2, namely the m^6A writer complex (Wang et al. 2021) and the TCP22 transcription factor (Mo et al. 2022). Both the m^6A writer complex and TCP22 are known to localize to CRY2 nuclear speckles under blue light, contributing to the regulation of downstream processes in conjunction with CRY2 (Mo et al. 2022; Wang et al. 2021). Notably, my study has unveiled a light-independent interaction between CRY2 and the ISWI complex, thus expanding the roster of light-independent interactors associated with CRY2. Consequently, it is of interest for future investigations to explore whether the ISWI complex also localizes to CRY2 nuclear speckles under blue light, akin to the m^6A writer complex and TCP22 (Mo et al. 2022; Wang et al. 2021). In summary, the emergence of light-

independent interactors of CRY2 underscores the complexity and versatility of this blue light receptor, emphasizing the need for further research to comprehensively elucidate its regulatory mechanisms.

4.3.3 Cryptochromes associate with both the SWR1 and the ISWI chromatin remodeling complexes

Before, it was shown that CRY2 interacts with the SWR1 complex, which belongs to the INOSITOL REQUIRING 80 (INO80) family of chromatin remodelers. Specifically, CRY2 interacts with the SWR1 COMPLEX SUBUNIT 6 (SWC6) and ACTIN-RELATED PROTEIN 6 (ARP6) subunits. The ELONGATED HYPOCOTYL 5 (HY5) transcription factor also interacts with the SWR1 complex and recruits SWR1 to its target genes, facilitating the exchange of histone H2A for H2A.Z and promoting transcription (Mao et al. 2021). Recently, it was found that the SWR1 complex associates with the ISWI remodelers CHR11 and CHR17 via common binding to METHYL-CPG-BINDING DOMAIN 9 (MBD9) (Luo et al. 2020), but not with the ISWI accessory subunits RLT1/2 and ARID5 (Luo et al. 2020). My discovery that CRY2 forms a complex with the ISWI complex, including the accessory subunits, indicates that CRY2 can regulate different chromatin remodeler complexes. There might be competition between the SWR1 complex and the ISWI complex for the CHR11/17 subunits, which may regulate the blue light signaling pathway since both complexes interact with CRY2. This hypothesized competition between SWR1 and ISWI in CRY2 signaling is consistent with the opposite phenotypes of *swc6* and *arp6* mutants (long hypocotyl) (Mao et al. 2021) and *rlt1rlt2* and *arid5* mutants (short hypocotyl) under blue light.

4.3.4 Mechanism of gene transcription regulation by the CRY2-ISWI complex

Previous studies have identified target genes of the ARID5 subunit of the ISWI complex and have shown that loss of function of *ARID5* can lead to both upregulation and downregulation of these target genes (Tan et al. 2020), highlighting the complex and context-dependent role of the ISWI complex in regulating transcription. While the ISWI complex has been shown *in vitro* to possess the ability to evenly space nucleosomes (Lieleg et al. 2015). Disruption of ISWI genes, including *RLT1/2*

and *ARID5*, in *Arabidopsis* leads to a disruption of the evenly-spaced nucleosome pattern in the 1 kb downstream of TSS of protein coding genes (Corcoran et al. 2022). However, the changes in nucleosome spacing are global, affecting both differentially and non-differentially expressed genes in the *rlt1rlt2* and *arid5* mutants (Corcoran et al. 2022), suggesting that the nucleosome spacing activity of the ISWI complex, which is the most studied activity *in vitro*, is not solely responsible for the regulation of gene transcription *in vivo*. Therefore, there might be other activities of the ISWI complex *in vivo* that regulate gene expression at specific loci. The interaction between CRY2 and the ISWI complex provides a mechanism for targeting the ISWI complex to specific genomic loci, possibly with the help of CRY2-interacting transcription factors such as CIB1 (Liu et al. 2018) and PIF4/5 (Pedmale et al. 2016), to fine-tune gene expression.

In conclusion, my study has made significant contributions to the understanding of the complex CRY-mediated blue light signaling pathway by identifying the CRA ISWI complex as novel interactors of CRY2. Notably, my findings have shed light on a previously unknown molecular mechanism underlying the long-established role of CRYs in higher-order chromatin regulation. Specifically, I have demonstrated that the ISWI complex acts downstream of CRY2, exerting regulatory control over large-scale chromatin condensation. This discovery provides valuable insights into the intricate mechanisms through which CRYs participate in chromatin remodeling processes. By unraveling these molecular mechanisms, my research paves the way for further investigations and opens up new avenues for understanding the broader impact of CRY-dependent processes in plant biology.

4.4 Materials and methods

4.4.1 Plant genotypes and growth conditions

Arabidopsis thaliana Columbia (Col-0) ecotype served as the genetic background for mutants and transgenic lines. The *cry2-1* (Lin et al. 1998), *rlt1-1rlt2-1* (Corcoran et al. 2022), and *arid5* mutants (Tan et al. 2020) were previously described. After surface sterilization, seeds were planted on 0.5×

Linsmaier and Skoog (LS) medium (HiMedia Laboratories) containing 0.8% agar, stratified in darkness for two days at 4°C, and then grown at 22°C under a 100 μmol m^{-2} s^{-1} white LED light source in a growth chamber (Percival Scientific) unless otherwise specified. To generate the *cry2rlt1rlt2* triple mutant, the *cry2-1* mutant was crossed with the *rlt1-1rlt2-1* mutant. Similarly, to generate the *cry2arid5* double mutant, the *cry2-1* mutant was crossed with the *arid5* mutant.

4.4.2 Molecular cloning

The $UBQ10_{pro}$:UBP13-HA, $UBQ10_{pro}$:FLAG-mCitrine, $UBQ10_{pro}$:FLAG-CRY2, and pTNT-MYC-CRY2 constructs were previously described (Lindback et al. 2022). To generate the $UBQ10_{pro}$:UBP13-MYC, $UBQ10_{pro}$:MYC-CHR11, $UBQ10_{pro}$:RLT1-HA, $UBQ10_{pro}$:ARID5-HA, pTNT-FLAG-CIB1, and pTNT-FLAG-CHR11 plasmids, the cDNA or genomic sequences of UBP13, CHR11, RLT1, ARID5, CIB1, and CHR11 were amplified and cloned into pDONR221 vectors (Thermo Fisher Scientific) using BP Clonase II (Thermo Fisher Scientific), followed by recombination into destination vectors using LR Clonase II (Thermo Fisher Scientific). The UBP13 cDNA was amplified from a cDNA pool from Col-0 as previously described (Lindback et al. 2022), while the RLT1 genomic DNA sequence was amplified from a plasmid containing the genomic DNA sequence from Dr. Ryan Lister's laboratory. The CIB1 and ARID5 cDNA sequences were amplified from plasmids containing the cDNA sequence from Dr. Doreen Ware's laboratory. The CHR11 cDNA sequence was commercially synthesized (GenScript).

4.4.3 Co-immunoprecipitation of proteins

Co-IP in *N. benthamiana* was performed as previously described with some modifications (Lindback et al. 2022). The constructs used were $UBQ10_{pro}$:FLAG-CRY2, $UBQ10_{pro}$:FLAG-mCitrine, $UBQ10_{pro}$:MYC-CHR11, $UBQ10_{pro}$:UBP13-MYC, $UBQ10_{pro}$:UBP13-HA, $UBQ10_{pro}$:RLT1-HA and $UBQ10_{pro}$:ARID5-HA. The SII buffer was replaced with a different co-IP buffer (150 mM Tris-HCl, 150 mM NaCl, 10% glycerol, 10 mM ethylenediaminetetraacetic acid (EDTA), 20 mM NaF, 10 mM dithiothreitol (DTT), 0.1% Tween-20, 1 mM phenylmethylsulfonyl fluoride (PMSF), 1× EDTA-free

protease inhibitor cocktail (Cat#11836170001, Roche), pH 7.5) for resuspending the ground frozen tissue and washing the protein G-beads. *In vitro* co-IP was performed as previously described with some modifications (Lindback et al. 2022). The constructs used were pTNT-MYC-CRY2, pTNT-FLAG-CIB1, and pTNT-FLAG-CHR11. For the dark *in vitro* co-IP, protein synthesis, immunoprecipitation, and washing steps were conducted in a darkroom with dim red light.

4.4.4 Flowering time assay

Seeds were surface sterilized with 75% ethanol, resuspended in 0.1% agarose, and stratified in the dark at 4°C for two days. Afterward, the seeds were planted in soil. For each genotype, 22 plants were planted and the flowering time was recorded. The flowering time was defined as the days passed from planting on soil to the appearance of the first visible flower bud.

4.4.5 Hypocotyl length measurement

Hypocotyl length measurements were performed as previously described (Lindback et al. 2022), with the exception that a lower light intensity of blue light (0.8 μmol m^{-2} s^{-1}) was used. The seedlings were grown under these conditions for four days prior to hypocotyl length measurement.

4.4.6 DAPI staining and image analysis

Seedlings of the corresponding genotypes are grown in the dark for four days, then transferred to blue light (471 nm, 30 μmol m^{-2} s^{-1}) for 24 hours. Seedlings are then fixed and nuclei were stained and imaged as previously described (Bourbousse et al. 2015). To calculate RHF, images were processed and analyzed as previously described (Johann to Berens et al. 2022).

Chapter 5. Role of cryptochromes and the ISWI complex in histone methylation

5.1 Introduction

Histone modifications are crucial regulators of gene expression during development in eukaryotic organisms (Gibney and Nolan 2010). Post-translational modifications, such as phosphorylation, acetylation, and methylation, occur on specific amino acids within histones (Gibney and Nolan 2010). Two extensively studied histone modifications, namely tri-methylation of histone H3 at lysine 4 (H3K4me3) and lysine 27 (H3K27me3), are closely associated with gene activation and repression, respectively (Macrae et al. 2023). While there is evidence that supports H3K4me3 as a record of transcription, such as the requirement for yeast Pol II-associated factor 1 (Paf1) elongation complex in the recruitment of Set1-containing COMPASS complex to RNA polymerase II after transcription initiation (Krogan et al. 2003), a recent study has demonstrated the instructive role of H3K4me3 in transcription through releasing paused RNA polymerase II in mammalian embryonic stem cells (Wang et al. 2023). This highlights the importance of investigating the functional roles of histone modifications in regulating gene expression.

Changes in light signal from the environment have been shown to regulate histone modifications in plants, particularly H3K4me3 and H3K27me3 (Charron et al. 2010; Guo et al. 2008). Extended darkness increases deposition of H3K4me3 at genes related to senescence and autophagy pathways, consistent with the leaf senescence phenotypes observed under extended darkness (Yan et al. 2019). ELONGATED HYPOCOTYL 5 (HY5), a master transcription factor regulating photomorphogenesis, promotes the deposition of H3K27me3 at its target genes involved in cell elongation (Jing et al. 2013). However, the PICKLE chromatin remodeler interacts with HY5 to bind to HY5-trageted hypocotyl elongation-promoting genes and inhibits the deposition of H3K27me3 at

these genes, thereby acting as a negative regulator of HY5 activity and photomorphogenesis (Jing et al. 2013). Therefore, histone modifications, such as H3K4me3 and H3K27me3, play important roles in plant light signaling pathway. However, the detailed mechanism through which light signaling components modulate histone modifications at the genome-wide level remains poorly understood.

In Chapter 4 of this thesis, I have identified the ISWI complex as interactors of CRY2. Notably, one of the subunits of the ISWI complex, ARID5, has been found to bind to the H3K4me3 histone modification (Tan et al. 2020). Based on these findings, I propose that the ISWI complex, in conjunction with CRY2, may regulate the deposition of H3K4me3. To test this hypothesis, I conducted chromatin immunoprecipitation coupled with high-throughput sequencing (ChIP-seq) experiments for H3K4me3, along with a suppressive histone modification involved in light signaling, H3K27me3, in 10-day-old light-grown WT, *cry2*, *cry1cry2*, and *arid5* seedlings. Additionally, in the same plants used for the ChIP-seq, I performed RNA-sequencing (RNA-seq) experiments to examine whether changes in H3K4me3 and H3K27me3 in *cry* and *arid5* mutants affect gene expression. my ChIP-seq and RNA-seq analyses revealed genome-wide alterations in H3K4me3 and H3K27me3 deposition in *cry1cry2* and *arid5* mutants. Furthermore, I observed a positive correlation between gene expression and H3K4me3 deposition, as well as a negative correlation between gene expression and H3K27me3 deposition. Importantly, I found that the flowering promoting gene, *SUPPRESSOR OF OVEREXPRESSION OF CO 1* (*SOC1*) (Lee and Lee 2010), exhibited reduced expression, decreased deposition of H3K4me3, and increased deposition of H3K27me3 in *cry1cry2*, consistent with the late flowering phenotype of this mutant. Additionally, another flowering-promoting gene, *SUMO-TARGETED UBIQUITIN E3 LIGASE 4* (*STUBL4*) (Elrouby et al. 2013), displayed elevated expression, higher H3K4me3 deposition, and lower H3K27me3 deposition in *arid5* mutants compared to WT, aligning with the early flowering phenotype of this mutant. Taken together, my results demonstrate that both CRYs and the ISWI complex modulate the deposition of H3K4me3 and H3K27me3 at genes involved in flowering time control, indicating the complex regulation of epigenetic marks by the CRY-ISWI complex.

5.2 Results

5.2.1 Genome-wide H3K4me3 changes positively correlate with gene expression changes in *cry1cry2* and *arid5* mutants.

In Chapter 4, I established that CRY2 interacts with the ISWI complex, composed of CHR11, CHR17, RLT1, RLT2, and ARID5, and that CRY2 and ISWI together regulate several processes in *Arabidopsis* such as floral transition, hypocotyl growth in blue light and heterochromatin condensation during seedling development. However, the underlying mechanism of how CRY2 and ISWI function together in light signaling remains to be explored. Since both CRY2 and ISWI are associated with the chromatin (Bourbousse et al. 2020; Erdel and Rippe 2011; Pedmale et al. 2016), further characterization is required to investigate whether and how they regulate chromatin-related processes. ARID5, an ISWI complex component which interacts with CRY2, has a plant homeodomain (PHD) known to bind to the H3K4me3 histone modification (Tan et al. 2020). H3K4me3 is a well-known marker for active gene transcription that has recently been shown to enhance transcription elongation of stalled RNA polymerases (Wang et al. 2023). In contrast, H3K27me3 is often connected with transcriptional repression and has been found to form bivalent marks with H3K4me3 in mammalian stem cells to regulate differentiation (Macrae et al. 2023). To evaluate the chromatin-related changes in the absence of CRYs and the ISWI complex and to test how these changes affect gene transcription, I performed a ChIP-seq experiment to examine H3K4me3 and H3K27me3 deposition and a parallel RNA-seq experiment to determine associated changes in gene expression. I used 10-day-old WT, *cry2*, *cry1cry2* and *arid5* seedlings grown under continuous white light for both the RNA-seq and ChIP-seq experiments (Figure 5.1A). For the ChIP-seq experiment, I used anti-H3K4me3 and anti-H3K27me3 antibodies, along with the anti-IgG antibody as a control (Figure 5.1 A).

For the RNA-seq experiment, two biological replicates were used for each genotype. Both RNA-seq replicates exhibited a strong correlation, as indicated by a high Pearson's correlation coefficient (0.99-1) and their close proximity in the principal component analysis (PCA) map (Figures

5.1B and 5.1C). To identify differentially expressed genes, I compared the *cry2*, *cry1cry2*, and *arid5* mutants to the WT. In the *cry2* mutant, I observed 82 upregulated genes and 125 downregulated genes compared to the WT (Figure 5.1D). In contrast, the *cry1cry2* mutant displayed a more pronounced alteration in gene expression, with 897 upregulated genes and 1540 downregulated genes compared to the WT (Figure 5.1D). Notably, 55 of the 82 upregulated genes in *cry2* overlapped with the upregulated genes in *cry1cry2*, while 100 of the 125 downregulated genes in *cry2* overlapped with the downregulated genes in *cry1cry2* (Figure 5.1D). These results suggest that the transcriptional changes in *cry2* are largely similar to those in *cry1cry2*. Therefore, I focused my downstream analysis on the *cry1cry2* mutant rather than the *cry2* mutant to study gene expression changes resulted from loss of function of cryptochromes.

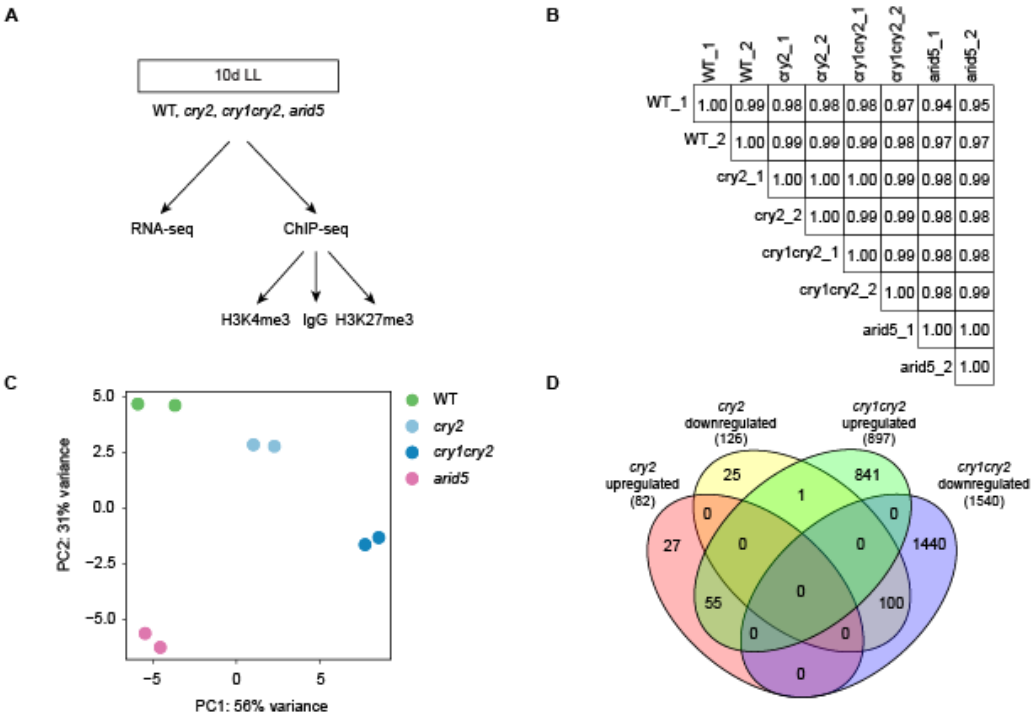

Figure 5.1: CRYs and the ISWI complex regulate genome-wide changes in RNA transcripts and histone H3K4me3 and H3K27me3 deposition levels.
(A) A schematic diagram illustrating the RNA-seq and ChIP-seq experiments performed in this study. Ten-day-old WT, *cry2*, *cry1cry2*, and *arid5* seedlings grown in continuous white light (LL) were harvested for both RNA-seq and ChIP-seq experiments. ChIP-seq was performed using three different antibodies, anti-IgG (serving as control), anti-H3K4me3, and anti-H3K27me3. (B) A plot of the Pearson's correlation coefficient between all eight RNA-seq samples calculated using the FPKM values of all genes. (C) Principal component analysis (PCA) plot of all eight RNA-seq samples. Different colors indicate the different genotypes, and round dots with the same color indicate biological replicates. (D) A Venn diagram showing the overlap between four different sets of genes: upregulated genes in *cry2*, downregulated genes in *cry2*, upregulated genes in *cry1cry2*, and downregulated genes in *cry1cry2*, compared to WT.

To analyze genome-wide differential enrichment of H3K4me3 deposition, I used MAnorm software (Shao et al. 2012) to compare H3K4me3 deposition in *cry1cry2* and *arid5* to WT, respectively. First, MAnorm compares common peaks between two ChIP-seq samples and assumes that the real read intensity of most common peaks between the two samples should be similar, using this assumption to normalize all peaks between the two samples (Shao et al. 2012). MAnorm then compares the normalized read intensity between the two samples and identifies differentially enriched peaks (Shao et al. 2012). Using this method, I found 2432 peaks depleted of H3K4me3 and 2523 peaks enriched with H3K4me3 in *cry1cry2* compared to WT (Figure 5.2A), and 651 peaks depleted of H3K4me3 and 1388 peaks enriched with H3K4me3 in *arid5* compared to WT (Figure 5.2B). To validate these differentially enriched peaks of H3K4me3, I identified genes where the transcription start sites were within 1 kilobase pairs of the differentially enriched peaks and plotted the H3K4me3 read intensity over these genes. The profile of average peak intensity of these identified genes and the heatmap of read intensities of individual genes both showed the corresponding increase or decrease in H3K4me3 deposition in *cry1cry2* and *arid5* (Figures 5.2C and 5.2D), suggesting that loss of function of *CRY1* and *CRY2* or *ARID5* result in substantial changes in H3K4me3 deposition at the genome-wide level.

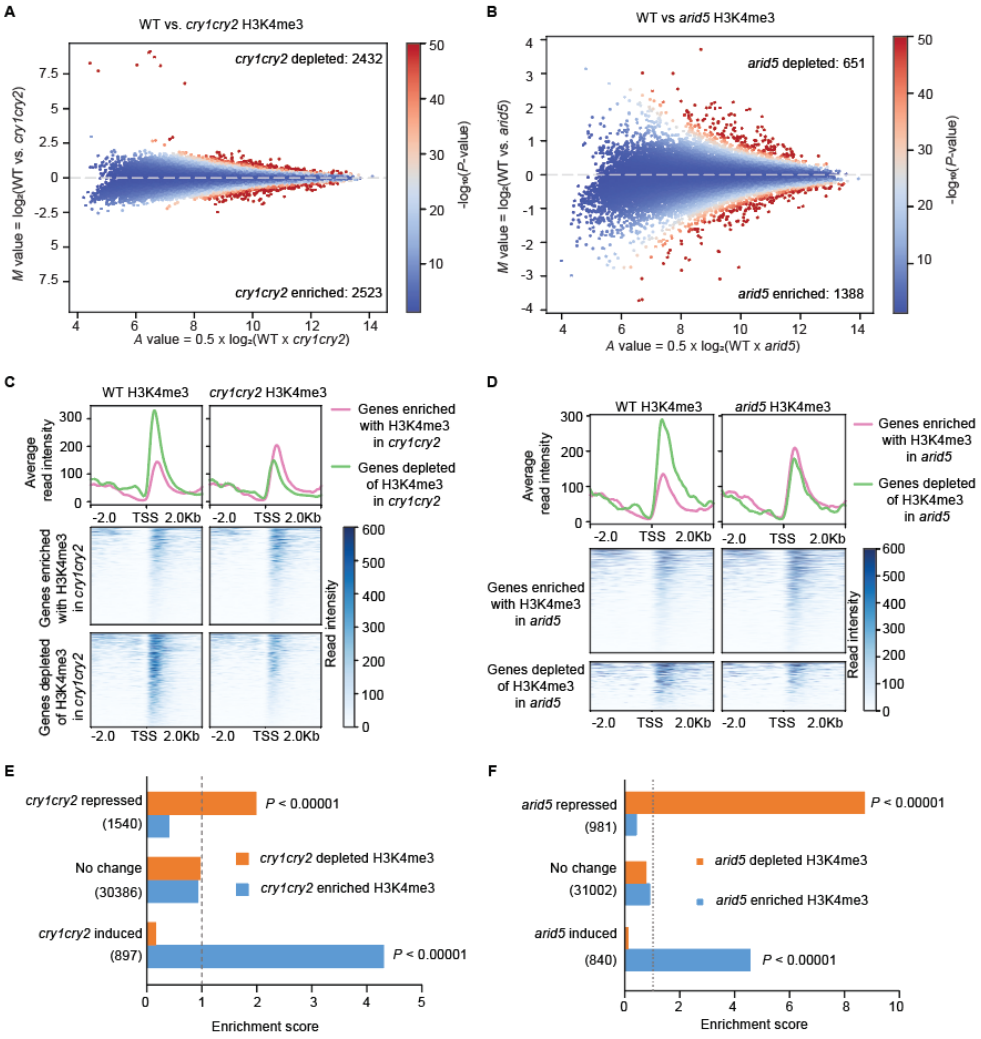

Figure 5.2: *cry1cry2* and *arid5* mutation result in substantial changes in genomic deposition of H3K4me3 that positively correlate with changes in gene expression.
(A) MA plot of H3K4me3 peaks generated by MAnorm, comparing WT and *cry1cry2*. The x-axis shows the A value of each peak (average read intensity), and the y-axis shows the M value as $\log_2$(difference in read intensity). Positive and negative M values represent increased and decreased H3K4me3 levels in WT compared to *cry1cry2*, respectively. The color range represents $-\log_{10}$(*P* values) associated with each normalized H3K4me3 peak. Two biological replicates of the ChIP–seq samples were analyzed. (B) MA plot of H3K4me3 peaks generated by MAnorm, comparing WT and *arid5*. (C) Plots of the average H3K4me3 ChIP-seq read intensity and heatmap of H3K4me3 ChIP-seq read intensity for gene groups enriched with or depleted of H3K4me3 in *cry1cry2* compared to WT. Genes are aligned at the transcription start site, and the region 2 kb upstream and downstream of the TSS is plotted. (D) Plots of the average H3K4me3 ChIP-seq read intensity and heatmap of H3K4me3 ChIP-seq read intensity for gene groups enriched with or depleted of H3K4me3 in *arid5* compared to WT. (E) Enrichment analysis of the overlap between repressed and induced genes in *cry1cry2* and genes enriched with or depleted of H3K4me3 in *cry1cry2* compared to WT. Each enrichment analysis was compared to the expected random overlap of the two sets of genes (shown as a vertical dotted line with an enrichment score of 1). The *P*-value was calculated using Fisher's exact test. (F) Enrichment analysis of the overlap between repressed and induced genes in *arid5* and genes enriched with or depleted of H3K4me3 in *arid5* compared to WT.

As H3K4me3 is a marker for active gene transcription (Wang et al. 2023), I investigated whether the differentially enriched H3K4me3 peaks identified in *cry1cry2* and *arid5* compared to WT correlated with changes in the expression of nearby genes. To do so, I overlapped the upregulated or downregulated genes identified in RNA-seq with genes enriched with or depleted of H3K4me3 (Figures 5.2E and 5.2F). In *cry1cry2* and *arid5* mutants, I observed a significant overlap between the upregulated genes and genes enriched with H3K4me3, with enrichment scores (indicative of the amount of overlap relative to random overlap between two datasets) of 4.3 and 4.6, respectively (see Figures 5.2E and 5.2F). Furthermore, the downregulated genes in *cry1cry2* and *arid5* mutants exhibited a significant overlap with genes depleted of H3K4me3, with enrichment scores of 2 and 8.7, respectively (see Figures 5.2E and 5.2F). These findings indicate that the *cry1cry2* and *arid5* mutations led to genome-wide changes in H3K4me3 deposition, which positively correlated with alterations in gene expression.

5.2.2 Depletion of *CRY1* and *CRY2* or *ARID5* lead to concordant changes in expression of and H3K4me3 deposition at genes controlling hypocotyl elongation and floral transition

As demonstrated in Chapter 4, *CRY2* and *ARID5* exhibit antagonistic effects on both hypocotyl elongation and floral transition, operating in an epistatic manner. To gain further insights into how the changes in H3K4me3 deposition observed in *cry1cry2* and *arid5* mutants contribute to their phenotypes, I analyzed genes with altered H3K4me3 deposition that positively correlate with changes in gene expression in both mutants. Among the many genes with altered expression and H3K4me3 deposition, I identified *SHADE AVOIDANCE 3* (*SAV3*) and *AT-HOOK MOTIF NUCLEAR-LOCALIZED PROTEIN 22* (*AHL22*) as upregulated genes with increased H3K4me3 deposition in *cry1cry2* compared to WT (Figures 5.3A and 5.3B). SAV3 is involved in the biosynthesis of the phytohormone auxin, which is required for hypocotyl elongation in plant response to both shade and high temperature conditions (Tao et al. 2008), suggesting that enriched H3K4me3 deposition and upregulated expression of *SAV3* (Figure 5.3A) may explain the elongated hypocotyl phenotype of *cry1cry2*. AHL22 is a AT-hook DNA-binding motif-containing protein involved in floral transition, and overexpression of *AHL22*

gene results in delayed flowering (Xiao et al. 2009). I observed that *AHL22* gene is upregulated and had increased H3K4me3 deposition in *cry1cry2* compared to WT (Figure 5.3B), suggesting that CRYs might inhibit *AHL22* gene expression through downregulating H3K4me3 deposition.

I also observed downregulated genes depleted of H3K4me3 in *cry1cry2*, including *PSEUDO-RESPONSE REGULATOR 9* (*PRR9*) and *SOC1* (Figures 5.3C and 5.3D). PRR9 is a core component of the circadian clock feedback loop in *Arabidopsis*. Loss of function of both PRR9 and PRR7 results in longer hypocotyls than WT under photoperiodic conditions, suggesting that PRR9 and PRR7 represses photoperiodic hypocotyl growth (Li et al. 2020). Therefore, the downregulation of *PRR9* gene expression and decreased H3K4me3 deposition at *PRR9* gene in *cry1cry2* (Figure 5.3C) may be associated with the elongated hypocotyl phenotype of the *cry1cry2* mutant. SOC1 integrates various signaling pathways to promote floral transition (Lee and Lee 2010). Therefore, the downregulation and decreased H3K4me3 deposition at the *SOC1* gene in *cry1cry2* compared to WT (Figure 5.3D) may account for the late flowering phenotype of this mutant. My findings highlight novel potential downstream regulators of CRYs that modulate hypocotyl growth and floral transition, which may be regulated by CRYs through changes in the deposition of H3K4me3.

The *arid5* mutant exhibits an early flowering phenotype and a short hypocotyl in blue light, which is opposite to the *cry2* mutant (see Chapter 4, Figure 4.2). Through my integration analysis of RNA-seq and H3K4me3 ChIP-seq data from the *arid5* mutant, I identified *PHYB ACTIVATION TAGGED SUPPRESSOR 1* (*BAS1*) and *STUBL4* as upregulated genes with enriched H3K4me3 peaks in *arid5* (Figures 5.3E and 5.3F). BAS1 is an enzyme mediating the inactivation of brassinosteroids (Turk et al. 2003), which are plant hormones that promote hypocotyl elongation (Nolan et al. 2020). Overexpression of *BAS1* results in a short hypocotyl phenotype (Turk et al. 2005), suggesting that BAS1 is a negative regulator of hypocotyl growth. Therefore, the upregulation of and enriched H3K4me3 deposition at *BAS1* correlate with the short hypocotyl phenotype of *arid5* mutant (Figure 5.3E). STUBL4 is a E3 that promotes floral transition (Elrouby et al. 2013). Over-expression of *STUBL4* leads to reduced CDF2 protein levels, which results in de-repression of the *CO* gene

transcription (Elrouby et al. 2013), thus promoting floral transition. Therefore, the upregulation of and increased H3K4me3 deposition at *STUBL4* in *arid5* thus correlates with the early flowering phenotype of this mutant (Figure 5.3F). Examining the downregulated genes with decreased H3K4me3 deposition in *arid5* revealed two downregulated genes: *TCP DOMAIN PROTEIN 17* (*TCP17*) and *FLOWERING LOCUS C* (*FLC*) (Figures 5.3G and 5.3H). TCP17 positively regulates high temperature-induced hypocotyl elongation by enhancing *PHYTOCHROME INTERACTING FACTOR 4* (*PIF4*) transcriptional activity (Zhou et al. 2019). Therefore, the downregulation of and decreased H3K4me3 deposition at *TCP17* gene in *arid5* might explain its short hypocotyl phenotype (Figure 5.3G). *FLC*, another gene downregulated and depleted of H3K4me3 in *arid5*, is a well-known repressor of floral transition through the inhibition of *FLOWERING LOCUS T* (*FT*) transcription (Helliwell et al. 2006). Therefore, the downregulation and depletion of H3K4me3 deposition of the *FLC* gene in *arid5* correlates with the early flowering phenotype of this mutant (Figure 5.3H). Overall, my integration analysis of RNA-seq and H3K4me3 ChIP-seq data revealed promising candidate genes with correlated changes in transcription and H3K4me3 deposition that could function downstream of CRYs and ARID5 to regulate hypocotyl elongation and floral transition.

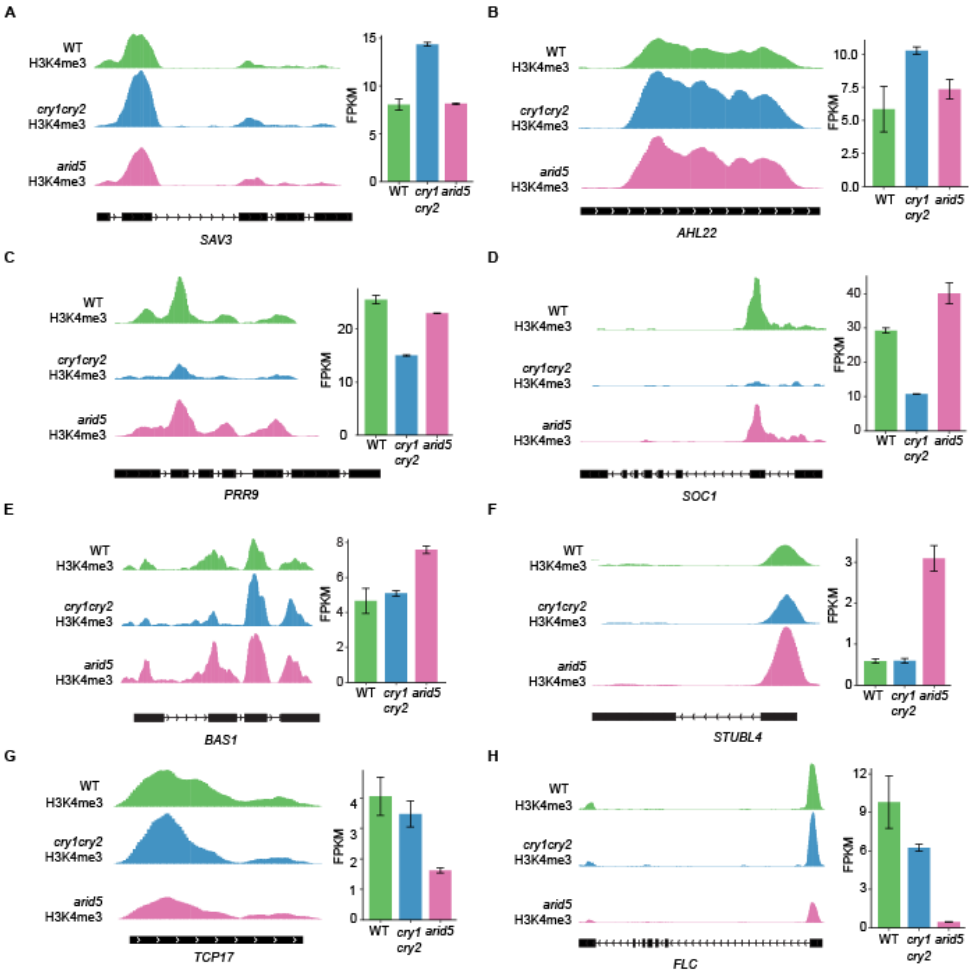

Figure 5.3: *cry1cry2* and *arid5* mutations result in positively correlated changes in transcription and H3K4me3 deposition at genes regulating hypocotyl elongation and floral transition.
(A) Integrative Genomics Viewer (IGV) screenshot depicting the H3K4me3 read intensity at the genomic locus of *SAV3* gene in WT, *cry1cry2*, and *arid5* along with a bar plot showing the gene expression (in fragments per kilobase of transcript per million mapped reads, FPKM) of *SAV3* in the respective genotypes. (B) IGV screenshot displaying the H3K4me3 read intensity at the genomic locus of *AHL22* gene in WT, *cry1cry2*, and *arid5* along with a bar plot showing the gene expression of *AHL22* in the respective genotypes. (C) IGV screenshot depicting the H3K4me3 read intensity at the genomic locus of *PRR9* gene in WT, *cry1cry2*, and *arid5* along with a bar plot showing the gene expression of *PRR9* in the respective genotypes. (D) IGV screenshot depicting the H3K4me3 read intensity at the genomic locus of *SOC1* gene in WT, *cry1cry2*, and *arid5* along with a bar plot showing the gene expression of *SOC1* in the respective genotypes. (E) IGV screenshot depicting the H3K4me3 read intensity at the genomic locus of *BAS1* gene in WT, *cry1cry2*, and *arid5* along with a bar plot showing the gene expression of *BAS1* in the respective genotypes. (F) IGV screenshot depicting the H3K4me3 read intensity at the genomic locus of *STUBL4* gene in WT, *cry1cry2*, and *arid5* along with a bar plot showing the gene expression of *STUBL4* in the respective genotypes. (G) IGV screenshot depicting the H3K4me3 read intensity at the genomic locus of *TCP17* gene in WT, *cry1cry2*, and *arid5* along with a bar plot showing the gene expression of *TCP17* in the respective genotypes. (H) IGV screenshot depicting the H3K4me3 read intensity at the genomic locus of *FLC* gene in WT, *cry1cry2*, and *arid5* along with a bar plot showing the gene expression of *FLC* in the respective genotypes.

5.2.3 Genome wide changes in H3K27me3 deposition negatively correlates with changes in gene expression in *cry1cry2* and *arid5*

H3K27me3 is a known marker for repression of gene transcription (Wiles and Selker 2017), and unlike H3K4me3, which is associated with a large number of actively transcribed genes (Wang et al. 2023), H3K27me3 is associated with a smaller proportion of genes in the genome (Zhou et al. 2018). From my H3K27me3 ChIP-seq data, I identified 7117 H3K27me3-associated genes defined by genes with at least one H3K27me3 peak within one kilobase pairs upstream or downstream of their transcription start sites. To validate the H3K27me3 ChIP-seq data, I compared it with a previously published H3K27me3 ChIP-seq dataset (Kralemann et al. 2020). Interestingly, out of the 6851 genes associated with H3K27me3 in WT identified in a previous study (Kralemann et al. 2020), 4955 genes overlapped with my study (Figure 5.4A). These results suggest that my H3K27me3 ChIP-seq effectively identified the correct set of peaks associated with *Arabidopsis* genes.

Next, I used the MAnorm software to identify differentially enriched peaks of H3K27me3 in *cry1cry2* and *arid5* mutants to examine genome-wide changes. I identified 440 peaks depleted of H3K27me3 and 1005 peaks enriched with H3K27me3 in *cry1cry2* and 717 peaks depleted of H3K27me3 and 954 peaks enriched with H3K27me3 in *arid5* (Figures 5.4B and 5.4C). To validate these differentially enriched H3K27me3 peaks, I plotted the read intensity heatmap of these peaks and the overall average read intensity profile over the associated genes. Unlike H3K4me3 deposition that is enriched at the transcriptional start site (Figures 5.2C and 5.2D), H3K27me3 deposition is present throughout the gene body (Figures 5.4D and 5.4E), consistent with the literature (Zhang et al. 2020). The plotted H3K27me3 read intensity showed the corresponding increase or decrease in H3K27me3 deposition in both *cry1cry2* and *arid5* mutants (Figures 5.4D and 5.4E), indicating that the MAnorm analysis accurately identified the differentially enriched H3K27me3 peaks.

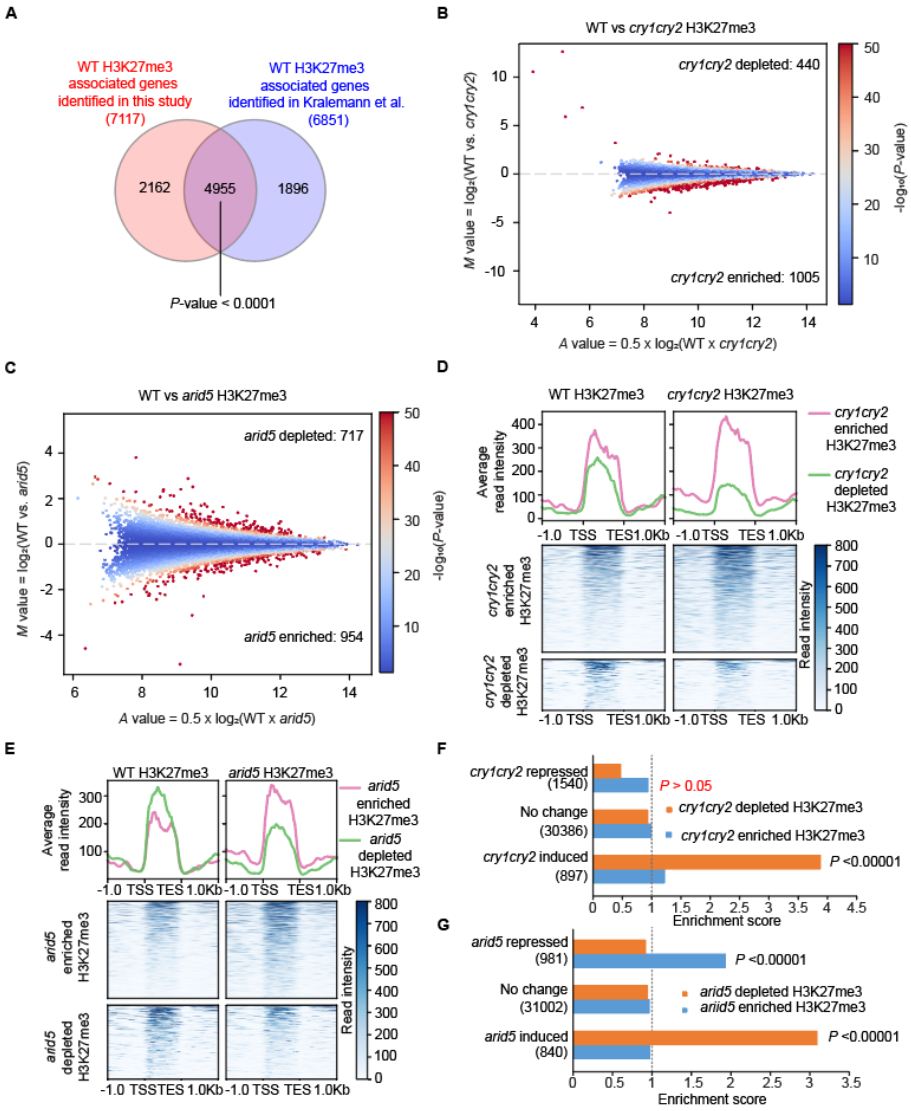

Figure 5.4: Genome wide H3K27me3 deposition changes negatively correlates with gene expression changes in *cry1cry2* and *arid5* mutants, except for downregulated genes in *cry1cry2*. (A) Venn diagram showing the overlap between genes associated with H3K27me3 peaks in WT identified in this study and those identified in Kralemann et al (Kralemann et al. 2020). The significance of the overlap was determined using Fisher's exact test. (B) MA plot of H3K27me3 peaks from WT and *cry1cry2* generated by MAnorm. (C) MA plot of H3K27me3 peaks from WT and *arid5* generated by MAnorm. (D) Plots of the average H3K27me3 ChIP-seq read intensity and heatmap of H3K27me3 ChIP-seq read intensity for gene groups enriched with or depleted of H3K27me3 in *cry1cry2* compared to WT. Genes are length-normalized and aligned at the transcription start site and the transcription end site, and the region 1 kb upstream of the TSS and 1 kb downstream of the TES is plotted. (E) Plots of the average H3K27me3 ChIP-seq read intensity and heatmap of H3K27me3 ChIP-seq read intensity for gene groups enriched with or depleted of H3K27me3 in *arid5* compared to WT. (F) Enrichment analysis of the overlap between repressed and induced genes in *cry1cry2* and genes enriched with or depleted of H3K27me3 in *cry1cry2* compared to WT. Each enrichment analysis was compared to the expected random overlap of the two sets of genes (shown as a vertical dotted line with an enrichment score of 1). The *P*-value was calculated using Fisher's exact test. (G) Enrichment analysis of the overlap between repressed and induced genes in *arid5* and genes enriched with or depleted of H3K27me3 in *arid5* compared to WT. The *P*-value was calculated using Fisher's exact test.

Next, I investigated whether the differentially enriched H3K27me3 peaks in *cry1cry2* and *arid5* mutants are associated with changes in gene expression. I compared the upregulated genes in each mutant with genes depleted of H3K27me3 and the downregulated genes with genes enriched with H3K27me3 (Figures 5.4F and 5.4G). I calculated the enrichment score and overlapping significance to determine the relationship between H3K27me3 deposition and gene expression. In *cry1cry2*, I found a strong overlap between the upregulated genes and genes depleted of H3K27me3 deposition (Figure 5.4F). However, I did not observe significant overlap between the downregulated genes and genes enriched with H3K27me3 in *cry1cry2* mutant (Figure 5.4F), indicating that CRYs might induce gene transcription mainly through mechanisms that are independent of decreasing H3K27me3 deposition. In *arid5*, I found significant overlap between the upregulated genes and genes depleted of H3K27me3, as well as between the downregulated genes and genes enriched with H3K27me3 (Figure 5.4G). These results suggest that CRYs and ARID5 modulates gene expression changes by regulating H3K27me3 deposition.

5.2.4 CRYs and ARID5 regulate floral transition by concurrently modulating the H3K4me3 and H3K27me3 deposition at regulated genes

To investigate the mechanism underlying the opposite effects of *cry1cry2* and *arid5* on hypocotyl growth and flowering time, particularly through H3K27me3 deposition, I analyzed the differentially expressed genes in *cry1cry2* and *arid5* that are associated with differentially enriched H3K27me3 peaks in the opposite direction (upregulated genes with depleted peaks of H3K27me3 and downregulated genes with enriched peaks of H3K27me3). Remarkably, *SOC1*, a downregulated gene in *cry1cry2*, which was depleted of H3K4me3 (Figure 5.3D), was also enriched with H3K27me3 compared to WT (Figure 5.5A). This finding suggests that CRY1 and CRY2 might enhance the transcription of *SOC1* by both increasing H3K4me3 deposition and decreasing H3K27me3 deposition at this locus. The potential mechanism for the regulation of both H3K4me3 and H3K27me3 deposition at the same genomic loci is further discussed in section 5.3.2 of this thesis. Additionally, the highly

upregulated gene in *arid5*, *STUBL4*, which was enriched with H3K4me3 (Figure 5.3F), was also depleted of H3K27me3 (Figure 5.5B). This indicates that ARID5 might suppress the gene expression of *STUBL4* by both decreasing H3K4me3 deposition and increasing H3K27me3 deposition. Furthermore, another downregulated gene in *arid5*, *MADS AFFECTING FLOWERING 4* (*MAF4*), which is a homolog of *FLC* and also functions as a floral transition repressor (Ratcliffe et al. 2003), was also enriched with H3K27me3 compared to WT (Figure 5.5C). Therefore, the increased H3K27me3 deposition and downregulation of the *MAF4* gene correlate with the early flowering phenotype of the *arid5* mutant. In conclusion, both CRY1/2 and ARID5 regulate the transcription of genes important for flowering time and hypocotyl growth by modulating the deposition of H3K4me3 and H3K27me3 at these genes.

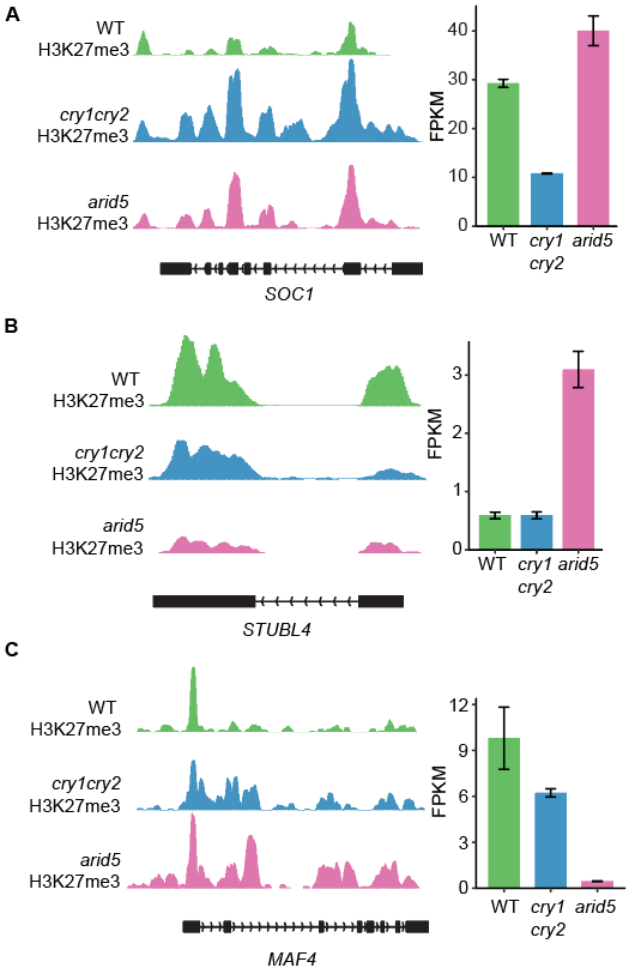

Figure 5.5: CRY1/2 and ARID5 regulate the transcription and H3K27me3 deposition of genes involved in floral transition.
(A) IGV screenshot depicting the H3K27me3 read intensity at the genomic locus of *SOC1* gene in WT, *cry1cry2*, and *arid5* along with a bar plot showing the gene expression (in FPKM) of *SOC1* in the respective genotypes. (B) IGV screenshot depicting the H3K27me3 read intensity at the genomic locus of *STUBL4* gene in WT, *cry1cry2*, and *arid5* along with a bar plot showing the gene expression of *STUBL4* in the respective genotypes. (C) IGV screenshot depicting the H3K27me3 read intensity at the genomic locus of *MAF4* gene in WT, *cry1cry2*, and *arid5* along with a bar plot showing the gene expression of *MAF4* in the respective genotypes.

5.3 Discussion

In this study, my objective was to investigate the underlying mechanism of how CRYs and the ISWI complex modulate hypocotyl growth and floral transition, especially through modulating histone modifications. I employed parallel RNA-seq and H3K4me3/H3K27me3 ChIP-seq experiments to shed light on the underlying mechanisms for the observed hypocotyl and flowering phenotypes in *cry2* and *arid5* mutants. My results demonstrate that there is a positive correlation between H3K4me3 deposition and changes in gene transcription in *cry1cry2* and *arid5* mutants, which is in line with the known role of H3K4me3 in gene activation (Wang et al. 2023). Importantly, I observed that many genes associated with hypocotyl growth and floral transition were dysregulated in both mutants, with changes in gene transcription and H3K4me3 deposition occurring in the same direction. For example, the hypocotyl growth-promoting gene *SAV3* is upregulated and accumulates more H3K4me3 deposition in *cry1cry2* mutant, consistent with the long hypocotyl phenotype of *cry1cry2*. In contrast, *TCP17*, a positive regulator of hypocotyl elongation, is downregulated and exhibits decreased H3K4me3 deposition in *arid5* mutant, consistent with the short hypocotyl phenotype of *arid5*. These results strongly suggest that CRYs and ARID5 regulate hypocotyl growth and floral transition at the epigenetic level by adjusting H3K4me3 deposition to fine-tune gene expression. Furthermore, I revealed that *SOC1* gene is downregulated in *cry1cry2* and exhibited decreased H3K4me3 deposition and increased H3K27me3 deposition. Similarly, *STUBL4* gene is upregulated in *arid5* mutant and exhibits increased H3K4me3 deposition and decreased H3K27me3 deposition. These results suggest that CRYs and the ISWI complex may regulate flowering time by modulating the deposition of both H3K4me3 and H3K27me3 at the same genomic loci.

5.3.1 Role of CRYs and the ISWI complex in regulation of H3K4me3 and H3K27me3 deposition

Although I have identified that CRYs and the ISWI complex may regulate gene expression by modulating H3K4me3 or H3K27me3 deposition or removal, the detailed mechanism behind this

regulation is currently unknown. Previous studies have shown that light-activated gene expression during de-etiolation is associated with an increase of H3K4me3 at the transcription start sites (TSS) of these genes (Guo et al. 2008). Several H3K4me3 writers, such as the SET DOMAIN PROTEIN 2 (SDG2), have been implicated in the deposition of H3K4me3 at light-inducible genes (Fiorucci et al. 2019), indicating that the light signaling pathway is associated with H3K4me3 writers to regulate gene expression. My results show that loss of *CRY1* and *CRY2* genes results in the increase of H3K4me3 at *SAV3* and *AHL22* genes, and the decrease of H3K4me3 at *PRR9* and *SOC1* genes. These findings suggest that CRYs may regulate H3K4me3 writer or eraser activity, and these differentially methylated genes could serve as potential novel targets of the CRY-mediated blue light signaling pathway.

ARID5, one of the components of the ISWI complex, has an AT-RICH INTERACTING DOMAIN (ARID) and a PHD domain that can specifically bind H3K4me3. It is possible that ARID5 could direct the ISWI complex to the genes with H3K4me3 deposition and interact with another complex with histone methyltransferase or demethylase activity to modulate the deposition of H3K4me3 and further fine-tune transcription. The interaction between chromatin remodeling complexes and histone methyltransferases has been reported previously. For example, the INO80 chromatin remodeling complex, can form a larger complex with the COMPASS H3K4 methylase complex (Shang et al. 2021). Similar to the INO80 complex, it is possible that the ISWI complex might associate with the COMPASS complex or another methylase or demethylase complex to regulate the H3K4me3 deposition. Interestingly, the CHR17 subunit of the ISWI complex was found to associate with the INO80 protein in an affinity purification-mass spectrometry experiment using CHR17-GFP as the bait (Smaczniak et al. 2012). This suggests that the ISWI complex may interact with the INO80 complex and further with the COMPASS complex to regulate H3K4me3 deposition. However, further research is needed to elucidate the precise molecular mechanisms underlying the role of CRYs and the ISWI complex in regulating the deposition of H3K4me3 and gene expression.

My results indicate that the mutation of both *CRY1* and *CRY2* genes resulted in changes in H3K27me3 deposition, but only the upregulated genes in *cry1cry2* had significant overlap with genes

depleted of H3K27me3, while the downregulated genes in *cry1cry2* did not significantly overlap with genes enriched with H3K27me3. One possible explanation for this discrepancy is that CRY1 and CRY2 may induce gene expression mainly through other regulatory means instead of modulating H3K27me3 deposition, such as regulating transcription factors CIB1 (Liu et al., 2008a) and PIF4/5 (Pedmale et al. 2016). Another possible explanation is that CRYs may mainly positively regulate H3K27me3 deposition instead of negatively regulate H3K27me3 deposition. CRY2 could be associated with the polycomb repressive complex 2 (PRC2) complex since CRY2 and the PRC2 complex interact with the deubiquitinases UBP12 and UBP13 (Kralemann et al. 2020; Derkacheva et al. 2016; Lindback et al. 2022). Therefore, it is possible that CRYs associate with PRC complexes to increase H3K27me3 deposition at some of their target genes to downregulate their expression. Further studies are needed to investigate the mechanism underlying the regulation of H3K27me3 deposition by CRYs and the PRC1/2 complexes.

5.3.2 Regulation of SOC1 and STUBL4-mediated floral transition by CRYs and the ISWI complex

In this ChIP-seq study, I observed that the *SOC1* and *STUBL4* genes, which are involved in flowering time regulation, are regulated through both the H3K4me3 and H3K27me3 deposition, reminiscent of the bivalent histone modification identified in mammalian cells (Macrae et al. 2023). In human embryonic stem cells, it was found that many development-relevant genes have both the activating marker H3K4me3 and the repressive marker H3K27me3 near the promoter regions (Macrae et al. 2023). Later studies suggest that these bivalent marks function to prime the gene for rapid activation upon entering a specific developmental stage or that bivalency at these genes could prevent the DNA methylation-induced irreversible silencing of these genes (Macrae et al. 2023). The study of bivalent chromatin in plants also suggests that there are bivalent marks in genes involved in floral transition, development of gametes, and potentially stress responses (Faivre and Schubert 2023). Interestingly, one of the genes previously identified to have a bivalent mark is *SOC1* (Qian et al. 2018).

Therefore, my study, which identified *SOC1* to be regulated at both the H3K4me3 and H3K27me3 levels in *cry1cry2*, is consistent with the previously reported bivalent marks on the *SOC1* gene (Qian et al. 2018). This also suggests that both of these two histone modifications at the bivalent site can be regulated simultaneously to fine-tune developmental processes, and CRYs might be important regulators of the bivalent chromatin state at the *SOC1* gene.

Furthermore, it has been demonstrated that one of the H3K4me3 methylases, ARABIDOPSIS TRITHORAX 1 (ATX1), can physically interact with the EMBRYONIC FLOWER 1 (EMF1) subunit of the PRC2 complex, providing a potential mechanism for the concurrent regulation of both H3K4me3 and H3K27me3 at genes with bivalent histone marks (Xu et al. 2018). This indicates a possible interaction between the H3K4me3 and H3K27me3 modification machineries, further emphasizing the potential importance of bivalent histone marks in regulating gene expression. My study provides evidence for the regulation of both H3K4me3 and H3K27me3 at bivalent sites in plants and suggests that CRYs and the ISWI complex may play a role in regulating these bivalent chromatin states, potentially contributing to the precise control of developmental processes in plants.

5.4 Materials and Methods

5.4.1 ChIP-sequencing

Seeds of WT, *cry2*, *cry1cry2*, and *arid5* were sterilized in 70% EtOH for five minutes and then sown onto 0.5× Linsmaier and Skoog (LS) medium (HiMedia Laboratories) containing 0.8% agar. After stratification for two days in darkness at 4°C, the seeds were grown at 22°C under continuous white light (100 μmol m^{-2} s^{-1}) from an LED source in a growth chamber (Percival Scientific) for 10 days before the tissue was harvested. Two biological replicates of tissue were collected for each genotype.

Two grams of harvested tissue per genotype per replicate were fixed in 1% formaldehyde (Cat #F8775, Sigma) prepared in fixation buffer (10 mM HEPES-NaOH, pH7.4). The fixation was

performed using a vacuum pump with three vacuum cycles of 5 min, 10 min, and 5 min. After vacuum fixation, the formaldehyde was quenched by adding a final concentration of 0.125 M of glycine to the fixation buffer with the tissue. The fixed tissue was rinsed twice with deionized water and dried using paper towels. The fixed and dried seedlings were then snap-frozen in liquid nitrogen and ground into a fine powder.

Ground tissue was mixed with 25 mL of nuclear isolation buffer (60 mM HEPES, 1 M sucrose, 5 mM KCl, 5 mM $MgCl_2$, 5 mM EDTA, 0.6% Triton X-100, 0.4 mM PMSF, and 1× EDTA-free protease inhibitor cocktail (Cat#11836170001, Roche), pH 8.0). The mixture was filtered through one layer of miracloth and centrifuged for 20 min at 4°C at 4000 rpm. After discarding the supernatant, the pellet was resuspended in 1 mL extraction buffer (0.25 M sucrose, 10 mM Tris-HCl, 10 mM $MgCl_2$, 1% Triton X-100, 5 mM BME, 0.1 mM PMSF, and 1× EDTA-free protease inhibitor cocktail (Cat#11836170001, Roche), pH 8). The mixture was centrifuged again for 10 min at 4°C at 11400 rpm, and the supernatant was discarded. The pellet was then resuspended in 300 µl of nuclei lysis buffer (50 mM Tris-HCl, 10 mM EDTA, 1% SDS, 0.1 mM PMSF, and 1× EDTA-free protease inhibitor cocktail (Cat#11836170001, Roche), pH 8) and incubated with rotation at 4°C for 20 min. ChIP dilution buffer (1.1% Triton X-100, 1.2 mM EDTA, 16.7 mM Tris-HCl, 167 mM NaCl, 0.1 mM PMSF, and 1× EDTA-free protease inhibitor cocktail (Cat#11836170001, Roche), pH 8) was added to each sample to make the final volume 2 mL.

The chromatin was sonicated using a Bioruptor sonicator (Diagenode) with the following setting: 4°C, 0.5 min on, 0.5 min off, 12 cycles. The sonicated chromatin mixture was then centrifuged for 10 min at 5000 rpm at 4°C, and the supernatant was transferred to a new tube and diluted to a final volume of 1.5 mL with the ChIP dilution buffer. Next, 300 µl of the diluted sample was saved as non-immunoprecipitated input chromatin, and the remaining chromatin sample was split into three volumes of 400 µl to be used for IgG, H3K4me3, and H3K27me3 IP, respectively. For each sample, the appropriate antibodies were added as follows: 5 µl of anti-H3K4me3 antibody (Cat#04-745, Sigma), 5 µg of anti-H3K27me3 antibody (Cat#07-449, Sigma), or 5 µg of normal rabbit IgG antibody (Cat#12-

370, Sigma). The sonicated chromatin added with antibodies was incubated with rotation at 4°C overnight.

The following day, each sample was mixed with 40 µl of protein-A beads (Cat#10008D, Thermo Fisher) prewashed with ChIP dilution buffer and incubated with rotation at 4°C for one hour. The beads were then sequentially washed with three different wash buffers: 1 mL of low salt buffer (150 mM NaCl, 0.1% SDS, 1% Triton X-100, 2 mM EDTA, 20 mM Tris-HCl, pH 8), 1 mL of high salt wash buffer (500 mM NaCl, 0.1% SDS, 1% Triton X-100, 2 mM EDTA, 20 mM Tris-HCl, pH 8), and 1 mL of LiCl wash buffer (0.25 M LiCl, 1% NP-40, 1% sodium deoxycholate, 1 mM EDTA, 10 mM Tris-HCl, pH 8). Each wash was performed for 5 min at 4°C. After the washes, the beads were rinsed once on a magnet stand with 1 mL of TE buffer (10 mM Tris-HCl, 1 mM EDTA, pH 8) and resuspended in 150 µl of elution buffer (50 mM Tris-HCl, 10 mM EDTA, 1% SDS, pH 8). The immunoprecipitated DNA-histone complexes were eluted by incubating the tubes at 65°C for 15 min. A second round of elution buffer (150 µl) was added to the beads and incubated for 15 min. The eluates from the two rounds of elution were combined into 300 µl of eluted solution for each antibody per genotype per replicate.

To release the DNA from the immunoprecipitated DNA-histone complexes and the input chromatin, eluted and input samples were added with 12 µl of 5 M NaCl, 30 µl of 1 M DTT, and 30 µl of 1 M NaHCO3 and incubated overnight at 65°C. The following day, 6 µl of 0.5 M EDTA, 12 µl of 1 M Tris-HCl (pH 8), and 2 µl of proteinase K solution (20 mg/mL, Thermo Fisher) were added to each of the immunoprecipitated and input samples and incubated at 65°C for one hour. After proteinase K treatment, an equal volume of phenol/chloroform/isoamyl alcohol (25:24:1, pH 8.0, Thermo Fisher) was added to each sample, vortexed, and centrifuged at 19,000 g for 5 min. The supernatant was transferred to a new tube and added with an equal volume of chloroform. The mixture was vortexed and centrifuged again at 19,000 g for 5 min, and the supernatant was transferred to a new tube. NaCl was added to a final concentration of 0.2 M into the transferred supernatant, along with glycogen (final concentration of 0.25 µg/µl) and 2.5 volumes of 100% ethanol. The samples were then incubated at -

80°C for at least three hours and centrifuged for 30 min at 13,000 rpm at 4°C. The supernatant was discarded, and the pellet was washed twice with 1 mL of 75% ethanol. Finally, the washed pellet was air-dried and resuspended with 50 µl of deionized water.

Following the ChIP procedure described above, the ChIP DNA samples were used to generate sequencing libraries using the NEBNext Ultra II DNA Library Prep Kit for Illumina (New England Biolabs), following the manufacturer's instructions. The ChIP-seq libraries were sequenced on the NextSeq500 (Illumina) platform with single-end sequencing of 76 bp, yielding an average of more than 37 million reads per sample.

5.4.2 mRNA-sequencing

Ten-day-old WT, *cry2*, *cry1cry2*, and *arid5* seedlings, grown under the same conditions as the ChIP-seq samples, were harvested for RNA extraction. Two biological replicates were collected, and total RNA was isolated using the Direct-zol RNA miniprep kit (Zymo Research) and quantified using a Qubit fluorometer (Thermo Fisher Scientific). Poly(A) mRNA was isolated from 1 µg of total RNA from each sample using the NEBNext poly(A) mRNA Magnetic Isolation Module (New England Biolabs), and the purified mRNA was used to construct libraries with the NEBNext Ultra II Directional RNA Library Prep Kit for Illumina (New England Biolabs), following the manufacturer's instructions. Single-end sequencing of 76 bp was performed on the NextSeq500 (Illumina) platform, generating more than 45 million reads per sample on average.

5.4.3 mRNA-seq analysis

The RNA-seq reads were aligned to the *Arabidopsis thaliana* Col-0 genome (TAIR10) using STAR version 2.7.5c (Dobin et al. 2013). Differential gene expression analysis was performed using Cufflinks version 2.2.1 (Trapnell et al. 2010). First, the FPKM values of all genes in all RNA-seq samples were calculated using the Cufflinks function. Then, the Cuffdiff function was used to derive the differentially expressed genes between the *cry2*, *cry1cry2*, *arid5* mutants and WT, respectively. To plot the Pearson's correlation coefficient between all RNA-seq samples, the "corrplot" package

(version 0.92) from R version 4.2.2 was used to calculate the coefficient and plot the coefficient values based on the FPKM values of all samples. The unnormalized counts for each gene for each sample generated by STAR were used as input for the "DESeq2" package (version 1.38.3) in R to plot the PCA map (Love et al. 2014).

5.4.4 ChIP-seq analysis

To map ChIP-seq reads to the *Arabidopsis thaliana* Col-0 genome (TAIR10), I used Bowtie2 software version 2.4.4 to generate SAM format mapping files (Langmead and Salzberg 2012). The resulting SAM files were then converted to BAM format files using SAMtools software version 1.10 (Li et al. 2009). Next, the BAM files were sorted and filtered to remove duplicated, multi-mapping, and unmapped reads, and then indexed using Sambamba software version 0.8.0 (Tarasov et al. 2015). To visualize the read coverage of the ChIP-seq at specific genomic loci, I used deepTools software (bamCoverage function) version 3.5.1 (Ramírez et al. 2014) to create BIGWIG format files with the BAM files as inputs, which were then visualized in IGV software version 2.8.2 (Robinson et al. 2011). I used two different peak calling software: MACS3 software version 3.0.0b1 (Zhang et al. 2008) to call peaks for H3K4me3 reads, and epic2 software version 0.0.51 (Stovner and Sætrom 2019) to call peaks for H3K27me3 reads. The resulting H3K4me3 and H3K27me3 peaks information generated by the two software were stored as BED format files.

The BAM files and BED files containing the peak information were used as inputs for MAnorm version 1.3.0 (Shao et al. 2012) to derive the differentially enriched H3K4me3 and H3K27me3 peaks. The resulting genomic coordinates of the peaks were manually formatted as BED files and then input into the R package "ChIPseeker" (version 1.34.1) to determine the nearest genes associated with each differentially enriched peak (Yu et al. 2015). Genes with a differentially enriched peak within 1 kb upstream or downstream of their transcriptional start site were manually defined as the genes associated with differentially enriched peaks. The coordinates of the start and end positions of these genes, enriched with or depleted of a histone mark, were obtained using the ATG number of the genes and the

GTF files from *Arabidopsis thaliana* genome assembly TAIR10. The resulting coordinates of the genes associated with a histone mark and the BIGWIG files were then used as inputs for deepTools software (plotHeatmap function) version 3.5.1 to generate plots showing the read intensity over individual genes and the average read intensity profile over all genes.

The overlap enrichment analysis between the differentially expressed genes obtained from the RNA-seq and the genes associated with differentially enriched ChIP-seq peaks was performed using Fisher's exact test, following the method previously reported by Zhou et al (Zhou et al. 2018).

Chapter 6. Conclusions and perspectives

6.1 Summary of findings

In this thesis, I have investigated and shed light on the novel roles of plant cryptochromes (CRYs) in regulating essential chromatin-related processes, including DNA damage response and chromatin remodeling. Notably, I have successfully characterized the involvement of CRYs, in conjunction with their interacting partners, deubiquitinases UBIQUITIN-SPECIFIC PROTEASE 12 and 13 (UBP12/13) (Lindback et al. 2022), in the pivotal task of regulating plant resistance against UVC-induced DNA damage.

CRYs have evolved from photolyases, enzymes specialized in repairing UV-induced DNA damage (Chaves et al. 2006). However, both animal and plant CRYs have lost their enzymatic activity of directly repairing DNA damage (Chaves et al. 2011). Nonetheless, mammalian CRYs have been found to play a crucial role in regulating the transcriptional response to DNA damage (Papp et al. 2015; Shafi et al. 2021). With this in mind, I aimed to investigate whether plant CRYs also retain a residual function in DNA damage response. My research focused on characterizing the function of CRYs and their negative regulators, deubiquitinases UBP12/13 (Lindback et al. 2022), in the context of DNA damage response. To achieve this, I subjected *cry1cry2* and *ubp12ubp13* mutants to treatment with UVC, a DNA damage-inducing agent (Molinier et al. 2005). My experimental results revealed that the *cry1cry2* mutant displayed hypersensitivity to UVC treatment, while the *ubp12ubp13* mutant exhibited resistance to UVC, compared to wild type (WT). Interestingly, the *UBP13* overexpression line (*UBP13oe*) also showed hypersensitivity to UVC treatment, while the sensitivity to UVC in *cry1cry2* and *cry1cry2;UBP13oe* was similar. These findings suggest that CRYs and UBP12/13 function together in the same genetic pathway to regulate plant resistance to UVC-induced DNA damage. As UVC primarily induces cyclobutane pyrimidine dimer (CPD)-type DNA damage (Gill et al. 2015), I proceeded to monitor the levels of CPD in *cry1cry2* and *ubp12ubp13* plants following UVC treatment

to assess their DNA repair progress. Notably, the CPD levels in *cry1cry2* remained mostly unchanged for up to three hours after an acute three-minute UVC treatment, while CPD levels decreased by approximately 25% during the three-hour recovery period in WT. This data strongly suggests that CRYs are functionally necessary for the repair of UVC-induced CPD-type DNA damage. In contrast, the repairing rate of CPD during the three-hour recovery period was faster in *ubp12ubp13* mutants compared to the WT, indicating that UBP12/13 negatively regulated CPD repair.

To delve into the underlying mechanism by which CRYs and UBP12/13 antagonistically regulate UVC resistance and DNA damage repair, I conducted an RNA sequencing (RNA-seq) time course experiment at 0 (untreated), 15, 60, and 180 minutes after UVC treatment in WT, *cry1cry2*, and *ubp12ubp13*. Through the RNA-seq analysis, I found that the UVC-induced transcriptional response was dampened in the *cry1cry2* mutant and enhanced in the *ubp12ubp13* mutant compared to WT, respectively. More precisely, WT plants exhibited activation of numerous stress response pathways upon UVC treatment, while these stress responses were attenuated in the *cry1cry2* mutant and amplified in the *ubp12ubp13* mutant. These findings shed light on the contrasting regulatory roles of CRYs and UBP12/13 in fine-tuning plant transcriptional response to UVC-induced DNA damage.

To gain further insights into the transcription factors responsible for the differential transcriptional response observed in *cry1cry2* and *ubp12ubp13* mutants, I conducted gene regulatory network analysis. My analysis revealed that in WT plants, the induction of gene transcription upon UVC treatment was predicted to be mediated by transcription factors including SUPPRESSOR OF GAMMA RADIATION 1 (SOG1), WRKYs, and CALMODULIN-BINDING TRANSCRIPTION ACTIVATORs (CAMTAs). Interestingly, these same three groups of transcription factors were also predicted to be involved in inducing gene expression in the *ubp12ubp13* mutant upon UVC. However, in *cry1cry2*, only SOG1 and WRKYs were predicted to regulate UVC-induced gene regulatory network, but not CAMTAs, indicating an impaired CAMTA-induced transcriptional response in *cry1cry2* following UVC treatment. This prompted us to closely examine the transcription of *CAMTA* genes following UVC treatment. I found that *CAMTA3* gene transcription was induced to a lesser extent in

cry1cry2 and to a greater extent in *ubp12ubp13* mutants compared to WT, suggesting that CAMTAs may function downstream of CRYs and UBP12/13 to modulate gene transcription. Furthermore, I examined whether CAMTAs are functionally required for plant UVC resistance. I conducted UVC treatment on *camta1camta2camta3* triple mutant plants and discovered that this mutant displayed hypersensitivity to UVC, similar to the *cry1cry2* mutant. This indicates that the function of CAMTA1, CAMTA2, and CAMTA3 is necessary for plant UVC resistance. Furthermore, CAMTA3 target genes were less induced in *cry1cry2* and more induced in *ubp12ubp13* mutants compared to WT upon UVC treatment, suggesting that CRYs and UBP12/13 oppositely regulate the CAMTA-mediated transcriptional response upon UVC treatment. Notably, the UVC-inducible CAMTA3 target genes were enriched in gene ontology (GO) terms related to stress responses, indicating that CAMTAs may operate downstream of CRYs and UBP12/13 to regulate UVC-induced stress responses at the transcriptional level.

My investigation has uncovered that CRYs and UBP12/13 function within the same genetic pathway to regulate plant response to UVC and exhibit antagonistic roles in DNA damage repair and DNA damage-induced transcriptional response, mirroring the negative regulation of CRY2 by UBP12/13 in blue light (Lindback et al. 2022). In light of these findings, I sought to further explore the molecular relationship between UBP12/13 and CRYs specifically under UVC conditions. Given that UBP13 has been shown to interact with CRY2 in a blue light-dependent manner (Lindback et al. 2022), I first examined whether the interaction between UBP13 and CRY2 is influenced by UVC. Intriguingly, my results demonstrated a considerably stronger interaction between CRY2 and UBP13 in the presence of UVC compared to in the dark, indicating that UVC enhances the interaction between CRY2 and UBP13, akin to blue light conditions (Lindback et al. 2022). As UBP12/13 are known to promote the destabilization of CRY2 protein in blue light (Lindback et al. 2022), I proceeded to investigate whether CRY2 undergoes destabilization upon UVC treatment and whether this process is dependent on UBP12/13. Interestingly, I observed that UVC exposure induced a transient destabilization of the CRY2 protein, and this destabilization is indeed reliant on the presence of UBP12/13. Subsequently, I aimed

to ascertain if CRY2 could be activated by UVC light, given its enhanced interaction with UBP13 and its UBP12/13-dependent destabilization under UVC. Notably, one of the early events in CRY2 photoactivation is the formation of CRY2 nuclear speckles (Wang et al. 2021). Therefore, I examined whether CRY2 forms nuclear speckles under UVC treatment using a UVC light-emitting diode (LED) light source devoid of UVA or blue light emissions. Surprisingly, my results revealed that UVC light indeed induces CRY2 nuclear speckle formation, similar to the response observed in blue light conditions (Wang et al. 2021). This intriguing observation suggests that UVC light could activate the CRY2 protein, thereby implying a potential role for CRY2 in sensing UVC light.

The subsequent phase of my dissertation delved into investigating the involvement of CRY2 in another crucial chromatin-related process: chromatin remodeling. Previous studies have established the requirement of CRYs in driving large-scale chromatin changes in *Arabidopsis*, such as the decondensation of chromatin during floral transition and during reduction in environmental light intensity (van Zanten et al. 2012). Additionally, CRYs have been implicated in the condensation of heterochromatin in cotyledon cell nuclei during early seedling development under blue light (Bourbousse et al. 2015). Despite significant progress in understanding the blue light signaling pathway mediated by CRYs, particularly regarding hypocotyl growth and floral transition (Liu et al., 2016a), the precise molecular mechanism underlying the function of CRYs in orchestrating large-scale chromatin changes remains largely unknown. Notably, the currently known CRY2 interactors do not have explicit roles in mediating large-scale chromatin changes. To identify novel CRY2 interactors, my laboratory conducted an affinity purification experiment targeting the CRY2 protein, followed by mass spectrometry analysis (Lindback et al. 2022). This experimental approach successfully identified five chromatin-related proteins as potential interactors of CRY2, namely CHROMATIN-REMODELING PROTEIN 11 (CHR11), CHR17, RINGLET 1 (RLT1), RLT2, and AT-RICH INTERACTING DOMAIN 5 (ARID5). These proteins collectively form one of the IMITATION SWITCH (ISWI) chromatin remodeling complexes in plants (Tan et al. 2020).

To validate the interaction between CRY2 and the ISWI complex, I conducted co-immunoprecipitation experiments specifically targeting the interaction between CRY2 and components of the ISWI complex, namely CHR11, RLT1, and ARID5. Notably, the pull-down of CRY2 successfully co-immunoprecipitated all three proteins: CHR11, RLT1, and ARID5. This observation strongly suggests that CRY2 interacts with distinct components of the ISWI complex. Subsequently, I aimed to investigate the light dependency of the interaction between CRY2 and the ISWI complex. To achieve this, *in vitro* co-immunoprecipitation experiments were conducted between CRY2 and the ATPase subunit of the ISWI complex, CHR11, in both light and dark conditions. Surprisingly, the results demonstrated that CRY2 and CHR11 interacted *in vitro* in a light-independent manner. This intriguing finding suggests that CRY2 establishes a constitutive interaction with the ISWI complex, while the activation of CRY2 by blue light may modulate the overall functionality of the CRY2-ISWI complex.

After confirming the interaction between CRY2 and the ISWI complex, I proceeded to investigate the functional relationship between CRY2 and ISWI. It is already established that both CRY2 and the ISWI complex regulate flowering time in plants (Tan et al. 2020), but in opposite ways: the *cry2* mutant exhibits late flowering (Guo et al. 1998), while the *chr11chr17*, *rlt1rlt2*, and *arid5* mutants flower early (Tan et al. 2020). To further understand the genetic interaction between CRY2 and ISWI, I generated *cry2rlt1rlt2* and *cry2arid5* higher-order mutants to examine their flowering time phenotype. Interestingly, both *cry2rlt1rlt2* and *cry2arid5* mutants flowered around the same time as the WT, with flowering times much closer to that of *rlt1rlt2* and *arid5* mutants rather than that of *cry2*. This indicates that the *RLT1/2* and *ARID5* genes are epistatic to the *CRY2* gene in regulating flowering time.

Next, I aimed to determine whether the ISWI complex is also involved in another CRY2-regulated response: the inhibition of hypocotyl growth in blue light (Lin et al. 1998). Interestingly, the *rlt1rlt2* and *arid5* mutants exhibited shorter hypocotyls under low intensities of blue light compared to WT, indicating that the ISWI complex promotes hypocotyl growth in blue light, contrary to CRY2.

More importantly, the *cry2rlt1rlt2* and *cry2arid5* higher-order mutants displayed shorter hypocotyls than the WT, suggesting that the *RLT1/2* and *ARID5* genes are epistatic to the *CRY2* gene in regulating blue light-mediated hypocotyl growth inhibition.

As mentioned earlier, CRY2 is known to regulate large-scale chromatin changes (van Zanten et al. 2012), although the underlying mechanism remains poorly understood. Interestingly, the ISWI complex in fruit flies is also required for higher-order chromatin condensation processes (Corona et al. 2007). Therefore, I investigated whether the ISWI complex could function together with CRY2 to regulate large-scale chromatin condensation during seedling development. Examination of the nucleus phenotype of WT, *cry2*, *rlt1rlt2*, and *arid5* mutants revealed that, in contrast to *cry2*, which exhibited less heterochromatin condensation in blue light, both *rlt1rlt2* and *arid5* mutants had higher levels of heterochromatin condensation than the WT. This suggests that the ISWI complex indeed regulates blue light-mediated large-scale chromatin condensation in plants. Importantly, the *cry2arid5* double mutant also exhibited increased heterochromatin condensation, similar to the *arid5* mutant, indicating that the *ARID5* gene is epistatic to the *CRY2* gene in the regulation of heterochromatin condensation.

Taken together, these results strongly indicate that the ISWI complex functions within the same genetic pathway as CRY2, regulating three crucial processes of the CRY2 signaling pathway: hypocotyl growth in blue light, flowering time, and blue light-mediated heterochromatin condensation during early seedling development. These findings provide valuable insights into the coordinated action of CRY2 and the ISWI complex in shaping important aspects of plant physiology and chromatin dynamics.

To gain further insight into the underlying mechanism and downstream processes by which CRY2 and the ISWI complex regulate the blue light signaling pathway in plants, I conducted a comprehensive RNA-seq experiment in conjunction with chromatin immunoprecipitation sequencing (ChIP-seq) analysis for trimethylation of histone H3 at lysine 4 (H3K4me3) and trimethylation of histone H3 at lysine 27 (H3K27me3). These experiments were performed in WT, *cry2*, *cry1cry2*, and *arid5* plants to investigate how CRY1/2 and ARID5 influence gene expression through histone modifications. Under the specific growth conditions employed for the RNA-seq experiment, I observed

that the *cry2* mutant exhibited a lower number of differentially expressed genes (DEGs) than the *cry1cry2* mutant, when compared to WT. Moreover, a significant proportion of the DEGs identified in the *cry2* mutant were also present in the DEGs identified in the *cry1cry2* mutant. These findings suggest that mutation of the *CRY2* gene led to a similar, albeit more subtle, transcriptomic alteration in comparison to the mutation of both the *CRY1* and *CRY2* genes. Consequently, my subsequent analyses for the RNA-seq and ChIP-seq data focused on the *cry1cry2* instead of *cry2*, comparing *cry1cry2* to both the WT and *arid5* samples.

In the RNA-seq and ChIP-seq analyses, I observed differential enrichment of H3K4me3 deposition in numerous protein-coding genes in *cry1cry2* and *arid5*, as compared to WT. Notably, the changes in deposition of H3K4me3 exhibited a positive correlation with changes in gene expression in *cry1cry2* and *arid5*, consistent with previous studies highlighting H3K4me3 as a marker for transcriptional activation (Howe et al. 2017). Conversely, I also detected differential enrichment of H3K27me3 peaks in *cry1cry2* and *arid5*, relative to WT, and noted a negative correlation between H3K27me3 deposition and gene expression, consistent with the previous studies (Wiles and Selker 2017).

In my investigation, I observed a notable reduction in the expression of the flowering-promoting gene *SUPPRESSOR OF OVEREXPRESSION OF CO 1* (*SOC1*) (Lee and Lee 2010) in the *cry1cry2* mutant, which is consistent with the delayed flowering phenotype observed in this mutant (Guo et al. 1998). Intriguingly, I found that the deposition of H3K4me3 at the *SOC1* gene was decreased in *cry1cry2* compared to the WT, while the deposition of H3K27me3 at this gene was increased in *cry1cry2* relative to the WT. These findings suggest that CRYs modulate *SOC1* gene expression by concurrently influencing the deposition of both H3K4me3 and H3K27me3. Similarly, I observed a significant induction in the expression of the flowering-promoting gene *SUMO-TARGETED UBIQUITIN E3 LIGASE 4* (*STUBL4*) (Elrouby et al. 2013) in the *arid5* mutant, accompanied by an increase in H3K4me3 deposition and a decrease in H3K27me3 deposition at this gene. These results

imply that CRY1/2 and ARID5 regulate the floral transition by modulating the transcription of key flowering time-regulating genes through the modulation of both H3K4me3 and H3K27me3 deposition.

In summary, this thesis offers valuable insights into the relatively understudied roles of plant CRYs in chromatin-related processes, such as DNA damage response and chromatin remodeling (Figure 6.1). Through this research, I have uncovered the intricate involvement of CRYs and UBP12/13 deubiquitinases in finely tuning the plant DNA damage response (Figure 6.1). Moreover, I have elucidated the physical interaction between plant CRY2 and the ISWI complex, which plays a crucial role in modulating various biological processes, including blue light-mediated hypocotyl growth inhibition, blue light-induced heterochromatin condensation in cotyledon cells, and regulation of flowering time (Figure 6.1). These findings contribute to our understanding of the diverse functions of plant CRYs in chromatin dynamics and plant development.

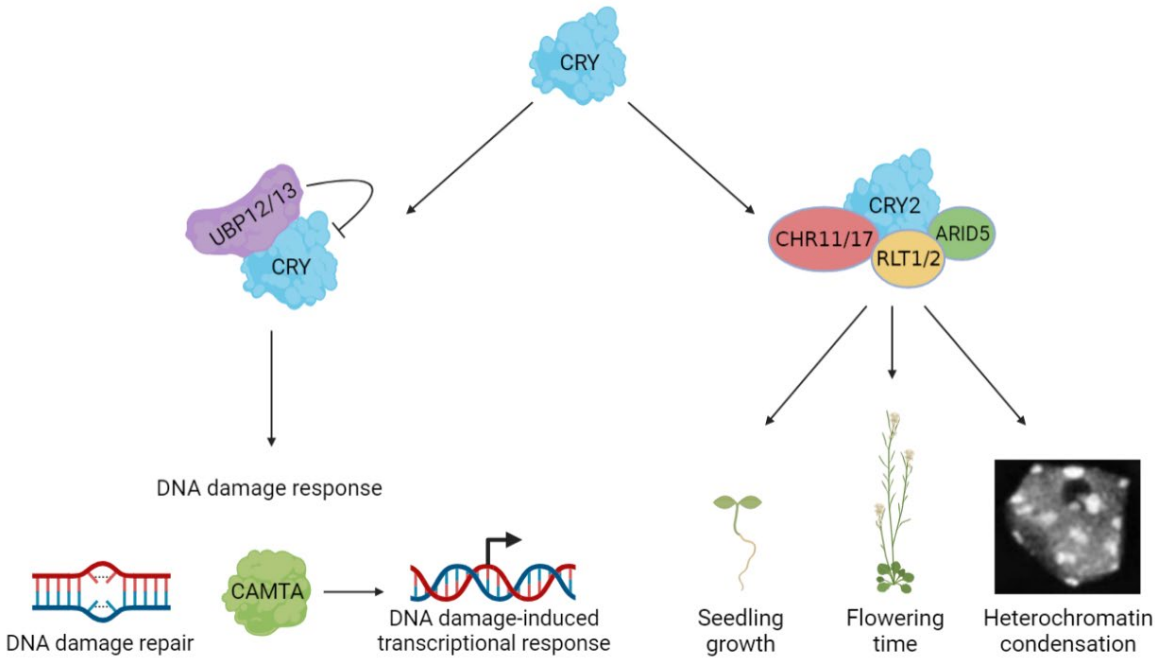

Figure 6.1 Diagram showing the role of CRYs in the regulation of DNA damage response and chromatin remodeling.

CRY proteins form two distinct complexes with distinct functional roles in chromatin-related processes: CRYs engage with UBP12/13, orchestrating DNA damage responses, while CRY2 interacts with CHR11/17, RLT1/2, and ARID5 to modulate chromatin remodeling processes. CRYs positively regulate the DNA damage response through promoting DNA damage repair and CAMTA-mediated transcription response to DNA damage. CRY2 physically interact with an ISWI complex consisting of CHR11/17, RLT1/2 and ARID5. This interaction assumes significance as CRY2 and the ISWI complex antagonistically regulate seedling growth, flowering time and heterochromatin condensation.

6.2 Impacts on the field

6.2.1 Role of CRYs in regulating higher-order chromatin changes

CRYs play a vital role in regulating essential developmental processes in *Arabidopsis*, such as the inhibition of hypocotyl growth in response to blue light and the photoperiodic control of flowering time (Guo et al. 1998; Lin et al. 1998). CRYs are also required for higher-order chromatin changes during floral transition, shift in light intensity and seedling development under blue light (van Zanten et al. 2012; Bourbousse et al. 2015). While the molecular mechanisms by which CRYs regulate hypocotyl growth and floral transition has been extensively studied, the involvement of CRYs in large-scale chromatin changes is still not well understood.

To date, only two downstream factors of CRYs have been implicated in the regulation of large-scale chromatin changes: COP1 and DE-ETIOLATED 1 (DET1) (Bourbousse et al. 2015). COP1, as an interactor of CRYs, is associated with the Cullin 4-RING ubiquitin E3 ligase (CRL4) complex (Chen et al. 2010). The CRL4 complex is part of a larger complex called COP/DET/ FUSCA (FUS) (Chen et al. 2006), which also includes the DET1 protein. Notably, DET1 protein can bind to nonacetylated histone H2B (Benvenuto et al. 2002), serving as a potential link between CRY signaling and chromatin regulation. Interestingly, DET1 and COP1 are known to be required for maintaining heterochromatin in a decondensed state in dark-grown seedling cotyledon cells (Bourbousse et al. 2015). However, the precise mechanisms by which COP1 and DET1 regulate large-scale chromatin condensation, as well as the genetic relationship between COP1/DET1 and CRYs in this process, remain to be explored.

My discovery of the physical interaction between CRY2 and the ISWI chromatin remodeling complex establishes a significant link between CRYs and large-scale chromatin changes. The ISWI chromatin remodeling complex has been well-documented to play a critical role in both chromatin condensation and decondensation (Corona et al. 2007). For instance, in *Drosophila*, the depletion of the ISWI ATPase leads to abnormal chromosomal decondensation (Corona et al. 2007). Similarly, depletion of the human ISWI ATPase SWI/SNF RELATED, MATRIX ASSOCIATED, ACTIN

DEPENDENT REGULATOR OF CHROMATIN, SUBFAMILY A, MEMBER 5 (SMARCA5) results in the over-compaction of newly synthesized chromatin, indicating a positive role for SMARCA5 in chromatin decondensation (Poot et al. 2004). In my study, I found that CRY2 and the ISWI complex antagonistically regulate heterochromatin condensation, revealing the conserved role of the plant ISWI chromatin remodelers in chromatin condensation (Corona et al. 2007). Furthermore, my study advances the field by identifying a novel factor involved in CRY-mediated signaling, ISWI complex, that contributes to the regulation of large-scale chromatin dynamics.

6.2.2 CRYs and UBP12/13 deubiquitinases regulate plant DNA damage response to UVC

CRYs evolved from photolyases (Chaves et al. 2006) but lost the enzymatic activity to directly repair DNA damage (Chaves et al. 2011). Nevertheless, several studies have demonstrated the involvement of mammalian CRYs in the DNA damage response (Papp et al. 2015; Shafi et al. 2021). However, the role of plant CRYs in the DNA damage response has remained elusive. My study represents the first comprehensive characterization of the detailed function of plant CRYs in the DNA damage response, revealing the requirement of CRYs in plant resistance against the genotoxin UVC and the repair of UV-induced DNA damage. Similar to findings on mammalian CRYs (Papp et al. 2015; Shafi et al. 2021), I observed destabilization of the plant CRY2 protein upon UVC exposure, while CRY1 and CRY2 positively regulate the plant's transcriptional response to UVC-induced DNA damage. Importantly, I have uncovered mechanistic insights into the regulation of DNA damage-induced transcriptional response by CRYs. Specifically, I have identified CAMTA transcription factors as crucial regulators of DNA damage-induced transcriptional response, with my results suggesting that CAMTAs function downstream of CRYs to regulate transcriptional response to DNA damage.

The results of my study demonstrate that CPD repair is impaired in *cry1cry2* mutant but enhanced in *ubp12ubp13* mutant. In *Arabidopsis*, CPD repair under light conditions is primarily mediated by the photolyase PHR1 (Jiang et al. 1997). Previous reports suggested that the *det1-1* mutant exhibited improved CPD repair after UVC treatment, associated with upregulated levels of *PHR1*

transcripts (Castells et al. 2010). However, in my investigation, the *PHR1* gene did not show differential expression in *cry1cry2* or *ubp12ubp13* mutants compared to the WT at all four time points (0, 15, 60, and 180 min) in the RNA-seq analysis (data not shown). Therefore, although CRYs and UBP12/13 regulate CPD repair under light conditions, they do not appear to modulate the transcript level of the *PHR1* gene. This suggests that CRYs and UBP12/13 might exert their effects on CPD repair through post-transcriptional regulation of PHR1. One possible post-transcriptional regulation mechanism could involve the modulation of PHR1 protein levels. To explore this, immunoblotting with an antibody specific to native PHR1 protein could be performed to measure PHR1 protein levels in WT, *cry1cry2*, and *ubp12ubp13* mutants before and after UVC treatment at different time points. Additionally, crossing the *cry1cry2* mutant with the *phr1* mutant and assessing the CPD repair and UVC resistance in the resulting *cry1cry2phr1* triple mutant would be another approach to investigate whether CRYs regulate CPD repair and UVC resistance through PHR1. If CRYs and PHR1 function in the same pathway for CPD repair, the *cry1cry2phr1* triple mutant should exhibit impaired CPD repair and hypersensitivity to UVC, similar to either the *cry1cry2* or *phr1* mutant. These proposed experiments have the potential to elucidate the molecular mechanism by which CRYs and UBP12/13 regulate CPD repair.

Deubiquitinases play crucial roles in the DNA damage response in animals (Le et al. 2019). For example, animal deubiquitinases can directly deubiquitinate DNA repair proteins, stabilizing them and promoting DNA damage repair (Le et al. 2019). However, the literature regarding the role of deubiquitinases in plant DNA damage response remains limited. My study provides significant insights into the mechanistic characterization of plant DUBs in the DNA damage response. Specifically, I have identified UBP12/13 as negative regulators of plant resistance to UVC and the repair of UV-induced DNA damage. Notably, my findings demonstrate that UBP12/13 DUBs antagonize the function of CRYs, suggesting that they serve as inhibitory components for the CRY-mediated DNA damage response to UVC.

During my investigation into the roles of UBP12/13 and CRYs in plant DNA damage response, I made a novel discovery: UVC light can regulate CRY2 in a manner similar to blue light. Specifically, I observed that UVC light triggers the formation of CRY2 nuclear speckles, strengthens the interaction between CRY2 and UBP13, and induces UBP12/13-dependent destabilization of CRY2 protein. These findings suggest that CRY2 may function as a potential UVC light receptor. This discovery is particularly surprising considering that CRY2 is well characterized as a receptor for UVA/blue light (Wang et al. 2014), and no functional roles of CRY2 in UVC response have been previously revealed. However, a study published over 60 years ago revealed that the chromophore of CRY2, FAD, exhibits an absorption peak in the UVC light spectrum in addition to two other absorption peaks in the UVA and blue light spectra (YAGI et al. 1959). Nevertheless, the functional relevance of UVC light for FAD-based light receptors has not been explored. Therefore, my study is the first to demonstrate the functional activation of a FAD-based light receptor, CRY2, by UVC light. This role of UVC in activating CRY2 provides a partial explanation for the specific involvement of CRYs in regulating DNA damage response to UVC, as evidenced by the lack of hypersensitivity in the *cry1cry2* mutant to another genotoxic agent, zeocin, which primarily induces DNA double-strand breaks.

6.3 Future directions

6.3.1 Establishing a molecular connection between CRYs and the CAMTA transcription factors

In my study, I found that CAMTAs are required for plant resistance to UVC and mediate the transcriptional response to UVC. Notably, I observed a reduction in the CAMTA-mediated transcriptional response in the *cry1cry2* mutant compared to the WT upon UVC treatment. This observation strongly indicates that CAMTAs function downstream of CRYs in regulating the plant's response to UVC. However, to establish a definitive and comprehensive relationship between CRYs and CAMTAs, further experimentation is required.

Firstly, experiments should be performed to address whether *CRY1/2* and *CAMTA1/2/3* function in the same genetic pathway to regulate plant UVC resistance. To achieve this, I propose crossing the *cry1cry2* double mutant with the *camta123* triple mutant, leading to the generation of the quintuple mutant *cry1cry2camta123*, wherein all five genes are mutated. Subsequently, this *cry1cry2camta123* quintuple mutant should be subjected to UVC treatment, and its fresh weight measured. On the one hand, if *CRY1/2* and *CAMTA1/2/3* indeed function in the same genetic pathway to regulate UVC resistance, it is expected that the *cry1cry2camta123* quintuple mutant would exhibit a lower relative fresh weight compared to the WT when subjected to UVC treatment. Additionally, the relative fresh weight of *cry1cry2camta123* would be similar to that of the *cry1cry2* mutant upon UVC treatment. On the other hand, if *CRY1/2* and *CAMTA1/2/3* function in separate parallel pathways, the *cry1cry2camta123* quintuple mutant would display a lower relative fresh weight than both the *cry1cry2* and *camta123* mutants after UVC treatment.

Alternatively, an additional approach to study the genetic interaction between *CRY1/2* and *CAMTA3* gene can be adopted by crossing the *camta3-3D* mutant, which expresses a constitutively active version of the CAMTA3 protein (Jing et al., 2011), with the *cry1cry2* mutant to generate the *cry1cry2camta3-3D* triple mutant. In this case, the *cry1cry2camta3-3D* mutant would possess constitutive CAMTA3 protein activity. If *CRY1/2* and *CAMTA3* function within the same genetic pathway to regulate UVC resistance, the *cry1cry2camta3-3D* mutant is anticipated to display a higher relative fresh weight compared to the *cry1cry2* mutant.

Moreover, the molecular mechanisms through which CRYs regulate CAMTAs remain unexplored and warrant further investigation. CAMTA transcription factors are known to interact with calmodulins (Iqbal et al. 2020). In *Arabidopsis*, one specific calmodulin protein, CALMODULIN 7 (CAM7), is recognized as a regulator of the light signaling pathway (Abbas et al. 2014; Kushwaha et al. 2008). CAM7 physically interacts with the HY5 transcription factor (Abbas et al. 2014), which is also associated with CRYs (Ponnu and Hoecker 2022). CAM7 and HY5 jointly bind to the promoter of *HY5* to enhance its gene expression (Abbas et al. 2014). Remarkably, the overexpression of *CAM7*

partially rescues the long hypocotyl phenotype observed in *hy5* mutations, indicating that CAM7 and HY5 function within the same genetic pathway to regulate light-mediated hypocotyl elongation inhibition (Kushwaha et al. 2008). An intricate relationship also exists between CRYs and HY5 (Ponnu and Hoecker 2022). On one hand, CRYs directly interact with COP1, which in turn interacts with HY5 (Ponnu and Hoecker 2022). On the other hand, CRYs are known to interact with subunits of the SWI2/SNF2-RELATED 1 (SWR1) complex, namely SWR1 COMPLEX SUBUNIT 6 (SWC6), and ACTIN-RELATED PROTEIN 6 (ARP6) (Mao et al. 2021). HY5 can also physically interact with SWC6 and ARP6, directing the SWR1 complex towards HY5 target genes (Mao et al. 2021). Consequently, CRYs can physically associate with the HY5 transcription factor through their common interaction with SWC6 and ARP6 (Mao et al. 2021). Considering these associations, it is reasonable to hypothesize that a potential interaction between CRYs and CAM7 may exist. Moreover, CAM7 might play a role in mediating the regulation of CAMTA transcription factors by CRYs. To validate these hypotheses, further experimentation involving biochemical and genetic interaction studies is warranted.

To investigate the potential physical interaction between CRYs and CAM7, co-IP experiments should be conducted using plant tissue co-expressing CRY1/2 together with CAM7. If a physical interaction between CRYs and CAM7 is confirmed, further experiments should be undertaken to explore the functional role of CAM7 in UVC resistance. Considering that *Arabidopsis* has seven *CAM* genes (*CAM1-7*), it is essential to evaluate UVC resistance in *CAM7* overexpression lines. If CAM7 positively regulates UVC resistance, it is expected that *CAM7* overexpression lines will display increased resistance to UVC treatment. Additionally, to investigate whether CAM7 functions in the same pathway as CRYs to regulate UVC resistance, *CAM7* overexpression lines in the *cry1cry2* background (*cry1cry2;CAM7oe*) should be generated and evaluated for UVC resistance. If CRY1/2 and CAM7 indeed function in the same pathway to regulate UVC resistance, it is expected that the overexpression of *CAM7* will, at least partially, rescue the UVC hypersensitivity phenotype of the *cry1cry2* mutant. Conducting these experiments will provide valuable insights into the potential interplay between CRYs and CAM7 in the context of UVC response, contributing to a comprehensive

understanding of the molecular mechanisms governing plant resistance against UVC-induced DNA damage.

6.3.2 Toward a functional mechanism of how CRYs and the ISWI complex regulate gene transcription at specific genomic loci

My study has revealed the physical and genetic interactions between CRYs and the ISWI complex, which play antagonistic roles in regulating two important CRY-mediated processes: hypocotyl growth inhibition by blue light and flowering time. To further our understanding, future experiments should focus on elucidating the molecular mechanism by which CRYs and the ISWI complex jointly regulate gene expression. It is likely that both CRYs and the ISWI complex interact with transcription factors to be targeted to specific genes. In the case of CRYs, they have been shown to interact with multiple transcription factors, thereby modulating the expression of genes involved in the regulation of hypocotyl growth and flowering time (Ponnu and Hoecker 2022). Notable examples of transcription factors that interact with CRYs include CIB1, CO, PIF4/5, and TCP DOMAIN PROTEIN (TCP) transcription factors (Liu et al., 2008a, 2018; Pedmale et al., 2016; Mo et al., 2022; Zhou et al., 2019). On the other hand, the ISWI complex, being a chromatin remodeling complex, typically forms complexes with transcription factors or non-coding RNAs to be directed to specific genomic loci (Tyagi et al. 2016). A possible hypothesis for the regulation of specific genes by the CRY2-ISWI complex is that one or more transcription factors interact with both CRY2 and the ISWI complex, directing them to genomic loci. Furthermore, it is conceivable that CRY2 and the ISWI complex have antagonistic roles in modulating transcriptional activity, given the opposite phenotypes of the *cry* and *iswi* mutants.

To shed light on potential transcription factors that may direct CRY2-ISWI complex to specific genomic loci, I conducted a preliminary analysis on common target genes of CRY2 and ARID5. ChIP-seq studies have been reported for both CRY2 and ARID5 (Pedmale et al. 2016; Tan et al. 2020). I found that out of the 6249 CRY2 target genes and 2864 ARID5 target genes, 1236 genes are common

targets of both CRY2 and ARID5 (data not shown). Importantly, a GO term analysis of these common target genes showed a significant enrichment for pathways related to light signaling (data not shown). This observation suggests that CRY2 and the ISWI complex may potentially localize to similar genomic target genes involved in regulating the light signaling pathway.

To explore the potential transcription factors involved in directing CRY2 and the ISWI complex to these common target genes, I performed a *de novo* motif search using the promoter sequences of the shared target genes. Interestingly, the top motifs identified from this motif search corresponded to known binding motifs of the TCP and PIF transcription factor families (data now shown). Notably, previous research has demonstrated that CRYs interact with both TCP and PIF transcription factors to coordinate the regulation of hypocotyl growth during thermomorphogenesis (Zhou et al. 2019). Consequently, it would be intriguing to conduct additional experiments to determine whether TCP/PIF transcription factors can direct CRY2 and the ISWI complex to the promoter regions of the common target genes involved in the light signaling pathway.

To investigate the potential interplay between CRY2, the ISWI complex, and TCP/PIF transcription factors, several experiments could be performed. Firstly, co-IP assays will be conducted to assess the physical interaction between the ISWI complex and TCP/PIF transcription factors. Additionally, ChIP-seq experiments will be performed for CRY2, ARID5, TCP, and PIF proteins to identify their shared target genes. To gain further insights into the regulatory mechanism, CRY2 and ARID5 ChIP-seq will be conducted in both the WT background and the *tcp* or *pif* mutant backgrounds. This will allow us to determine whether the binding of CRY2 and ARID5 to target genes is dependent on the presence of TCP or PIF transcription factors. The outcomes of these experiments will provide crucial information on whether TCP/PIF transcription factors play a functional role in facilitating CRY2 and the ISWI complex's binding to specific target genes to regulate gene expression.

In my study, I have observed dysregulation in the deposition of H3K27me3 within the *cry1cry2* mutant when compared to the WT, but the mechanism underlying this dysregulation remains to be explored. It is established in the literature that CRY2 can interact with UBP12 and UBP13

deubiquitinases (Lindback et al. 2022), both of which exhibit interactions with LIKE HETEROCHROMATIN PROTEIN 1 (LHP1) (Derkacheva et al. 2016), a critical component of the *Arabidopsis* Polycomb complex (Derkacheva et al. 2016). The catalytic activity of the Polycomb complexes is responsible for the deposition of H3K27me3 (Kralemann et al. 2020), and previous research has indicated that UBP12 and UBP13 are indispensable for the proper placement of H3K27me3 on select Polycomb target genes (Kralemann et al. 2020), thereby facilitating gene repression (Kralemann et al. 2020). Hence, it becomes plausible that CRYs may play a role in regulating the Polycomb systems, potentially influencing the deposition of H3K27me3 at specific target genes. To explore this hypothesis, co-IP experiments can be conducted to examine whether CRYs form complexes with LHP1 or other constituents of the Polycomb complexes. Should CRYs indeed exhibit interactions with Polycomb complexes, the next step would be to examine whether the regulation of H3K27me3 deposition by CRYs depends on the presence of the Polycomb complex. This could be effectively addressed by generating a *cry1cry2lhp1* triple mutant through crossing *cry1cry2* mutant with *lhp1* mutant. The rationale behind this genetic cross lies in the established understanding that H3K27me3 deposition at specific Polycomb target genes is dysregulated in the *lhp1* mutant (Veluchamy et al. 2016). By assessing the H3K27me3 deposition landscape in the *cry1cry2lhp1* mutant through ChIP-seq, valuable insights could be gained into whether CRYs exert their regulatory influence on H3K27me3 deposition through the mediation of Polycomb complexes. The findings from these experiments have the potential to unravel the intricate molecular mechanisms underlying the role of CRYs in modulating the deposition of pivotal epigenetic marks, like H3K27me3.

In summary, my analysis unveiled a significant overlap in the target genes of CRY2 and ARID5, indicating a potential collaboration between CRYs and the ISWI complex in the regulation of the light signaling pathway. The potential involvement of TCP/PIF transcription factors in directing CRY2 and ISWI complex to their common target genes presents an exciting avenue for further experimentation, contributing to unraveling the functional mechanism of how CRYs and the ISWI complex regulate gene transcription at specific genomic loci to modulate plant growth and development.

References

Abbas N, Maurya JP, Senapati D, Gangappa SN, Chattopadhyay S. 2014. *Arabidopsis* CAM7 and HY5 Physically Interact and Directly Bind to the *HY5* Promoter to Regulate Its Expression and Thereby Promote Photomorphogenesis. *Plant Cell* **26**: 1036–1052.

Abbotts R, Wilson DM. 2017. Coordination of DNA single strand break repair. *Free Radic Biol Med* **107**: 228–244.

Abdelhaleem M. 2009. Helicases: An Overview. pp. 1–12.

Ahmad M, Cashmore AR. 1993. HY4 gene of A. thaliana encodes a protein with characteristics of a blue-light photoreceptor. *Nature* **366**: 162–166. http://www.nature.com/articles/366162a0.

Akutsu M, Dikic I, Bremm A. 2016. Ubiquitin chain diversity at a glance. *J Cell Sci*.

Alhmoud JF, Woolley JF, Al Moustafa A-E, Malki MI. 2020. DNA Damage/Repair Management in Cancers. *Cancers (Basel)* **12**: 1050. https://www.mdpi.com/2072-6694/12/4/1050.

Al Khateeb WM, Sher AA, Marcus JM, Schroeder DF. 2019. UVSSA, UBP12, and RDO2/TFIIS Contribute to Arabidopsis UV Tolerance. *Front Plant Sci* **10**. https://www.frontiersin.org/article/10.3389/fpls.2019.00516/full.

Alonso-de Vega I, Martín Y, Smits VA. 2014. USP7 controls Chk1 protein stability by direct deubiquitination. *Cell Cycle* **13**: 3921–3926. https://www.tandfonline.com/doi/full/10.4161/15384101.2014.973324.

An Z, Liu Y, Ou Y, Li J, Zhang B, Sun D, Sun Y, Tang W. 2018. Regulation of the stability of RGF1 receptor by the ubiquitin-specific proteases UBP12/UBP13 is critical for root meristem maintenance. *Proceedings of the National Academy of Sciences* **115**: 1123–1128.

Aydin ÖZ, Marteijn JA, Ribeiro-Silva C, Rodríguez López A, Wijgers N, Smeenk G, van Attikum H, Poot RA, Vermeulen W, Lans H. 2014a. Human ISWI complexes are targeted by SMARCA5 ATPase and SLIDE domains to help resolve lesion-stalled transcription. *Nucleic Acids Res* **42**: 8473–8485.

Aydin ÖZ, Vermeulen W, Lans H. 2014b. ISWI chromatin remodeling complexes in the DNA damage response. *Cell Cycle* **13**: 3016–3025. http://www.tandfonline.com/doi/full/10.4161/15384101.2014.956551.

Bagnall DavidJ, King RodW, Hangarter RogerP. 1996. Blue-light promotion of flowering is absent in hy4 mutants of Arabidopsis. *Planta* **200**.

Ball HL, Myers JS, Cortez D. 2005. ATRIP Binding to Replication Protein A-Single-stranded DNA Promotes ATR–ATRIP Localization but Is Dispensable for Chk1 Phosphorylation. *Mol Biol Cell* **16**: 2372–2381.

Ban C. 1998. Structural basis for MutH activation in E.coli mismatch repair and relationship of MutH to restriction endonucleases. *EMBO J* **17**: 1526–1534.

Banerjee R, Schleicher E, Meier S, Viana RM, Pokorny R, Ahmad M, Bittl R, Batschauer A. 2007. The Signaling State of Arabidopsis Cryptochrome 2 Contains Flavin Semiquinone. *Journal of Biological Chemistry* **282**: 14916–14922. https://linkinghub.elsevier.com/retrieve/pii/S0021925820636468.

Bao Y, Shen X. 2007. INO80 subfamily of chromatin remodeling complexes. *Mutation Research/Fundamental and Molecular Mechanisms of Mutagenesis* **618**: 18–29.

Barisic D, Stadler MB, Iurlaro M, Schübeler D. 2019. Mammalian ISWI and SWI/SNF selectively mediate binding of distinct transcription factors. *Nature* **569**: 136–140. http://www.nature.com/articles/s41586-019-1115-5.

Barrero JM, Downie AB, Xu Q, Gubler F. 2014. A Role for Barley CRYPTOCHROME1 in Light Regulation of Grain Dormancy and Germination. *Plant Cell* **26**: 1094–1104.

Barski A, Cuddapah S, Cui K, Roh TY, Schones DE, Wang Z, Wei G, Chepelev I, Zhao K. 2007. High-Resolution Profiling of Histone Methylations in the Human Genome. *Cell* **129**: 823–837. https://linkinghub.elsevier.com/retrieve/pii/S0092867407006009.

Bartholomew B. 2014. ISWI chromatin remodeling: one primary actor or a coordinated effort? *Curr Opin Struct Biol* **24**: 150–155.
Bas-Orth C, Tan Y-W, Oliveira AMM, Bengtson CP, Bading H. 2016. The calmodulin-binding transcription activator CAMTA1 is required for long-term memory formation in mice. *Learning & Memory* **23**: 313–321. http://learnmem.cshlp.org/lookup/doi/10.1101/lm.041111.115.
Basta J, Rauchman M. 2015. The nucleosome remodeling and deacetylase complex in development and disease. *Translational Research* **165**: 36–47.
Battey NH, Tooke F. 2002. Molecular control and variation in the floral transition. *Curr Opin Plant Biol* **5**: 62–68.
Bedrosian TA, Nelson RJ. 2017. Timing of light exposure affects mood and brain circuits. *Transl Psychiatry* **7**: e1017–e1017.
Benayoun BA, Pollina EA, Ucar D, Mahmoudi S, Karra K, Wong ED, Devarajan K, Daugherty AC, Kundaje AB, Mancini E, et al. 2015. H3K4me3 Breadth Is Linked to Cell Identity and Transcriptional Consistency. *Cell* **163**: 1281–1286.
Benn G, Wang C-Q, Hicks DR, Stein J, Guthrie C, Dehesh K. 2014. A key general stress response motif is regulated non-uniformly by CAMTA transcription factors. *The Plant Journal* **80**: 82–92. https://onlinelibrary.wiley.com/doi/10.1111/tpj.12620.
Benvenuto G, Formiggini F, Laflamme P, Malakhov M, Bowler C. 2002. The Photomorphogenesis Regulator DET1 Binds the Amino-Terminal Tail of Histone H2B in a Nucleosome Context. *Current Biology* **12**: 1529–1534.
Besteiro MAG, Bartels S, Albert A, Ulm R. 2011. Arabidopsis MAP kinase phosphatase 1 and its target MAP kinases 3 and 6 antagonistically determine UV-B stress tolerance, independent of the UVR8 photoreceptor pathway. *Plant Journal* **68**: 727–737. https://onlinelibrary.wiley.com/doi/10.1111/j.1365-313X.2011.04725.x.
Biswas S, Rao CM. 2018. Epigenetic tools (The Writers, The Readers and The Erasers) and their implications in cancer therapy. *Eur J Pharmacol* **837**: 8–24.
Blackford AN, Jackson SP. 2017. ATM, ATR, and DNA-PK: The Trinity at the Heart of the DNA Damage Response. *Mol Cell* **66**: 801–817.
Bogliolo M, Surrallés J. 2015. Fanconi anemia: a model disease for studies on human genetics and advanced therapeutics. *Curr Opin Genet Dev* **33**: 32–40.
Boisvert RA, Howlett NG. 2014. The Fanconi anemia ID2 complex: Dueling saxes at the crossroads. *Cell Cycle* **13**: 2999–3015.
Bouché N, Scharlat A, Snedden W, Bouchez D, Fromm H. 2002. A Novel Family of Calmodulin-binding Transcription Activators in Multicellular Organisms. *Journal of Biological Chemistry* **277**: 21851–21861. https://linkinghub.elsevier.com/retrieve/pii/S002192582070445X.
Bouly J-P, Schleicher E, Dionisio-Sese M, Vandenbussche F, Van Der Straeten D, Bakrim N, Meier S, Batschauer A, Galland P, Bittl R, et al. 2007. Cryptochrome Blue Light Photoreceptors Are Activated through Interconversion of Flavin Redox States. *Journal of Biological Chemistry* **282**: 9383–9391.
Bourbousse C, Barneche F, Laloi C. 2020. Plant Chromatin Catches the Sun. *Front Plant Sci* **10**. https://www.frontiersin.org/article/10.3389/fpls.2019.01728/full.
Bourbousse C, Mestiri I, Zabulon G, Bourge M, Formiggini F, Koini MA, Brown SC, Fransz P, Bowler C, Barneche F. 2015. Light signaling controls nuclear architecture reorganization during seedling establishment. *Proceedings of the National Academy of Sciences* **112**.
Bourbousse C, Vegesna N, Law JA. 2018. SOG1 activator and MYB3R repressors regulate a complex DNA damage network in *Arabidopsis*. *Proceedings of the National Academy of Sciences* **115**: E12453–E12462. https://pnas.org/doi/full/10.1073/pnas.1810582115.
Bowman GD, McKnight JN. 2017. Sequence-specific targeting of chromatin remodelers organizes precisely positioned nucleosomes throughout the genome. *BioEssays* **39**: e201600183.

Brinkmann K, Schell M, Hoppe T, Kashkar H. 2015. Regulation of the DNA damage response by ubiquitin conjugation. *Front Genet* **6**. http://journal.frontiersin.org/Article/10.3389/fgene.2015.00098/abstract.

Brocken DJW, Tark-Dame M, Dame RT. 2018. dCas9: A Versatile Tool for Epigenome Editing. *Curr Issues Mol Biol* 15–32.

Brooks CL, Gu W. 2011. p53 regulation by ubiquitin. *FEBS Lett* **585**: 2803–2809. http://doi.wiley.com/10.1016/j.febslet.2011.05.022.

Brown EJ, Baltimore D. 2000. *ATR* disruption leads to chromosomal fragmentation and early embryonic lethality. *Genes Dev* **14**: 397–402.

Brownell JE, Zhou J, Ranalli T, Kobayashi R, Edmondson DG, Roth SY, Allis CD. 1996. Tetrahymena Histone Acetyltransferase A: A Homolog to Yeast Gcn5p Linking Histone Acetylation to Gene Activation. *Cell* **84**: 843–851.

Burdge GC, Hanson MA, Slater-Jefferies JL, Lillycrop KA. 2007. Epigenetic regulation of transcription: a mechanism for inducing variations in phenotype (fetal programming) by differences in nutrition during early life? *British Journal of Nutrition* **97**: 1036–1046.

Burma S, Chen BP, Murphy M, Kurimasa A, Chen DJ. 2001. ATM Phosphorylates Histone H2AX in Response to DNA Double-strand Breaks. *Journal of Biological Chemistry* **276**: 42462–42467.

Busino L, Bassermann F, Maiolica A, Lee C, Nolan PM, Godinho SIH, Draetta GF, Pagano M. 2007. SCF ^{Fbxl3} Controls the Oscillation of the Circadian Clock by Directing the Degradation of Cryptochrome Proteins. *Science (1979)* **316**: 900–904.

Cano-Rodriguez D, Gjaltema RAF, Jilderda LJ, Jellema P, Dokter-Fokkens J, Ruiters MHJ, Rots MG. 2016. Writing of H3K4Me3 overcomes epigenetic silencing in a sustained but context-dependent manner. *Nat Commun* **7**: 12284.

Cao J, Yan Q. 2012. Histone Ubiquitination and Deubiquitination in Transcription, DNA Damage Response, and Cancer. *Front Oncol* **2**.

Cao X, Xu P, Liu Y, Yang G, Liu M, Chen L, Cheng Y, Xu P, Miao L, Mao Z, et al. 2021. *Arabidopsis* cryptochrome 1 promotes stomatal development through repression of AGB1 inhibition of SPEECHLESS DNA-binding activity. *J Integr Plant Biol* **63**: 1967–1981.

Carell T, Burgdorf LT, Kundu LM, Cichon M. 2001. The mechanism of action of DNA photolyases. *Curr Opin Chem Biol* **5**: 491–498.

Cashmore AR, Jarillo JA, Wu YJ, Liu D. 1999. Cryptochromes: Blue light receptors for plants and animals. *Science (1979)* **284**: 760–765. https://www.science.org/doi/10.1126/science.284.5415.760.

Castells E, Molinier J, Benvenuto G, Bourbousse C, Zabulon G, Zalc A, Cazzaniga S, Genschik P, Barneche F, Bowler C. 2011. The conserved factor DE-ETIOLATED 1 cooperates with CUL4-DDB1 DDB2 to maintain genome integrity upon UV stress. *EMBO J* **30**: 1162–1172. http://emboj.embopress.org/cgi/doi/10.1038/emboj.2011.20.

Castells E, Molinier J, Drevensek S, Genschik P, Barneche F, Bowler C. 2010. det1-1-induced UV-C hyposensitivity through UVR3 and PHR1 photolyase gene over-expression. *The Plant Journal* **63**: 392–404. https://onlinelibrary.wiley.com/doi/10.1111/j.1365-313X.2010.04249.x.

Centore RC, Sandoval GJ, Soares LMM, Kadoch C, Chan HM. 2020. Mammalian SWI/SNF Chromatin Remodeling Complexes: Emerging Mechanisms and Therapeutic Strategies. *Trends in Genetics* **36**: 936–950.

Chang HHY, Lieber MR. 2016. Structure-Specific nuclease activities of Artemis and the Artemis: DNA-PKcs complex. *Nucleic Acids Res* **44**: 4991–4997.

Chang HHY, Pannunzio NR, Adachi N, Lieber MR. 2017. Non-homologous DNA end joining and alternative pathways to double-strand break repair. *Nat Rev Mol Cell Biol* **18**: 495–506.

Chan SH, Yu AM, McVey M. 2010. Dual Roles for DNA Polymerase Theta in Alternative End-Joining Repair of Double-Strand Breaks in Drosophila. *PLoS Genet* **6**: e1001005.

Chapman JR, Taylor MRG, Boulton SJ. 2012. Playing the End Game: DNA Double-Strand Break Repair Pathway Choice. *Mol Cell* **47**: 497–510.

Charron J-BF, He H, Elling AA, Deng XW. 2010. Dynamic Landscapes of Four Histone Modifications during Deetiolation in *Arabidopsis* . *Plant Cell* **21**: 3732–3748.
Chatterjee N, Walker GC. 2017. Mechanisms of DNA damage, repair, and mutagenesis. *Environ Mol Mutagen* **58**: 235–263. https://onlinelibrary.wiley.com/doi/10.1002/em.22087.
Chaves I, Pokorny R, Byrdin M, Hoang N, Ritz T, Brettel K, Essen LO, Van Der Horst GTJ, Batschauer A, Ahmad M. 2011. The cryptochromes: Blue light photoreceptors in plants and animals. *Annu Rev Plant Biol* **62**: 335–364. http://www.annualreviews.org/doi/10.1146/annurev-arplant-042110-103759.
Chaves I, Yagita K, Barnhoorn S, Okamura H, van der Horst GTJ, Tamanini F. 2006. Functional Evolution of the Photolyase/Cryptochrome Protein Family: Importance of the C Terminus of Mammalian CRY1 for Circadian Core Oscillator Performance. *Mol Cell Biol* **26**: 1743–1753.
Che DL, Duan L, Zhang K, Cui B. 2015. The Dual Characteristics of Light-Induced Cryptochrome 2, Homo-oligomerization and Heterodimerization, for Optogenetic Manipulation in Mammalian Cells. *ACS Synth Biol* **4**: 1124–1135. https://pubs.acs.org/doi/10.1021/acssynbio.5b00048.
Chen C-C, Feng W, Lim PX, Kass EM, Jasin M. 2018. Homology-Directed Repair and the Role of BRCA1, BRCA2, and Related Proteins in Genome Integrity and Cancer. *Annu Rev Cancer Biol* **2**: 313–336.
Chen H, Huang X, Gusmaroli G, Terzaghi W, Lau OS, Yanagawa Y, Zhang Y, Li J, Lee J-H, Zhu D, et al. 2010. Arabidopsis CULLIN4-Damaged DNA Binding Protein 1 Interacts with CONSTITUTIVELY PHOTOMORPHOGENIC1-SUPPRESSOR OF PHYA Complexes to Regulate Photomorphogenesis and Flowering Time. *Plant Cell* **22**: 108–123. https://academic.oup.com/plcell/article/22/1/108/6094855.
Chen H, Shen Y, Tang X, Yu L, Wang J, Guo L, Zhang Y, Zhang H, Feng S, Strickland E, et al. 2006. *Arabidopsis* CULLIN4 Forms an E3 Ubiquitin Ligase with RBX1 and the CDD Complex in Mediating Light Control of Development. *Plant Cell* **18**: 1991–2004.
Chen K, Chen Z, Wu D, Zhang L, Lin X, Su J, Rodriguez B, Xi Y, Xia Z, Chen X, et al. 2015. Broad H3K4me3 is associated with increased transcription elongation and enhancer activity at tumor-suppressor genes. *Nat Genet* **47**: 1149–1157.
Chen X, Wei M, Liu X, Song S, Wang L, Yang X, Song Y. 2019. Construction and validation of the CRISPR/dCas9-EZH2 system for targeted H3K27Me3 modification. *Biochem Biophys Res Commun* **511**: 246–252.
Chen Y, Hu X, Liu S, Su T, Huang H, Ren H, Gao Z, Wang X, Lin D, Wohlschlegel JA, et al. 2021. Regulation of Arabidopsis photoreceptor CRY2 by two distinct E3 ubiquitin ligases. *Nat Commun* **12**: 2155. http://www.nature.com/articles/s41467-021-22410-x.
Choi HH, Zou S, Wu J, Wang H, Phan L, Li K, Zhang P, Chen D, Liu Q, Qin B, et al. 2020. EGF Relays Signals to COP1 and Facilitates FOXO4 Degradation to Promote Tumorigenesis. *Advanced Science* **7**: 2000681.
Chory J. 2010. Light signal transduction: an infinite spectrum of possibilities. *The Plant Journal* **61**: 982–991.
Clapier CR, Cairns BR. 2012. Regulation of ISWI involves inhibitory modules antagonized by nucleosomal epitopes. *Nature* **492**: 280–284.
Clapier CR, Cairns BR. 2009. The Biology of Chromatin Remodeling Complexes. *Annu Rev Biochem* **78**: 273–304.
Clapier CR, Iwasa J, Cairns BR, Peterson CL. 2017. Mechanisms of action and regulation of ATP-dependent chromatin-remodelling complexes. *Nat Rev Mol Cell Biol* **18**: 407–422.
Clouaire T, Webb S, Skene P, Illingworth R, Kerr A, Andrews R, Lee J-H, Skalnik D, Bird A. 2012. Cfp1 integrates both CpG content and gene activity for accurate H3K4me3 deposition in embryonic stem cells. *Genes Dev* **26**: 1714–1728.
Clough SJ, Bent AF. 1998. Floral dip: a simplified method forAgrobacterium-mediated transformation ofArabidopsis thaliana. *The Plant Journal* **16**: 735–743. http://doi.wiley.com/10.1046/j.1365-313x.1998.00343.x.

Coleman KA, Greenberg RA. 2011. The BRCA1-RAP80 Complex Regulates DNA Repair Mechanism Utilization by Restricting End Resection. *Journal of Biological Chemistry* **286**: 13669–13680.
Cong L, Ran FA, Cox D, Lin S, Barretto R, Habib N, Hsu PD, Wu X, Jiang W, Marraffini LA, et al. 2013. Multiplex Genome Engineering Using CRISPR/Cas Systems. *Science (1979)* **339**: 819–823.
Corcoran ET, LeBlanc C, Huang Y-C, Arias Tsang M, Sarkiss A, Hu Y, Pedmale U V, Jacob Y. 2022. Systematic histone H4 replacement in Arabidopsis thaliana reveals a role for H4R17 in regulating flowering time. *Plant Cell* koac211. https://doi.org/10.1093/plcell/koac211.
Corona DFV, Tamkun JW. 2004. Multiple roles for ISWI in transcription, chromosome organization and DNA replication. *Biochimica et Biophysica Acta (BBA) - Gene Structure and Expression* **1677**: 113–119.
Corona DF V, Siriaco G, Armstrong JA, Snarskaya N, McClymont SA, Scott MP, Tamkun JW. 2007. ISWI Regulates Higher-Order Chromatin Structure and Histone H1 Assembly In Vivo. *PLoS Biol* **5**: e232.
Cowan AD, Ciulli A. 2022. Driving E3 Ligase Substrate Specificity for Targeted Protein Degradation: Lessons from Nature and the Laboratory. *Annu Rev Biochem* **91**: 295–319.
Cui X, Lu F, Li Y, Xue Y, Kang Y, Zhang S, Qiu Q, Cui X, Zheng S, Liu B, et al. 2013. Ubiquitin-Specific Proteases UBP12 and UBP13 Act in Circadian Clock and Photoperiodic Flowering Regulation in Arabidopsis . *Plant Physiol* **162**: 897–906. https://academic.oup.com/plphys/article/162/2/897/6110775.
Culligan KM, Robertson CE, Foreman J, Doerner P, Britt AB. 2006. ATR and ATM play both distinct and additive roles in response to ionizing radiation. *Plant Journal* **48**: 947–961. http://doi.wiley.com/10.1111/j.1365-313X.2006.02931.x.
Cummins JM, Rago C, Kohli M, Kinzler KW, Lengauer C, Vogelstein B. 2004. Disruption of HAUSP gene stabilizes p53. *Nature* **428**: 1–2.
Cutler SR, Ehrhardt DW, Griffitts JS, Somerville CR. 2000. Random GFP∶∶cDNA fusions enable visualization of subcellular structures in cells of *Arabidopsis* at a high frequency. *Proceedings of the National Academy of Sciences* **97**: 3718–3723. https://pnas.org/doi/full/10.1073/pnas.97.7.3718.
Cutter AR, Hayes JJ. 2015. A brief review of nucleosome structure. *FEBS Lett* **589**: 2914–2922.
Daley JM, Sung P. 2014. 53BP1, BRCA1, and the Choice between Recombination and End Joining at DNA Double-Strand Breaks. *Mol Cell Biol* **34**: 1380–1388.
Damulewicz M, Mazzotta GM. 2020. One Actor, Multiple Roles: The Performances of Cryptochrome in Drosophila. *Front Physiol* **11**.
Dang W, Bartholomew B. 2007. Domain Architecture of the Catalytic Subunit in the ISW2-Nucleosome Complex. *Mol Cell Biol* **27**: 8306–8317.
Danon A, Rotari VI, Gordon A, Mailhac N, Gallois P. 2004. Ultraviolet-C Overexposure Induces Programmed Cell Death in Arabidopsis, Which Is Mediated by Caspase-like Activities and Which Can Be Suppressed by Caspase Inhibitors, p35 and Defender against Apoptotic Death. *Journal of Biological Chemistry* **279**: 779–787. https://linkinghub.elsevier.com/retrieve/pii/S0021925818528738.
de Bie P, Ciechanover A. 2011. Ubiquitination of E3 ligases: self-regulation of the ubiquitin system via proteolytic and non-proteolytic mechanisms. *Cell Death Differ* **18**: 1393–1402.
De La Fuente R, Baumann C, Viveiros MM. 2011. Role of ATRX in chromatin structure and function: implications for chromosome instability and human disease. *REPRODUCTION* **142**: 221–234.
Deng XW, Matsui M, Wei N, Wagner D, Chu AM, Feldmann KA, Quail PH. 1992. COP1, an arabidopsis regulatory gene, encodes a protein with both a zinc-binding motif and a Gβ homologous domain. *Cell* **71**: 791–801. https://linkinghub.elsevier.com/retrieve/pii/009286749290555Q.

Derkacheva M, Liu S, Figueiredo DD, Gentry M, Mozgova I, Nanni P, Tang M, Mannervik M, Köhler C, Hennig L. 2016. H2A deubiquitinases UBP12/13 are part of the Arabidopsis polycomb group protein system. *Nat Plants* **2**: 16126. https://www.nature.com/articles/nplants2016126.

Deuring R, Fanti L, Armstrong JA, Sarte M, Papoulas O, Prestel M, Daubresse G, Verardo M, Moseley SL, Berloco M, et al. 2000. The ISWI Chromatin-Remodeling Protein Is Required for Gene Expression and the Maintenance of Higher Order Chromatin Structure In Vivo. *Mol Cell* **5**: 355–365.

Dharmasiri N, Dharmasiri S, Estelle M. 2005. The F-box protein TIR1 is an auxin receptor. *Nature* **435**: 441–445. http://www.nature.com/articles/nature03543.

Ding Y, Avramova Z, Fromm M. 2011. Two Distinct Roles of ARABIDOPSIS HOMOLOG OF TRITHORAX1 (ATX1) at Promoters and within Transcribed Regions of ATX1-Regulated Genes . *Plant Cell* **23**: 350–363.

Dobin A, Davis CA, Schlesinger F, Drenkow J, Zaleski C, Jha S, Batut P, Chaisson M, Gingeras TR. 2013. STAR: Ultrafast universal RNA-seq aligner. *Bioinformatics* **29**: 15–21. https://academic.oup.com/bioinformatics/article-lookup/doi/10.1093/bioinformatics/bts635.

Doil C, Mailand N, Bekker-Jensen S, Menard P, Larsen DH, Pepperkok R, Ellenberg J, Panier S, Durocher D, Bartek J, et al. 2009. RNF168 Binds and Amplifies Ubiquitin Conjugates on Damaged Chromosomes to Allow Accumulation of Repair Proteins. *Cell* **136**: 435–446. https://linkinghub.elsevier.com/retrieve/pii/S009286740900004X.

Duan R, Du W, Guo W. 2020. EZH2: a novel target for cancer treatment. *J Hematol Oncol* **13**: 104.

Dumbliauskas E, Lechner E, Jaciubek M, Berr A, Pazhouhandeh M, Alioua M, Cognat V, Brukhin V, Koncz C, Grossniklaus U, et al. 2011. The Arabidopsis CUL4-DDB1 complex interacts with MSI1 and is required to maintain *MEDEA* parental imprinting. *EMBO J* **30**: 731–743.

Duncan T, Trewick SC, Koivisto P, Bates PA, Lindahl T, Sedgwick B. 2002. Reversal of DNA alkylation damage by two human dioxygenases. *Proceedings of the National Academy of Sciences* **99**: 16660–16665.

El-Din El-Assal S, Alonso-Blanco C, Peeters AJM, Wagemaker C, Weller JL, Koornneef M. 2003. The Role of Cryptochrome 2 in Flowering in Arabidopsis. *Plant Physiol* **133**: 1504–1516. https://academic.oup.com/plphys/article/133/4/1504/6103465.

Elrouby N, Bonequi MV, Porri A, Coupland G. 2013. Identification of *Arabidopsis* SUMO-interacting proteins that regulate chromatin activity and developmental transitions. *Proceedings of the National Academy of Sciences* **110**: 19956–19961.

Emery P, So WV, Kaneko M, Hall JC, Rosbash M. 1998. CRY, a Drosophila Clock and Light-Regulated Cryptochrome, Is a Major Contributor to Circadian Rhythm Resetting and Photosensitivity. *Cell* **95**: 669–679.

Emery P, Stanewsky R, Helfrich-Förster C, Emery-Le M, Hall JC, Rosbash M. 2000. Drosophila CRY Is a Deep Brain Circadian Photoreceptor. *Neuron* **26**: 493–504.

Engeland K. 2022. Cell cycle regulation: p53-p21-RB signaling. *Cell Death Differ* **29**: 946–960.

Erdel F, Krug J, Längst G, Rippe K. 2011. Targeting chromatin remodelers: Signals and search mechanisms. *Biochimica et Biophysica Acta (BBA) - Gene Regulatory Mechanisms* **1809**: 497–508.

Erdel F, Rippe K. 2011. Chromatin remodelling in mammalian cells by ISWI-type complexes - where, when and why? *FEBS Journal* **278**: 3608–3618. https://onlinelibrary.wiley.com/doi/10.1111/j.1742-4658.2011.08282.x.

Ernst J, Vainas O, Harbison CT, Simon I, Bar-Joseph Z. 2007. Reconstructing dynamic regulatory maps. *Mol Syst Biol* **3**: 74. https://onlinelibrary.wiley.com/doi/10.1038/msb4100115.

Erpapazoglou Z, Walker O, Haguenauer-Tsapis R. 2014. Versatile Roles of K63-Linked Ubiquitin Chains in Trafficking. *Cells* **3**: 1027–1088.

Escribano-Díaz C, Orthwein A, Fradet-Turcotte A, Xing M, Young JTF, Tkáč J, Cook MA, Rosebrock AP, Munro M, Canny MD, et al. 2013. A Cell Cycle-Dependent Regulatory Circuit

Composed of 53BP1-RIF1 and BRCA1-CtIP Controls DNA Repair Pathway Choice. *Mol Cell* **49**: 872–883.
Estavoyer B, Messmer C, Echbicheb M, Rudd CE, Milot E, Affar EB. 2022. Mechanisms orchestrating the enzymatic activity and cellular functions of deubiquitinases. *Journal of Biological Chemistry* **298**: 102198.
Euskirchen G, Auerbach RK, Snyder M. 2012. SWI/SNF Chromatin-remodeling Factors: Multiscale Analyses and Diverse Functions. *Journal of Biological Chemistry* **287**: 30897–30905.
Eustermann S, Schall K, Kostrewa D, Lakomek K, Strauss M, Moldt M, Hopfner K-P. 2018. Structural basis for ATP-dependent chromatin remodelling by the INO80 complex. *Nature* **556**: 386–390.
Exner V, Alexandre C, Rosenfeldt G, Alfarano P, Nater M, Caflisch A, Gruissem W, Batschauer A, Hennig L. 2010. A Gain-of-Function Mutation of Arabidopsis CRYPTOCHROME1 Promotes Flowering. *Plant Physiol* **154**: 1633–1645.
Faivre L, Schubert D. 2023. Facilitating transcriptional transitions: an overview of chromatin bivalency in plants ed. D. Gibbs. *J Exp Bot* **74**: 1770–1783. https://academic.oup.com/jxb/article/74/6/1770/6992876.
Fan H, Lu J, Guo Y, Li D, Zhang Z-M, Tsai Y-H, Pi W-C, Ahn JH, Gong W, Xiang Y, et al. 2020. BAHCC1 binds H3K27me3 via a conserved BAH module to mediate gene silencing and oncogenesis. *Nat Genet* **52**: 1384–1396.
Fedeles BI, Singh V, Delaney JC, Li D, Essigmann JM. 2015. The AlkB Family of Fe(II)/α-Ketoglutarate-dependent Dioxygenases: Repairing Nucleic Acid Alkylation Damage and Beyond. *Journal of Biological Chemistry* **290**: 20734–20742.
Fernandez DC, Fogerson PM, Lazzerini Ospri L, Thomsen MB, Layne RM, Severin D, Zhan J, Singer JH, Kirkwood A, Zhao H, et al. 2018. Light Affects Mood and Learning through Distinct Retina-Brain Pathways. *Cell* **175**: 71-84.e18.
Fiorucci A-S, Bourbousse C, Concia L, Rougée M, Deton-Cabanillas A-F, Zabulon G, Layat E, Latrasse D, Kim SK, Chaumont N, et al. 2019. Arabidopsis S2Lb links AtCOMPASS-like and SDG2 activity in H3K4me3 independently from histone H2B monoubiquitination. *Genome Biol* **20**: 100.
Flanagan JF, Mi L-Z, Chruszcz M, Cymborowski M, Clines KL, Kim Y, Minor W, Rastinejad F, Khorasanizadeh S. 2005. Double chromodomains cooperate to recognize the methylated histone H3 tail. *Nature* **438**: 1181–1185.
Flick K, Ouni I, Wohlschlegel JA, Capati C, McDonald WH, Yates JR, Kaiser P. 2004. Proteolysis-independent regulation of the transcription factor Met4 by a single Lys 48-linked ubiquitin chain. *Nat Cell Biol* **6**: 634–641.
Fousteri M, Mullenders LH. 2008. Transcription-coupled nucleotide excision repair in mammalian cells: molecular mechanisms and biological effects. *Cell Res* **18**: 73–84.
Fradet-Turcotte A, Canny MD, Escribano-Díaz C, Orthwein A, Leung CCY, Huang H, Landry M-C, Kitevski-LeBlanc J, Noordermeer SM, Sicheri F, et al. 2013. 53BP1 is a reader of the DNA-damage-induced H2A Lys 15 ubiquitin mark. *Nature* **499**: 50–54.
French ME, Koehler CF, Hunter T. 2021. Emerging functions of branched ubiquitin chains. *Cell Discov* **7**: 6.
Fukushima HS, Takeda H, Nakamura R. 2019. Targeted in vivo epigenome editing of H3K27me3. *Epigenetics Chromatin* **12**: 17.
Gao L, Liu Q, Zhong M, Zeng N, Deng W, Li Y, Wang D, Liu S, Wang Q. 2022. Blue light-induced phosphorylation of *Arabidopsis* cryptochrome 1 is essential for its photosensitivity. *J Integr Plant Biol* **64**: 1724–1738.
Garaycoechea JI, Crossan GP, Langevin F, Daly M, Arends MJ, Patel KJ. 2012. Genotoxic consequences of endogenous aldehydes on mouse haematopoietic stem cell function. *Nature* **489**: 571–575.
Gartner A, Engebrecht J. 2022. DNA repair, recombination, and damage signaling. *Genetics* **220**.

George AJ, Hoffiz YC, Charles AJ, Zhu Y, Mabb AM. 2018. A Comprehensive Atlas of E3 Ubiquitin Ligase Mutations in Neurological Disorders. *Front Genet* **9**.
Gerhold CB, Gasser SM. 2014. INO80 and SWR complexes: relating structure to function in chromatin remodeling. *Trends Cell Biol* **24**: 619–631.
Ghosh S, Saha T. 2012. Central Role of Ubiquitination in Genome Maintenance: DNA Replication and Damage Repair. *ISRN Mol Biol* **2012**: 1–9.
Gibney ER, Nolan CM. 2010. Epigenetics and gene expression. *Heredity (Edinb)* **105**: 4–13.
Gill SS, Anjum NA, Gill R, Jha M, Tuteja N. 2015. DNA Damage and Repair in Plants under Ultraviolet and Ionizing Radiations. *The Scientific World Journal* **2015**: 1–11. http://www.hindawi.com/journals/tswj/2015/250158/.
Godinho SIH, Maywood ES, Shaw L, Tucci V, Barnard AR, Busino L, Pagano M, Kendall R, Quwailid MM, Romero MR, et al. 2007. The After-Hours Mutant Reveals a Role for Fbxl3 in Determining Mammalian Circadian Period. *Science (1979)* **316**: 897–900.
Goldmark JP, Fazzio TG, Estep PW, Church GM, Tsukiyama T. 2000. The Isw2 Chromatin Remodeling Complex Represses Early Meiotic Genes upon Recruitment by Ume6p. *Cell* **103**: 423–433.
Graf N, Ang WH, Zhu G, Myint M, Lippard SJ. 2011. Role of Endonucleases XPF and XPG in Nucleotide Excision Repair of Platinated DNA and Cisplatin/Oxaliplatin Cytotoxicity. *ChemBioChem* **12**: 1115–1123.
Grawunder U, Wilm M, Wu X, Kulesza P, Wilson TE, Mann M, Lieber MR. 1997. Activity of DNA ligase IV stimulated by complex formation with XRCC4 protein in mammalian cells. *Nature* **388**: 492–495.
Greenberg RA, Sobhian B, Pathania S, Cantor SB, Nakatani Y, Livingston DM. 2006. Multifactorial contributions to an acute DNA damage response by BRCA1/BARD1-containing complexes. *Genes Dev* **20**: 34–46.
Grilley M, Welsh KM, Su SS, Modrich P. 1989. Isolation and Characterization of the Escherichia coli mutL Gene Product. *Journal of Biological Chemistry* **264**: 1000–1004.
Groelly FJ, Fawkes M, Dagg RA, Blackford AN, Tarsounas M. 2022. Targeting DNA damage response pathways in cancer. *Nat Rev Cancer*. https://www.nature.com/articles/s41568-022-00535-5.
Gross S, Rahal R, Stransky N, Lengauer C, Hoeflich KP. 2015. Targeting cancer with kinase inhibitors. *Journal of Clinical Investigation* **125**: 1780–1789. http://www.jci.org/articles/view/76094.
Grunstein M. 1997. Histone acetylation in chromatin structure and transcription. *Nature* **389**: 349–352.
Guo H, Yang H, Mockler TC, Lin C. 1998. Regulation of flowering time by Arabidopsis photoreceptors. *Science (1979)* **279**: 1360–1363. https://www.sciencemag.org/lookup/doi/10.1126/science.279.5355.1360.
Guo L, Zhou J, Elling AA, Charron J-BF, Deng XW. 2008. Histone Modifications and Expression of Light-Regulated Genes in Arabidopsis Are Cooperatively Influenced by Changing Light Conditions . *Plant Physiol* **147**: 2070–2083.
Gupta A, Hunt CR, Chakraborty S, Pandita RK, Yordy J, Ramnarain DB, Horikoshi N, Pandita TK. 2014. Role of 53BP1 in the Regulation of DNA Double-Strand Break Repair Pathway Choice. *Radiat Res* **181**: 1–8.
Haahr P, Hoffmann S, Tollenaere MAX, Ho T, Toledo LI, Mann M, Bekker-Jensen S, Räschle M, Mailand N. 2016. Activation of the ATR kinase by the RPA-binding protein ETAA1. *Nat Cell Biol* **18**: 1196–1207.
Hafner A, Bulyk ML, Jambhekar A, Lahav G. 2019. The multiple mechanisms that regulate p53 activity and cell fate. *Nat Rev Mol Cell Biol* **20**: 199–210. http://www.nature.com/articles/s41580-019-0110-x.

Han X, Huang X, Deng XW. 2020. The Photomorphogenic Central Repressor COP1: Conservation and Functional Diversification during Evolution. *Plant Commun* **1**: 100044.
Hargreaves DC, Crabtree GR. 2011. ATP-dependent chromatin remodeling: genetics, genomics and mechanisms. *Cell Res* **21**: 396–420.
Harris JL, Khanna KK. 2011. BRCA1 A-Complex fine tunes repair functions of BRCA1. *Aging* **3**: 461–463.
Hauk G, McKnight JN, Nodelman IM, Bowman GD. 2010. The Chromodomains of the Chd1 Chromatin Remodeler Regulate DNA Access to the ATPase Motor. *Mol Cell* **39**: 711–723.
Heimbucher T, Hunter T. 2015. The *C. elegans* Ortholog of USP7 controls DAF-16 stability in Insulin/IGF-1-like signaling. *Worm* **4**: e1103429.
Heinz S, Benner C, Spann N, Bertolino E, Lin YC, Laslo P, Cheng JX, Murre C, Singh H, Glass CK. 2010. Simple Combinations of Lineage-Determining Transcription Factors Prime cis-Regulatory Elements Required for Macrophage and B Cell Identities. *Mol Cell* **38**: 576–589. https://linkinghub.elsevier.com/retrieve/pii/S1097276510003667.
He J, Zhu Q, Wani G, Sharma N, Han C, Qian J, Pentz K, Wang Q, Wani AA. 2014. Ubiquitin-specific Protease 7 Regulates Nucleotide Excision Repair through Deubiquitinating XPC Protein and Preventing XPC Protein from Undergoing Ultraviolet Light-induced and VCP/p97 Protein-regulated Proteolysis. *Journal of Biological Chemistry* **289**: 27278–27289. https://linkinghub.elsevier.com/retrieve/pii/S0021925820371805.
Helliwell CA, Wood CC, Robertson M, James Peacock W, Dennis ES. 2006. The Arabidopsis FLC protein interacts directly *in vivo* with *SOC1* and *FT* chromatin and is part of a high-molecular-weight protein complex. *The Plant Journal* **46**: 183–192.
Hergeth SP, Schneider R. 2015. The H1 linker histones: multifunctional proteins beyond the nucleosomal core particle. *EMBO Rep* **16**: 1439–1453.
Herhaus L, Perez-Oliva AB, Cozza G, Gourlay R, Weidlich S, Campbell DG, Pinna LA, Sapkota GP. 2015. Casein kinase 2 (CK2) phosphorylates the deubiquitylase OTUB1 at Ser ^{16} to trigger its nuclear localization. *Sci Signal* **8**.
He Y, Yu Y, Wang X, Qin Y, Su C, Wang L. 2022. Aschoff's rule on circadian rhythms orchestrated by blue light sensor CRY2 and clock component PRR9. *Nat Commun* **13**: 5869.
Hicke L. 2001. Protein regulation by monoubiquitin. *Nat Rev Mol Cell Biol* **2**: 195–201.
Hirano A, Nakagawa T, Yoshitane H, Oyama M, Kozuka-Hata H, Lanjakornsiripan D, Fukada Y. 2016. USP7 and TDP-43: Pleiotropic Regulation of Cryptochrome Protein Stability Paces the Oscillation of the Mammalian Circadian Clock. ed. M.L. Block. *PLoS One* **11**: e0154263. http://www.ncbi.nlm.nih.gov/pubmed/27123980.
Hirota T, Lee JW, St. John PC, Sawa M, Iwaisako K, Noguchi T, Pongsawakul PY, Sonntag T, Welsh DK, Brenner DA, et al. 2012. Identification of Small Molecule Activators of Cryptochrome. *Science (1979)* **337**: 1094–1097.
Hjerpe R, Aillet F, Lopitz-Otsoa F, Lang V, England P, Rodriguez MS. 2009. Efficient protection and isolation of ubiquitylated proteins using tandem ubiquitin-binding entities. *EMBO Rep* **10**: 1250–1258.
Hofstatter PG, Lahr DJG. 2021. Complex Evolution of the Mismatch Repair System in Eukaryotes is Illuminated by Novel Archaeal Genomes. *J Mol Evol* **89**: 12–18.
Holtkotte X, Ponnu J, Ahmad M, Hoecker U. 2017. The blue light-induced interaction of cryptochrome 1 with COP1 requires SPA proteins during Arabidopsis light signaling ed. C. Fankhauser. *PLoS Genet* **13**: e1007044. https://dx.plos.org/10.1371/journal.pgen.1007044.
Horvath BM, Kourova H, Nagy S, Nemeth E, Magyar Z, Papdi C, Ahmad Z, Sanchez-Perez GF, Perilli S, Blilou I, et al. 2017. Arabidopsis RETINOBLASTOMA RELATED directly regulates DNA damage responses through functions beyond cell cycle control. *EMBO J* **36**: 1261–1278. https://onlinelibrary.wiley.com/doi/10.15252/embj.201694561.
Howe FS, Fischl H, Murray SC, Mellor J. 2017. Is H3K4me3 instructive for transcription activation? *BioEssays* **39**: e201600095.

Hsu DS, Zhao X, Zhao S, Kazantsev A, Wang R-P, Todo T, Wei Y-F, Sancar A. 1996. Putative Human Blue-Light Photoreceptors hCRY1 and hCRY2 Are Flavoproteins. *Biochemistry* **35**: 13871–13877. https://pubs.acs.org/doi/10.1021/bi962209o.

Huang J, Zhao X, Chory J. 2019. The Arabidopsis Transcriptome Responds Specifically and Dynamically to High Light Stress. *Cell Rep* **29**: 4186-4199.e3.

Huang R, Zhou P-K. 2021. DNA damage repair: historical perspectives, mechanistic pathways and clinical translation for targeted cancer therapy. *Signal Transduct Target Ther* **6**: 254. https://www.nature.com/articles/s41392-021-00648-7.

Huang Y, Leung JWC, Lowery M, Matsushita N, Wang Y, Shen X, Huong D, Takata M, Chen J, Li L. 2014. Modularized Functions of the Fanconi Anemia Core Complex. *Cell Rep* **7**: 1849–1857.

Huen MSY, Grant R, Manke I, Minn K, Yu X, Yaffe MB, Chen J. 2007. RNF8 Transduces the DNA-Damage Signal via Histone Ubiquitylation and Checkpoint Protein Assembly. *Cell* **131**: 901–914.

Hu Y, Rosado D, Lindbäck LN, Micko J, Pedmale U V. 2023. Cryptochromes and UBP12/13 deubiquitinases antagonistically regulate DNA damage response in Arabidopsis. *bioRxiv* 2023.01.15.524001. http://biorxiv.org/content/early/2023/01/16/2023.01.15.524001.abstract.

International Light Technologies. 2022. UVC LED Module Array Data Sheet. https://www.intl-lighttech.com/sites/default/files/downloads/e275-80-module_uvc_led_array_data_sheet.pdf.

Iqbal Z, Shariq Iqbal M, Singh SP, Buaboocha T. 2020. Ca2+/Calmodulin Complex Triggers CAMTA Transcriptional Machinery Under Stress in Plants: Signaling Cascade and Molecular Regulation. *Front Plant Sci* **11**. https://www.frontiersin.org/articles/10.3389/fpls.2020.598327/full.

Iyer RR, Pluciennik A, Burdett V, Modrich PL. 2006. DNA Mismatch Repair: Functions and Mechanisms. *Chem Rev* **106**: 302–323.

Jackson SP, Bartek J. 2009. The DNA-damage response in human biology and disease. *Nature* **461**: 1071–1078. https://www.nature.com/articles/nature08467.

Jang I-C, Yang J-Y, Seo HS, Chua N-H. 2005. HFR1 is targeted by COP1 E3 ligase for post-translational proteolysis during phytochrome A signaling. *Genes Dev* **19**: 593–602.

Jeggo PA, Pearl LH, Carr AM. 2016. DNA repair, genome stability and cancer: a historical perspective. *Nat Rev Cancer* **16**: 35–42.

Jeong JS, Jung C, Seo JS, Kim J-K, Chua N-H. 2017. The Deubiquitinating Enzymes UBP12 and UBP13 Positively Regulate MYC2 Levels in Jasmonate Responses. *Plant Cell* **29**: 1406–1424. https://academic.oup.com/plcell/article/29/6/1406-1424/6099366.

Jiang C-Z, Yee J, Mitchell DL, Britt AB. 1997. Photorepair mutants of Arabidopsis. *Proceedings of the National Academy of Sciences* **94**: 7441–7445. https://pnas.org/doi/full/10.1073/pnas.94.14.7441.

Jing Y, Zhang D, Wang X, Tang W, Wang W, Huai J, Xu G, Chen D, Li Y, Lin R. 2013. Arabidopsis Chromatin Remodeling Factor PICKLE Interacts with Transcription Factor HY5 to Regulate Hypocotyl Cell Elongation. *Plant Cell* **25**: 242–256. https://academic.oup.com/plcell/article/25/1/242/6097817.

Jin H. 2000. Transcriptional repression by AtMYB4 controls production of UV-protecting sunscreens in Arabidopsis. *EMBO J* **19**: 6150–6161. http://emboj.embopress.org/cgi/doi/10.1093/emboj/19.22.6150.

Jiricny J. 2006. The multifaceted mismatch-repair system. *Nat Rev Mol Cell Biol* **7**: 335–346.

Johann to Berens P, Schivre G, Theune M, Peter J, Sall SO, Mutterer J, Barneche F, Bourbousse C, Molinier J. 2022. Advanced Image Analysis Methods for Automated Segmentation of Subnuclear Chromatin Domains. *Epigenomes* **6**: 34.

Jones SN, Roe AE, Donehower LA, Bradley A. 1995. Rescue of embryonic lethality in Mdm2-deficient mice by absence of p53. *Nature* **378**: 206–208. http://www.nature.com/articles/378206a0.

Judd J, Duarte FM, Lis JT. 2021. Pioneer-like factor GAF cooperates with PBAP (SWI/SNF) and NURF (ISWI) to regulate transcription. *Genes Dev* **35**: 147–156.
Kang C-Y, Lian H-L, Wang F-F, Huang J-R, Yang H-Q. 2009. Cryptochromes, Phytochromes, and COP1 Regulate Light-Controlled Stomatal Development in *Arabidopsis* . *Plant Cell* **21**: 2624–2641.
Kang T-H, Leem S-H. 2014. Modulation of ATR-mediated DNA damage checkpoint response by cryptochrome 1. *Nucleic Acids Res* **42**: 4427–4434. https://academic.oup.com/nar/article-lookup/doi/10.1093/nar/gku094.
Kannan K, Nelson ADL, Shippen DE. 2008. Dyskerin Is a Component of the Arabidopsis Telomerase RNP Required for Telomere Maintenance. *Mol Cell Biol* **28**: 2332–2341. https://journals.asm.org/doi/10.1128/MCB.01490-07.
Karanja KK, Cox SW, Duxin JP, Stewart SA, Campbell JL. 2012. DNA2 and EXO1 in replication-coupled, homology-directed repair and in the interplay between HDR and the FA/BRCA network. *Cell Cycle* **11**: 3983–3996.
Karimi M, Bleys A, Vanderhaeghen R, Hilson P. 2007. Building Blocks for Plant Gene Assembly. *Plant Physiol* **145**: 1183–1191. https://academic.oup.com/plphys/article/145/4/1183/6107194.
Karl LA, Peritore M, Galanti L, Pfander B. 2022. DNA Double Strand Break Repair and Its Control by Nucleosome Remodeling. *Front Genet* **12**.
Kato K, Nakajima K, Ui A, Muto-Terao Y, Ogiwara H, Nakada S. 2014. Fine-Tuning of DNA Damage-Dependent Ubiquitination by OTUB2 Supports the DNA Repair Pathway Choice. *Mol Cell* **53**: 617–630.
Kee Y, Huang TT. 2016. Role of Deubiquitinating Enzymes in DNA Repair. *Mol Cell Biol* **36**: 524–544.
Kehle J. 1998. dMi-2, a Hunchback-Interacting Protein That Functions in Polycomb Repression. *Science (1979)* **282**: 1897–1900.
Kemp MG, Akan Z, Yilmaz S, Grillo M, Smith-Roe SL, Kang T-H, Cordeiro-Stone M, Kaufmann WK, Abraham RT, Sancar A, et al. 2010. Tipin-Replication Protein A Interaction Mediates Chk1 Phosphorylation by ATR in Response to Genotoxic Stress. *Journal of Biological Chemistry* **285**: 16562–16571. https://linkinghub.elsevier.com/retrieve/pii/S0021925819355814.
Kenzelmann Broz D, Spano Mello S, Bieging KT, Jiang D, Dusek RL, Brady CA, Sidow A, Attardi LD. 2013. Global genomic profiling reveals an extensive p53-regulated autophagy program contributing to key p53 responses. *Genes Dev* **27**: 1016–1031.
Kim H, Chen J, Yu X. 2007. Ubiquitin-Binding Protein RAP80 Mediates BRCA1-Dependent DNA Damage Response. *Science (1979)* **316**: 1202–1205.
Kim Y, Gilmour SJ, Chao L, Park S, Thomashow MF. 2020. Arabidopsis CAMTA Transcription Factors Regulate Pipecolic Acid Biosynthesis and Priming of Immunity Genes. *Mol Plant* **13**: 157–168. https://linkinghub.elsevier.com/retrieve/pii/S167420521930365X.
Kinoshita A, Richter R. 2020. Genetic and molecular basis of floral induction in Arabidopsis thaliana. *J Exp Bot* **71**: 2490–2504.
Kliebenstein DJ, Lim JE, Landry LG, Last RL. 2002. Arabidopsis UVR8 regulates ultraviolet-B signal transduction and tolerance and contains sequence similarity to human Regulator of Chromatin Condensation 1. *Plant Physiol* **130**: 234–243. https://academic.oup.com/plphys/article/130/1/234/6110373.
Kobor MS, Venkatasubrahmanyam S, Meneghini MD, Gin JW, Jennings JL, Link AJ, Madhani HD, Rine J. 2004. A protein complex containing the conserved Swi2/Snf2-related ATPase Swr1p deposits histone variant H2A.Z into euchromatin ed. Peter Becker. *PLoS Biol* **2**: e131. https://dx.plos.org/10.1371/journal.pbio.0020131.
Koh K, Zheng X, Sehgal A. 2006. JETLAG Resets the *Drosophila* Circadian Clock by Promoting Light-Induced Degradation of TIMELESS. *Science (1979)* **312**: 1809–1812.

Koike N, Yoo S-H, Huang H-C, Kumar V, Lee C, Kim T-K, Takahashi JS. 2012. Transcriptional Architecture and Chromatin Landscape of the Core Circadian Clock in Mammals. *Science (1979)* **338**: 349–354.
Kokic G, Chernev A, Tegunov D, Dienemann C, Urlaub H, Cramer P. 2019. Structural basis of TFIIH activation for nucleotide excision repair. *Nat Commun* **10**: 2885.
Kolas NK, Chapman JR, Nakada S, Ylanko J, Chahwan R, Sweeney FD, Panier S, Mendez M, Wildenhain J, Thomson TM, et al. 2007. Orchestration of the DNA-Damage Response by the RNF8 Ubiquitin Ligase. *Science (1979)* **318**: 1637–1640.
Komander D, Clague MJ, Urbé S. 2009. Breaking the chains: structure and function of the deubiquitinases. *Nat Rev Mol Cell Biol* **10**: 550–563.
Kozuka T, Oka Y, Kohzuma K, Kusaba M. 2023. Cryptochromes suppress leaf senescence in response to blue light in Arabidopsis. *Plant Physiol* **191**: 2506–2518.
Krais JJ, Wang Y, Patel P, Basu J, Bernhardy AJ, Johnson N. 2021. RNF168-mediated localization of BARD1 recruits the BRCA1-PALB2 complex to DNA damage. *Nat Commun* **12**: 5016. https://www.nature.com/articles/s41467-021-25346-4.
Kralemann LEM, Liu S, Trejo-Arellano MS, Muñoz-Viana R, Köhler C, Hennig L. 2020. Removal of H2Aub1 by ubiquitin-specific proteases 12 and 13 is required for stable Polycomb-mediated gene repression in Arabidopsis. *Genome Biol* **21**: 144. https://genomebiology.biomedcentral.com/articles/10.1186/s13059-020-02062-8.
Krogan NJ, Dover J, Wood A, Schneider J, Heidt J, Boateng MA, Dean K, Ryan OW, Golshani A, Johnston M, et al. 2003. The Paf1 Complex Is Required for Histone H3 Methylation by COMPASS and Dot1p: Linking Transcriptional Elongation to Histone Methylation. *Mol Cell* **11**: 721–729.
Krokan HE, Bjoras M. 2013. Base Excision Repair. *Cold Spring Harb Perspect Biol* **5**: a012583–a012583.
Kushwaha R, Singh A, Chattopadhyay S. 2008. Calmodulin7 Plays an Important Role as Transcriptional Regulator in *Arabidopsis* Seedling Development. *Plant Cell* **20**: 1747–1759.
Lai KP, Chen J, Tse WKF. 2020. Role of Deubiquitinases in Human Cancers: Potential Targeted Therapy. *Int J Mol Sci* **21**: 2548. https://www.mdpi.com/1422-0067/21/7/2548.
Lamia KA, Papp SJ, Yu RT, Barish GD, Uhlenhaut NH, Jonker JW, Downes M, Evans RM. 2011. Cryptochromes mediate rhythmic repression of the glucocorticoid receptor. *Nature* **480**: 552–556.
Lane DP. 1992. p53, guardian of the genome. *Nature* **358**: 15–16.
Lange SM, Armstrong LA, Kulathu Y. 2022. Deubiquitinases: From mechanisms to their inhibition by small molecules. *Mol Cell* **82**: 15–29.
Langmead B, Salzberg SL. 2012. Fast gapped-read alignment with Bowtie 2. *Nat Methods* **9**: 357–359.
Lauberth SM, Nakayama T, Wu X, Ferris AL, Tang Z, Hughes SH, Roeder RG. 2013. H3K4me3 Interactions with TAF3 Regulate Preinitiation Complex Assembly and Selective Gene Activation. *Cell* **152**: 1021–1036.
Lau K, Podolec R, Chappuis R, Ulm R, Hothorn M. 2019. Plant photoreceptors and their signaling components compete for COP 1 binding via VP peptide motifs . *EMBO J* **38**.
Laurent BC, Yang X, Carlson M. 1992. An Essential *Saccharomyces cerevisiae* Gene Homologous to *SNF2* Encodes a Helicase-Related Protein in a New Family. *Mol Cell Biol* **12**: 1893–1902.
Lavin MF, Gueven N. 2006. The complexity of p53 stabilization and activation. *Cell Death Differ* **13**: 941–950.
Lecona E, Narendra V, Reinberg D. 2015. USP7 Cooperates with SCML2 To Regulate the Activity of PRC1. *Mol Cell Biol* **35**: 1157–1168.
Lee C-M, Li M-W, Feke A, Liu W, Saffer AM, Gendron JM. 2019. GIGANTEA recruits the UBP12 and UBP13 deubiquitylases to regulate accumulation of the ZTL photoreceptor complex. *Nat Commun* **10**: 3750.

Lee J, He K, Stolc V, Lee H, Figueroa P, Gao Y, Tongprasit W, Zhao H, Lee I, Xing WD. 2007. Analysis of transcription factor HY5 genomic binding sites revealed its hierarchical role in light regulation of development. *Plant Cell* **19**: 731–749. https://academic.oup.com/plcell/article/19/3/731/6091800.

Lee J-H, Paull TT. 2005. ATM Activation by DNA Double-Strand Breaks Through the Mre11-Rad50-Nbs1 Complex. *Science (1979)* **308**: 551–554.

Lee J-H, Skalnik DG. 2008. Wdr82 Is a C-Terminal Domain-Binding Protein That Recruits the Setd1A Histone H3-Lys4 Methyltransferase Complex to Transcription Start Sites of Transcribed Human Genes. *Mol Cell Biol* **28**: 609–618.

Lee J, Lee I. 2010. Regulation and function of SOC1, a flowering pathway integrator. *J Exp Bot* **61**: 2247–2254. https://academic.oup.com/jxb/article-lookup/doi/10.1093/jxb/erq098.

Lee J, Zhou P. 2007. DCAFs, the Missing Link of the CUL4-DDB1 Ubiquitin Ligase. *Mol Cell* **26**: 775–780. https://linkinghub.elsevier.com/retrieve/pii/S1097276507003619.

Le J, Perez E, Nemzow L, Gong F. 2019. Role of deubiquitinases in DNA damage response. *DNA Repair (Amst)* **76**: 89–98. https://linkinghub.elsevier.com/retrieve/pii/S1568786418303082.

Levendosky RF, Bowman GD. 2019. Asymmetry between the two acidic patches dictates the direction of nucleosome sliding by the ISWI chromatin remodeler. *Elife* **8**.

Levy S, Somasundaram L, Raj IX, Ic-Mex D, Phal A, Schmidt S, Ng WI, Mar D, Decarreau J, Moss N, et al. 2022. dCas9 fusion to computer-designed PRC2 inhibitor reveals functional TATA box in distal promoter region. *Cell Rep* **38**: 110457.

Lian HL, He SB, Zhang YC, Zhu DM, Zhang JY, Jia KP, Sun SX, Li L, Yang HQ. 2011. Blue-light-dependent interaction of cryptochrome 1 with SPA1 defines a dynamic signaling mechanism. *Genes Dev* **25**: 1023–1028. http://genesdev.cshlp.org/lookup/doi/10.1101/gad.2025111.

Lieleg C, Ketterer P, Nuebler J, Ludwigsen J, Gerland U, Dietz H, Mueller-Planitz F, Korber P. 2015. Nucleosome Spacing Generated by ISWI and CHD1 Remodelers Is Constant Regardless of Nucleosome Density. *Mol Cell Biol* **35**: 1588–1605.

Li G, Liu S, Wang J, He J, Huang H, Zhang Y, Xu L. 2014. ISWI proteins participate in the genome-wide nucleosome distribution in Arabidopsis. *The Plant Journal* **78**: 706–714. https://onlinelibrary.wiley.com/doi/10.1111/tpj.12499.

Li G-M. 2008. Mechanisms and functions of DNA mismatch repair. *Cell Res* **18**: 85–98.

Li G, Zhang J, Li J, Yang Z, Huang H, Xu L. 2012. Imitation Switch chromatin remodeling factors and their interacting RINGLET proteins act together in controlling the plant vegetative phase in Arabidopsis. *The Plant Journal* **72**: 261–270. https://onlinelibrary.wiley.com/doi/10.1111/j.1365-313X.2012.05074.x.

Li H, Handsaker B, Wysoker A, Fennell T, Ruan J, Homer N, Marth G, Abecasis G, Durbin R. 2009. The Sequence Alignment/Map format and SAMtools. *Bioinformatics* **25**: 2078–2079.

Li M, Brooks CL, Kon N, Gu W. 2004a. A Dynamic Role of HAUSP in the p53-Mdm2 Pathway. *Mol Cell* **13**: 879–886.

Li M, Chen D, Shiloh A, Luo J, Nikolaev AY, Qin J, Gu W. 2002. Deubiquitination of p53 by HAUSP is an important pathway for p53 stabilization. *Nature* **416**: 648–653. http://www.nature.com/articles/nature737.

Lin C, Robertson DE, Ahmad M, Raibekas AA, Jorns MS, Dutton PL, Cashmore AR. 1995. Association of Flavin Adenine Dinucleotide with the *Arabidopsis* Blue Light Receptor CRY1. *Science (1979)* **269**: 968–970.

Lin C, Todo T. 2005. The cryptochromes. *Genome Biol* **6**: 220.

Lin C, Yang H, Guo H, Mockler T, Chen J, Cashmore AR. 1998. Enhancement of blue-light sensitivity of Arabidopsis seedlings by a blue light receptor cryptochrome 2. *Proceedings of the National Academy of Sciences* **95**: 2686–2690. https://pnas.org/doi/full/10.1073/pnas.95.5.2686.

Lindback LN, Hu Y, Ackermann A, Artz O, Pedmale U V. 2022. UBP12 and UBP13 deubiquitinases destabilize the CRY2 blue light receptor to regulate Arabidopsis growth. *Current Biology* **32**: 1–11.

Linzer DIH, Levine AJ. 1979. Characterization of a 54K Dalton cellular SV40 tumor antigen present in SV40-transformed cells and uninfected embryonal carcinoma cells. *Cell* **17**: 43–52. https://linkinghub.elsevier.com/retrieve/pii/0092867479902939.

Li N, Zhang Y, He Y, Wang Y, Wang L. 2020. Pseudo Response Regulators Regulate Photoperiodic Hypocotyl Growth by Repressing *PIF4* / *5* Transcription. *Plant Physiol* **183**: 686–699. https://academic.oup.com/plphys/article/183/2/686-699/6116297.

Li S, Lavagnino Z, Lemacon D, Kong L, Ustione A, Ng X, Zhang Y, Wang Y, Zheng B, Piwnica-Worms H, et al. 2019. Ca2+-Stimulated AMPK-Dependent Phosphorylation of Exo1 Protects Stressed Replication Forks from Aberrant Resection. *Mol Cell* **74**: 1123-1137.e6. https://linkinghub.elsevier.com/retrieve/pii/S1097276519302734.

Liu B, Yang Z, Gomez A, Liu B, Lin C, Oka Y. 2016a. Signaling mechanisms of plant cryptochromes in Arabidopsis thaliana. *J Plant Res* **129**: 137–148.

Liu B, Zuo Z, Liu H, Liu X, Lin C. 2011. *Arabidopsis* cryptochrome 1 interacts with SPA1 to suppress COP1 activity in response to blue light. *Genes Dev* **25**: 1029–1034.

Liu H, Yu X, Li K, Klejnot J, Yang H, Lisiero D, Lin C. 2008a. Photoexcited CRY2 interacts with CIB1 to regulate transcription and floral initiation in Arabidopsis. *Science (1979)* **322**: 1535–1539. http://www.ncbi.nlm.nih.gov/pubmed/18988809.

Liu L-J, Zhang Y-C, Li Q-H, Sang Y, Mao J, Lian H-L, Wang L, Yang H-Q. 2008b. COP1-Mediated Ubiquitination of CONSTANS Is Implicated in Cryptochrome Regulation of Flowering in *Arabidopsis*. *Plant Cell* **20**: 292–306.

Liu Q, Su T, He W, Ren H, Liu S, Chen Y, Gao L, Hu X, Lu H, Cao S, et al. 2020. Photooligomerization Determines Photosensitivity and Photoreactivity of Plant Cryptochromes. *Mol Plant* **13**: 398–413. https://linkinghub.elsevier.com/retrieve/pii/S1674205220300022.

Liu Q, Wang Q, Deng W, Wang X, Piao M, Cai D, Li Y, Barshop WD, Yu X, Zhou T, et al. 2017. Molecular basis for blue light-dependent phosphorylation of Arabidopsis cryptochrome 2. *Nat Commun* **8**: 15234. https://www.nature.com/articles/ncomms15234.

Liu Q, Wang Q, Liu B, Wang W, Wang X, Park J, Yang Z, Du X, Bian M, Lin C. 2016b. The Blue Light-Dependent Polyubiquitination and Degradation of Arabidopsis Cryptochrome2 Requires Multiple E3 Ubiquitin Ligases. *Plant Cell Physiol* **57**: 2175–2186. https://academic.oup.com/pcp/article-lookup/doi/10.1093/pcp/pcw134.

Liu S, Kong D. 2021. End resection: a key step in homologous recombination and DNA double-strand break repair. *Genome Instab Dis* **2**: 39–50.

Liu S, Zhang L, Gao L, Chen Z, Bie Y, Zhao Q, Zhang S, Hu X, Liu Q, Wang X, et al. 2022. Differential photoregulation of the nuclear and cytoplasmic CRY1 in Arabidopsis. *New Phytologist* **234**: 1332–1346. https://onlinelibrary.wiley.com/doi/10.1111/nph.18007.

Liu Y, Li X, Ma D, Chen Z, Wang J, Liu H. 2018. CIB1 and CO interact to mediate CRY2-dependent regulation of flowering. *EMBO Rep* **19**: 1–10. https://www.embopress.org/doi/10.15252/embr.201845762.

Liu Y, Wang F, Zhang H, He H, Ma L, Deng XW. 2008c. Functional characterization of the Arabidopsis *ubiquitin-specific protease* gene family reveals specific role and redundancy of individual members in development. *The Plant Journal* **55**: 844–856.

Livak KJ, Schmittgen TD. 2001. Analysis of Relative Gene Expression Data Using Real-Time Quantitative PCR and the 2−ΔΔCT Method. *Methods* **25**: 402–408. https://linkinghub.elsevier.com/retrieve/pii/S1046202301912629.

Li W, Chen C, Markmann-Mulisch U, Timofejeva L, Schmelzer E, Ma H, Reiss B. 2004b. The Arabidopsis AtRAD51 gene is dispensable for vegetative development but required for meiosis. *Proceedings of the National Academy of Sciences* **101**: 10596–10601. https://pnas.org/doi/full/10.1073/pnas.0404110101.

Li W, Ye Y. 2008. Polyubiquitin chains: functions, structures, and mechanisms. *Cellular and Molecular Life Sciences* **65**: 2397–2406.

Li X, Heyer W-D. 2008. Homologous recombination in DNA repair and DNA damage tolerance. *Cell Res* **18**: 99–113.
Li Y, Gong H, Wang P, Zhu Y, Peng H, Cui Y, Li H, Liu J, Wang Z. 2021. The emerging role of ISWI chromatin remodeling complexes in cancer. *Journal of Experimental & Clinical Cancer Research* **40**: 346.
Lombardi R, Circelli P, Villani ME, Buriani G, Nardi L, Coppola V, Bianco L, Benvenuto E, Donini M, Marusic C. 2009. High-level HIV-1 Nef transient expression in Nicotiana benthamiana using the P19 gene silencing suppressor protein of Artichoke Mottled Crinckle Virus. *BMC Biotechnol* **9**: 96.
Long C, Grueter CE, Song K, Qin S, Qi X, Kong YM, Shelton JM, Richardson JA, Zhang C-L, Bassel-Duby R, et al. 2014. Ataxia and Purkinje cell degeneration in mice lacking the CAMTA1 transcription factor. *Proceedings of the National Academy of Sciences* **111**: 11521–11526. https://pnas.org/doi/full/10.1073/pnas.1411251111.
Lou Z, Minter-Dykhouse K, Franco S, Gostissa M, Rivera MA, Celeste A, Manis JP, van Deursen J, Nussenzweig A, Paull TT, et al. 2006. MDC1 Maintains Genomic Stability by Participating in the Amplification of ATM-Dependent DNA Damage Signals. *Mol Cell* **21**: 187–200.
Love MI, Huber W, Anders S. 2014. Moderated estimation of fold change and dispersion for RNA-seq data with DESeq2. *Genome Biol* **15**: 550. http://genomebiology.biomedcentral.com/articles/10.1186/s13059-014-0550-8.
Lujan SA, Clausen AR, Clark AB, MacAlpine HK, MacAlpine DM, Malc EP, Mieczkowski PA, Burkholder AB, Fargo DC, Gordenin DA, et al. 2014. Heterogeneous polymerase fidelity and mismatch repair bias genome variation and composition. *Genome Res* **24**: 1751–1764.
Luo Y, Hou X, Zhang C, Tan L, Shao C, Lin R, Su Y, Cai X, Li L, Chen S, et al. 2020. A plant-specific SWR1 chromatin-remodeling complex couples histone H2A.Z deposition with nucleosome sliding. *EMBO J* **39**. https://onlinelibrary.wiley.com/doi/10.15252/embj.2019102008.
Macrae TA, Fothergill-Robinson J, Ramalho-Santos M. 2023. Regulation, functions and transmission of bivalent chromatin during mammalian development. *Nat Rev Mol Cell Biol* **24**: 6–26. https://www.nature.com/articles/s41580-022-00518-2.
Ma D, Li X, Guo Y, Chu J, Fang S, Yan C, Noel JP, Liu H. 2016. Cryptochrome 1 interacts with PIF4 to regulate high temperature-mediated hypocotyl elongation in response to blue light. *Proceedings of the National Academy of Sciences* **113**: 224–229.
Maertens GN, El Messaoudi-Aubert S, Elderkin S, Hiom K, Peters G. 2010. Ubiquitin-specific proteases 7 and 11 modulate Polycomb regulation of the INK4a tumour suppressor. *EMBO J* **29**: 2553–2565.
Maier A, Schrader A, Kokkelink L, Falke C, Welter B, Iniesto E, Rubio V, Uhrig JF, Hülskamp M, Hoecker U. 2013. Light and the E3 ubiquitin ligase COP1/SPA control the protein stability of the MYB transcription factors PAP1 and PAP2 involved in anthocyanin accumulation in Arabidopsis. *The Plant Journal* **74**: 638–651.
Mailand N, Bekker-Jensen S, Faustrup H, Melander F, Bartek J, Lukas C, Lukas J. 2007. RNF8 Ubiquitylates Histones at DNA Double-Strand Breaks and Promotes Assembly of Repair Proteins. *Cell* **131**: 887–900.
Ma L, Guan Z, Wang Q, Yan X, Wang J, Wang Z, Cao J, Zhang D, Gong X, Yin P. 2020a. Structural insights into the photoactivation of Arabidopsis CRY2. *Nat Plants* **6**: 1432–1438.
Mallette FA, Richard S. 2012. K48-linked ubiquitination and protein degradation regulate 53BP1 recruitment at DNA damage sites. *Cell Res* **22**: 1221–1223.
Ma L, Wang X, Guan Z, Wang L, Wang Y, Zheng L, Gong Z, Shen C, Wang J, Zhang D, et al. 2020b. Structural insights into BIC-mediated inactivation of Arabidopsis cryptochrome 2. *Nat Struct Mol Biol* **27**: 472–479.
Manova V, Gruszka D. 2015. DNA damage and repair in plants – from models to crops. *Front Plant Sci* **6**.

Mansour WY, Rhein T, Dahm-Daphi J. 2010. The alternative end-joining pathway for repair of DNA double-strand breaks requires PARP1 but is not dependent upon microhomologies. *Nucleic Acids Res* **38**: 6065–6077.
Mao J, Zhang Y-C, Sang Y, Li Q-H, Yang H-Q. 2005. A role for *Arabidopsis* cryptochromes and COP1 in the regulation of stomatal opening. *Proceedings of the National Academy of Sciences* **102**: 12270–12275.
Mao Z, Wei X, Li L, Xu P, Zhang J, Wang W, Guo T, Kou S, Wang W, Miao L, et al. 2021. Arabidopsis cryptochrome 1 controls photomorphogenesis through regulation of H2A.Z deposition. *Plant Cell* **33**: 1961–1979. https://academic.oup.com/plcell/article/33/6/1961/6188635.
March E, Farrona S. 2018. Plant Deubiquitinases and Their Role in the Control of Gene Expression Through Modification of Histones. *Front Plant Sci* **8**. http://journal.frontiersin.org/article/10.3389/fpls.2017.02274/full.
Marechal A, Zou L. 2013. DNA Damage Sensing by the ATM and ATR Kinases. *Cold Spring Harb Perspect Biol* **5**: a012716–a012716.
Marfella CGA, Imbalzano AN. 2007. The Chd family of chromatin remodelers. *Mutation Research/Fundamental and Molecular Mechanisms of Mutagenesis* **618**: 30–40.
Marteijn JA, Lans H, Vermeulen W, Hoeijmakers JHJ. 2014. Understanding nucleotide excision repair and its roles in cancer and ageing. *Nat Rev Mol Cell Biol* **15**: 465–481. http://www.nature.com/articles/nrm3822.
Matsumura M, Nomoto M, Itaya T, Aratani Y, Iwamoto M, Matsuura T, Hayashi Y, Mori T, Skelly MJ, Yamamoto YY, et al. 2022. Mechanosensory trichome cells evoke a mechanical stimuli–induced immune response in Arabidopsis thaliana. *Nat Commun* **13**: 1216. https://www.nature.com/articles/s41467-022-28813-8.
Mattiroli F, Penengo L. 2021. Histone Ubiquitination: An Integrative Signaling Platform in Genome Stability. *Trends in Genetics* **37**: 566–581. https://linkinghub.elsevier.com/retrieve/pii/S0168952520303358.
Mattiroli F, Vissers JHA, van Dijk WJ, Ikpa P, Citterio E, Vermeulen W, Marteijn JA, Sixma TK. 2012. RNF168 Ubiquitinates K13-15 on H2A/H2AX to Drive DNA Damage Signaling. *Cell* **150**: 1182–1195.
Mavragani I V., Nikitaki Z, Kalospyros SA, Georgakilas AG. 2019. Ionizing Radiation and Complex DNA Damage: From Prediction to Detection Challenges and Biological Significance. *Cancers (Basel)* **11**: 1789.
Mayer C, Neubert M, Grummt I. 2008. The structure of NoRC-associated RNA is crucial for targeting the chromatin remodelling complex NoRC to the nucleolus. *EMBO Rep* **9**: 774–780.
McNellis TW, von Arnim AG, Deng XW. 1994. Overexpression of Arabidopsis COP1 results in partial suppression of light-mediated development: evidence for a light-inactivable repressor of photomorphogenesis. *Plant Cell* **6**: 1391–1400.
Mei Q, Dvornyk V. 2015. Evolutionary History of the Photolyase/Cryptochrome Superfamily in Eukaryotes. *PLoS One* **10**: e0135940.
Mevissen TET, Komander D. 2017. Mechanisms of Deubiquitinase Specificity and Regulation. *Annu Rev Biochem* **86**: 159–192.
Miao L, Zhao J, Yang G, Xu P, Cao X, Du S, Xu F, Jiang L, Zhang S, Wei X, et al. 2022. Arabidopsis cryptochrome 1 undergoes COP1 and LRBs-dependent degradation in response to high blue light. *New Phytologist* **234**: 1347–1362. https://onlinelibrary.wiley.com/doi/10.1111/nph.17695.
Mi H, Ebert D, Muruganujan A, Mills C, Albou L-P, Mushayamaha T, Thomas PD. 2021. PANTHER version 16: a revised family classification, tree-based classification tool, enhancer regions and extensive API. *Nucleic Acids Res* **49**: D394–D403.
Mi H, Thomas P. 2009. PANTHER Pathway: An Ontology-Based Pathway Database Coupled with Data Analysis Tools. pp. 123–140 http://link.springer.com/10.1007/978-1-60761-175-2_7.

Millán-Zambrano G, Burton A, Bannister AJ, Schneider R. 2022. Histone post-translational modifications — cause and consequence of genome function. *Nat Rev Genet* **23**: 563–580.
Milne TA, Dou Y, Martin ME, Brock HW, Roeder RG, Hess JL. 2005. MLL associates specifically with a subset of transcriptionally active target genes. *Proceedings of the National Academy of Sciences* **102**: 14765–14770.
Mockler TC, Guo H, Yang H, Duong H, Lin C. 1999. Antagonistic actions of Arabidopsis cryptochromes and phytochrome B in the regulation of floral induction. *Development* **126**: 2073–2082. https://journals.biologists.com/dev/article/126/10/2073/40321/Antagonistic-actions-of-Arabidopsis-cryptochromes.
Modrich P. 2016. Mechanisms in *E. coli* and Human Mismatch Repair (Nobel Lecture). *Angewandte Chemie International Edition* **55**: 8490–8501.
Mofers A, Pellegrini P, Linder S, D'Arcy P. 2017. Proteasome-associated deubiquitinases and cancer. *Cancer and Metastasis Reviews* **36**: 635–653. http://link.springer.com/10.1007/s10555-017-9697-6.
Molinier J, Lechner E, Dumbliauskas E, Genschik P. 2008. Regulation and role of arabidopsis CUL4-DDB1A-DDB2 in maintaining genome integrity upon UV stress. *PLoS Genet* **4**.
Molinier J, Oakeley EJ, Niederhauser O, Kovalchuk I, Hohn B. 2005. Dynamic response of plant genome to ultraviolet radiation and other genotoxic stresses. *Mutation Research - Fundamental and Molecular Mechanisms of Mutagenesis* **571**: 235–247. https://linkinghub.elsevier.com/retrieve/pii/S002751070400497X.
Mordes DA, Glick GG, Zhao R, Cortez D. 2008. TopBP1 activates ATR through ATRIP and a PIKK regulatory domain. *Genes Dev* **22**: 1478–1489.
Morgan MAJ, Shilatifard A. 2020. Reevaluating the roles of histone-modifying enzymes and their associated chromatin modifications in transcriptional regulation. *Nat Genet* **52**: 1271–1281.
Mo W, Zhang J, Zhang L, Yang Z, Yang L, Yao N, Xiao Y, Li T, Li Y, Zhang G, et al. 2022. Arabidopsis cryptochrome 2 forms photobodies with TCP22 under blue light and regulates the circadian clock. *Nat Commun* **13**: 2631. https://www.nature.com/articles/s41467-022-30231-9.
Mueller T, Breuer P, Schmitt I, Walter J, Evert BO, Wüllner U. 2009. CK2-dependent phosphorylation determines cellular localization and stability of ataxin-3. *Hum Mol Genet* **18**: 3334–3343.
Mu J-J, Wang Y, Luo H, Leng M, Zhang J, Yang T, Besusso D, Jung SY, Qin J. 2007. A Proteomic Analysis of Ataxia Telangiectasia-mutated (ATM)/ATM-Rad3-related (ATR) Substrates Identifies the Ubiquitin-Proteasome System as a Regulator for DNA Damage Checkpoints. *Journal of Biological Chemistry* **282**: 17330–17334.
Narlikar GJ, Sundaramoorthy R, Owen-Hughes T. 2013. Mechanisms and Functions of ATP-Dependent Chromatin-Remodeling Enzymes. *Cell* **154**: 490–503.
Niedernhofer LJ. 2007. The Fanconi Anemia Signalosome Anchor. *Mol Cell* **25**: 487–490.
Nisa MU, Huang Y, Benhamed M, Raynaud C. 2019. The plant DNA damage response: Signaling pathways leading to growth inhibition and putative role in response to stress conditions. *Front Plant Sci* **10**. https://www.frontiersin.org/article/10.3389/fpls.2019.00653/full.
Nitabach MN, Taghert PH. 2008. Organization of the Drosophila Circadian Control Circuit. *Current Biology* **18**: R84–R93.
Nito K, Wong CCL, Yates JR, Chory J. 2013. Tyrosine Phosphorylation Regulates the Activity of Phytochrome Photoreceptors. *Cell Rep* **3**: 1970–1979.
Nolan TM, Vukašinović N, Liu D, Russinova E, Yin Y. 2020. Brassinosteroids: Multidimensional Regulators of Plant Growth, Development, and Stress Responses. *Plant Cell* **32**: 295–318.
Oberle C, Blattner C. 2010. Regulation of the DNA Damage Response to DSBs by Post-Translational Modifications. *Curr Genomics* **11**: 184–198. http://www.eurekaselect.com/openurl/content.php?genre=article&issn=1389-2029&volume=11&issue=3&spage=184.

Ocampo J, Chereji R V., Eriksson PR, Clark DJ. 2016. The ISW1 and CHD1 ATP-dependent chromatin remodelers compete to set nucleosome spacing *in vivo*. *Nucleic Acids Res* **44**: 4625–4635.

O'Geen H, Ren C, Nicolet CM, Perez AA, Halmai J, Le VM, Mackay JP, Farnham PJ, Segal DJ. 2017. dCas9-based epigenome editing suggests acquisition of histone methylation is not sufficient for target gene repression. *Nucleic Acids Res* **45**: 9901–9916.

Ogita N, Okushima Y, Tokizawa M, Yamamoto YY, Tanaka M, Seki M, Makita Y, Matsui M, Okamoto-Yoshiyama K, Sakamoto T, et al. 2018. Identifying the target genes of SUPPRESSOR OF GAMMA RESPONSE 1, a master transcription factor controlling DNA damage response in Arabidopsis. *Plant Journal* **94**: 439–453.

Ohtake F, Tsuchiya H. 2016. The emerging complexity of ubiquitin architecture. *J Biochem* mvw088.

Ohtake F, Tsuchiya H, Saeki Y, Tanaka K. 2018. K63 ubiquitylation triggers proteasomal degradation by seeding branched ubiquitin chains. *Proceedings of the National Academy of Sciences* **115**.

Oppikofer M, Bai T, Gan Y, Haley B, Liu P, Sandoval W, Ciferri C, Cochran AG. 2017. Expansion of the ISWI chromatin remodeler family with new active complexes. *EMBO Rep* **18**: 1697–1706. https://onlinelibrary.wiley.com/doi/abs/10.15252/embr.201744011.

Ozer G, Luque A, Schlick T. 2015. The chromatin fiber: multiscale problems and approaches. *Curr Opin Struct Biol* **31**: 124–139.

Özgür S, Sancar A. 2003. Purification and Properties of Human Blue-Light Photoreceptor Cryptochrome 2. *Biochemistry* **42**: 2926–2932. https://pubs.acs.org/doi/10.1021/bi026963n.

Ozturk N, VanVickle-Chavez SJ, Akileswaran L, Van Gelder RN, Sancar A. 2013. Ramshackle (Brwd3) promotes light-induced ubiquitylation of *Drosophila* Cryptochrome by DDB1-CUL4-ROC1 E3 ligase complex. *Proceedings of the National Academy of Sciences* **110**: 4980–4985.

Palayam M, Ganapathy J, Guercio AM, Tal L, Deck SL, Shabek N. 2021. Structural insights into photoactivation of plant Cryptochrome-2. *Commun Biol* **4**: 28. http://www.nature.com/articles/s42003-020-01531-x.

Papamichos-Chronakis M, Watanabe S, Rando OJ, Peterson CL. 2011. Global regulation of H2A.Z localization by the INO80 chromatin-remodeling enzyme is essential for genome integrity. *Cell* **144**: 200–213. https://linkinghub.elsevier.com/retrieve/pii/S0092867410014790.

Papp SJ, Huber AL, Jordan SD, Kriebs A, Nguyen M, Moresco JJ, Yates JR, Lamia KA. 2015. DNA damage shifts circadian clock time via Hausp-dependent Cry1 stabilization. *Elife* **4**. https://elifesciences.org/articles/04883.

Park S, Jeong JS, Seo JS, Park BS, Chua N. 2019. Arabidopsis ubiquitin-specific proteases UBP12 and UBP13 shape ORE1 levels during leaf senescence induced by nitrogen deficiency. *New Phytologist* **223**: 1447–1460. https://onlinelibrary.wiley.com/doi/10.1111/nph.15879.

Partch CL, Green CB, Takahashi JS. 2014. Molecular architecture of the mammalian circadian clock. *Trends Cell Biol* **24**: 90–99.

Pedmale UV, Huang SC, Zander M, Cole BJ, Hetzel J, Ljung K, Reis PAB, Sridevi P, Nito K, Nery JR, et al. 2016. Cryptochromes Interact Directly with PIFs to Control Plant Growth in Limiting Blue Light. *Cell* **164**: 233–245. https://linkinghub.elsevier.com/retrieve/pii/S0092867415016426.

Pedmale U V., Liscum E. 2007. Regulation of Phototropic Signaling in Arabidopsis via Phosphorylation State Changes in the Phototropin 1-interacting Protein NPH3. *Journal of Biological Chemistry* **282**: 19992–20001.

Peschel N, Chen KF, Szabo G, Stanewsky R. 2009. Light-Dependent Interactions between the Drosophila Circadian Clock Factors Cryptochrome, Jetlag, and Timeless. *Current Biology* **19**: 241–247.

Peschel N, Veleri S, Stanewsky R. 2006. *Veela* defines a molecular link between Cryptochrome and Timeless in the light-input pathway to *Drosophila* 's circadian clock. *Proceedings of the National Academy of Sciences* **103**: 17313–17318.

Peterson CL, Laniel M-A. 2004. Histones and histone modifications. *Current Biology* **14**: R546–R551.
Petruseva IO, Evdokimov AN, Lavrik OI. 2014. Molecular mechanism of global genome nucleotide excision repair. *Acta Naturae* **6**: 23–34.
Petty E, Pillus L. 2013. Balancing chromatin remodeling and histone modifications in transcription. *Trends in Genetics* **29**: 621–629.
Pfeifer GP, You YH, Besaratinia A. 2005. Mutations induced by ultraviolet light. *Mutation Research - Fundamental and Molecular Mechanisms of Mutagenesis* **571**: 19–31. https://linkinghub.elsevier.com/retrieve/pii/S0027510704004804.
PIN PA, NILSSON O. 2012. The multifaceted roles of FLOWERING LOCUS T in plant development. *Plant Cell Environ* **35**: 1742–1755.
Piovesan A, Pelleri MC, Antonaros F, Strippoli P, Caracausi M, Vitale L. 2019. On the length, weight and GC content of the human genome. *BMC Res Notes* **12**: 106.
Ponnu J, Hoecker U. 2022. Signaling Mechanisms by Arabidopsis Cryptochromes. *Front Plant Sci* **13**. https://www.frontiersin.org/articles/10.3389/fpls.2022.844714/full.
Ponnu J, Riedel T, Penner E, Schrader A, Hoecker U. 2019. Cryptochrome 2 competes with COP1 substrates to repress COP1 ubiquitin ligase activity during Arabidopsis photomorphogenesis. *Proc Natl Acad Sci U S A* **116**: 27133–27141.
Poot RA, Bozhenok L, van den Berg DLC, Steffensen S, Ferreira F, Grimaldi M, Gilbert N, Ferreira J, Varga-Weisz PD. 2004. The Williams syndrome transcription factor interacts with PCNA to target chromatin remodelling by ISWI to replication foci. *Nat Cell Biol* **6**: 1236–1244.
Porebski S, Bailey LG, Baum BR. 1997. Modification of a CTAB DNA extraction protocol for plants containing high polysaccharide and polyphenol components. *Plant Mol Biol Report* **15**: 8–15. http://link.springer.com/10.1007/BF02772108.
Pozhidaeva A, Bezsonova I. 2019. USP7: Structure, substrate specificity, and inhibition. *DNA Repair (Amst)* **76**: 30–39. https://linkinghub.elsevier.com/retrieve/pii/S156878641830301X.
Qian S, Lv X, Scheid RN, Lu L, Yang Z, Chen W, Liu R, Boersma MD, Denu JM, Zhong X, et al. 2018. Dual recognition of H3K4me3 and H3K27me3 by a plant histone reader SHL. *Nat Commun* **9**: 2425.
Quennet V, Beucher A, Barton O, Takeda S, Löbrich M. 2011. CtIP and MRN promote non-homologous end-joining of etoposide-induced DNA double-strand breaks in G1. *Nucleic Acids Res* **39**: 2144–2152.
Rai N, Neugart S, Yan Y, Wang F, Siipola SM, Lindfors A V., Winkler JB, Albert A, Brosché M, Lehto T, et al. 2019. How do cryptochromes and UVR8 interact in natural and simulated sunlight? *J Exp Bot* **70**: 4975–4990. https://academic.oup.com/jxb/article/70/18/4975/5491325.
Rai N, O'Hara A, Farkas D, Safronov O, Ratanasopa K, Wang F, Lindfors A V., Jenkins GI, Lehto T, Salojärvi J, et al. 2020. The photoreceptor UVR8 mediates the perception of both UV-B and UV-A wavelengths up to 350 nm of sunlight with responsivity moderated by cryptochromes. *Plant Cell Environ* **43**: 1513–1527. https://onlinelibrary.wiley.com/doi/10.1111/pce.13752.
Ramadan A, Nemoto K, Seki M, Shinozaki K, Takeda H, Takahashi H, Sawasaki T. 2015. Wheat germ-based protein libraries for the functional characterisation of the Arabidopsis E2 ubiquitin conjugating enzymes and the RING-type E3 ubiquitin ligase enzymes. *BMC Plant Biol* **15**: 275.
Ramírez F, Dündar F, Diehl S, Grüning BA, Manke T. 2014. deepTools: a flexible platform for exploring deep-sequencing data. *Nucleic Acids Res* **42**: W187–W191.
Rastogi RP, Richa, Kumar A, Tyagi MB, Sinha RP. 2010. Molecular Mechanisms of Ultraviolet Radiation-Induced DNA Damage and Repair. *J Nucleic Acids* **2010**: 1–32.
Ratcliffe OJ, Kumimoto RW, Wong BJ, Riechmann JL. 2003. Analysis of the Arabidopsis *MADS AFFECTING FLOWERING* Gene Family: *MAF2* Prevents Vernalization by Short Periods of Cold [W]. *Plant Cell* **15**: 1159–1169.
Reyes AA, Marcum RD, He Y. 2021. Structure and Function of Chromatin Remodelers. *J Mol Biol* **433**: 166929.

Rittinger K, Ikeda F. 2017. Linear ubiquitin chains: enzymes, mechanisms and biology. *Open Biol* **7**: 170026.
Rizzini L, Levine DC, Perelis M, Bass J, Peek CB, Pagano M. 2019. Cryptochromes-Mediated Inhibition of the CRL4Cop1-Complex Assembly Defines an Evolutionary Conserved Signaling Mechanism. *Current Biology* **29**: 1954-1962.e4.
Robinson JT, Thorvaldsdóttir H, Winckler W, Guttman M, Lander ES, Getz G, Mesirov JP. 2011. Integrative genomics viewer. *Nat Biotechnol* **29**: 24–26.
Rodriguez E, Chevalier J, El Ghoul H, Voldum-Clausen K, Mundy J, Petersen M. 2018. DNA damage as a consequence of NLR activation ed. J.D.G. Jones. *PLoS Genet* **14**: e1007235. https://dx.plos.org/10.1371/journal.pgen.1007235.
Roldán-Arjona T, Ariza RR. 2009. Repair and tolerance of oxidative DNA damage in plants. *Mutation Research/Reviews in Mutation Research* **681**: 169–179. https://linkinghub.elsevier.com/retrieve/pii/S1383574208001154.
Rona GB, Eleutherio ECA, Pinheiro AS. 2016. PWWP domains and their modes of sensing DNA and histone methylated lysines. *Biophys Rev* **8**: 63–74.
Rosato E, Tauber E, Kyriacou CP. 2006. Molecular genetics of the fruit-fly circadian clock. *European Journal of Human Genetics* **14**: 729–738.
Sahu RK, Singh S, Tomar RS. 2020. The mechanisms of action of chromatin remodelers and implications in development and disease. *Biochem Pharmacol* **180**: 114200.
Saldivar JC, Cortez D, Cimprich KA. 2017. The essential kinase ATR: ensuring faithful duplication of a challenging genome. *Nat Rev Mol Cell Biol* **18**: 622–636.
Sallmyr A, Tomkinson AE. 2018. Repair of DNA double-strand breaks by mammalian alternative end-joining pathways. *Journal of Biological Chemistry* **293**: 10536–10546.
Sancar A. 1994. Structure and function of DNA photolyase. *Biochemistry* **33**: 2–9. https://pubs.acs.org/doi/abs/10.1021/bi00167a001.
Sancar A. 2003. Structure and Function of DNA Photolyase and Cryptochrome Blue-Light Photoreceptors. *Chem Rev* **103**: 2203–2238.
Sanchez R, Zhou M-M. 2011. The PHD finger: a versatile epigenome reader. *Trends Biochem Sci*.
Sanchez R, Zhou M-M. 2009. The role of human bromodomains in chromatin biology and gene transcription. *Curr Opin Drug Discov Devel* **12**: 659–65.
Sanchez Y, Wong C, Thoma RS, Richman R, Wu Z, Piwnica-Worms H, Elledge SJ. 1997. Conservation of the Chk1 Checkpoint Pathway in Mammals: Linkage of DNA Damage to Cdk Regulation Through Cdc25. *Science (1979)* **277**: 1497–1501. https://www.science.org/doi/10.1126/science.277.5331.1497.
Sang Y, Li Q-H, Rubio V, Zhang Y-C, Mao J, Deng X-W, Yang H-Q. 2005. N-Terminal Domain–Mediated Homodimerization Is Required for Photoreceptor Activity of Arabidopsis CRYPTOCHROME 1. *Plant Cell* **17**: 1569–1584.
Santoro R, Li J, Grummt I. 2002. The nucleolar remodeling complex NoRC mediates heterochromatin formation and silencing of ribosomal gene transcription. *Nat Genet* **32**: 393–396.
Santos-Rosa H, Schneider R, Bannister AJ, Sherriff J, Bernstein BE, Emre NCT, Schreiber SL, Mellor J, Kouzarides T. 2002. Active genes are tri-methylated at K4 of histone H3. *Nature* **419**: 407–411.
Saridakis V, Sheng Y, Sarkari F, Holowaty MN, Shire K, Nguyen T, Zhang RG, Liao J, Lee W, Edwards AM, et al. 2005. Structure of the p53 Binding Domain of HAUSP/USP7 Bound to Epstein-Barr Nuclear Antigen 1. *Mol Cell* **18**: 25–36.
Sartori AA, Lukas C, Coates J, Mistrik M, Fu S, Bartek J, Baer R, Lukas J, Jackson SP. 2007. Human CtIP promotes DNA end resection. *Nature* **450**: 509–514.
Sasidharan R, Pierik R. 2010. Cell wall modification involving XTHs controls phytochrome-mediated petiole elongation in *Arabidopsis thaliana*. *Plant Signal Behav* **5**: 1491–1492.

Savage KI, Harkin DP. 2015. BRCA1, a 'complex' protein involved in the maintenance of genomic stability. *FEBS J* **282**: 630–646.
Savitsky K, Bar-Shira A, Gilad S, Rotman G, Ziv Y, Vanagaite L, Tagle DA, Smith S, Uziel T, Sfez S, et al. 1995. A Single Ataxia Telangiectasia Gene with a Product Similar to PI-3 Kinase. *Science (1979)* **268**: 1749–1753. https://www.science.org/doi/10.1126/science.7792600.
Scharer OD. 2013. Nucleotide Excision Repair in Eukaryotes. *Cold Spring Harb Perspect Biol* **5**: a012609–a012609.
Scheffner M, Nuber U, Huibregtse JM. 1995. Protein ubiquitination involving an E1–E2–E3 enzyme ubiquitin thioester cascade. *Nature* **373**: 81–83.
Schneider CA, Rasband WS, Eliceiri KW. 2012. NIH Image to ImageJ: 25 years of image analysis. *Nat Methods* **9**: 671–675. http://www.nature.com/articles/nmeth.2089.
Schraivogel D, Weinmann L, Beier D, Tabatabai G, Eichner A, Zhu JY, Anton M, Sixt M, Weller M, Beier CP, et al. 2011. CAMTA1 is a novel tumour suppressor regulated by miR-9/9 * in glioblastoma stem cells. *EMBO J* **30**: 4309–4322. http://emboj.embopress.org/cgi/doi/10.1038/emboj.2011.301.
Schulz MH, Devanny WE, Gitter A, Zhong S, Ernst J, Bar-Joseph Z. 2012. DREM 2.0: Improved reconstruction of dynamic regulatory networks from time-series expression data. *BMC Syst Biol* **6**: 104. http://bmcsystbiol.biomedcentral.com/articles/10.1186/1752-0509-6-104.
Scully R, Panday A, Elango R, Willis NA. 2019. DNA double-strand break repair-pathway choice in somatic mammalian cells. *Nat Rev Mol Cell Biol* **20**: 698–714. http://www.nature.com/articles/s41580-019-0152-0.
Sekiguchi M, Matsushita N. 2022. DNA Damage Response Regulation by Histone Ubiquitination. *Int J Mol Sci* **23**: 8187.
Seo HS, Yang J-Y, Ishikawa M, Bolle C, Ballesteros ML, Chua N-H. 2003. LAF1 ubiquitination by COP1 controls photomorphogenesis and is stimulated by SPA1. *Nature* **423**: 995–999.
Shafi AA, McNair CM, McCann JJ, Alshalalfa M, Shostak A, Severson TM, Zhu Y, Bergman A, Gordon N, Mandigo AC, et al. 2021. The circadian cryptochrome, CRY1, is a pro-tumorigenic factor that rhythmically modulates DNA repair. *Nat Commun* **12**: 401. https://www.nature.com/articles/s41467-020-20513-5.
Shang J-Y, Lu Y-J, Cai X-W, Su Y-N, Feng C, Li L, Chen S, He X-J. 2021. COMPASS functions as a module of the INO80 chromatin remodeling complex to mediate histone H3K4 methylation in Arabidopsis. *Plant Cell* **33**: 3250–3271.
Shao G, Lilli DR, Patterson-Fortin J, Coleman KA, Morrissey DE, Greenberg RA. 2009. The Rap80-BRCC36 de-ubiquitinating enzyme complex antagonizes RNF8-Ubc13-dependent ubiquitination events at DNA double strand breaks. *Proceedings of the National Academy of Sciences* **106**: 3166–3171.
Shao Z, Zhang Y, Yuan G-C, Orkin SH, Waxman DJ. 2012. MAnorm: a robust model for quantitative comparison of ChIP-Seq data sets. *Genome Biol* **13**: R16. http://genomebiology.biomedcentral.com/articles/10.1186/gb-2012-13-3-r16.
Sharma N, Zhu Q, Wani G, He J, Wang QE, Wani AA. 2014. USP3 counteracts RNF168 via deubiquitinating H2A and γh2AX at lysine 13 and 15. *Cell Cycle* **13**: 106–114. http://www.tandfonline.com/doi/abs/10.4161/cc.26814.
Shen T, Huang S. 2012. The Role of Cdc25A in the Regulation of Cell Proliferation and Apoptosis. *Anticancer Agents Med Chem* **12**: 631–639.
Shi D, Grossman SR. 2010. Ubiquitin becomes ubiquitous in cancer. *Cancer Biol Ther* **10**: 737–747.
Shin JY, Muniyappan S, Tran N-N, Park H, Lee SB, Lee B-H. 2020. Deubiquitination Reactions on the Proteasome for Proteasome Versatility. *Int J Mol Sci* **21**: 5312.
Shrestha RK, Ronau JA, Davies CW, Guenette RG, Strieter ER, Paul LN, Das C. 2014. Insights into the Mechanism of Deubiquitination by JAMM Deubiquitinases from Cocrystal Structures of the Enzyme with the Substrate and Product. *Biochemistry* **53**: 3199–3217.

Siepka SM, Yoo S-H, Park J, Song W, Kumar V, Hu Y, Lee C, Takahashi JS. 2007. Circadian Mutant Overtime Reveals F-box Protein FBXL3 Regulation of Cryptochrome and Period Gene Expression. *Cell* **129**: 1011–1023.
Sinha RP, Häder D-P. 2002. UV-induced DNA damage and repair: a review. *Photochemical & Photobiological Sciences* **1**: 225–236.
Siriaco G, Deuring R, Chioda M, Becker PB, Tamkun JW. 2009. Drosophila ISWI Regulates the Association of Histone H1 With Interphase Chromosomes *in Vivo*. *Genetics* **182**: 661–669.
Smaczniak C, Immink RGH, Muiño JM, Blanvillain R, Busscher M, Busscher-Lange J, Dinh QD (Peter), Liu S, Westphal AH, Boeren S, et al. 2012. Characterization of MADS-domain transcription factor complexes in *Arabidopsis* flower development. *Proceedings of the National Academy of Sciences* **109**: 1560–1565.
Smeenk G, Wiegant WW, Marteijn JA, Luijsterburg MS, Sroczynski N, Costelloe T, Romeijn RJ, Pastink A, Mailand N, Vermeulen W, et al. 2012. Poly(ADP-ribosyl)ation links the chromatin remodeler SMARCA5/SNF2H to RNF168-dependent DNA damage signaling. *J Cell Sci*.
Smith J, Mun Tho L, Xu N, A. Gillespie D. 2010. The ATM–Chk2 and ATR–Chk1 Pathways in DNA Damage Signaling and Cancer. pp. 73–112 https://linkinghub.elsevier.com/retrieve/pii/B9780123808882000030.
Soll JM, Sobol RW, Mosammaparast N. 2017. Regulation of DNA Alkylation Damage Repair: Lessons and Therapeutic Opportunities. *Trends Biochem Sci* **42**: 206–218.
Song H, Spichiger-Haeusermann C, Basler K. 2009. The ISWI-containing NURF complex regulates the output of the canonical Wingless pathway. *EMBO Rep* **10**: 1140–1146.
Song K, Backs J, McAnally J, Qi X, Gerard RD, Richardson JA, Hill JA, Bassel-Duby R, Olson EN. 2006. The Transcriptional Coactivator CAMTA2 Stimulates Cardiac Growth by Opposing Class II Histone Deacetylases. *Cell* **125**: 453–466. https://linkinghub.elsevier.com/retrieve/pii/S0092867406004429.
Soppe WJJ, Jasencakova Z, Houben A, Kakutani T, Meister A, Huang MS, Jacobsen SE, Schubert I, Fransz PF. 2002. DNA methylation controls histone H3 lysine 9 methylation and heterochromatin assembly in Arabidopsis. *EMBO J* **21**: 6549–59.
Spivak G. 2015. Nucleotide excision repair in humans. *DNA Repair (Amst)* **36**: 13–18.
Stanewsky R, Kaneko M, Emery P, Beretta B, Wager-Smith K, Kay SA, Rosbash M, Hall JC. 1998. The cryb Mutation Identifies Cryptochrome as a Circadian Photoreceptor in Drosophila. *Cell* **95**: 681–692. https://linkinghub.elsevier.com/retrieve/pii/S0092867400816384.
Stovner EB, Sætrom P. 2019. epic2 efficiently finds diffuse domains in ChIP-seq data. *Bioinformatics* **35**: 4392–4393.
Stucki M, Clapperton JA, Mohammad D, Yaffe MB, Smerdon SJ, Jackson SP. 2005. MDC1 Directly Binds Phosphorylated Histone H2AX to Regulate Cellular Responses to DNA Double-Strand Breaks. *Cell* **123**: 1213–1226.
Sung P, Robberson DL. 1995. DNA strand exchange mediated by a RAD51-ssDNA nucleoprotein filament with polarity opposite to that of RecA. *Cell* **82**: 453–461.
Swatek KN, Komander D. 2016. Ubiquitin modifications. *Cell Res* **26**: 399–422. http://www.nature.com/articles/cr201639.
Sy SMH, Jiang J, O WS, Deng Y, Huen MSY. 2013. The ubiquitin specific protease USP34 promotes ubiquitin signaling at DNA double-strand breaks. *Nucleic Acids Res* **41**: 8572–8580. https://academic.oup.com/nar/article-lookup/doi/10.1093/nar/gkt622.
Takahashi JS. 2017. Transcriptional architecture of the mammalian circadian clock. *Nat Rev Genet* **18**: 164–179.
Takahashi N, Inagaki S, Nishimura K, Sakakibara H, Antoniadi I, Karady M, Ljung K, Umeda M. 2021. Alterations in hormonal signals spatially coordinate distinct responses to DNA double-strand breaks in Arabidopsis roots. *Sci Adv* **7**. https://www.science.org/doi/10.1126/sciadv.abg0993.

Tamura K, Adachi Y, Chiba K, Oguchi K, Takahashi H. 2002. Identification of Ku70 and Ku80 homologues in Arabidopsis thaliana: Evidence for a role in the repair of DNA double-strand breaks. *Plant Journal* **29**: 771–781. https://onlinelibrary.wiley.com/doi/abs/10.1046/j.1365-313X.2002.01258.x.

Tang L, Nogales E, Ciferri C. 2010. Structure and function of SWI/SNF chromatin remodeling complexes and mechanistic implications for transcription. *Prog Biophys Mol Biol* **102**: 122–128.

Tan LM, Liu R, Gu BW, Zhang CJ, Luo J, Guo J, Wang Y, Chen L, Du X, Li S, et al. 2020. Dual recognition of H3K4me3 and DNA by the ISWI component ARID5 regulates the floral transition in Arabidopsis. *Plant Cell* **32**: 2178–2195. http://www.plantcell.org/lookup/doi/10.1105/tpc.19.00944.

Tao Y, Ferrer J-L, Ljung K, Pojer F, Hong F, Long JA, Li L, Moreno JE, Bowman ME, Ivans LJ, et al. 2008. Rapid Synthesis of Auxin via a New Tryptophan-Dependent Pathway Is Required for Shade Avoidance in Plants. *Cell* **133**: 164–176.

Tarasov A, Vilella AJ, Cuppen E, Nijman IJ, Prins P. 2015. Sambamba: fast processing of NGS alignment formats. *Bioinformatics* **31**: 2032–2034.

Taylor EM, Cecillon SM, Bonis A, Chapman JR, Povirk LF, Lindsay HD. 2010. The Mre11/Rad50/Nbs1 complex functions in resection-based DNA end joining in Xenopus laevis. *Nucleic Acids Res* **38**: 441–454.

Tessadori F, Schulkes RK, Driel R van, Fransz P. 2007. Light-regulated large-scale reorganization of chromatin during the floral transition in Arabidopsis. *The Plant Journal* **50**: 848–857. https://onlinelibrary.wiley.com/doi/10.1111/j.1365-313X.2007.03093.x.

Thompson M V., Wolniak SM. 2008. A Plasma Membrane-Anchored Fluorescent Protein Fusion Illuminates Sieve Element Plasma Membranes in Arabidopsis and Tobacco. *Plant Physiol* **146**: 1599–1610. https://academic.oup.com/plphys/article/146/4/1599/6107123.

Thorslund T, Ripplinger A, Hoffmann S, Wild T, Uckelmann M, Villumsen B, Narita T, Sixma TK, Choudhary C, Bekker-Jensen S, et al. 2015. Histone H1 couples initiation and amplification of ubiquitin signalling after DNA damage. *Nature* **527**: 389–393.

Tian G, Lu Q, Kohalmi SE, Rothstein SJ, Cui Y. 2012. Evidence that the Arabidopsis Ubiquitin C-terminal Hydrolases 1 and 2 associate with the 26S proteasome and the TREX-2 complex. *Plant Signal Behav* **7**: 1415–1419.

Tissot N, Ulm R. 2020. Cryptochrome-mediated blue-light signalling modulates UVR8 photoreceptor activity and contributes to UV-B tolerance in Arabidopsis. *Nat Commun* **11**: 1323. http://www.nature.com/articles/s41467-020-15133-y.

Toiber D, Erdel F, Bouazoune K, Silberman DM, Zhong L, Mulligan P, Sebastian C, Cosentino C, Martinez-Pastor B, Giacosa S, et al. 2013. SIRT6 Recruits SNF2H to DNA Break Sites, Preventing Genomic Instability through Chromatin Remodeling. *Mol Cell* **51**: 454–468.

Toto M, D'Angelo G, Corona DF V. 2014. Regulation of ISWI chromatin remodelling activity. *Chromosoma* **123**: 91–102.

Tracz M, Bialek W. 2021. Beyond K48 and K63: non-canonical protein ubiquitination. *Cell Mol Biol Lett* **26**: 1. https://cmbl.biomedcentral.com/articles/10.1186/s11658-020-00245-6.

Trapnell C, Roberts A, Goff L, Pertea G, Kim D, Kelley DR, Pimentel H, Salzberg SL, Rinn JL, Pachter L. 2012. Differential gene and transcript expression analysis of RNA-seq experiments with TopHat and Cufflinks. *Nat Protoc* **7**: 562–578. http://www.nature.com/articles/nprot.2012.016.

Trapnell C, Williams BA, Pertea G, Mortazavi A, Kwan G, van Baren MJ, Salzberg SL, Wold BJ, Pachter L. 2010. Transcript assembly and quantification by RNA-Seq reveals unannotated transcripts and isoform switching during cell differentiation. *Nat Biotechnol* **28**: 511–515.

Tsurumoto T, Fujikawa Y, Onoda Y, Ochi Y, Ohta D, Okazawa A. 2022. Transcriptome and metabolome analyses revealed that narrowband 280 and 310 nm UV-B induce distinctive responses in Arabidopsis. *Sci Rep* **12**: 4319. https://www.nature.com/articles/s41598-022-08331-9.

Turk EM, Fujioka S, Seto H, Shimada Y, Takatsuto S, Yoshida S, Denzel MA, Torres QI, Neff MM. 2003. CYP72B1 Inactivates Brassinosteroid Hormones: An Intersection between Photomorphogenesis and Plant Steroid Signal Transduction. *Plant Physiol* **133**: 1643–1653.
Turk EM, Fujioka S, Seto H, Shimada Y, Takatsuto S, Yoshida S, Wang H, Torres QI, Ward JM, Murthy G, et al. 2005. BAS1 and SOB7 act redundantly to modulate Arabidopsis photomorphogenesis via unique brassinosteroid inactivation mechanisms. *The Plant Journal* **42**: 23–34.
Turner BM. 2007. Defining an epigenetic code. *Nat Cell Biol* **9**: 2–6.
Tyagi M, Imam N, Verma K, Patel AK. 2016. Chromatin remodelers: We are the drivers!! *Nucleus* **7**: 388–404. https://www.tandfonline.com/doi/full/10.1080/19491034.2016.1211217.
Uckelmann M, Sixma TK. 2017. Histone ubiquitination in the DNA damage response. *DNA Repair (Amst)* **56**: 92–101.
Udugama M, Sabri A, Bartholomew B. 2011. The INO80 ATP-Dependent Chromatin Remodeling Complex Is a Nucleosome Spacing Factor. *Mol Cell Biol* **31**: 662–673.
Ulm R, Baumann A, Oravecz A, Máté Z, Ádám É, Oakeley EJ, Schäfer E, Nagy F. 2004. Genome-wide analysis of gene expression reveals function of the bZIP transcription factor HY5 in the UV-B response of Arabidopsis. *Proceedings of the National Academy of Sciences* **101**: 1397–1402. https://pnas.org/doi/full/10.1073/pnas.0308044100.
Ulm R, Revenkova E, di Sansebastiano G-P, Bechtold N, Paszkowski J. 2001. Mitogen-activated protein kinase phosphatase is required for genotoxic stress relief in Arabidopsis. *Genes Dev* **15**: 699–709. http://genesdev.cshlp.org/lookup/doi/10.1101/gad.192601.
Uziel T. 2003. Requirement of the MRN complex for ATM activation by DNA damage. *EMBO J* **22**: 5612–5621.
Valles GJ, Bezsonova I, Woodgate R, Ashton NW. 2020. USP7 Is a Master Regulator of Genome Stability. *Front Cell Dev Biol* **8**. https://www.frontiersin.org/article/10.3389/fcell.2020.00717/full.
van der Weegen Y, Golan-Berman H, Mevissen TET, Apelt K, González-Prieto R, Goedhart J, Heilbrun EE, Vertegaal ACO, van den Heuvel D, Walter JC, et al. 2020. The cooperative action of CSB, CSA, and UVSSA target TFIIH to DNA damage-stalled RNA polymerase II. *Nat Commun* **11**: 2104.
van Haaften G, Romeijn R, Pothof J, Koole W, Mullenders LHF, Pastink A, Plasterk RHA, Tijsterman M. 2006. Identification of Conserved Pathways of DNA-Damage Response and Radiation Protection by Genome-Wide RNAi. *Current Biology* **16**: 1344–1350.
Vanhaeren H, Chen Y, Vermeersch M, De Milde L, De Vleeschhauwer V, Natran A, Persiau G, Eeckhout D, De Jaeger G, Gevaert K, et al. 2020. UBP12 and UBP13 negatively regulate the activity of the ubiquitin-dependent peptidases DA1, DAR1 and DAR2. *Elife* **9**.
van Zanten M, Koini MA, Geyer R, Liu Y, Brambilla V, Bartels D, Koornneef M, Fransz P, Soppe WJJ. 2011. Seed maturation in *Arabidopsis thaliana* is characterized by nuclear size reduction and increased chromatin condensation. *Proceedings of the National Academy of Sciences* **108**: 20219–20224.
van Zanten M, Tessadori F, Bossen L, Peeters AJM, Fransz P. 2010a. Large-scale chromatin de-compaction induced by low light is not accompanied by nucleosomal displacement. *Plant Signal Behav* **5**: 1677–1678.
van Zanten M, Tessadori F, McLoughlin F, Smith R, Millenaar FF, van Driel R, Voesenek LACJ, Peeters AJM, Fransz P. 2010b. Photoreceptors CRYTOCHROME2 and phytochrome B control chromatin compaction in arabidopsis. *Plant Physiol* **154**: 1686–1696. http://www.plantphysiol.org/lookup/doi/10.1104/pp.110.164616.
van Zanten M, Tessadori F, Peeters AJM, Fransz P. 2012. Shedding Light on Large-Scale Chromatin Reorganization in Arabidopsis thaliana. *Mol Plant* **5**: 583–590.

Veluchamy A, Jégu T, Ariel F, Latrasse D, Mariappan KG, Kim S-K, Crespi M, Hirt H, Bergounioux C, Raynaud C, et al. 2016. LHP1 Regulates H3K27me3 Spreading and Shapes the Three-Dimensional Conformation of the Arabidopsis Genome. *PLoS One* **11**: e0158936.
Vierstra RD. 2009. The ubiquitin–26S proteasome system at the nexus of plant biology. *Nat Rev Mol Cell Biol* **10**: 385–397.
Walden H, Deans AJ. 2014. The Fanconi Anemia DNA Repair Pathway: Structural and Functional Insights into a Complex Disorder. *Annu Rev Biophys* **43**: 257–278.
Wallace SS. 2014. Base excision repair: A critical player in many games. *DNA Repair (Amst)* **19**: 14–26.
Wang H, Fan Z, Shliaha P V., Miele M, Hendrickson RC, Jiang X, Helin K. 2023. H3K4me3 regulates RNA polymerase II promoter-proximal pause-release. *Nature* **615**: 339–348. https://www.nature.com/articles/s41586-023-05780-8.
Wang H, Ma L-G, Li J-M, Zhao H-Y, Deng XW. 2001. Direct Interaction of *Arabidopsis* Cryptochromes with COP1 in Light Control Development. *Science (1979)* **294**: 154–158.
Wang J. 2001. DNA damage and apoptosis. *Cell Death Differ* **8**: 1047–1048.
Wang M, Wu W, Wu W, Rosidi B, Zhang L, Wang H, Iliakis G. 2006. PARP-1 and Ku compete for repair of DNA double strand breaks by distinct NHEJ pathways. *Nucleic Acids Res* **34**: 6170–6182.
Wang Q, Barshop WD, Bian M, Vashisht AA, He R, Yu X, Liu B, Nguyen P, Liu X, Zhao X, et al. 2015. The Blue Light-Dependent Phosphorylation of the CCE Domain Determines the Photosensitivity of Arabidopsis CRY2. *Mol Plant* **8**: 631–643.
Wang Q, Lin C. 2020. Mechanisms of Cryptochrome-Mediated Photoresponses in Plants. *Annu Rev Plant Biol* **71**: 103–129.
Wang Q, Zuo Z, Wang X, Gu L, Yoshizumi T, Yang Z, Yang L, Liu Q, Liu W, Han Y-J, et al. 2016. Photoactivation and inactivation of *Arabidopsis* cryptochrome 2. *Science (1979)* **354**: 343–347. https://www.sciencemag.org/lookup/doi/10.1126/science.aaf9030.
Wang W, Xu J, Limbo O, Fei J, Kassavetis GA, Chong J, Kadonaga JT, Russell P, Li B, Wang D. 2019. Molecular basis of chromatin remodeling by Rhp26, a yeast CSB ortholog. *Proceedings of the National Academy of Sciences* **116**: 6120–6129.
Wang X, Jiang B, Gu L, Chen Y, Mora M, Zhu M, Noory E, Wang Q, Lin C. 2021. A photoregulatory mechanism of the circadian clock in Arabidopsis. *Nat Plants* **7**: 1397–1408. https://www.nature.com/articles/s41477-021-01002-z.
Wang X, Wang L, Huang Y, Deng Z, Li C, Zhang J, Zheng M, Yan S. 2022. A plant-specific module for homologous recombination repair. *Proceedings of the National Academy of Sciences* **119**. https://pnas.org/doi/full/10.1073/pnas.2202970119.
Wang X, Wang Q, Nguyen P, Lin C. 2014. Cryptochrome-Mediated Light Responses in Plants. pp. 167–189 https://linkinghub.elsevier.com/retrieve/pii/B9780128019221000075 (Accessed May 17, 2023).
Weber S. 2005. Light-driven enzymatic catalysis of DNA repair: a review of recent biophysical studies on photolyase. *Biochimica et Biophysica Acta (BBA) - Bioenergetics* **1707**: 1–23.
Weidemüller P, Kholmatov M, Petsalaki E, Zaugg JB. 2021. Transcription factors: Bridge between cell signaling and gene regulation. *Proteomics* **21**: 2000034.
Weidler G, zur Oven-Krockhaus S, Heunemann M, Orth C, Schleifenbaum F, Harter K, Hoecker U, Batschauer A. 2012. Degradation of *Arabidopsis* CRY2 Is Regulated by SPA Proteins and Phytochrome A. *Plant Cell* **24**: 2610–2623.
Weinert TA, Kiser GL, Hartwell LH. 1994. Mitotic checkpoint genes in budding yeast and the dependence of mitosis on DNA replication and repair. *Genes Dev* **8**: 652–665. http://genesdev.cshlp.org/lookup/doi/10.1101/gad.8.6.652.
Wiles ET, McNaught KJ, Kaur G, Selker JML, Ormsby T, Aravind L, Selker EU. 2020. Evolutionarily ancient BAH–PHD protein mediates Polycomb silencing. *Proceedings of the National Academy of Sciences* **117**: 11614–11623.

Wiles ET, Selker EU. 2017. H3K27 methylation: a promiscuous repressive chromatin mark. *Curr Opin Genet Dev* **43**: 31–37.
Wilkinson KD. 2000. Ubiquitination and deubiquitination: Targeting of proteins for degradation by the proteasome. *Semin Cell Dev Biol* **11**: 141–148.
Winter D, Vinegar B, Nahal H, Ammar R, Wilson G V., Provart NJ. 2007. An "Electronic Fluorescent Pictograph" Browser for Exploring and Analyzing Large-Scale Biological Data Sets ed. I. Baxter. *PLoS One* **2**: e718. https://dx.plos.org/10.1371/journal.pone.0000718.
Wisor JP, O'Hara BF, Terao A, Selby CP, Kilduff TS, Sancar A, Edgar DM, Franken P. 2002. A role for cryptochromes in sleep regulation. *BMC Neurosci* **3**: 20.
Workman CT, Mak HC, McCuine S, Tagne J-B, Agarwal M, Ozier O, Begley TJ, Samson LD, Ideker T. 2006. A Systems Approach to Mapping DNA Damage Response Pathways. *Science (1979)* **312**: 1054–1059.
Wright WD, Shah SS, Heyer W-D. 2018. Homologous recombination and the repair of DNA double-strand breaks. *Journal of Biological Chemistry* **293**: 10524–10535.
Wu G, Spalding EP. 2007. Separate functions for nuclear and cytoplasmic cryptochrome 1 during photomorphogenesis of *Arabidopsis* seedlings. *Proceedings of the National Academy of Sciences* **104**: 18813–18818.
Xiao C, Chen F, Yu X, Lin C, Fu Y-F. 2009. Over-expression of an AT-hook gene, AHL22, delays flowering and inhibits the elongation of the hypocotyl in Arabidopsis thaliana. *Plant Mol Biol* **71**: 39–50.
Xu F, Kuo T, Rosli Y, Liu M-S, Wu L, Chen L-FO, Fletcher JC, Sung ZR, Pu L. 2018. Trithorax Group Proteins Act Together with a Polycomb Group Protein to Maintain Chromatin Integrity for Epigenetic Silencing during Seed Germination in Arabidopsis. *Mol Plant* **11**: 659–677. https://linkinghub.elsevier.com/retrieve/pii/S1674205218300509.
Xu G, Jaffrey SR. 2011. The new landscape of protein ubiquitination. *Nat Biotechnol* **29**: 1098–1100.
YAGI K, OZAWA T, HARADA M. 1959. Change of Absorption Spectrum of Flavin Adenine Dinucleotide byits Binding with both D-Amino Acid Oxidase Apo-Protein and Benzoate. *Nature* **184**: 1938–1939. https://www.nature.com/articles/1841938a0.
Yang Q, Zhao J, Chen D, Wang Y. 2021. E3 ubiquitin ligases: styles, structures and functions. *Molecular Biomedicine* **2**: 23.
Yan H, Liu Y, Zhang K, Song J, Xu W, Su Z. 2019. Chromatin State-Based Analysis of Epigenetic H3K4me3 Marks of Arabidopsis in Response to Dark Stress. *Front Genet* **10**. https://www.frontiersin.org/article/10.3389/fgene.2019.00306/full.
Yan J, Zhang C, Gu M, Bai Z, Zhang W, Qi T, Cheng Z, Peng W, Luo H, Nan F, et al. 2009. The Arabidopsis CORONATINE INSENSITIVE1 Protein Is a Jasmonate Receptor. *Plant Cell* **21**: 2220–2236. https://academic.oup.com/plcell/article/21/8/2220/6095498.
Yan L, Chen Z. 2020. A Unifying Mechanism of DNA Translocation Underlying Chromatin Remodeling. *Trends Biochem Sci* **45**: 217–227.
Yan N, Doelling JH, Falbel TG, Durski AM, Vierstra RD. 2000. The Ubiquitin-Specific Protease Family from Arabidopsis. *At* UBP1 and 2 Are Required for the Resistance to the Amino Acid Analog Canavanine. *Plant Physiol* **124**: 1828–1843.
Ye H, Park YC, Kreishman M, Kieff E, Wu H. 1999. The Structural Basis for the Recognition of Diverse Receptor Sequences by TRAF2. *Mol Cell* **4**: 321–330.
Yi C, He C. 2013. DNA Repair by Reversal of DNA Damage. *Cold Spring Harb Perspect Biol* **5**: a012575–a012575.
Yokoyama H, Rybina S, Santarella-Mellwig R, Mattaj IW, Karsenti E. 2009. ISWI is a RanGTP-dependent MAP required for chromosome segregation. *Journal of Cell Biology* **187**: 813–829.
Yoo S-H, Mohawk JA, Siepka SM, Shan Y, Huh SK, Hong H-K, Kornblum I, Kumar V, Koike N, Xu M, et al. 2013. Competing E3 Ubiquitin Ligases Govern Circadian Periodicity by Degradation of CRY in Nucleus and Cytoplasm. *Cell* **152**: 1091–1105.

Yoshiyama K, Conklin PA, Huefner ND, Britt AB. 2009. Suppressor of gamma response 1 (SOG1) encodes a putative transcription factor governing multiple responses to DNA damage. *Proc Natl Acad Sci U S A* **106**: 12843–12848. http://www.pnas.org/cgi/doi/10.1073/pnas.0810304106.
Yoshiyama KO. 2015. SOG1: a master regulator of the DNA damage response in plants. *Genes Genet Syst* **90**: 209–216.
Yuan J, Luo K, Zhang L, Cheville JC, Lou Z. 2010. USP10 Regulates p53 Localization and Stability by Deubiquitinating p53. *Cell* **140**: 384–396.
Yudkovsky N, Logie C, Hahn S, Peterson CL. 1999. Recruitment of the SWI/SNF chromatin remodeling complex by transcriptional activators. *Genes Dev* **13**: 2369–2374.
Yue X, Bai C, Xie D, Ma T, Zhou P-K. 2020. DNA-PKcs: A Multi-Faceted Player in DNA Damage Response. *Front Genet* **11**.
Yu G, Wang L-G, He Q-Y. 2015. ChIPseeker: an R/Bioconductor package for ChIP peak annotation, comparison and visualization. *Bioinformatics* **31**: 2382–2383.
Yu H, Zhu S, Zhou B, Xue H, Han J-DJ. 2008. Inferring causal relationships among different histone modifications and gene expression. *Genome Res* **18**: 1314–1324.
Yu X, Klejnot J, Zhao X, Shalitin D, Maymon M, Yang H, Lee J, Liu X, Lopez J, Lin C. 2007. Arabidopsis Cryptochrome 2 Completes Its Posttranslational Life Cycle in the Nucleus. *Plant Cell* **19**: 3146–3156. https://academic.oup.com/plcell/article/19/10/3146/6092230.
Yu X, Liu H, Klejnot J, Lin C. 2010. The Cryptochrome Blue Light Receptors. *Arabidopsis Book* **8**: e0135.
Yu X, Sayegh R, Maymon M, Warpeha K, Klejnot J, Yang H, Huang J, Lee J, Kaufman L, Lin C. 2009. Formation of Nuclear Bodies of Arabidopsis CRY2 in Response to Blue Light Is Associated with Its Blue Light–Dependent Degradation. *Plant Cell* **21**: 118–130. https://academic.oup.com/plcell/article/21/1/118/6095881.
Yu Y, Chen Y, Kim B, Wang H, Zhao C, He X, Liu L, Liu W, Wu LMN, Mao M, et al. 2013. Olig2 Targets Chromatin Remodelers to Enhancers to Initiate Oligodendrocyte Differentiation. *Cell* **152**: 248–261.
Zahid S, Seif El Dahan M, Iehl F, Fernandez-Varela P, Le Du M-H, Ropars V, Charbonnier JB. 2021. The Multifaceted Roles of Ku70/80. *Int J Mol Sci* **22**: 4134.
Zeng Z, Wei J, Liu Y, Zhang W, Mabe T. 2018. Magnetoreception of Photoactivated Cryptochrome 1 in Electrochemistry and Electron Transfer. *ACS Omega* **3**: 4752–4759. https://pubs.acs.org/doi/10.1021/acsomega.8b00645.
Zhang B, Holmlund M, Lorrain S, Norberg M, Bakó L, Fankhauser C, Nilsson O. 2017. BLADE-ON-PETIOLE proteins act in an E3 ubiquitin ligase complex to regulate PHYTOCHROME INTERACTING FACTOR 4 abundance. *Elife* **6**.
Zhang Y, Hunter T. 2014. Roles of Chk1 in cell biology and cancer therapy. *Int J Cancer* **134**: 1013–1023.
Zhang Y, Liu T, Meyer CA, Eeckhoute J, Johnson DS, Bernstein BE, Nusbaum C, Myers RM, Brown M, Li W, et al. 2008. Model-based Analysis of ChIP-Seq (MACS). *Genome Biol* **9**: R137.
Zhang Y, Mayba O, Pfeiffer A, Shi H, Tepperman JM, Speed TP, Quail PH. 2013. A Quartet of PIF bHLH Factors Provides a Transcriptionally Centered Signaling Hub That Regulates Seedling Morphogenesis through Differential Expression-Patterning of Shared Target Genes in Arabidopsis. *PLoS Genet* **9**: e1003244.
Zhang Y-Z, Yuan J, Zhang L, Chen C, Wang Y, Zhang G, Peng L, Xie S-S, Jiang J, Zhu J-K, et al. 2020. Coupling of H3K27me3 recognition with transcriptional repression through the BAH-PHD-CPL2 complex in Arabidopsis. *Nat Commun* **11**: 6212.
Zhao B, Bhuripanyo K, Schneider J, Zhang K, Schindelin H, Boone D, Yin J. 2012. Specificity of the E1-E2-E3 Enzymatic Cascade for Ubiquitin C-Terminal Sequences Identified by Phage Display. *ACS Chem Biol* **7**: 2027–2035.
Zhao B, Rothenberg E, Ramsden DA, Lieber MR. 2020. The molecular basis and disease relevance of non-homologous DNA end joining. *Nat Rev Mol Cell Biol* **21**: 765–781.

Zhao H, Watkins JL, Piwnica-Worms H. 2002. Disruption of the checkpoint kinase 1/cell division cycle 25A pathway abrogates ionizing radiation-induced S and G $_2$ checkpoints. *Proceedings of the National Academy of Sciences* **99**: 14795–14800.

Zhao Y, Majid MC, Soll JM, Brickner JR, Dango S, Mosammaparast N. 2015. Noncanonical regulation of alkylation damage resistance by the OTUD 4 deubiquitinase. *EMBO J* **34**: 1687–1703. https://onlinelibrary.wiley.com/doi/10.15252/embj.201490497.

Zhou B-BS, Elledge SJ. 2000. The DNA damage response: putting checkpoints in perspective. *Nature* **408**: 433–439.

Zhou Y, Park S-H, Soh MY, Chua N-H. 2021. Ubiquitin-specific proteases UBP12 and UBP13 promote shade avoidance response by enhancing PIF7 stability. *Proceedings of the National Academy of Sciences* **118**. https://pnas.org/doi/full/10.1073/pnas.2103633118.

Zhou Y, Wang Y, Krause K, Yang T, Dongus JA, Zhang Y, Turck F. 2018. Telobox motifs recruit CLF/SWN–PRC2 for H3K27me3 deposition via TRB factors in Arabidopsis. *Nat Genet* **50**: 638–644. http://www.nature.com/articles/s41588-018-0109-9.

Zhou Y, Xun Q, Zhang D, Lv M, Ou Y, Li J. 2019. TCP Transcription Factors Associate with PHYTOCHROME INTERACTING FACTOR 4 and CRYPTOCHROME 1 to Regulate Thermomorphogenesis in Arabidopsis thaliana. *iScience* **15**: 600–610.

Zhu Q, Ding N, Wei S, Li P, Wani G, He J, Wani AA. 2020. USP7-mediated deubiquitination differentially regulates CSB but not UVSSA upon UV radiation-induced DNA damage. *Cell Cycle* **19**: 124–141.

Zhu Q, Sharma N, He J, Wani G, Wani AA. 2015. USP7 deubiquitinase promotes ubiquitin-dependent DNA damage signaling by stabilizing RNF168*. *Cell Cycle* **14**: 1413–1425. https://www.tandfonline.com/doi/full/10.1080/15384101.2015.1007785.

Zuo Z-C, Meng Y-Y, Yu X-H, Zhang Z-L, Feng D-S, Sun S-F, Liu B, Lin C-T. 2012. A Study of the Blue-Light-Dependent Phosphorylation, Degradation, and Photobody Formation of Arabidopsis CRY2. *Mol Plant* **5**: 726–733. https://linkinghub.elsevier.com/retrieve/pii/S1674205214600204.

Appendix

Attached in this appendix section is my co-authored paper describing a histone H4 replacement system developed for the model plant species *Arabidopsis thaliana*. This paper results from a collaboration between me and Dr. Yannick Jacob's laboratory at Yale University. My work in this paper mainly involves generating mutant lines. This paper is previously published in *The Plant Cell** (2022), Volume 34, Issue 10, Pages 3611–3631 under the title "Systematic histone H4 replacement in *Arabidopsis thaliana* reveals a role for H4R17 in regulating flowering time" by Emma Tung Corcoran, Chantal LeBlanc, Yi-Chun Huang, Mia Arias Tsang, Anthony Sarkiss, Yuzhao Hu, Ullas V Pedmale and Yannick Jacob (Corcoran et al. 2022).

https://doi.org/10.1093/plcell/koac211 THE PLANT CELL 2022: 34: 3611–3631

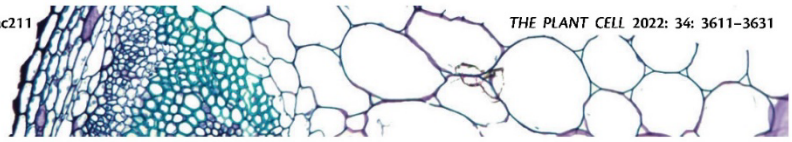

Research Article

Systematic histone H4 replacement in *Arabidopsis thaliana* reveals a role for H4R17 in regulating flowering time

Emma Tung Corcoran [1], **Chantal LeBlanc** [1], **Yi-Chun Huang** [1], **Mia Arias Tsang**[1], **Anthony Sarkiss** [1], **Yuzhao Hu** [2], **Ullas V. Pedmale** [2] and **Yannick Jacob** [1,*]

1 Faculty of Arts and Sciences, Department of Molecular, Cellular and Developmental Biology, Yale University, New Haven, CT 06511, USA
2 Cold Spring Harbor Laboratory, Cold Spring Harbor, NY 11724, USA

*Author for correspondence: yannick.jacob@yale.edu

Y.J. and E.T.C. designed the experiments and wrote the article with contributions from C.L. Constructs were generated by E.T.C. and Y.-C.H. Plant transformations were performed by E.T.C., A.S., C.L., and Y.J. Genotyping was performed by E.T.C., A.S., M.A.T., C.L., and Y.J. RNA extractions and RT-qPCR were done by E.T.C., C.L., and Y.J. Flowering time measurements were obtained by E.T.C., M.A.T., and C.L. Plant pictures were taken by E.T.C., M.A.T., C.L., and Y.J. Some of the mutants used in this work were generated by Y.H. and U.V.P. Y.-C.H. performed the in vitro binding assays. C.L. performed the RNA-seq and MNase-seq experiments. E.T.C. did the bioinformatics analyses of all RNA-seq and MNase-seq experiments.
The author responsible for distribution of materials integral to the findings presented in this article in accordance with the policy described in the Instructions for Authors (https://academic.oup.com/plcell) is: Yannick Jacob (yannick.jacob@yale.edu).

Abstract

Despite the broad array of roles for epigenetic mechanisms on regulating diverse processes in eukaryotes, no experimental system is currently available in plants for the direct assessment of histone function. In this work, we present the development of a genetic strategy in Arabidopsis (*Arabidopsis thaliana*) whereby modified histone H4 transgenes can completely replace the expression of endogenous histone *H4* genes. Accordingly, we established a collection of plants expressing different *H4* point mutants targeting residues that may be post-translationally modified in vivo. To demonstrate its utility, we screened this new *H4* mutant collection to uncover substitutions in H4 that alter flowering time. We identified different mutations in the H4 tail (H4R17A) and the H4 globular domain (H4R36A, H4R39K, H4R39A, and H4K44A) that strongly accelerate the floral transition. Furthermore, we identified a conserved regulatory relationship between H4R17 and the ISWI chromatin remodeling complex in plants: As with other biological systems, H4R17 regulates nucleosome spacing via ISWI. Overall, this work provides a large set of H4 mutants to the plant epigenetics community that can be used to systematically assess histone H4 function in Arabidopsis and a roadmap to replicate this strategy for studying other histone proteins in plants.

Introduction

In eukaryotic cells, genomic DNA is organized into chromatin, whose basic unit is the nucleosome, which consists of 147 bp of DNA wrapped around one histone octamer made up of two copies of the histone proteins H2A, H2B, H3, and H4 (Luger et al., 1997). Histones play a significant role in regulatory processes operating at the chromatin level, such as transcription and DNA replication, and can therefore exert widespread effects on organismal growth, development, and fitness (Kouzarides, 2007). One mechanism by which

Received January 18, 2022. Accepted July 15, 2022. Advance access publication July 26, 2022

histones contribute to these processes is through the post-translational modifications (PTMs) of histone residues. Traditionally, the functional significance of histone PTMs has primarily been deduced through the analysis of phenotypes resulting from the mutation of histone-modifying enzymes or histone-reading proteins. However, while this method has been successful at identifying functions for many histone PTMs, there are several limitations to this approach. For example, this strategy presents difficulties if there are many redundant proteins writing or reading the same PTM, or if the writers or readers of a specific histone PTM have not been identified. Moreover, histone-modifying enzymes often target non-histone substrates in addition to histones, complicating the analysis of mutant phenotypes (Glozak et al., 2005).

To circumvent these obstacles, one effective strategy to study the functions of histone PTMs is to mutate the acceptor histone residue to a nonmodifiable residue and then assess the resulting phenotype(s). One inherent advantage of this strategy is that it can be applied to investigate the roles of modifiable and nonmodifiable residues of histones. In addition, this histone replacement strategy can be used in biological backgrounds expressing wild-type histone genes, or in backgrounds where expression of endogenous histone genes is partially or completely eliminated. A major advantage of removing endogenous histones in this strategy is that it increases the likelihood of detecting phenotypes associated with the expression of genes encoding histone mutants, which may otherwise be masked if competing wild-type histones are also present. Systematic mutagenesis experiments with core histones were initially conducted in budding yeast (*Saccharomyces cerevisiae*) and revealed many new insights into histone function (Dai et al., 2008; Nakanishi et al., 2008; Govin et al., 2010; Fu et al., 2021). These experiments utilized histone shuffle systems to either provide an episomal plasmid expressing histone mutant genes in a background from which the endogenous histone genes had been deleted, or to directly mutate the endogenous histone gene copies using homologous recombination. The most recent system developed in yeast utilized an efficient clustered regularly interspaced short palindromic repeats (CRISPR)-associated nuclease 9 (Cas9)-based histone shuffle strategy that allows for the rapid development of multiplex histone mutations (Fu et al., 2021). In multicellular eukaryotes, Drosophila (*Drosophila melanogaster*) was the first organism in which systematic histone mutagenesis was performed, by using site-specific transgenesis to replace the endogenous histone coding region with that of a modified histone gene or histone array (Hodl and Basler, 2009, 2012; Gunesdogan et al., 2010; McKay et al., 2015). Additionally, high-throughput screens of histones H3 and H4 were recently conducted in Drosophila using a CRISPR/Cas9-mediated knock-in technology for histone gene replacement at the endogenous histone locus (Zhang et al., 2019).

In contrast to the aforementioned biological model systems, plant systems present additional challenges to implementing complete histone gene replacement. While all replication-dependent histone genes are clustered at a single genomic locus in Drosophila (Lifton et al., 1978), and yeast contains only two copies of each core histone gene at the haploid cell stage (Fu et al., 2021), there are 47 genes, dispersed throughout the genome, that encode H2A, H2B, H3, and H4 in Arabidopsis (*Arabidopsis thaliana*) (Tenea et al., 2009). Because the histone genes are not clustered together in plants, the establishment of complex histone deletion mutants necessary for partially or completely replacing endogenous histone genes with modified histone genes is more challenging. Histone replacement was however recently reported in Arabidopsis, using a combination of the traditional crossing of histone mutants and artificial microRNAs to generate backgrounds largely depleted of wild-type histone H3.1 (Jiang et al., 2017). Notably, this strategy is relatively time-consuming and may not completely eliminate endogenous histones. While the earliest strategies used to implement histone gene replacement in both yeast and Drosophila were not applicable to plants due to their reliance on either the plasmid shuffle strategy and/or site-specific recombination systems, some aspects of the newest histone replacement strategies in other systems should facilitate the establishment of complete histone gene replacement in plants. For example, recent advancements in the deployment of multiplex CRISPR/Cas9-based technologies in plants make it possible to create mutations in large gene families like those of histones.

While histones contribute to diverse processes in plants, a system enabling histone gene replacement would allow plant researchers to further elucidate the biological roles of histones in a more high-throughput manner. One of the most important developmental decisions during the plant life cycle is the transition from vegetative growth to reproductive development (Andres and Coupland, 2012; Song et al., 2015). Thus, the ways in which epigenetic mechanisms regulate the floral transition is a major area of research that could benefit from the application of histone replacement strategies. Diverse histone PTMs, including histone H3 lysine 4 (H3K4) methylation, H3K36 di- and tri-methylation, H3K9 methylation, H3K27 methylation, and H3 acetylation have been shown to regulate the expression of key flowering time regulatory genes such as *FLOWERING LOCUS C* (*FLC*) and *FLOWERING LOCUS T* (*FT*) (Bastow et al., 2004; He et al., 2004; Kim et al., 2005; Deng et al., 2007; Jiang et al., 2008; Pien et al., 2008; Xu et al., 2008; He, 2009; Yu et al., 2011; Bu et al., 2014; Crevillen et al., 2014, 2019; Cui et al., 2016; Pajoro et al., 2017; Ning et al., 2019; Zheng et al., 2019). However, compared with H3, the role of H4 in regulating the floral transition has been characterized to a much lesser extent.

Here, we present the establishment of a CRISPR-based histone mutagenesis platform in the plant model system Arabidopsis that allows for complete histone replacement. As a proof-of-concept, we targeted histone H4, which is encoded by the largest number of endogenous genes (eight genes) among functionally distinct plant histone proteins

(Okada et al., 2005; Wierzbicki and Jerzmanowski, 2005; Tenea et al., 2009), for a systematic assessment of the roles of modifiable residues on this protein. After in vivo validation of our histone replacement strategy, we generated a large population of H4 point mutants to study the role(s) of 38 histone H4 residues. Using this H4 population, we identified a role for H4R17 in the regulation of flowering time. Furthermore, we demonstrated the functional relationship between H4R17 and an imitation switch (ISWI) chromatin-remodeling complex. Overall, this study demonstrates the utility of implementing histone replacement strategies in plants and provides a new resource that the plant community can use to probe for H4 functions in various aspects of plant growth and development.

Results

Generation of an Arabidopsis mutant expressing a single histone H4 gene

To create a library of Arabidopsis plants with replacement of endogenous histone H4 with H4 point mutants, we first generated a histone H4-depleted background using multiplex CRISPR/Cas9. The eight histone *H4* genes in Arabidopsis (Columbia-0 [Col-0] accession) all code for the same histone H4 protein, which is 98% identical to human histone H4 (100/102 identical amino acids [aa]; with conservative substitutions at aa 60 and 77) (Supplemental Figure S1A). We designed three single-guide RNAs (sgRNAs) that can target Cas9 to seven of the eight endogenous *H4* genes (Supplemental Figure S1B). We then transformed Col-0 plants via Agrobacterium (*Agrobacterium tumefaciens*) using a multiplex Cas9/sgRNA construct containing the three sgRNAs against the *H4* genes, selected primary transformants (T_1), and exposed these T_1 plants to repeated heat stress treatments at 37°C for 30 h to increase the efficiency of targeted mutagenesis by Cas9 (LeBlanc et al., 2017). We assessed CRISPR/Cas9 activity at all seven *H4* genes via PCR and sequencing in T_1 plants, leading to the identification in the T_2 generation of one plant with homozygous loss-of-function mutations in all seven targeted *H4* genes (hereafter referred to as the *H4* septuple mutant) (Supplemental Figure S1B). Morphological and molecular characterization of the *H4* septuple mutant plants showed that they are slightly smaller than wild-type Col-0 plants and display a serrated leaf phenotype (Figure 1A). In addition, fertility was much lower in the *H4* septuple mutant compared with Col-0 plants (Figure 1B). We determined that the transcript levels of the remaining endogenous *H4* gene (At3g53730) is upregulated approximately two-fold in the *H4* septuple mutant relative to Col-0, likely to compensate for H4 depletion due to the loss of function mutations in the other seven *H4* genes (Figure 1C). The *H4* septuple mutant exhibited misregulation of markers of genomic and epigenomic instability, including upregulation of the DNA damage response gene *BREAST CANCER SUSCEPTIBILITY1* (*BRCA1*) and transcriptional derepression of the heterochromatic DNA repeat *TRANSCRIPTIONNALLY SILENT INFORMATION* (*TSI*) (Figure 1, D and E). Additionally, we observed that the *H4* septuple mutant displays similar morphological phenotypes (small serrated leaves, abnormal silique phyllotaxy, and partial sterility) and a high overlap of differentially expressed genes (DEGs) with a mutant (*fas1-4* in *FASCIATA1*) lacking the histone chaperone chromatin assembly factor-1 (CAF-1) that loads histones H3.1/H4 during replication (e.g. 62% of downregulated DEGs and 55% of upregulated DEGs in the *H4* septuple mutant are shared with *fas1-4*) (Supplemental Figure S2). These findings strongly suggest that reduced H4 levels result in issues with replication due to an insufficient amount of histones for replication forks to proceed normally. Overall, our results demonstrate that multiplex CRISPR/Cas9 can be used to rapidly create an Arabidopsis mutant background containing a minimal number of functional genes coding for a specific histone.

Establishment of a histone H4 replacement system in Arabidopsis

To set up a complete histone H4 replacement in plants, we designed an *H4* replacement plasmid that contains (1) a sgRNA targeting the last remaining endogenous *H4* gene (At3g53730) and (2) a Cas9-resistant *H4* gene allowing for expression of At3g53730 under its native promoter (i.e. *H4* replacement gene). Our strategy was to transform the *H4* septuple mutant, which already expresses *Cas9*, with the *H4* replacement plasmid and select T_1 plants that contain mutations at the endogenous At3g53730 gene. To prevent Cas9 from targeting the replacement *H4* gene, we introduced two silent mutations in the transgene that prevent recognition from the sgRNA targeting the endogenous At3g53730 gene (Figure 1F). After transformation of the *H4* septuple mutant with the *H4* replacement plasmid, we recovered many T_1 transformants expressing the replacement *H4* gene (hereafter referred to as *rH4* plants); in contrast to the *H4* septuple mutant, all *rH4* plants were normal in size, did not exhibit serrated leaves, and showed normal fertility (Figure 1, A and B). Moreover, the relative transcript levels of *BRCA1* and *TSI* in *rH4* plants were comparable to those of Col-0 (Figure 1, D and E). The expression of At3g53730 in first-generation *rH4* plants was upregulated approximately four- to nine-fold relative to Col-0 (Figure 1C). These results indicate that high expression levels of the replacement *H4* gene in *rH4* plants are responsible for suppressing the morphological phenotypes of the *H4* septuple mutant.

We then used site-directed mutagenesis to create a large library of *H4* replacement plasmids carrying different point mutations in the *H4* replacement gene. We generated mutations covering every amino acid (i.e. lysine, arginine, threonine, serine, and tyrosine) in the encoded H4 that could theoretically be post-translationally modified in vivo. To this end, we mutated each modifiable amino acid to a residue that cannot be post-translationally modified (i.e. alanine, valine, or phenylalanine). We also changed lysine and arginine residues to residues with similar biochemical properties (i.e. arginine and lysine, respectively). In total, we modified

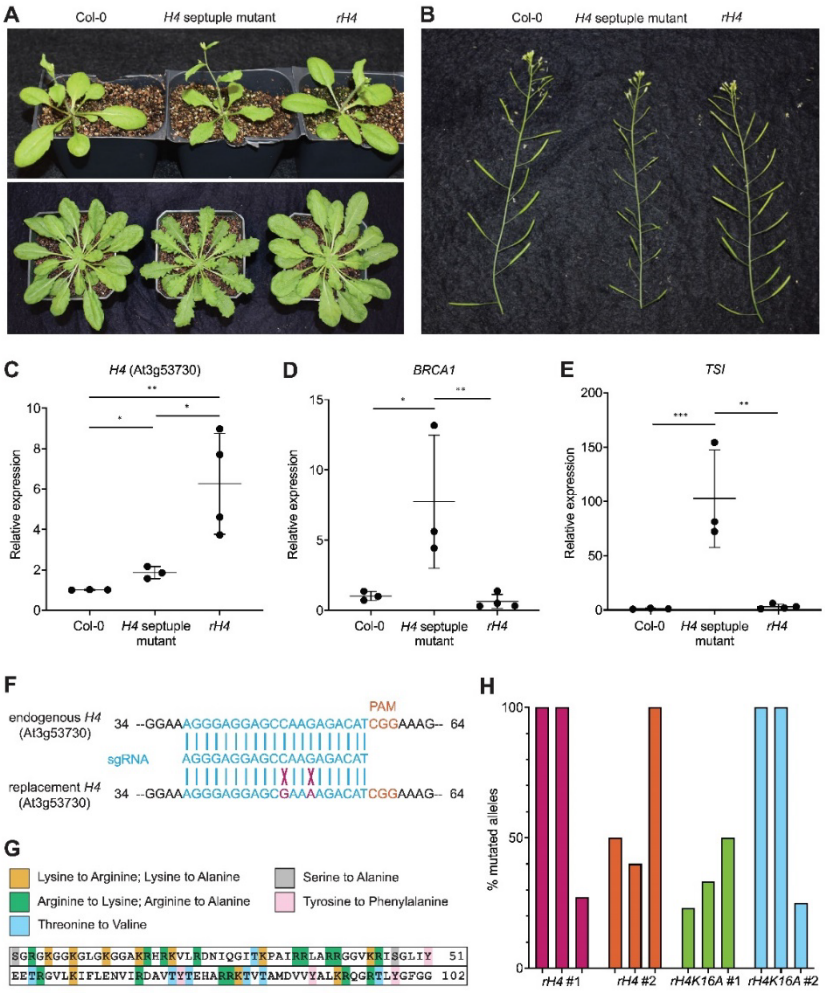

Figure 1 A CRISPR-based genetic system for expression of *H4* point mutant constructs in Arabidopsis. A, Morphological phenotypes of Col-0, *H4* septuple mutant, and *rH4* plants grown in long-day conditions for 24 days (top) and short-day conditions for 7 weeks (bottom). B, Siliques of Col-0, *H4* septuple mutant, and *rH4* plants grown in long-day conditions for 4 weeks. C–E, RT-qPCR analysis of (C) *H4* (At3g53730), (D) *BRCA1*, and (E) *TSI* in Col-0, the *H4* septuple mutant, and four independent *rH4* T_1 lines. Three biological replicates were included for Col-0 and *H4* septuple mutant plants. Horizontal bars indicate the mean. Error bars show standard deviation. $^*P < 0.05$; $^{**}P < 0.005$; $^{***}P < 0.0005$, as determined by unpaired Student's *t* test. F, Design of the sgRNA targeting the remaining endogenous *H4* gene (At3g53730) in the *H4* septuple mutant. Mismatches of the replacement *H4* gene with the sgRNA shown with an X. G, Schematic of point mutations in the *H4* replacement plasmid library. H, Percentage of mutated alleles in six *rH4* plants and six *rH4K16A* plants. Each plant assessed was from the T_2 generation; three plants from the same T_1 parent were used in this experiment (i.e. two independent T_2 lines per genotype).

38 amino acid residues of H4 to generate 63 different *H4* replacement genes containing a specific point mutation (Figure 1G). We subcloned these *H4* mutant genes into the *H4* replacement plasmid and individually transformed them into the *H4* septuple mutant. We selected two independent transgenic lines for each *H4* mutant, except for plants expressing the *H4* replacement genes *H4R40A*, *H4R45A*, *H4K59A*, *H4R78A*, *H4K79R*, and *H4R92K* due to lethality induced by these mutations (Supplemental Figure S3A). Again, we exposed all T_1 plants to repeated heat stress

treatments to maximize the efficiency of targeted mutagenesis of the remaining endogenous *H4* gene by Cas9. To estimate the frequency of mutations at the remaining endogenous *H4* gene in the plants expressing each *H4* replacement gene, we genotyped three plants each from two independent *rH4* lines and two independent *rH4K16A* lines at the T_2 generation stage. We amplified the remaining endogenous *H4* gene (At3g53730) from these T_2 plants, cloned the resulting PCR products and sequenced at least 10 individual clones corresponding to each plant, and calculated the percentage of mutated alleles. Approximately half of the plants were characterized by a complete elimination of the wild-type At3g53730 allele, while the other plants varied from 50% to 75% wild-type alleles remaining (Figure 1H). Taking into account that expression of the *H4* replacement gene was either equivalent or much higher compared with the remaining endogenous *H4* gene (Figure 1C), these results suggest that the chromatin of most T_2 plants in our H4 replacement collection contains large amounts of H4 point mutants. Overall, these results show that our CRISPR/Cas9 strategy was successful in creating a large collection of Arabidopsis plants expressing different *H4* point mutants replacing wild-type H4 proteins.

Differential regulation of flowering time in plants expressing histone H4 mutants

To demonstrate the utility of the H4 replacement collection in identifying pathways regulated by H4 in Arabidopsis, we initiated a screen of the plants expressing *H4* mutants for defects in flowering time. The transition between vegetative and reproductive development is sensitive to various chromatin disruptions in Arabidopsis, but most of the findings in this field have focused on the roles of PTMs on histone H3 (He and Amasino, 2005; He, 2009; Srikanth and Schmid, 2011; Yaish et al., 2011; Berry and Dean, 2015).

We grew our collection of *H4* mutants using plants from two independent T_2 lines for each *H4* mutant and measured flowering time (as days to flowering and leaf number) when grown under both short-day conditions (8-h light, 16-h dark) and long-day conditions (16-h light, 8-h dark). We observed many morphological and developmental phenotypes at the vegetative stage of growth in T_2 plants expressing the different *H4* mutants (Figure 2A and Supplemental Figure S4A), which demonstrates that our H4 replacement strategy can be used to reveal various developmental phenotypes associated with mutations on histone H4. In regard to flowering time, plants expressing *H4* point mutants were not associated with a consistent and significant late flowering-time phenotype compared with *rH4* plants (i.e. replacement with the intact *H4* gene) for both transgenic lines corresponding to the same mutation in either long-day or short-day conditions. By contrast, we identified 16 *rH4* mutants with early flowering phenotype using the same criteria (Figure 2, B and C, Supplemental Figures S4, B and C and S5). Many *rH4* mutant lines exhibited early flowering in both long-day and short-day conditions, with the *rH4R17A*, *rH4R36A*, *rH4R39K*, *rH4R39A*, and *rH4K44A* mutants exhibiting the most consistent and drastic acceleration of flowering time (Supplemental Figure S3B). To reduce the dimensionality of the data, we performed a principal component analysis of the mean values for the four flowering time variables measured in our analyses: number of days in long-day conditions, leaf number in long-day conditions, number of days in short-day conditions, and leaf number in short-day conditions (Figure 2D). We performed *k*-means clustering on principle component 1 (PC1) and PC2, which together explained 98% of the standing variance (Supplemental Figure S4D) and revealed three clusters in the data. Cluster a, corresponding to a flowering response most similar to that of wild-type plants, contained Col-0, the *H4* septuple mutant, *rH4*, *rH4K16A*, *rH4K20R*, and *rH4K20A*. Cluster b, corresponding to a moderately early flowering time phenotype, contained *rH4R17K*, *rH4R35K*, *rH4R35A*, *rH4R36K*, *rH4R40K*, and *rH4K44R*. Cluster c, corresponding to a drastically early flowering time phenotype, contained *rH4R17A*, *rH4R36A*, *rH4R39K*, *rH4R39A*, and *rH4K44A*. The two *rH4K16R* lines were split between Cluster a and Cluster b, and the two *rH4T80V* lines were split between Cluster b and Cluster c. While the *rH4K16R*, *rH4K16A*, *rH4K20R*, and *rH4K20A* mutants appeared slightly early flowering relative to *rH4* plants (Figure 2, B and C and Supplemental Figure S4, B and C), all of these mutant lines, except for a single *rH4K16R* line, clustered within the wild-type cluster (Cluster a) through these analyses. Due to the differences in the flowering time responses of the two independent transgenic lines expressing the *rH4K16R* and *rH4K20R* mutants, we performed RT-qPCR on *H4* (At3g53730) and established that the early flowering lines (*rH4K16R* #1 and *rH4K20R* #2) also display higher *H4* expression (Supplemental Figure S4E), thus supporting the hypothesis that a higher expression of the mutant *H4* transgene causes earlier flowering for these mutants. We also performed RT-qPCR analyses on the key genes *FT* and *SUPPRESSOR OF OVEREXPRESSION OF CO 1* (*SOC1*) regulating flowering time in selected *rH4* mutants and observed their upregulation, consistent with the early flowering behavior of *rH4* mutants from Cluster c (Figure 2, E and F). Taken together, our histone H4 replacement system enables the assessment of expressing histone *H4* mutants on flowering time regulation, thus demonstrating the usefulness of the system for probing histone H4 function in plants.

In vivo modulation of PRMT7 activity does not replicate the early flowering phenotype of *rH4R17A* plants

Of the five H4 mutations (*H4R17A*, *H4R36A*, *H4R39K*, *H4R39A*, and *H4K44A*) identified in our screen that cause the strongest effect on flowering time, only one (*H4R17A*) mapped to the N-terminal tail (aa 1-20) of H4, where most histone PTMs are made. Mutations in the unstructured N-terminal tail of H4 are less likely to affect flowering time by disrupting histone H4 folding and/or nucleosome structure

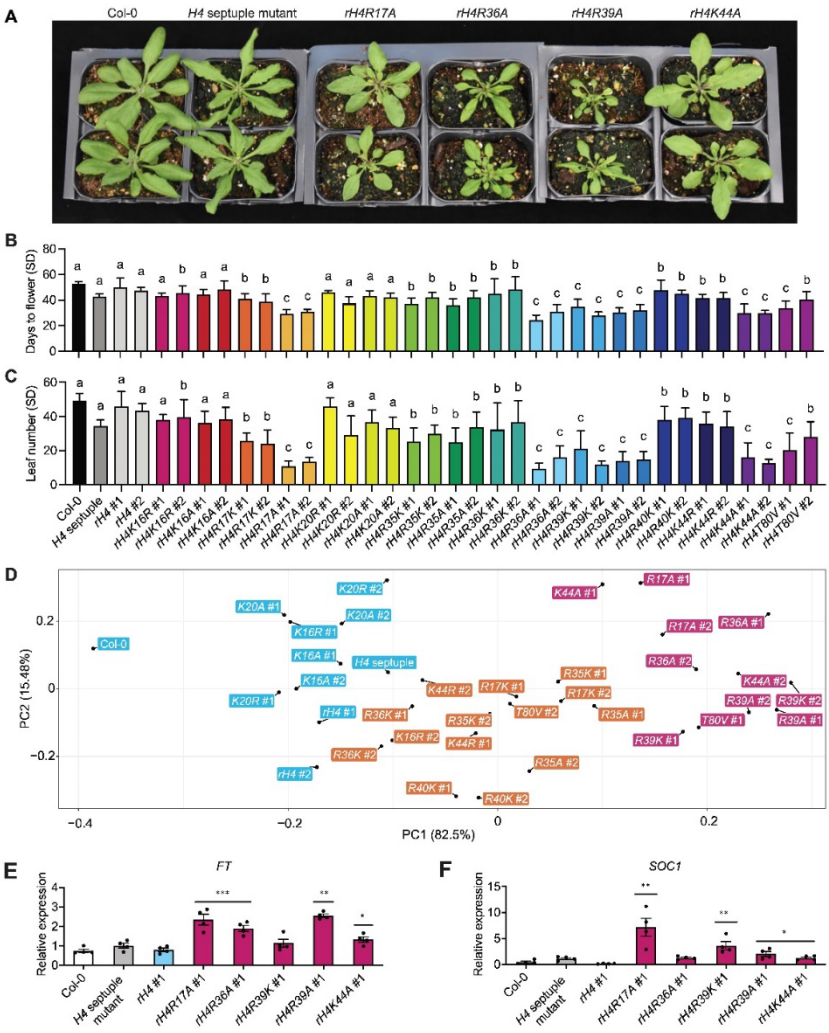

Figure 2 Mutations in specific residues of histone H4 generate early flowering phenotypes in Arabidopsis. A, Rosette phenotype of Col-0, the *H4* septuple mutant, *rH4R17A*, *rH4R36A*, *rH4R39A*, and rH4K44A mutant lines grown in long-day conditions for 3 weeks. For the *rH4* plants, individual T_2 plants (top and bottom) from independent T_1 parents are shown. B and C, Mean days to flower (B) and rosette leaf number (C) at flowering in short-day (SD) conditions for Col-0, the *H4* septuple mutant, and various *H4* replacement backgrounds (two independent T_2 transgenic lines each). Error bars show standard deviation ($n \geq 7$). Lowercase letters indicate cluster identified by *k*-means clustering. D, Principal component analysis for flowering time data along the first two principal components PC1 and PC2. Variance explained by each principal component is indicated on the respective axis. The three clusters produced by *k*-means clustering are represented in blue (cluster a), orange (cluster b), and pink (cluster c). E and F, RT-qPCR analysis of *FT* (E) and *SOC1* (F) in Col-0, the *H4* septuple mutant, *rH4* #1, *rH4R17A* #1, *rH4R36A* #1, *rH4R39K* #1, *rH4R39A* #1, and *rH4K44A* #1 plants. Error bars show standard deviation. *$P < 0.05$; **$P < 0.005$; ***$P < 0.0005$, as determined by unpaired Student's *t* test. Bar colors represent cluster assignment from (D).

than mutations in the histone-fold domain. Therefore, we focused our subsequent analyses on trying to elucidate the mechanism by which the H4R17A mutation affects the timing of the transition to reproductive development. For this work, we used *H4* replacement plants for which there was a complete replacement of the endogenous histone *H4*

with the *H4R17A* mutant (Supplemental Figure S6A). In addition to a significantly earlier floral transition, we observed that the *H4R17A* mutation also causes other developmental phenotypes, including smaller, upwardly curled leaves, and reduced fertility compared with wild-type plants (Figure 3, A and B). When we introduced the *H4R17A* replacement construct in wild-type Col-0 instead of the *H4* septuple mutant background, we noticed an attenuation of the effects of *H4R17A* on plant development when the normal H4 protein content of Arabidopsis competes with the H4 point mutant for insertion on chromatin (Supplemental Figure S6, B and C).

One hypothesis regarding the mechanism by which the *H4R17A* mutation causes early flowering is that the encoded variant H4 protein prevents deposition of a PTM on H4R17. PROTEIN ARGININE METHYLTRANSFERASE 7 (PRMT7) is the only known histone-modifying enzyme that targets H4R17 in eukaryotes, as it has been shown to monomethylate H4R17 in mammals (Feng et al., 2013, 2014; Jain and Clarke, 2019). The Arabidopsis genome contains a single

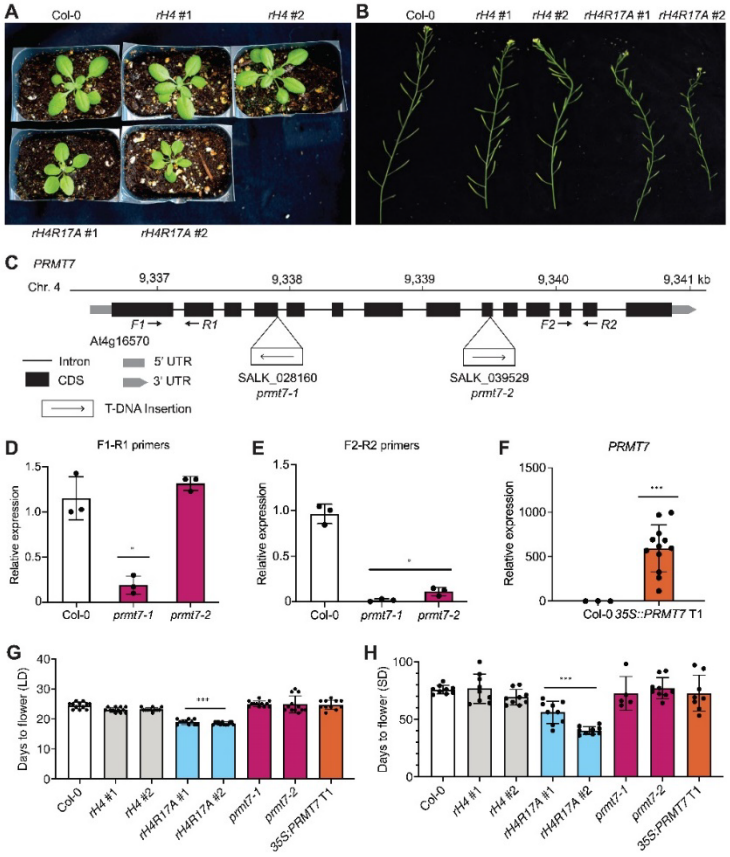

Figure 3 PRMT7 does not regulate the floral transition in Arabidopsis. A, Rosette phenotype of Col-0, *rH4* #1, *rH4* #2, *rH4R17A* #1, and *rH4R17A* #2 plants grown in long-day conditions for 3 weeks. B, Silique phenotype of Col-0, *rH4* #1, *rH4* #2, *rH4R17A* #1, and *rH4R17A* #2 plants grown in long-day conditions for 4 weeks. C, Schematic diagram of the *PRMT7* locus. The location of the T-DNA insertions and the primers (F1–R1 and F2–R2) used for gene expression analyses are shown. D–F, RT-qPCR showing relative *PRMT7* transcript levels in Col-0, *prmt7-1*, and *prmt7-2* plants (D and E), and Col-0 and *35S:PRMT7* T_1 plants (F). The average of three biological replicates and standard deviation are shown for Col-0 and *prmt7* mutants. For the *35S:PRMT7* plants, individual data points represent independent T_1 plants. $^*P < 0.05$; $^{**}P < 0.005$; $^{***}P < 0.0005$, as determined by unpaired Student's *t* test (sample versus Col-0). E and F, Mean days to flower in long-day (E) or short-day conditions (F) for Col-0, *rH4* #1, *rH4* #2, *rH4R17A* #1 and *rH4R17A* #2, *prmt7-1*, *prmt7-2*, and *35S:PRMT7* T_1 plants. Error bars show standard deviation. $^*P < 0.05$; $^{**}P < 0.005$; $^{***}P < 0.0005$, as determined by one-way ANOVA with Tukey's honestly significant difference (HSD) post hoc test. $n \geq 11$ for long days, $n \geq 5$ for short days.

orthologous gene for *PRMT7* (At4g16570), which has not been functionally characterized. To assess a potential role for PRMT7 in regulating flowering time via methylation of H4R17, we measured flowering time in *prmt7* mutants (SALK_028160 and SALK_039529) and in plants overexpressing the *PRMT7* gene (i.e. *35S:PRMT7*). We confirmed by RT-qPCR that both T-DNA alleles used in these experiments prevent the expression of a full-length *PRMT7* transcript and that *PRMT7* is overexpressed in the *35S:PRMT7* plants generated here (Figure 3, C–F). Importantly, neither *prmt7* mutants nor *PRMT7* overexpressing plants displayed altered flowering time in either long-day or short-day conditions (Figure 3, G and H and Supplemental Figure S7). In addition, we observed none of the other vegetative or reproductive phenotypes characteristic of *rH4R17A* plants in plants lacking or overexpressing *PRMT7*. These results strongly suggest that replacement of H4 with H4R17A does not affect development in Arabidopsis by interfering with PRMT7 activity on histone H4.

H4R17A interferes with the binding of the catalytic subunits of Arabidopsis ISWI to H4

In addition to affecting the deposition of PTMs, mutation of histone residues can prevent binding of proteins to chromatin (Hyland et al., 2005; Norris et al., 2008). Therefore, we next investigated the possibility that replacement of histone H4 with H4R17A affects plant development by negatively affecting the function of plant ISWI chromatin-remodeling complexes. In yeast and animals, R17 of H4 has been shown to directly interact with ISWI to regulate nucleosome remodeling activity in vitro and in vivo (Hamiche et al., 2001; Clapier et al., 2002; Fazzio et al., 2005; Yan et al., 2016; Dann et al., 2017). Replacement of H4 with H4R17A was shown to severely reduce the ability of ISWI from the fungus *Myceliophthora thermophila* to interact with H4 in isothermal titration calorimetry assays (Yan et al., 2016). Comparative analysis of the protein sequence of the ISWI catalytic subunits in Arabidopsis (CHROMATIN-REMODELING PROTEIN 11 [CHR11] and CHR17) revealed a strict conservation of the two amino acids (E474 and D524 in CHR11; E479 and D529 in CHR17) directly involved in making contacts with H4R17 in the ISWI orthologs from other species, in addition to high protein sequence identity across the H4R17-interacting domain (71%, 167/235 CHR11/CHR17 versus *M. thermophila* ISWI) (Figure 4A and Supplemental Figure S8). Therefore, we hypothesized that the H4R17A mutation might prevent binding of histone H4 to Arabidopsis ISWI enzymes (Yan et al., 2016, 2019). To test this hypothesis, we first assessed homology models of the structure of CHR11, which indicated conservation of the H4R17-binding pocket in the plant ISWI protein (Figure 4, B–G). We then performed in vitro binding assays with recombinant CHR11 or CHR17 and histone H4 and determined that plant ISWI subunits bind to intact histone H4, while we detected lower binding for the H4R17A mutant protein (Figure 4H). Taken together, these results suggest that expression of *H4R17A* in plants interferes with the function of the ISWI chromatin-remodeling complexes.

Functional relationship between H4R17 and ISWI in the regulation of flowering time

We next examined morphological phenotypes induced by mutations in genes encoding different Arabidopsis ISWI subunits (CHR11, CHR17, HOMEOBOX-1/RINGLET 1 [RLT1], RLT2 and AT-RICH INTERACTING DOMAIN5 [ARID5]). We observed that mutants alleles in these genes result in plants with similar phenotypes as *rH4R17A* mutant plants: early flowering, upwardly curled leaves, reduced fertility, and a small size relative to wild-type plants (Figure 5, A–D and Supplemental Figure S9; Li et al., 2012). Defects in the timing of the floral transition and other developmental aspects seen in the *rH4R17A* plants were more similar to those of the single mutant *arid5* defective in the ISWI accessory subunit or in the double mutant *rlt1 rlt2* (*RLT1* and *RLT2* were shown to act redundantly [Li et al., 2012]) than to mutations in the ISWI catalytic subunit genes *CHR11* and *CHR17* (also shown to act redundantly [Li et al., 2012]), which cause more severe developmental phenotypes (Figure 5, A–D and Supplemental Figure S9; Li et al., 2012). The increased severity of the phenotypes displayed by the *chr11 chr17* double mutant may be caused by the joint disruption of the ISWI and SWR1 chromatin-remodeling complexes, which both contain CHR11 and CHR17 (Luo et al., 2020). By contrast, ARID5 and RLT1/RLT2 are present in ISWI, but not in SWR1. In addition, RLT1 and RLT2 are only 2 of 12 DNA binding homeobox and Different Transcription (DDT) factors-domain proteins in Arabidopsis, and different ISWI complexes associate with different DDT-domain proteins in vivo (Dong et al., 2013; Tan et al., 2020).

To further investigate the interplay in plants between H4R17 and ISWI, we performed transcriptome deep sequencing (RNA-seq) analysis on the *rH4R17A*, *arid5*, *rlt1 rlt2*, *chr11 chr17*, and *pie1* (defective in the catalytic subunit of the SWR1 complex PIE1 [PHOTOPERIOD-INDEPENDENT EARLY FLOWERING 1]) mutants grown in short-day conditions. We identified 1,771 downregulated genes and 1,471 upregulated genes in the *chr11 chr17* double mutant (3,242 DEGs in total), while there were only 535 downregulated genes and 299 upregulated genes in the *rH4R17A* #1 mutant line (834 DEGs), and 410 downregulated genes and 375 upregulated genes in the *rH4R17A* #2 mutant line (785 DEGs), relative to wild-type plants (Figure 5E). In spite of the large difference in the total amount of DEGs between *chr11 chr17* mutants and the *rH4R17A* plants, we observed a high overlap between the DEGs in the *chr11 chr17* and *rH4R17A* #1 mutants (45.6%, 380/834), as well as between the DEGs in the *chr11 chr17* and *rH4R17A* #2 mutants (56.0%, 440/785) (Figure 5E). Additionally, we observed a high overlap of DEGs (average 50.0% *rH4R17A* versus *arid5*; average 52.5% *rH4R17A* versus *rlt1 rlt2*) when comparing the *rH4R17A* lines to the ISWI subunit mutants *arid5* and *rlt1 rlt2* (Figure 5, F and G). Furthermore, in the *rH4R17A*, *chr11*

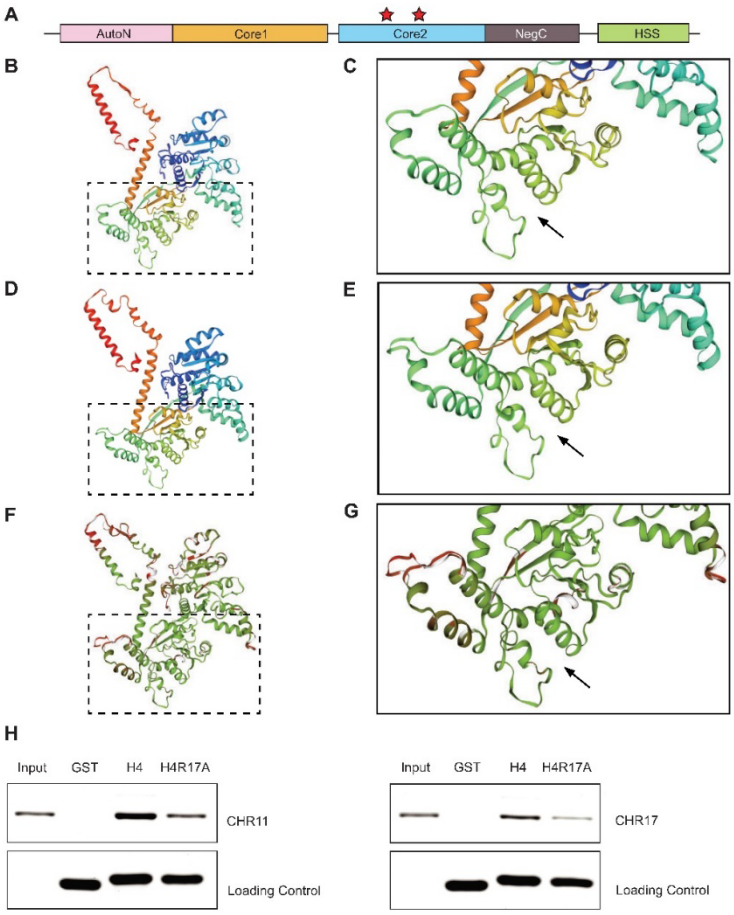

Figure 4 The H4R17A mutation prevents binding by Arabidopsis ISWI enzymes. A, Domain architecture of ISWI. HSS, HAND–SAND–SLIDE; core1, first RecA-like domain; core2, second RecA-like domain. Red stars indicate the residues implicated in binding H4R17 on the second RecA-like ATPase core domain (core2) identified in *M. thermophila* (Yan et al., 2016) and *S. cerevisiae* (Yan et al., 2019). B and C, Homology model of Arabidopsis CHR11 amino acids (aa) 176–706. D and E, Reference structure of *M. thermophila* ISWI (5JXR) aa 173–718. F and G, Superposition of Arabidopsis CHR11 and *M. thermophila* ISWI structures with consistency color scheme (green indicates more consistent and red indicates less consistent). Black arrow denotes the predicted (Arabidopsis) or validated (*M. thermophila*) binding pocket of histone H4 arginine 17 (Yan et al., 2016). The boxed regions are enlarged in (C), (E), and (G). H, In vitro pull-down assay with recombinant GST or GST-tagged histone proteins (H4 or H4R17A) and CHR11 (left) or CHR17 (right).

chr17, *arid5*, and *rlt1 rlt2* mutants, we detected a similar pattern of RNA expression not shared by *rH4* or Col-0 plants, as indicated by the clustering of both *rH4R17A* lines and all ISWI subunit mutants together (Figure 5H). As ARID5 was previously demonstrated to recognize the histone modification H3K4me3 (Tan et al., 2020), we investigated the relationship between DEGs in *rH4R17A* mutants and H3K4me3-enriched genes (Chica et al., 2013) and detected a significant overlap (64.7%, 540/834 for *rH4R17A* #1; 73.0%, 573/785 for *rH4R17A* #2) (Supplemental Figure S10A), further supporting a functional relationship between H4R17 and ARID5. By contrast, we observed a weaker extent of overlap (average 25.8%) between the DEGs identified in *pie1* mutants and the DEGs of *rH4R17A* mutants and we failed to observe similar patterns of RNA expression between *pie* and the *rH4R17A* lines (Figure 5H and Supplemental Figure S10B). Principal component analysis (PC1 and PC2 together explaining 60% of the variance) also indicated similarities between *rH4R17A* and ISWI subunit mutants, while Col-0 and *rH4* plants clustered separately (Supplemental Figure S10C).

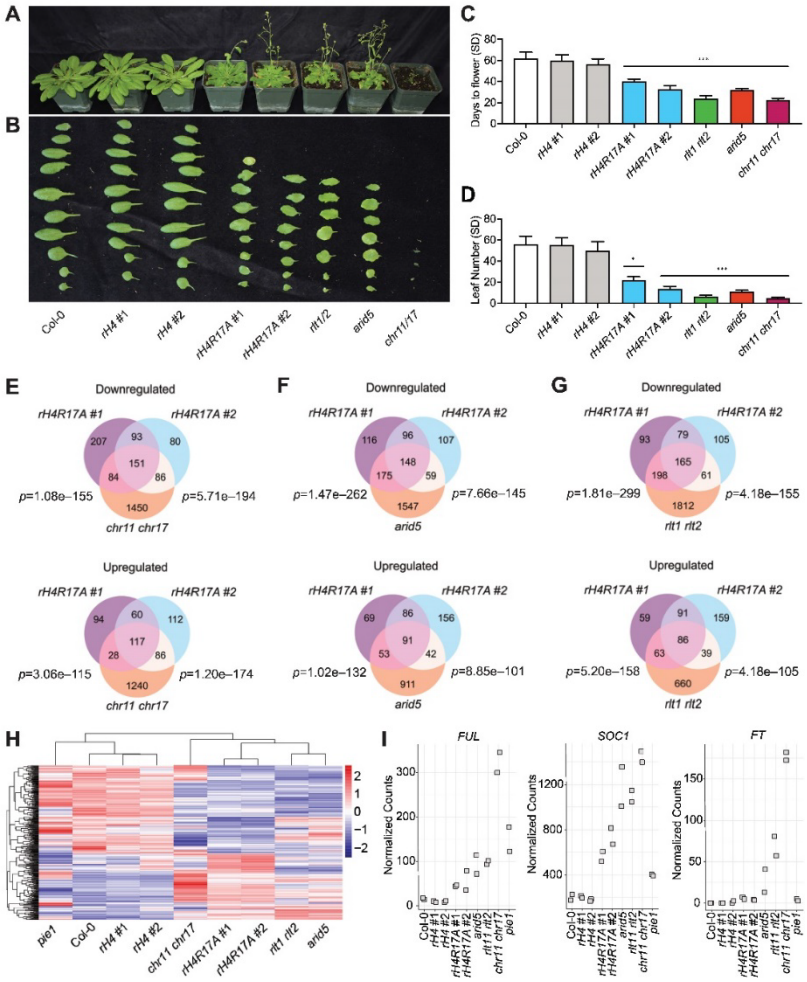

Figure 5 H4R17 and ISWI are functionally related and involved in the regulation of gene expression and plant development. A, Morphological phenotypes of Col-0, *rH4* #1, *rH4* #2, *rH4R17A* #1 and *rH4R17A* #2, *rlt1 rlt2*, *arid5*, and *chr11 chr17* plants grown in short-day conditions for 7 weeks. B, Rosette leaf phenotype of Col-0, *rH4* #1, *rH4* #2, *rH4R17A* #1 and *rH4R17A* #2, *rlt1 rlt2*, *arid5*, and *chr11 chr17* plants. Rosette leaves were cut from plants shortly after bolting in long-day conditions. C and D, Mean days to flower (C) and rosette leaf number (D) at flowering in short-day conditions for Col-0, *rH4* #1, *rH4* #2, *rH4R17A* #1 and *rH4R17A* #2, *rlt1 rlt2*, *arid5*, and *chr11 chr17* plants. Error bars show standard deviation. *$P < 0.01$; **$P < 0.001$; ***$P < 0.0001$, as determined by one-way ANOVA (genotype versus Col-0) with Tukey's HSD post hoc test. $n = 12$. E–G, Venn diagrams showing DEGs (relative to Col-0) identified by RNA-seq in *rH4R17A* and *chr11 chr17* (E), *rH4R17A* and *arid5* (F), and *rH4R17A* and *rlt1 rlt2* plants (G). Statistical analyses were performed using the hypergeometric test, assessing overlap between *rH4R17A* #1 or *rH4R17A* #2 and *chr11 chr17*, *arid5*, or *rlt1 rlt2* mutants, respectively (left *P*-value represents *rH4R17A* #1 versus ISWI subunit mutant and right *P*-value represents *rH4R17A* #2 versus ISWI subunit mutant). H, Heatmap representation of relative expression levels of shared DEGs identified in the *rH4R17A* #1 and *rH4R17A* #2 lines. Legend represents scaled Z-score of normalized read counts. Clustering of rows and columns was calculated using Euclidean distance. I, Normalized read counts for *FUL*, *SOC1*, and *FT* in Col-0, *rH4* #1, *rH4* #2, *rH4R17A* #1 and *rH4R17A* #2, *arid5*, *rlt1 rlt2*, *chr11 chr17*, and *pie1* plants.

We then investigated the expression of key flowering time regulatory genes and found that the flowering promoter genes *FRUITFULL* (*FUL*), *SOC1*, and *FT* are all co-upregulated in the *rH4R17A*, *rlt1 rlt2*, *arid5*, and *chr11 chr17* backgrounds (Figure 5I and Supplemental Figure S10D). We did not observe these patterns of co-expression when comparing *rlt1*

rlt2, *arid5*, and *chr11 chr17* mutants to *rH4* plants (Figure 5, H and I and Supplemental Figure S10D). We also performed Gene Ontology (GO) term enrichment analysis and identified multiple additional biological pathways co-regulated by H4R17 and ISWI, including flavonoid metabolism and biosynthesis, pattern specification, specification of symmetry, morphogenesis, the ultraviolet (UV) response pathway, and the regulation of cell death (Supplemental Figure S11 and Supplemental Data Set S1). The shared developmental phenotypes and transcriptional profiles of the *rH4R17A*, *rlt1 rlt2*, *arid5*, and *chr11 chr17* mutants suggest that H4R17 plays an important role in plants as in other eukaryotes in regulating the activity of ISWI on chromatin.

Effects of the H4R17A mutation on global nucleosome positioning

ISWI functions as a chromatin remodeling complex that properly organizes nucleosome spacing at transcriptionally active genes in eukaryotes (Clapier and Cairns, 2009; Gkikopoulos et al., 2011; Yadon and Tsukiyama, 2011; Li et al., 2014). Due to the similarity in the phenotypes and transcriptional profiles between *rH4R17A* plants and mutants in the Arabidopsis ISWI complex, we hypothesized that the expression of *H4R17A* interferes with nucleosome spacing in plants. To address this hypothesis, we assessed global nucleosome positioning in *rH4R17A* mutants using micrococcal nuclease digestion followed by deep sequencing (MNase-seq). Consistent with previous results, we detected a relatively lower nucleosome density in the 1-kb region upstream of the transcription start site (TSS) of protein-coding genes, and a relatively high, evenly spaced distribution of nucleosomes in the 1-kb region downstream of the TSS for Col-0 plants (Figure 6A and Supplemental Figure S12A; Li et al., 2014). Moreover, we observed that expressed protein-coding genes generally displayed more highly phased nucleosome arrays in the gene body and a sharper peak of nucleosome-free DNA in the promoter when compared with nonexpressed protein-coding genes, in line with previous studies (Figure 6, B and C and Supplemental Figure S12B; Li et al., 2014; Zhang et al., 2015). In terms of the different genotypes analyzed, *rH4* plants displayed highly similar nucleosome positioning patterns to those of Col-0, as expected. By contrast, while *rH4R17A*, *arid5*, and *rlt1 rlt2* mutants showed the same general pattern of lower nucleosome density upstream of the TSS and high nucleosome density downstream of the TSS, these genotypes all exhibited a reduction of evenly spaced nucleosome distributions in the gene body (Figure 6A and Supplemental Figure S12A), similar to the pattern reported for the *chr11 chr17* mutant (Li et al., 2014). Additionally, we analyzed the nucleosome distribution patterns at genes with expression changes in *rH4R17A*, *chr11 chr17*, *rlt1 rlt2*, and/or *arid5* mutants as well as genes without expression changes in these mutants. We determined that the nucleosome distribution patterns at DEGs and non-DEGs are both affected in *rH4R17A*, *arid5*, and *rlt1 rlt2* mutants (Figure 6, D and E and Supplemental Figure S12C and D), in line with previously published MNase-seq results for the *chr11 chr17* mutant (Li et al., 2014). Additionally, nucleosome distribution patterns at DEGs were affected in *rH4R17A*, *arid5*, and *rlt1 rlt2* mutants regardless of whether the expression of these genes was upregulated or downregulated (Figure 6, F and G). To provide a more quantitative assessment of nucleosome spacing in our assays, we calculated the average change in nucleosome occupancy at the +2 through +6 nucleosome peaks as a measure of nucleosome phasing. This analysis confirmed that the *rH4R17A*, *arid5*, and *rlt1 rlt2* mutations cause a significant reduction in regular nucleosome phasing in gene bodies (Figure 6, H–N). Taken together, these results indicate that H4R17 positively regulates the action of the ISWI complex to establish nucleosome arrays in protein-coding genes.

Discussion

A novel system for studying histone function in plants

In this study, we present a new histone replacement system that facilitates the analysis of histone H4 functions in plants. Our results serve as a proof-of-concept that complete histone replacement systems can be rapidly established in Arabidopsis. In the future, this approach may be applied to generate similar systems to study the functions of different histones or histone variants. The histone replacement system developed in this study for histone H4 will supplement already existing systems in yeast and Drosophila to offer new biological insights into the roles of H4 in plants. Our methodology provides extensive coverage of *H4* mutants in a multicellular eukaryote, as the histone replacement system generated in Drosophila has only been used to generate 14 *H4* point mutants (Zhang et al., 2019), compared with the 63 *H4* point mutants generated with our system, which have been made available through the Arabidopsis Biological Resource Center (ABRC).

This collection of *H4* point mutants has revealed a multitude of roles for H4 residues in plants. For example, six separate *H4* point mutations located in the globular domain appeared to cause lethality. Many of the equivalent mutations also cause lethality or reduced sporulation efficiency in yeast (Dai et al., 2008; Govin et al., 2010), revealing insights into the effect of these mutations on chromatin. One possibility is that the H4R40A and H4R45A substitutions disrupt the nucleosome entry site, which is highly sensitive to mutations that affect DNA wrapping around the nucleosome (Zhou et al., 2019). Additionally, H4R78A and H4K79A reside on the low sporulation patch identified in yeast (Govin et al., 2010), a region that lies in close proximity to contact sites with the DNA and has been demonstrated to affect meiosis. Similar functions could also result in the early flowering phenotypes observed for certain H4 globular domain mutants (e.g. *H4R35*, *H4R36*, *H4R39*, and *H4K44*, whose corresponding amino acid positions reside on the nucleosome entry site while that of *H4T80* is located on the low

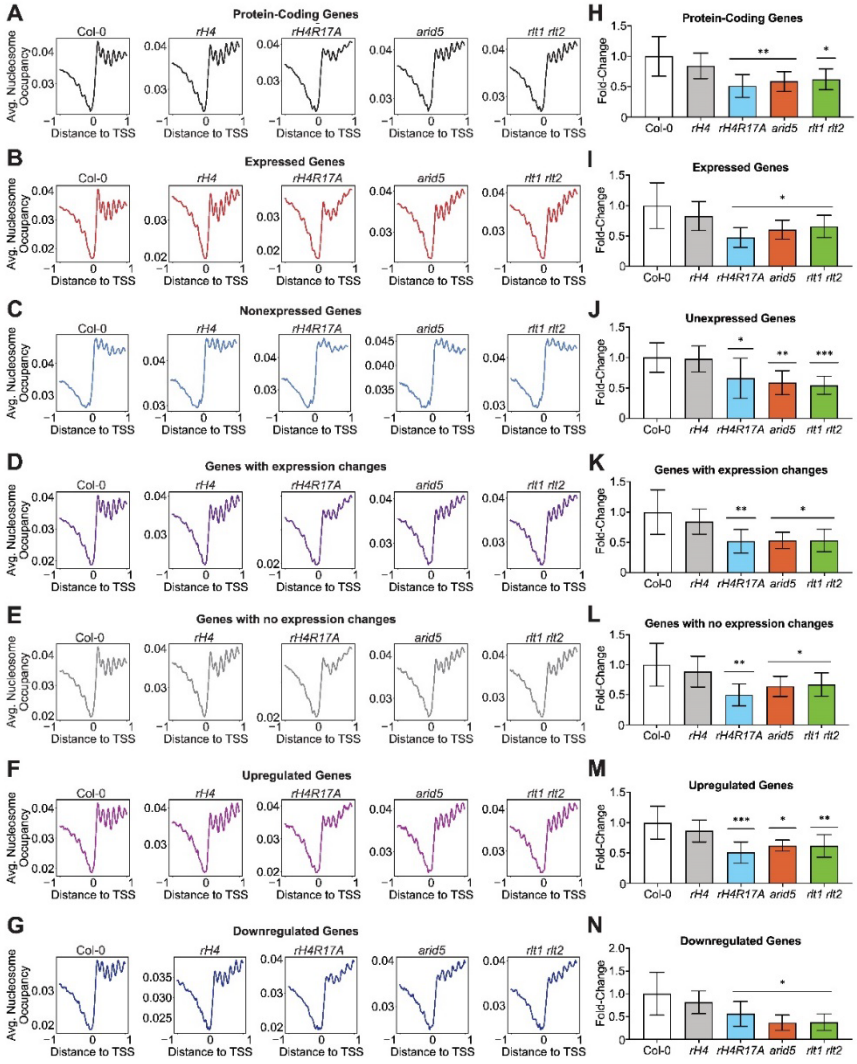

Figure 6 Determination of H4R17 function on regulating nucleosome positioning. A–G, Average nucleosome occupancy relative to the TSS (in kb) of all protein-coding genes (A), expressed protein-coding genes (B), non-expressed protein-coding genes (C), genes with expression changes in *rH4R17A*, *arid5*, *rlt1 rlt2*, and/or *chr11 chr17* mutants (D), genes with no expression changes in *rH4R17A*, *arid5*, *rlt1 rlt2*, and/or *chr11 chr17* mutants (E), upregulated genes (F) and downregulated genes (G) in *rH4R17A*, *arid5*, *rlt1 rlt2*, and/or *chr11 chr17* mutants. The MNase-seq results were generated from two independent biological replicates and RNA-seq data were obtained from the same tissues used for MNase-seq. Cutoffs were defined as follows: Expressed $\geq$0.5 TPM; nonexpressed $<$0.5 TPM. Genes with expression changes were defined as $>\pm$1.5-fold versus Col-0 and genes with no expression changes were defined as $<\pm$1.1-fold versus Col-0. H–N, Fold-change in Δnucleosome occupancy of +2 through +6 nucleosome peaks relative to Col-0 corresponding to all protein-coding genes (H), expressed protein-coding genes (I), unexpressed protein-coding genes (J), genes with expression changes in *rH4R17A*, *arid5*, *rlt1 rlt2*, and/or *chr11 chr17* mutants (K), genes with no expression changes in *rH4R17A*, *arid5*, *rlt1 rlt2*, and/or *chr11 chr17* mutants (L), upregulated genes (M) and downregulated genes (N) in *rH4R17A*, *arid5*, *rlt1 rlt2*, and/or *chr11 chr17* mutants. Error bars show standard deviation. *$P < 0.05$; **$P < 0.005$; ***$P < 0.0005$, as determined by paired Student's *t* test.

sporulation patch). In this way, experiments in plants build on knowledge gathered from other model systems to elucidate how histone residues regulate chromatin function.

Our CRISPR-based strategy to replace endogenous histones offers several advantages over other methods that can potentially be used to achieve complete histone replacement. For example, the successful generation of the *H4* septuple mutant in two generations in this work demonstrates that multiplex CRISPR/Cas9 can be used to efficiently inactivate many histone genes in plants (LeBlanc et al., 2017). Using CRISPR/Cas9 greatly reduces the amount of time and resources required to generate a histone depletion background, especially when compared with crossing individual histone mutants. The presence of tandem duplicated copies of histone genes (e.g. the *H3.1* genes At5g10390 and At5g10400) can also preclude using traditional crossing schemes to generate backgrounds lacking a specific histone or histone variant. In addition, deploying multiplex CRISPR/Cas9 to inactivate endogenous histones will allow researchers to rapidly re-establish histone replacement systems in a particular mutant background, for example, to screen for point mutations in histones that enhance or suppress a phenotype of interest. Another advantage of our histone H4 replacement strategy is that we consistently observed high expression of the *H4* replacement gene, which rescues the morphological phenotype of the *H4* septuple background in all of our T_1 plants (Figure 1, A–C). Several factors could contribute to this phenomenon. While T-DNA integration into the Arabidopsis genome occurs randomly, a requirement for minimal *H4* expression appears to shift the recovery of T-DNA insertions into more transcriptionally active chromatin regions (Koncz et al., 1989; Brunaud et al., 2002; Szabados et al., 2002; Alonso et al., 2003; Kim et al., 2007). Moreover, dosage compensation mechanisms acting to upregulate the expression of the endogenous histone *H4* gene At3g53730, as seen in this study (Figure 1C), may also act on the histone *H4* replacement gene, as the expression of both of these genes is driven by the At3g53730 promoter. Histone dosage compensation has also been observed in the histone replacement systems implemented in the multicellular eukaryote Drosophila (McKay et al., 2015; Zhang et al., 2019). These histone dosage compensation mechanisms may be related to the recently described process of transcriptional adaptation, in which mutant mRNA decay causes the upregulation of related genes (El-Brolosy et al., 2019; Serobyan et al., 2020). For both of the above reasons, transgenic plants lacking endogenous H4 proteins are observed, and therefore, *rH4* plants expressing exclusively mutant histones can predictably be obtained using our strategy.

Several changes may be implemented to improve future histone replacement systems in Arabidopsis and other plants. To control for differential effects caused by random T-DNA integration (Gelvin, 2017), in this study we characterized two independent transgenic lines expressing each *H4* replacement construct. Ideally, gene targeting would be utilized to introduce the *H4* mutations directly at an endogenous histone *H4* locus. While gene targeting technologies in plants relying on homologous recombination currently have very low efficiency compared with yeast and animals, as additional improvements in gene targeting are developed, in situ histone replacement systems in plants analogous to platforms already existing in yeast and Drosophila may also become feasible. Additionally, more precise control over the dosage of the replacement histone could also serve to improve this method. It was recently shown that while yeast histone replacement systems utilizing single-copy integrated histone genes expressing certain mutant histones cannot survive, the addition of a second copy of the mutant histone gene rescues this lethality (Jiang et al., 2017). In the system described here, we utilized a single endogenous histone *H4* gene as the *H4* replacement gene, rather than generating eight histone *H4* replacement constructs corresponding to each endogenous histone *H4* gene present in the Arabidopsis genome. While we observed that our *rH4* plants appear morphologically wild type due to high *H4* expression, it may be important to study the function of the other endogenous *H4* genes, or the requirement for Arabidopsis to have eight copies of the *H4* genes in its genome. Although labor-intensive, future strategies simultaneously using multiple endogenous *H4* genes as *H4* replacement genes could therefore be more reflective of the H4 supply available to wild-type plants.

H4R17 regulates nucleosome remodeling and developmental processes in plants

This study uncovered a role for H4R17 in regulating multiple developmental processes in Arabidopsis, including leaf development, fruit development, and flowering. Our findings suggest that this role for H4R17 is not mediated via PTM of this residue. Based on our results, we propose a model similar to that of animal systems where H4R17 regulates developmental processes in plants through its regulation of the ISWI complex (Figure 7; Hamiche et al., 2001; Clapier et al., 2001, 2002; Fazzio et al., 2005; Dann et al., 2017). In wild-type plants, H4R17 positively regulates the ISWI complex to slide nucleosomes and adequately establish the nucleosome positioning patterns in the gene bodies of protein-coding genes (Figure 7). In *rH4R17A* mutant plants however, the positive regulation of ISWI by histone H4 is impaired so that evenly spaced nucleosome distributions are no longer observed in gene bodies. The altered nucleosome positioning patterns in gene bodies and the large-scale transcriptional changes in turn cause the observed pleiotropic developmental phenotypes. Interestingly, while transcription and nucleosome positioning have been shown to be highly interconnected (Workman and Kingston, 1998; Jiang and Pugh, 2009; Hughes et al., 2012; Struhl and Segal, 2013), we and others have observed that mutations in H4R17 and plant ISWI complex subunits affect nucleosome positioning patterns in both differentially and non-DEGs (Li et al., 2014). Our results support previous work demonstrating that it is unlikely that the nucleosome positioning defects in ISWI

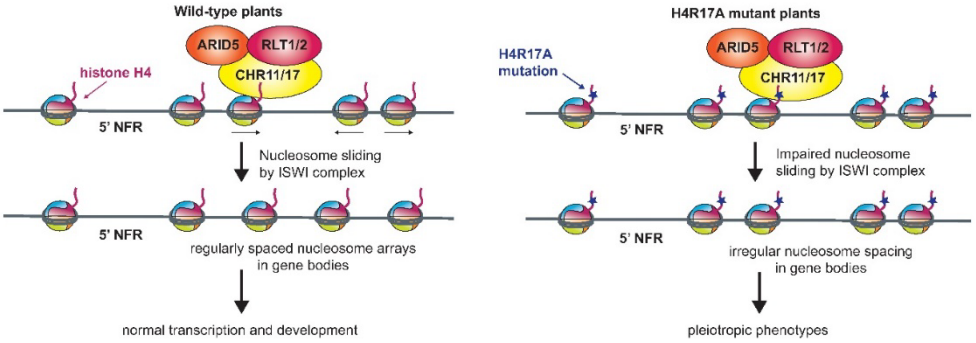

Figure 7 Model for the role of H4R17 in plants. Proposed model for the role of histone H4 arginine 17 in the regulation of ISWI complexes in Arabidopsis. 5′-NFR, 5′-nucleosome-free region.

mutants are caused by the transcriptional changes observed in these backgrounds (Li et al., 2014; Luo et al., 2020). Moreover, our results are consistent with the idea that many factors on top of nucleosome positioning in gene bodies affect the transcription levels of a gene, and thus in some cases, altered genic nucleosome positioning appears to majorly affect transcription, while in others, little change is observed (Jiang and Pugh, 2009; Bai and Morozov, 2010). Additionally, processes related to genetic robustness may also serve to counteract transcriptional fluctuations due to perturbations of nucleosome positioning (Masel and Siegal, 2009). For these reasons, we observed independence between the nucleosome positioning and transcriptional phenotypes of *rH4R17A* and mutants in ISWI components. While we cannot exclude the possibility that H4R17 interacts with other chromatin-associated factors to induce certain phenotypes when mutated, our genetic and biochemical evidence strongly supports our proposed model.

ISWI chromatin-remodeling complexes contain between two and four subunits in eukaryotes, consisting of a conserved ATPase catalytic subunit and at least one accessory subunit (Corona and Tamkun, 2004; Clapier and Cairns, 2009; Aydin et al., 2014). Multiple types of ISWI complexes have been identified in animals, and the different accessory subunits in these complexes have been proposed to modulate the activity of the shared catalytic subunit as well as the specificity and target recognition of the complex (Lusser et al., 2005; Aydin et al., 2014; Toto et al., 2014). In plants, three types of ISWI complexes have been identified: the plant-specific CHR11/CHR17-RLT1/RLT2-ARID5 (CRA)-type complex, the CHR11/CHR17-DDP1/2/3-MSI3 (CDM)-type complex, and the CHR11/CHR17-DDR1/3/4/5-DDW1 (CDD)-type complex (Tan et al., 2020). In addition, the shared ISWI catalytic subunits CHR11 and CHR17 were also recently demonstrated to act as accessory subunits of the SWR1 chromatin remodeling complex in plants (Luo et al., 2020). We observed that *rH4R17A* mutants exhibited less severe transcriptional defects than *arid5*, *rlt1 rlt2*, or *chr11 chr17* mutants. One explanation for this result is that the *rH4R17A* mutation could affect the action of all types of ISWI complexes in plants without completely abolishing their function, while the *arid5* and *rlt1 rlt2* mutations could have a more severe influence on only one specific type of ISWI complex (i.e. the CRA-type complex). For example, as ARID5 recognizes H3K4me3 (Tan et al., 2020), it may play a role in directing the ISWI complex to a specific subset of genes, and thus mutation of ARID5 could cause the mislocalization of the ISWI complex. These different mechanisms of action of the *rH4R17A* and ISWI accessory subunit mutations could induce the differing gene expression and nucleosome positioning phenotypes that we observed. Further characterization of the different ISWI complexes in plants, including their different targeting specificities to chromatin loci and the impact of the other identified CDM-type and CDD-type complexes on the regulation of global transcription and nucleosome positioning, will contribute to elucidating their specific consequences on chromatin regulation.

Materials and methods

Plant materials

All Arabidopsis (*A. thaliana*) plants were derived from the Columbia-0 (Col-0) accession and were grown in Pro-Mix BX Mycorrhizae soil under cool-white fluorescent lights (approximately 100 μmol m^{-2} s^{-1}). Seeds were surface-sterilized with a 70% (v/v) ethanol, 0.1% (v/v) Triton X-100 solution for 5 min, and then with 95% (v/v) ethanol for 1 min. Seeds were spread on sterilized paper, air-dried, and plated on half-strength Murashige–Skoog (MS) plates. Seeds were stratified in the dark at 4°C for 2–4 days, transferred to the growth chamber for 5 days, and then transplanted to soil. Plants were grown in long-day conditions (16-h light/8-h dark) or short-day conditions (8-h light/16-h dark), as indicated.

The *chr11* (GK-424F01) *chr17* (GK-424F04) double mutant was described previously (Li et al., 2012). The *fas1-4* (SAIL_662_D10), *arid5* (SALK_111627), *prmt7-1* (SALK_028160), and *prmt7-2* (SALK_039529) T-DNA insertion mutants were obtained from the ABRC. The *pie1* T-DNA insertion mutants were initially obtained from ABRC (SALK_096434) and the *pie1* mutants used in this study were seeds collected from homozygous *pie1* plants. The *rlt1* (SALK_099250) *rlt2* (SALK_132828) double mutant was generated by crossing. Due to severely reduced fertility, *chr11 chr17* and *arid5* mutants were maintained in a heterozygous state. All newly generated mutant lines are described in Supplemental Data Set S2.

Generation of transgenic Arabidopsis plants

Binary vectors were transformed into Agrobacterium (*A. tumefaciens*) strain GV3101, using heat shock; plants were transformed using the floral dip procedure as described previously (Clough and Bent, 1998). Transgenic plants for generation of the *H4* septuple mutant were selected on half-strength MS plates containing 1% (w/v) sucrose, carbenicillin (200 μg mL^{-1}), and kanamycin (100 μg mL^{-1}). Transgenic rH4 plants were selected on half-strength MS plates containing 1% (w/v) sucrose, carbenicillin (200 μg mL^{-1}), and glufosinate ammonium (25 μg mL^{-1}). Plants were subjected to heat stress treatments as described previously (LeBlanc et al., 2017). The plants were grown continuously at 22°C thereafter.

Scoring of flowering time, rosette leaf number, and rosette size

Days to flower were measured when a 1-cm bolting stem was visible. The number of rosette leaves was determined at the day of flowering. Rosette area was measured using the ARADEEPOPSIS workflow (Huther et al., 2020).

Dimensionality reduction and clustering

For flowering time data, principal component analysis of four variables (day number in long days, leaf number in long days, day number in short days, and leaf number in short days) was performed. We centered variables at mean 0 and set the standard deviation to 1. *k*-Means clustering was performed 40 times with random initializations on the first two principal components to identify three clusters. For RNA-seq data, principal component analysis of the 200 most variable DEGs in *rH4R17A* #1 and *rH4R17A* #2 lines was performed as described above. Analyses were executed in RStudio with R version 3.6.1 (R Development Core Team, 2018).

Plasmid construction

CRISPR constructs used to generate the *H4* septuple mutant were inserted into the pYAO-Cas9-SK vector as described previously (Yan et al., 2015).

The *H4* replacement plasmid was made by amplifying the promoter (from 967 bp upstream of the start codon to the start codon), gene body, and terminator (up to 503 bp downstream of the stop codon) of H4 (At3g53730) into pENTR/D (ThermoFisher Scientific, Waltham, MA, USA). Site-directed mutagenesis of *H4pro:H4* in pENTR/D was first performed using QuikChange II XL (Agilent Technologies, Santa Clara, CA, USA) to create plasmids with 10 silent mutations in the *H4* coding sequence. These silent mutations were engineered to test the resistance of the *H4* replacement gene against multiple sgRNAs. Additional site-directed mutagenesis of this vector was performed to generate a library of 63 *H4* point mutant genes.

Each *H4pro:H4* sequence was then transferred into the binary vector pB7WG, containing the *H4* sgRNA, using Gateway Technology. The binary vector pB7WG containing the *H4* sgRNA was generated as follows: The *AtU6-26*-sgRNA vector containing the sgRNA targeting *H4* (At3g53730) was first digested with the restriction enzymes SpeI and NheI, and the digestion products were run on a 1% (w/v) agarose gel. The band containing the *H4* sgRNA was then cut out and ligated into the binary vector pB7WG, which had been digested with the restriction enzyme SpeI.

The *PRMT7* overexpression construct was created by cloning the *PRMT7* genomic coding region (from ATG to stop codon, including introns) into pDONR207, and then subcloning the gene into pMDC32 (Curtis and Grossniklaus, 2003).

Constructs for the production of recombinant protein were generated as follows: Using the NdeI and BamHI restriction sites, the coding sequences of *H4* (aa 1–30) were cloned into pET28-Mff(1-61)-PP-GST (Addgene plasmid #73042; provided by D. Chan) and fused with a C-terminal glutathione-*S*-transferase (GST) tag (Davarinejad et al., 2022). Site-directed mutagenesis was used to create the H4R17A mutation (QuikChange II XL, Agilent Technologies). The coding sequences of *CHR11* (encoding fragment aa 409–750) and *CHR17* (encoding fragment aa 414–753) were cloned into the pET32a vector using the BamHI and SalI restriction sites.

DNA extraction, PCR, and sequencing analyses

Genomic DNA was extracted from Arabidopsis plants by grinding one leaf in 500 μL of extraction buffer (200 mM Tris–HCl pH 8.0, 250 mM NaCl, 25 mM ethylenediaminetetraacetic acid [EDTA] and 1% [w/v] SDS). Phenol/chloroform (50 μL) was added and tubes were vortexed, followed by centrifugation for 10 min at 3,220 × *g* at room temperature. The supernatant was transferred to a new tube and 70 μL of isopropanol was added, followed by centrifugation for 10 min at 3,200 × *g* at room temperature. The supernatant was removed and the DNA pellets were resuspended in 100 μL water.

PCR products were sequenced and analyzed using Sequencher 5.4.6 (Gene Codes Corporation, Ann Arbor, MI, USA) to identify CRISPR-induced mutations. To assess the rate of mutation of the remaining endogenous *H4* gene (At3g53730) in *rH4* plants by the sgRNA in the *H4* replacement plasmid, endogenous *H4* PCR products were cloned into TOPO TA cloning vectors (Invitrogen, Carlsbad, CA,

USA). Ten to sixteen individual clones corresponding to each plant were sequenced.

RT-qPCR

Total RNA was extracted from 18-day-old leaves from plants grown in long-day conditions with TRIzol (Invitrogen) and DNase I-treated using RQ1 RNase-Free DNase (Promega, Madison, WI, USA). Three biological replicates (different plants sampled simultaneously) were assessed. SuperScript II Reverse Transcriptase (Invitrogen) was used to generate first-strand cDNA from 1 μg of DNAse I-treated total RNA. Reverse transcription was initiated using random hexamers (Applied Biosystems, Foster City, CA, USA). Quantification of cDNA was done by qPCR using a CFX96 Real-Time PCR Detection System (Bio-Rad, Hercules, CA, USA) with KAPA SYBR FAST qPCR Master Mix (2×) Kit (Kapa Biosystems, Wilmington, MA, USA). Relative transcript levels were determined by using the comparative C_t method as follows: Relative quantity = $2^{(-((Ct\ GOI\ unknown - Ct\ normalizer\ unknown) - (Ct\ GOI\ calibrator - Ct\ normalizer\ calibrator)))}$, where GOI is the gene of interest (Livak and Schmittgen, 2001). *Actin* was used as reference transcript for normalization.

Recombinant protein production

To produce the recombinant proteins AtCHR11, AtCHR17, and the histone-GST fusion proteins, the Rosetta (DE3) *Escherichia coli* strain (#70954, Sigma, St. Louis, MO, USA) was used. The bacteria were grown in LB medium and protein production was induced with 1 mM IPTG (final concentration). To purify recombinant CHR11 and CHR17, with each protein harboring an N-terminal Trx-His-S tag and a C-terminal His tag, the cell pellets were first resuspended in NPI-10 buffer (50 mM NaH_2PO_4, 300 mM NaCl, 10 mM imidazole, pH 8) containing 1 mM PMSF and then sonicated. After centrifugation, the supernatant was passed through a Ni-NTA agarose column. The column was then washed with NPI-20 buffer (50 mM NaH_2PO_4, 300 mM NaCl, 20 mM imidazole, pH 8.0) and the recombinant proteins were eluted with NPI-250 buffer (50 mM NaH_2PO_4, 300 mM NaCl, 250 mM imidazole, pH 8.0). For purification of histone-GST proteins, the cell pellets were resuspended in 1× phosphate-buffered saline (PBS, 137 mM NaCl, 10 mM phosphate buffer pH 7.4, 2.7 mM KCl) with 1 mM PMSF before sonification and centrifugation. The supernatant was passed over a glutathione Sepharose 4B column and the bound proteins were washed with 1× PBS before being eluted with EB buffer (50 mM Tris–HCl pH 8.0, 50 mM NaCl, 30 mM reduced L-glutathione, 10% glycerol). The proteins were divided into aliquots and kept at −80°C.

In vitro binding assays

Four micrograms of recombinant CHR11 or CHR17 was combined with 4 μg of GST or GST-tagged histone proteins in 400 μL of binding buffer (25 mM Tris–HCl pH 8.0, 250 mM NaCl, 0.05% [v/v] NP-40) and incubated at 4°C for 12 h for the binding assay. Each tube received 20 μL of prewashed glutathione Sepharose 4B agarose beads, which were incubated for 30 min to draw down the GST-tagged histone proteins. The beads were washed twice with 1 mL of binding buffer, with rotation for 5 min at 4°C between washes. After the final wash, 15 μL of 2× SDS loading buffer was added to each tube and the proteins were eluted by boiling at 95°C for 5 min. A 10% (w/v) SDS–PAGE gel was used to separate the samples. The GST or GST-tagged histone N-terminal tail proteins were visualized on the gel using Coomassie staining.

Preparation of sequencing libraries

RNA-seq and MNase-seq libraries were prepared at the Yale Center for Genome Analysis (YCGA). For the analysis of the *H4* septuple mutant and *fas1-4* plants, unopened flowers from 6-week-old plants grown in long-day conditions were frozen in liquid nitrogen, ground with a pestle, and then RNA was extracted using a Direct-zol RNA Miniprep Plus Kit (Zymo Research, Irvine, CA, USA). For each biological replicate, pooled tissue collected simultaneously from three different plants was used. RNA quality was assessed with an Agilent Bioanalyzer 5300 using a DNF-471 RNA kit (Agilent) (Supplemental Figure S13A). For library preparation, mRNA was purified from 500 ng of total RNA with oligodT beads and sheared by incubation at 94°C in the presence of magnesium (KAPA mRNA HyperPrep). Following first-strand cDNA synthesis with random primers, second strand synthesis and A-tailing were performed with dUTP for generating strand-specific sequencing libraries. Adapter ligation with 3′ dTMP overhangs was ligated to library insert fragments. The library was then amplified to obtain fragments carrying the appropriate adapter sequences at both ends. Strands marked with dUTP were not amplified. Indexed libraries that met appropriate cut-offs for both for titer and quality were quantified by qPCR using a commercially available kit (KAPA Biosystems); insert size distribution was determined with LabChip GX or Agilent Bioanalyzer.

For the analysis of *rH4* #1, *rH4* #2, *rH4R17A* #1, *rH4R17A* #2, *arid5*, *rlt1 rlt2*, *chr11 chr17*, and *pie1* plants, leaves of 4-week-old plants grown in short-day conditions were frozen in liquid nitrogen, ground with a pestle, and then total RNA was extracted using an RNeasy Plant Mini Kit (Qiagen, Hilden, Germany). For each biological replicate, pooled leaf tissue collected simultaneously from three different plants was used. RNA quality was confirmed through analysis on an Agilent Bioanalyzer 2100 with an RNA Nano chip (Supplemental Figure S14). Library preparation was performed using an Illumina TruSeq Stranded Total RNA kit with Ribo-Zero for plant in which samples were normalized with a total RNA input of 1 μg and library amplification was carried out with eight PCR cycles.

MNase-digested DNA was collected as described previously (Pajoro et al., 2018) with the following modifications: 2 g of leaves from 4-week-old plants grown in short-day conditions was ground in liquid nitrogen and resuspended in 20 mL of lysis buffer for 15 min at 4°C. The resulting slurry was filtered through a 40-μm cell strainer into a 50-mL tube. Samples were centrifuged for 20 min at 3,200 ×*g* at 4°C.

The resulting pellets were resuspended in 10 mL of HBB buffer (25 mM Tris–HCl, pH 7.6, 0.44 M sucrose, 10 mM $MgCl_2$, 0.1% [v/v] Triton-X, and 10 mM β-mercaptoethanol) and centrifuged for 10 min at 1,500 × *g* at 4°C. Pellets were successively washed in 5 mL wash buffer and 5 mL reaction buffer. MNase-seq library preparation was performed using the KAPA Hyper Library Preparation kit (KAPA Biosystems, Part#KK8504). For each biological replicate, pooled leaf tissue collected simultaneously from three different plants was used. Libraries were validated using Agilent Bioanalyzer 2100 Hisense DNA assay and quantified using the KAPA Library Quantification Kit for Illumina Platforms kit. Sequencing was done on an Illumina NovaSeq 6000 using the S4 XP workflow.

RNA-seq processing and analysis

Two independent biological replicates for Col-0, *rH4* #1, *rH4* #2, *rH4R17A* #1, *rH4R17A* #2, *arid5*, *rlt1 rlt2*, *chr11 chr17*, and *pie1* were sequenced. Paired-end reads were filtered and trimmed using Trim Galore! (version 0.5.0) with default options for quality (https://github.com/FelixKrueger/TrimGalore). The resulting datasets were aligned to the Araport11 genome (Cheng et al., 2017) using STAR (version 2.7.2a) allowing two mismatches (–outFilterMismatchNmax 2) (Dobin et al., 2013). Statistics for mapping and coverage of the RNA-seq data are provided in Supplemental Data Set S3. Protein-coding genes were defined as described in the Araport11 genome annotation (Cheng et al., 2017). The program featureCounts (version 1.6.4) (-M –fraction) (Liao et al., 2014) was used to count the paired-end fragments overlapping with the annotated protein-coding genes. Differential expression analysis of protein-coding genes was performed using DESeq2 version 1.26 (Love et al., 2014) on raw read counts to obtain normalized fold-changes and *Padj*-values for each gene. Genes were considered to be differentially expressed if they showed $>\pm$2-fold-change and *Padj*-value <0.05. DEGs are described in Supplemental Data Set S4. Venn diagrams, correlation plots, and correlation matrices were plotted using RStudio with R version 3.6.1 (R Development Core Team, 2018). Heatmaps were plotted with the pheatmap package (version 1.0.12) in RStudio using default clustering parameters on rows and columns. Consistency between biological replicates was assessed by Spearman correlation using deepTools2 (version 2.7.15) (Supplemental Figures S13B and S15; Ramirez et al., 2016). deepTools2 was used to generate bam coverage profiles for visualization with Integrative Genomics Viewer version 2.8.9 (Robinson et al., 2011). The enrichGO method of clusterProfiler (version 3.14.3) was used for GO term enrichment analysis (ont = "BP," *P*-value cut-off = 0.05, *q*-value cut-off = 0.10). Hypergeometric tests were performed using the phyper function of R. H3K4me3-enriched genes were defined from a previously published ChIP-seq dataset gathered from wild-type plants grown in short-day conditions at the 17-leaf stage (Chica et al., 2013)

MNase-seq processing and analysis

Two independent biological replicates for Col-0, *rH4* #2, *rH4R17A* #1, *arid5*, and *rlt1 rlt2* were sequenced. Paired-end reads were filtered and trimmed using Trim Galore! (version 0.5.0) with default options for quality (https://github.com/FelixKrueger/TrimGalore). Bowtie2 version 2.4.2 (Langmead and Salzberg, 2012) was used to align the reads to the Araport11 genome (Cheng et al., 2017) with the –very-sensitive parameter. Statistics for mapping and coverage of the MNase-seq data are provided in Supplemental Data Set S3. Duplicate reads were removed using Picard toolkit version 2.9.0 (Toolkit, 2019) (MarkDuplicates with *REMOVE_DUPLICATES=true*) and the insertion size was filtered to be between 140 bp and 160 bp using SAMtools version 1.11 (Li et al., 2009). The average nucleosome occupancy corresponding to the regions 1 kb upstream and downstream of the TSS of all protein-coding genes was calculated using the bamCoverage (–MNase parameter specified) and computeMatrix functions of deepTools2 version 2.7.15 (Ramirez et al., 2016). Normalization was performed by scaling with the effective library size calculated by the calcNormFactors function using edgeR version 3.28.1 (Robinson et al., 2010). Consistency between biological replicates was confirmed by Spearman correlation using deepTools2 (Supplemental Figure S16). Fold-change in ΔNucleosome Occupancy of +2 through +6 nucleosome peaks relative to Col-0 was calculated with a custom Python script (https://github.com/etc27/MNaseseq-workflow/analysis/peak_height) as follows: ΔNucleosome Occupancy = peak maximum – (5′ peak minimum + 3′ peak minimum)/2.

Model building

The homology model for Arabidopsis CHR11 (aa 176-706) was built with Swiss-Model against the *M. thermophila* ISWI reference structure (5JXR) (Biasini et al., 2014; Yan et al., 2016).

Primers

All primers used in this study are listed in Supplemental Data Set S5 (Wu et al., 2008; Richter et al., 2019; Dong et al., 2021).

Statistical analyses

Statistical analysis data are provided in Supplemental Data Set S6. In general, we used unpaired *t* test and one-way ANOVA with Tukey's HSD post hoc test for statistical analyses.

Accession numbers

Accession numbers of genes reported in this study are: At3g53730 (*H4*), At1g07660 (*H4*), At1g07820 (*H4*), At2g28740 (*H4*), At3g45930 (*H4*), At5g59690 (*H4*), At3g46320 (*H4*), At5g59970 (*H4*), At4g21070 (*BRCA1*), At1g65470 (*FAS1*), At1g65480 (*FT*), At2g45660 (*SOC1*), At4g16570 (*PRMT7*), At3g06400 (*CHR11*), AT5g18620 (*CHR17*), At3g43240 (*ARID5*), At1g28420 (*RLT1*), At5g44180 (*RLT2*), At3g12810 (*PIE1*), At5g60910 (*FUL*), and At5g09810

(*ACTIN7*). Raw and processed RNA-seq and MNase-seq data have been deposited in the Gene Expression Omnibus database with the accession code GSE190317.

Supplemental data

The following materials are available in the online version of this article.

Supplemental Figure S1. CRISPR/Cas9-induced mutations in the *H4* septuple mutant of Arabidopsis.

Supplemental Figure S2. Co-regulation of biological processes in *H4* septuple and *fas1-4* mutants.

Supplemental Figure S3. Mapping of H4 globular domain mutations to the nucleosome structure.

Supplemental Figure S4. Impact of histone *H4* mutations on the floral transition in Arabidopsis.

Supplemental Figure S5. Phenotypes of early flowering histone *H4* mutants.

Supplemental Figure S6. Expression of *H4R17A* in wild-type Col-0 attenuates mutant phenotypes.

Supplemental Figure S7. Phenotypes of *rH4R17A* plants and *prmt7* mutants.

Supplemental Figure S8. Conservation of ISWI proteins.

Supplemental Figure S9. The effect of ISWI and *rH4R17A* mutations on the floral transition and development.

Supplemental Figure S10. Co-regulation of gene expression observed between *rH4R17A* and ISWI mutants.

Supplemental Figure S11. GO term enrichment analysis for *rH4R17A* and ISWI mutants.

Supplemental Figure S12. H4R17 and the ISWI complex regulate nucleosome positioning in plants.

Supplemental Figure S13. Quality control analysis of RNA-seq replicates.

Supplemental Figure S14. Bioanalyzer electropherograms of RNA-seq replicates.

Supplemental Figure S15. Spearman correlation of RNA-seq replicates.

Supplemental Figure S16. Spearman correlation of MNase-seq replicates.

Supplemental Data Set S1. GO term enrichment analysis.

Supplemental Data Set S2. Genetic materials module.

Supplemental Data Set S3. Statistics for mapping and coverage of sequencing data.

Supplemental Data Set S4. DEGs identified in RNA-seq.

Supplemental Data Set S5. Cloning and PCR primers.

Supplemental Data Set S6. Statistical analysis data.

Acknowledgments

We thank all current and former members of our laboratory for discussions and advice during the course of this work. We especially acknowledge the contributions of Axel Poulet, Gonzalo Villarino, Benoit Mermaz, and Anisa Iqbal. We also acknowledge Christopher Bolick and his staff at Yale for help with plant growth and maintenance and thank the Yale Science Building Facilities Staff for maintenance of the laboratory facilities. We also thank Franziska Bleichert from Yale University for her assistance with structural analyses, Paja Sijacic and Roger Deal from Emory University for their generous gift of *pie1* seeds, Lin Xu and Wu Liu from the National Laboratory of Plant Molecular Genetics, Shanghai Institute of Plant Physiology and Ecology, Shanghai Institutes for Biological Sciences, Chinese Academy of Sciences, China, for their generous gift of *chr11 chr17* mutant seeds. The authors declare that they have no competing interests.

Funding

This work was supported by grant #R35GM128661 from the National Institutes of Health to Y.J. E.T.C. was supported by a Yale University Gruber Science Fellowship, the NIH Predoctoral Program in Cellular and Molecular Biology Training Grant T32GM007233, and the National Science Foundation Graduate Research Fellowship #2139841. U.V.P. was supported by a grant from the National Institutes of Health R35GM125003.

Conflict of interest statement. None declared.

References

Alonso JM, Stepanova AN, Leisse TJ, Kim CJ, Chen H, Shinn P, Stevenson DK, Zimmerman J, Barajas P, Cheuk R, et al. (2003) Genome-wide insertional mutagenesis of *Arabidopsis thaliana*. Science **301**: 653–657

Andres F, Coupland G (2012) The genetic basis of flowering responses to seasonal cues. Nat Rev Genet **13**: 627–639

Aydin OZ, Vermeulen W, Lans H (2014) ISWI chromatin remodeling complexes in the DNA damage response. Cell Cycle **13**: 3016–3025

Bai L, Morozov AV (2010) Gene regulation by nucleosome positioning. Trends Genet **26**: 476–483

Bastow R, Mylne JS, Lister C, Lippman Z, Martienssen RA, Dean C (2004) Vernalization requires epigenetic silencing of FLC by histone methylation. Nature **427**: 164–167

Berry S, Dean C (2015) Environmental perception and epigenetic memory: mechanistic insight through FLC. Plant J **83**: 133–148

Biasini M, Bienert S, Waterhouse A, Arnold K, Studer G, Schmidt T, Kiefer F, Gallo Cassarino T, Bertoni M, Bordoli L, et al. (2014) SWISS-MODEL: modelling protein tertiary and quaternary structure using evolutionary information. Nucleic Acids Res **42**: W252–W258

Brunaud V, Balzergue S, Dubreucq B, Aubourg S, Samson F, Chauvin S, Bechtold N, Cruaud C, DeRose R, Pelletier G, et al. (2002) T-DNA integration into the Arabidopsis genome depends on sequences of pre-insertion sites. EMBO Rep **3**: 1152–1157

Bu Z, Yu Y, Li Z, Liu Y, Jiang W, Huang Y, Dong AW (2014) Regulation of Arabidopsis flowering by the histone mark readers MRG1/2 via interaction with CONSTANS to modulate FT expression. PLoS Genet **10**: e1004617

Cheng CY, Krishnakumar V, Chan AP, Thibaud-Nissen F, Schobel S, Town CD (2017) Araport11: a complete reannotation of the *Arabidopsis thaliana* reference genome. Plant J **89**: 789–804

Chica C, Szarzynska B, Chen-Min-Tao R, Duvernois-Berthet E, Kassam M, Colot V, Roudier F (2013) Profiling spatial enrichment of chromatin marks suggests an additional epigenomic dimension in gene regulation. Front Life Sci **7**: 80–87

Clapier CR, Cairns BR (2009) The biology of chromatin remodeling complexes. Annu Rev Biochem **78**: 273–304

Clapier CR, Langst G, Corona DF, Becker PB, Nightingale KP (2001) Critical role for the histone H4 N terminus in nucleosome remodeling by ISWI. Mol Cell Biol **21**: 875–883

Clapier CR, Nightingale KP, Becker PB (2002) A critical epitope for substrate recognition by the nucleosome remodeling ATPase ISWI. Nucleic Acids Res **30**: 649–655

Clough SJ, Bent AF (1998) Floral dip: a simplified method for Agrobacterium-mediated transformation of *Arabidopsis thaliana*. Plant J **16**: 735–743

Corona DF, Tamkun JW (2004) Multiple roles for ISWI in transcription, chromosome organization and DNA replication. Biochim Biophys Acta **1677**: 113–119

Crevillen P, Gomez-Zambrano A, Lopez JA, Vazquez J, Pineiro M, Jarillo JA (2019) Arabidopsis YAF9 histone readers modulate flowering time through NuA4-complex-dependent H4 and H2A.Z histone acetylation at FLC chromatin. New Phytol **222**: 1893–1908

Crevillen P, Yang H, Cui X, Greeff C, Trick M, Qiu Q, Cao X, Dean C (2014) Epigenetic reprogramming that prevents transgenerational inheritance of the vernalized state. Nature **515**: 587–590

Cui X, Lu F, Qiu Q, Zhou B, Gu L, Zhang S, Kang Y, Cui X, Ma X, Yao Q, et al. (2016) REF6 recognizes a specific DNA sequence to demethylate H3K27me3 and regulate organ boundary formation in Arabidopsis. Nat Genet **48**: 694–699

Curtis MD, Grossniklaus U (2003) A gateway cloning vector set for high-throughput functional analysis of genes in planta. Plant Physiol **133**: 462–469

Dai J, Hyland EM, Yuan DS, Huang H, Bader JS, Boeke JD (2008) Probing nucleosome function: a highly versatile library of synthetic histone H3 and H4 mutants. Cell **134**: 1066–1078

Dann GP, Liszczak GP, Bagert JD, Muller MM, Nguyen UTT, Wojcik F, Brown ZZ, Bos J, Panchenko T, Pihl R, et al. (2017) ISWI chromatin remodellers sense nucleosome modifications to determine substrate preference. Nature **548**: 607–611

Davarinejad H, Huang YC, Mermaz B, LeBlanc C, Poulet A, Thomson G, Joly V, Munoz M, Arvanitis-Vigneault A, Valsakumar D, et al. (2022) The histone H3.1 variant regulates TONSOKU-mediated DNA repair during replication. Science **375**: 1281–1286

Davey CA, Sargent DF, Luger K, Maeder AW, Richmond TJ (2002) Solvent mediated interactions in the structure of the nucleosome core particle at 1.9 a resolution. J Mol Biol **319**: 1097–1113

Deng W, Liu C, Pei Y, Deng X, Niu L, Cao X (2007) Involvement of the histone acetyltransferase AtHAC1 in the regulation of flowering time via repression of FLOWERING LOCUS C in Arabidopsis. Plant Physiol **143**: 1660–1668

Dobin A, Davis CA, Schlesinger F, Drenkow J, Zaleski C, Jha S, Batut P, Chaisson M, Gingeras TR (2013) STAR: ultrafast universal RNA-seq aligner. Bioinformatics **29**: 15–21.

Dong J, Gao Z, Liu S, Li G, Yang Z, Huang H, Xu L (2013) SLIDE, the protein interacting domain of Imitation Switch remodelers, binds DDT-domain proteins of different subfamilies in chromatin remodeling complexes. J Integr Plant Biol **55**: 928–937

Dong J, LeBlanc C, Poulet A, Mermaz B, Villarino G, Webb KM, Joly V, Mendez J, Voigt P, Jacob Y (2021) H3.1K27me1 maintains transcriptional silencing and genome stability by preventing GCN5-mediated histone acetylation. Plant Cell **33**: 961–979

El-Brolosy MA, Kontarakis Z, Rossi A, Kuenne C, Gunther S, Fukuda N, Kikhi K, Boezio GLM, Takacs CM, Lai SL, et al. (2019) Genetic compensation triggered by mutant mRNA degradation. Nature **568**: 193–197

Fazzio TG, Gelbart ME, Tsukiyama T (2005) Two distinct mechanisms of chromatin interaction by the Isw2 chromatin remodeling complex in vivo. Mol Cell Biol **25**: 9165–9174

Feng Y, Hadjikyriacou A, Clarke SG (2014) Substrate specificity of human protein arginine methyltransferase 7 (PRMT7): the importance of acidic residues in the double E loop. J Biol Chem **289**: 32604–32616

Feng Y, Maity R, Whitelegge JP, Hadjikyriacou A, Li Z, Zurita-Lopez C, Al-Hadid Q, Clark AT, Bedford MT, Masson JY, et al. (2013) Mammalian protein arginine methyltransferase 7 (PRMT7) specifically targets RXR sites in lysine- and arginine-rich regions. J Biol Chem **288**: 37010–37025

Fu Y, Zhu Z, Meng G, Zhang R, Zhang Y (2021). A CRISPR-Cas9 based shuffle system for endogenous histone H3 and H4 combinatorial mutagenesis. Sci Rep **11**: 3298

Gelvin SB (2017) Integration of Agrobacterium T-DNA into the plant genome. Annu Rev Genet **51**: 195–217

Gkikopoulos T, Schofield P, Singh V, Pinskaya M, Mellor J, Smolle M, Workman JL, Barton GJ, Owen-Hughes T (2011) A role for Snf2-related nucleosome-spacing enzymes in genome-wide nucleosome organization. Science **333**: 1758–1760

Glozak MA, Sengupta N, Zhang X, Seto E (2005) Acetylation and deacetylation of non-histone proteins. Gene **363**: 15–23

Govin J, Dorsey J, Gaucher J, Rousseaux S, Khochbin S, Berger SL (2010) Systematic screen reveals new functional dynamics of histones H3 and H4 during gametogenesis. Genes Dev **24**: 1772–1786

Gunesdogan U, Jackle H, Herzig A (2010) A genetic system to assess in vivo the functions of histones and histone modifications in higher eukaryotes. EMBO Rep **11**: 772–776

Hamiche A, Kang JG, Dennis C, Xiao H, Wu C (2001) Histone tails modulate nucleosome mobility and regulate ATP-dependent nucleosome sliding by NURF. Proc Natl Acad Sci USA **98**: 14316–14321

He Y (2009) Control of the transition to flowering by chromatin modifications. Mol Plant **2**: 554–564

He Y, Amasino RM (2005) Role of chromatin modification in flowering-time control. Trends Plant Sci **10**: 30–35

He Y, Doyle MR, Amasino RM (2004) PAF1-complex-mediated histone methylation of FLOWERING LOCUS C chromatin is required for the vernalization-responsive, winter-annual habit in Arabidopsis. Genes Dev **18**: 2774–2784

Hodl M, Basler K (2009) Transcription in the absence of histone H3.3. Curr Biol **19**: 1221–1226

Hodl M, Basler K (2012) Transcription in the absence of histone H3.2 and H3K4 methylation. Curr Biol **22**: 2253–2257

Hughes AL, Jin Y, Rando OJ, Struhl K (2012) A functional evolutionary approach to identify determinants of nucleosome positioning: a unifying model for establishing the genome-wide pattern. Mol Cell **48**: 5–15

Huther P, Schandry N, Jandrasits K, Bezrukov I, Becker C (2020) ARADEEPOPSIS, an automated workflow for top-view plant phenomics using semantic segmentation of leaf states. Plant Cell **32**: 3674–3688

Hyland EM, Cosgrove MS, Molina H, Wang D, Pandey A, Cottee RJ, Boeke JD (2005) Insights into the role of histone H3 and histone H4 core modifiable residues in *Saccharomyces cerevisiae*. Mol Cell Biol **25**: 10060–10070

Jain K, Clarke SG (2019) PRMT7 as a unique member of the protein arginine methyltransferase family: a review. Arch Biochem Biophys **665**: 36–45

Jiang C, Pugh BF (2009) Nucleosome positioning and gene regulation: advances through genomics. Nat Rev Genet **10**: 161–172

Jiang D, Wang Y, Wang Y, He Y (2008) Repression of FLOWERING LOCUS C and FLOWERING LOCUS T by the Arabidopsis Polycomb repressive complex 2 components. PLoS ONE **3**: e3404

Jiang S, Liu Y, Wang A, Qin Y, Luo M, Wu Q, Boeke JD, Dai J (2017) Construction of comprehensive dosage-matching core histone mutant libraries for *Saccharomyces cerevisiae*. Genetics **207**: 1263–1273

Kim SI, Gelvin SB (2007) Genome-wide analysis of Agrobacterium T-DNA integration sites in the Arabidopsis genome generated under non-selective conditions. Plant J **51**: 779–791

Kim SY, He Y, Jacob Y, Noh YS, Michaels S, Amasino R (2005) Establishment of the vernalization-responsive, winter-annual habit in Arabidopsis requires a putative histone H3 methyl transferase. Plant Cell **17**: 3301–3310

Koncz C, Martini N, Mayerhofer R, Koncz-Kalman Z, Korber H, Redei GP, Schell J (1989) High-frequency T-DNA-mediated gene tagging in plants. Proc Natl Acad Sci USA **86**: 8467–8471

Kouzarides T (2007) Chromatin modifications and their function. Cell **128**: 693–705

Langmead B, Salzberg SL (2012) Fast gapped-read alignment with Bowtie 2. Nat Methods **9**: 357–359

Larkin MA, Blackshields G, Brown NP, Chenna R, McGettigan PA, McWilliam H, Valentin F, Wallace IM, Wilm A, Lopez R, et al. (2007) Clustal W and Clustal X version 2.0. Bioinformatics **23**: 2947–2948

LeBlanc C, Zhang F, Mendez J, Lozano Y, Chatpar K, Irish V, Jacob Y (2017) Increased efficiency of targeted mutagenesis by CRISPR/Cas9 in plants using heat stress. Plant J **93**: 377–386

Li G, Liu S, Wang J, He J, Huang H, Zhang Y, Xu L (2014) ISWI proteins participate in the genome-wide nucleosome distribution in Arabidopsis. Plant J **78**: 706–714

Li G, Zhang J, Li J, Yang Z, Huang H, Xu L (2012) Imitation Switch chromatin remodeling factors and their interacting RINGLET proteins act together in controlling the plant vegetative phase in Arabidopsis. Plant J **72**: 261–270

Li H, Handsaker B, Wysoker A, Fennell T, Ruan J, Homer N, Marth G, Abecasis G, Durbin R, Genome Project Data Processing Subgroup (2009) The sequence alignment/map format and SAMtools. Bioinformatics **25**: 2078–2079

Liao Y, Smyth GK, Shi W (2014) featureCounts: an efficient general purpose program for assigning sequence reads to genomic features. Bioinformatics **30**: 923–930

Lifton RP, Goldberg ML, Karp RW, Hogness DS (1978) The organization of the histone genes in *Drosophila melanogaster*: functional and evolutionary implications. Cold Spring Harb Symp Quant Biol **42**: 1047–1051

Livak KJ, Schmittgen TD (2001) Analysis of relative gene expression data using real-time quantitative PCR and the 2(-Delta Delta C(T)) method. Methods **25**: 402–408

Love MI, Huber W, Anders S (2014) Moderated estimation of fold change and dispersion for RNA-seq data with DESeq2. Genome Biol **15**: 550

Luger K, Mader AW, Richmond RK, Sargent DF, Richmond TJ (1997) Crystal structure of the nucleosome core particle at 2.8 A resolution. Nature **389**: 251–260

Luo YX, Hou XM, Zhang CJ, Tan LM, Shao CR, Lin RN, Su YN, Cai XW, Li L, Chen S, et al. (2020) A plant-specific SWR1 chromatin-remodeling complex couples histone H2A.Z deposition with nucleosome sliding. EMBO J **39**: e102008

Lusser A, Urwin DL, Kadonaga JT (2005) Distinct activities of CHD1 and ACF in ATP-dependent chromatin assembly. Nat Struct Mol Biol **12**: 160–166

Masel J, Siegal ML (2009) Robustness: mechanisms and consequences. Trends Genet **25**: 395–403

McKay DJ, Klusza S, Penke TJR, Meers MP, Curry KP, McDaniel SL, Malek PY, Cooper SW, Tatomer DC, Lieb JD, et al. (2015) Interrogating the function of metazoan histones using engineered gene clusters. Dev Cell **32**: 373–386

Nakanishi S, Sanderson BW, Delventhal KM, Bradford WD, Staehling-Hampton K, Shilatifard A (2008) A comprehensive library of histone mutants identifies nucleosomal residues required for H3K4 methylation. Nat Struct Mol Biol **15**: 881–888

Ning YQ, Chen Q, Lin RN, Li YQ, Li L, Chen S, He XJ (2019) The HDA19 histone deacetylase complex is involved in the regulation of flowering time in a photoperiod-dependent manner. Plant J **98**: 448–464

Norris A, Bianchet MA, Boeke JD (2008) Compensatory interactions between Sir3p and the nucleosomal LRS surface imply their direct interaction. PLoS Genet **4**: e1000301

Okada T, Endo M, Singh MB, Bhalla PL (2005) Analysis of the histone H3 gene family in Arabidopsis and identification of the male-gamete-specific variant AtMGH3. Plant J **44**: 557–568

Pajoro A, Muino JM, Angenent GC, Kaufmann K (2018) Profiling nucleosome occupancy by MNase-seq: experimental protocol and computational analysis. Methods Mol Biol **1675**: 167–181

Pajoro A, Severing E, Angenent GC, Immink RGH (2017) Histone H3 lysine 36 methylation affects temperature-induced alternative splicing and flowering in plants. Genome Biol **18**: 102

Picard Toolkit (2019) Broad Institute, GitHub Repository. https://broadinstitute.github.io/picard/.

Pien S, Fleury D, Mylne JS, Crevillen P, Inze D, Avramova Z, Dean C, Grossniklaus U (2008) ARABIDOPSIS TRITHORAX1 dynamically regulates FLOWERING LOCUS C activation via histone 3 lysine 4 trimethylation. Plant Cell **20**: 580–588

R Development Core Team. (2018) R: A Language and Environment for Statistical Computing, R Foundation for Statistical Computing, Vienna, Austria

Ramirez F, Ryan DP, Gruning B, Bhardwaj V, Kilpert F, Richter AS, Heyne S, Dundar F, Manke T (2016) deepTools2: a next generation web server for deep-sequencing data analysis. Nucleic Acids Res **44**: W160–W165

Richter R, Kinoshita A, Vincent C, Martinez-Gallegos R, Gao H, van Driel AD, Hyun Y, Mateos JL, Coupland G (2019) Floral regulators FLC and SOC1 directly regulate expression of the B3-type transcription factor TARGET OF FLC AND SVP 1 at the Arabidopsis shoot apex via antagonistic chromatin modifications. PLoS Genet **15**: e1008065

Robinson JT, Thorvaldsdottir H, Winckler W, Guttman M, Lander ES, Getz G, Mesirov JP (2011) Integrative genomics viewer. Nat Biotechnol **29**: 24–26

Robinson MD, McCarthy DJ, Smyth GK (2010) edgeR: a bioconductor package for differential expression analysis of digital gene expression data. Bioinformatics **26**: 139–140

Serobyan V, Kontarakis Z, El-Brolosy MA, Welker JM, Tolstenkov O, Saadeldein AM, Retzer N, Gottschalk A, Wehman AM, Stainier DY (2020) Transcriptional adaptation in *Caenorhabditis elegans*. eLife **9**

Song YH, Shim JS, Kinmonth-Schultz HA, Imaizumi T (2015) Photoperiodic flowering: time measurement mechanisms in leaves. Annu Rev Plant Biol **66**: 441–464

Srikanth A, Schmid M (2011) Regulation of flowering time: all roads lead to Rome. Cell Mol Life Sci **68**: 2013–2037

Struhl K, Segal E (2013) Determinants of nucleosome positioning. Nat Struct Mol Biol **20**: 267–273

Szabados L, Kovacs I, Oberschall A, Abraham E, Kerekes I, Zsigmond L, Nagy R, Alvarado M, Krasovskaja I, Gal M, et al. (2002) Distribution of 1000 sequenced T-DNA tags in the Arabidopsis genome. Plant J **32**: 233–242

Tan LM, Liu R, Gu BW, Zhang CJ, Luo J, Guo J, Wang Y, Chen L, Du X, Li S, et al. (2020) Dual recognition of H3K4me3 and DNA by the ISWI component ARID5 regulates the floral transition in Arabidopsis. Plant Cell **32**: 2178–2195

Tenea GN, Spantzel J, Lee LY, Zhu Y, Lin K, Johnson SJ, Gelvin SB (2009) Overexpression of several Arabidopsis histone genes increases agrobacterium-mediated transformation and transgene expression in plants. Plant Cell **21**: 3350–3367

Toto M, D'Angelo G, Corona DF (2014) Regulation of ISWI chromatin remodelling activity. Chromosoma **123**: 91–102

Wierzbicki AT, Jerzmanowski A (2005) Suppression of histone H1 genes in Arabidopsis results in heritable developmental defects and stochastic changes in DNA methylation. Genetics **169**: 997–1008

Workman JL, Kingston RE (1998) Alteration of nucleosome structure as a mechanism of transcriptional regulation. Annu Rev Biochem **67**: 545–579

Wu JF, Wang Y, Wu SH (2008) Two new clock proteins, LWD1 and LWD2, regulate Arabidopsis photoperiodic flowering. Plant Physiol **148**: 948–959

Xu L, Zhao Z, Dong A, Soubigou-Taconnat L, Renou JP, Steinmetz A, Shen WH (2008) Di- and tri- but not monomethylation on histone H3 lysine 36 marks active transcription of genes involved in flowering time regulation and other processes in *Arabidopsis thaliana*. Mol Cell Biol **28**: 1348–1360

Yadon AN, Tsukiyama T (2011) SnapShot: chromatin remodeling: ISWI. Cell **144**: 453–453.e451

Yaish MW, Colasanti J, Rothstein SJ (2011) The role of epigenetic processes in controlling flowering time in plants exposed to stress. J Exp Bot **62**: 3727–3735

Yan L, Wang L, Tian Y, Xia X, Chen Z (2016) Structure and regulation of the chromatin remodeller ISWI. Nature **540**: 466–469

Yan L, Wei S, Wu Y, Hu R, Li H, Yang W, Xie Q (2015) High-efficiency genome editing in Arabidopsis using YAO promoter-driven CRISPR/Cas9 system. Mol Plant **8**: 1820–1823

Yan L, Wu H, Li X, Gao N, Chen Z (2019) Structures of the ISWI-nucleosome complex reveal a conserved mechanism of chromatin remodeling. Nat Struct Mol Biol **26**: 258–266

Yu CW, Liu X, Luo M, Chen C, Lin X, Tian G, Lu Q, Cui Y, Wu K (2011) HISTONE DEACETYLASE6 interacts with FLOWERING LOCUS D and regulates flowering in Arabidopsis. Plant Physiol **156**: 173–184

Zhang T, Zhang W, Jiang J (2015) Genome-wide nucleosome occupancy and positioning and their impact on gene expression and evolution in plants. Plant Physiol **168**: 1406–1416

Zhang W, Zhang X, Xue Z, Li Y, Ma Q, Ren X, Zhang J, Yang S, Yang L, Wu M, et al. (2019) Probing the function of metazoan histones with a systematic library of H3 and H4 mutants. Dev Cell **48**: 406–419.e405.

Zheng S, Hu H, Ren H, Yang Z, Qiu Q, Qi W, Liu X, Chen X, Cui X, Li S, et al. (2019) The Arabidopsis H3K27me3 demethylase JUMONJI 13 is a temperature and photoperiod dependent flowering repressor. Nat Commun **10**: 1303

Zhou K, Gaullier G, Luger K (2019) Nucleosome structure and dynamics are coming of age. Nat Struct Mol Biol **26**: 3–13